5-2019

Synthesis and Application of Oil-Soluble Polymer Brush-Grafted Silica Nanoparticles as Lubricant Additives for Friction and Wear Reduction

Bryan Thomas Seymour
University of Tennessee, bseymou2@vols.utk.edu

To the Graduate Council:

I am submitting herewith a dissertation written by Bryan Thomas Seymour entitled "Synthesis and Application of Oil-Soluble Polymer Brush-Grafted Silica Nanoparticles as Lubricant Additives for Friction and Wear Reduction." I have examined the final electronic copy of this dissertation for form and content and recommend that it be accepted in partial fulfillment of the requirements for the degree of Doctor of Philosophy, with a major in Chemistry.

Bin Zhao, Major Professor

We have read this dissertation and recommend its acceptance:

S. Michael Kilbey II, Ziling Xue, Hong Guo

Accepted for the Council:

Dixie L. Thompson

Vice Provost and Dean of the Graduate School

(Original signatures are on file with official student records.)

Synthesis and Application of Oil-Soluble Polymer Brush-Grafted Silica Nanoparticles as Lubricant Additives for Friction and Wear Reduction

A Dissertation Presented for the

Doctor of Philosophy

Degree

The University of Tennessee, Knoxville

Bryan Thomas Seymour

May 2019

Acknowledgments

I would first like to express my gratitude to my research advisor, Professor Bin Zhao, who has mentored and trained me to become a much better scientist. You taught me the importance of critical thinking, problem-solving, and how to learn from setbacks. Your enthusiasm for knowledge and professionalism is inspirational and I strive to emulate this throughout my career.

I would also like to thank my graduate committee: Prof. Michael Kilbey, Prof. Ben Xue, and Prof. Hong Guo. You all have been very gracious with your time and helpful in furthering my growth within the world of scientific research.

I would like to thank the US Department of Energy and the National Science Foundation for their funding, which has made all of this work possible.

Many thanks to my various collaborators including Dr. Jun Qu at Oak Ridge National Lab for allowing me to access his lab for tribological testing. Thank you to Dr. John Dunlap at JIAM for his training on the use of electron microscopy. I also sincerely thank Prof. Lei Zhu of Case Western Reserve University for collaborating with us on mesogen-free liquid crystalline polymers. Lastly, thank you to Dr. Ed Wright for training and allowing me to use the ultracentrifuge.

I would like to thank all of the members of Prof. Zhao's research group, both past and present, for their friendship and advice. My thanks to Dr. Daniel M. Henn, Dr. Bin Hu, Dr. Roger A. E. Wright, Sisi Jiang, Ethan Kent, Jessica Holmes, Evan Lewoczko, Caleb Bohannon, Andrew Chancellor, Michael Kelly, Nina Wang, Dr. Wenxin Fu, and Prof.

Chunhui Luo. I would like to give special thanks to Dr. Roger A. E. Wright, who helped mentor me in the synthesis and characterization of oil-soluble hairy nanoparticles.

I would like to thank my family for their support and encouragement through my graduate school career. Thank you to my mom, Sue; dad, Mike; step mom, Nona; and brothers, Eric and TJ for allowing this to be possible and for your consistent love and support throughout the journey. I would also like to thank all of my extended family and friends for being sources of inspiration and encouragement.

Finally, to my soon-to-be wife, Jessie, I would not have been able to do this without you. Thank you for your endless love and support.

Abstract

Although inorganic and metallic nanoparticles are potentially effective oil lubricant additives for friction and wear reduction, their high tendency to undergo aggregation and precipitation in base oils has been an obstacle for real-world applications. This dissertation research aims to develop oil-soluble, polymer brush-grafted nanoparticles (hairy NPs) for use as additives for base oils such as polyalphaolefin (PAO). Well-defined hairy NPs were synthesized by surface-initiated reversible addition-fragmentation chain transfer polymerization from chain transfer agent-functionalized, 23 nm silica NPs, and their lubrication properties were investigated in PAO by high-contact-stress ball-on-flat reciprocating sliding tribological tests.

The effects of alkyl pendant groups of poly(alkyl methacrylate) brushes on oil dispersibility, stability, and tribological properties of hairy NPs were studied. It was found that hairy NPs with sufficiently long alkyl pendants (> 8 carbon atoms, such as 12, 13, and 16) were readily dispersed in PAO and formed homogeneous, clear dispersions with long-term stability over a wide temperature range. Significant friction and wear reductions were achieved by using 1 wt% homogenous dispersions of hairy NPs in PAO. In an effort to increase the function of polymer brushes through the introduction of triboactive phosphorus into the grafted polymers, three phosphonate-containing monomers were synthesized and copolymerized with a long alkyl methacrylate. A significant amount of phosphonate can be incorporated into the brushes without comprising the dispersibility of hairy NPs in PAO. A synergistic effect of combining hairy NPs with a phosphonium-phosphate ionic liquid as PAO additives was discovered. The lubricating performance was

improved significantly when the two additives were mixed at certain ratios. Analysis showed that both silica NPs and the ionic liquid participated in the tribo-chemical reaction. These research efforts have shown that hairy NPs have promise for use as lubricant additives. Lastly, as a side project, a series of isotactic and atactic polyethers with monosulfone-containing pendants were synthesized by the reaction of corresponding poly(epichlorohydrin) with various *n*-alkanethiols and subsequent oxidation of thioether groups with a goal of seeking ferroelectric liquid crystalline polymers for use in solid state cooling. The isotactic poly((*R*)-epichlorohydrin) was synthesized by ring-opening polymerization of (*R*)-(-)-epichlorohydrin using a commercial methylaluminoxane as the catalyst.

Table of Contents

List of Tables

List of Figures

List of Schemes

List of Abbreviations

AIBN: Azobisisobutyronitrile

APTES: (3-Aminopropyl)triethoxysilane

ATRP: Atom transfer radical polymerization

COF: Coefficient of friction

COP: Coefficient of performance

CTA: Chain transfer agent

CTA-COOH: 4-(((Butylthio)carbonothioyl)thio)-4-cyanopentanoic acid

CTA-Silane: *n*-Butyl (2-cyano-5-oxo-5-((3-(triethoxysilyl)propyl)amino)pentan-2-yl)carbonotrithioate

Đ: Dispersity

DCC: Dicyclohexyl carbodiimide

DLS: Dynamic light scattering

DSC: Differential scanning calorimetry

Hairy NPs: Polymer brush-grafted nanoparticles

IL: [P8888][DEHP] Ionic liquid

LCPs: Liquid crystalline polymers

MAC2P: 2-(Diethoxyphosphoryl) ethyl methacrylate

MAC11P: 11-(Diethoxyphosphoryl)undecyl methacrylate

MAO: Methylaluminoxane

MIBK: Methyl isobutyl ketone

$M_{n,SEC}$: Number average molecular weight by size exclusion chromatography

NHS: N-hydroxy succinimide

NPs: Nanoparticles

NMR: Nuclear magnetic resonance

NMRP: Nitroxide-mediated radical polymerization

PAO: Polyalphaolefin

PC6MA: Poly(*n*-hexyl methacrylate)

PC8MA: Poly(ethylhexyl methacrylate)

PC12MA: Poly(lauryl methacrylate) (also PLMA)

PC13MA: Poly(tridecyl methacrylate)

PC16MA: Poly(hexadecyl methacrylate)

PDEGMMA: Poly(methoxydi(ethylene glycol)methacrylate)

PECH: Poly(epichlorohydrin)

PTEGMMA: Poly(methoxytri(ethylene glycol)methacrylate)

RAFT: Reversible addition-fragmentation chain transfer

ROP: Ring-opening polymerization

SAXS: Small-angle X-ray scattering

SEC: Size exclusion chromatography (also GPC)

SEM-EDS: Scanning electron microscopy-energy dispersive X-ray spectroscopy

SI: Surface-initiated

STEM: Scanning transmission electron microscopy

StP: Diethyl (4-vinylbenzyl)phosphonate

TGA: Thermogravimetric analysis

THF: Tetrahydrofuran

WAXS: Wide-angle X-ray scattering

XPS: X-ray photoelectron spectroscopy

ZDDP: Zinc dialkyldithiophosphonates

Chapter 1. Introduction

1.1 Introduction

This dissertation describes the design and synthesis of polymer brush-grafted nanoparticles (hairy NPs) for use as additives in lubricating base oil polyalphaolefin (PAO) for friction and wear reduction. These hairy NPs are composed of a core particle and a layer of polymer chains that are end-grafted on the surface of the core. Section 1.1.1. presents a general introduction to polymer brush-grafted nanoparticles and the synthesis of both single component and multicomponent polymer brush-grafted NPs. Nanoparticles have been explored for application as lubricant additives, dubbed as "nanolubricants", and have shown great promise. Various nanolubricants, including nanoparticle dispersions prepared by the use of dispersant or surface modification and oil-soluble polymer brush-grafted NPs, will be discussed in Section 1.1.2. An overview of this dissertation work is given in Section 1.2 at the end of this chapter.

1.1.1 Introduction to Polymer Brush-Grafted Nanoparticles

1.1.1.1 General Introduction

Polymer brush-grafted nanoparticles, or hairy NPs, are an interesting class of hybrid materials consisting of a core and an outer layer of polymer chains end-tethered to the core by a covalent bond. Many different types of materials can be used for the core NPs, including metals, metal oxides, latex particles, etc. At a sufficiently high grafting density, the grafted polymer chains are highly stretched, extending outwards from the surface of the core. Typically, the substrates for hairy NPs are spherical and solid, but NPs of other shapes and features, such as mesoporous or hollow structures are also utilized. The grafted

polymers could have different architectures, including linear or cyclic homopolymers, or multicomponent systems, such as binary mixed homopolymer brushes and block copolymer brushes, to name a few. Due to the many possible core compositions and polymer architectures, hairy NPs have been investigated for many different applications, such as drug delivery, sensing, oil lubrication, and catalysis. Nanoparticles are known to have a high tendency to undergo irreversible aggregation due to their small size and relatively high surface energy. With a canopy of end-grafted polymer chains, the stability of NPs in good solvents has been demonstrated to increase significantly. This is because the favorable enthalpic interactions of the grafted polymer chains with the good solvent can overcome the unfavorable contact between NPs and solvent and the van der Waals attractive forces among core NPs.

1.1.1.2 Synthesis of Single Component Polymer Brush-Grafted NPs by Surface-Initiated "Living"/Controlled Polymerization

There are two general methods commonly used for the synthesis of hairy NPs, "grafting to" and "grafting from" as illustrated in Scheme 1.1. "Grafting to" refers to the bonding of end-functionalized polymers to a substrate with complementary groups, where modification of the polymer and/or substrate is often required. This method is straightforward, but the polymer grafting density of hairy particles is often lower due to the steric hindrance of the already tethered polymer chains presented to incoming macromolecules. Commonly, polymer chains are end-functionalized with a thiol group for grafting to gold NPs.[1,2] The "grafting from" method is also referred to as surface-initiated polymerization, where the nanoparticles are surface-modified with an appropriate initiator

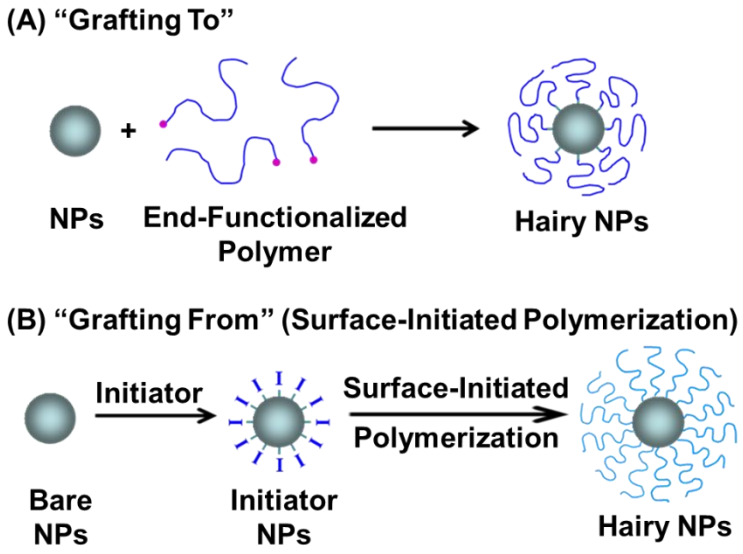

Scheme 1.1. Two General Methods for the Synthesis of Hairy NPs: (A) "Grafting To" and (B) "Grafting From".

for the polymerization technique used. Pruker and Rühe were one of the first to report on the use of surface-initiated polymerization to grow polymer brushes. They immobilized monochlorosilyl-functionalized azo-initiators onto various solid surfaces and grew linear polymer chains using conventional free radical polymerization.[3] Various "living"/controlled polymerization techniques have been used for surface-initiated polymerization from many different substrates, including atom transfer radical polymerization (ATRP), nitroxide mediated radical polymerization (NMRP), and reversible addition-fragmentation chain transfer (RAFT) polymerization, which will be discussed individually below. Surface-initiated "living"/controlled polymerizations allow for the synthesis of polymer brushes with well-controlled molecular weights, narrow dispersities, and high grafting densities. The drawback of "grafting from" is the difficulty in characterizing the grafted polymers. To directly characterize brush chains, one has to degraft the polymer chains from the surface for characterization by NMR spectroscopy and size exclusion chromatography (SEC) analysis. Often, a sacrificial initiator is added to the polymerization mixture to produce an analogous free polymer during the synthesis of hairy NPs, which are used for the estimation of the molecular weight of grafted polymer chains.[4]

One of the first to report on the use of surface-initiated ATRP (SI-ATRP) was Matyjaszewski et al., who synthesized hybrid NPs composed of polystyrene or polymethacrylates grafted on silica NPs.[5] The initiator-modified NPs were prepared by anchoring a 2-bromoisobutyrate initiator (Scheme 1.2A) onto the surface of NPs through silane chemistry, and well-defined homopolymer and block copolymer brushes were grown from the NP surface by SI-ATRP. Fukuda et al. synthesized a triethoxysilane-

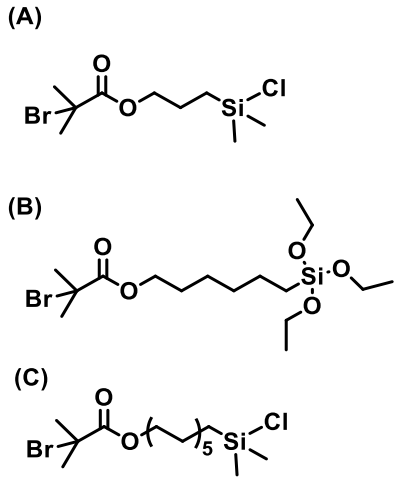

Scheme 1.2. Various Atom Transfer Radical Polymerization (ATRP) Initiators Used for Surface Modification of Nanoparticles for Surface-Initiated ATRP.[5-7]

functionalized ATRP initiator (Scheme 1.2B) and used it to modify the surface of silica particles in a mixture of ethanol, water, and ammonia.[6] SI-ATRP of methyl methacrylate from the initiator-functionalized particles produced well-defined grafted polymer brushes with molecular weights up to 480 kDa and grafting densities as high as 0.65 chains/nm^2. Thermosensitive polymer brushes have been successfully synthesized by SI-ATRP by Li et al.[7] For this work, an ATRP initiator with a longer spacer group (Scheme 1.2C) was used to functionalize silica particles and to grow poly(methoxydi(ethylene glycol) methacrylate) (PDEGMMA) and poly(methoxytri(ethylene glycol) methacrylate) (PTEGMMA) brushes. Note that the cloud points of PDEGMMA and PTEGMMA in water are 25 °C and 48 °C, respectively.

NMRP, another "living"/controlled radical polymerization technique, has been employed for the synthesis of hairy NPs. Hawker et al. demonstrated the preparation of polystyrene brushes from silica gel particles that were surface-functionalized with an alkoxyamine initiator (Figure 1.1A) by SI-NMRP.[8] A free initiator, 1-phenyl-1-(2',2',6',6'-tetramethyl-1'-piperidinyloxy) ethane, was added into the polymerization mixture to form free polystyrene during the polymerization. They cleaved the grafted polystyrene chains from the silica particles and compared it with the free polystyrene formed from the free initiator during the polymerization; they found little difference in regards to molecular weight and dispersity (Đ) of the grafted and free polymers (Figure 1.1B).

The third "living"/controlled radical polymerization technique that is widely used in the surface-initiated polymerization for the synthesis of polymer brush-grafted NPs is

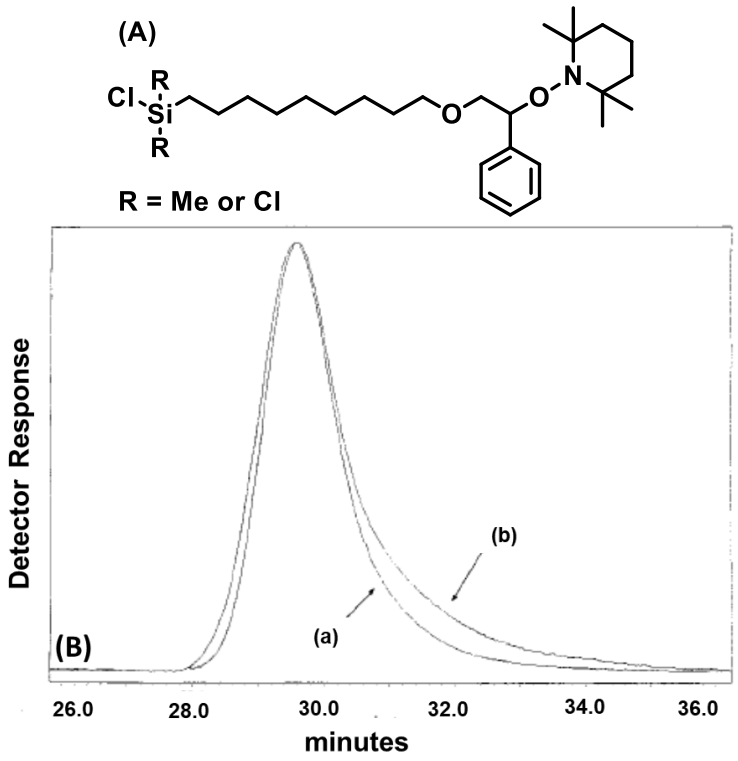

Figure 1.1. (A) Nitroxide mediated radical polymerization (NMRP) initiator used for the surface functionalization of silica nanoparticles and (B) GPC traces of cleaved (a) and free (b) polystyrene.[8] (Adapted from Ref. 8 with permission from the American Chemical Society)

RAFT polymerization. One early report of surface-initiated RAFT polymerization came from Fukuda et al.[9] They first immobilized an ATRP initiator (BCS, Scheme 1.3A) onto the surface of silica particles. After the surface-initiated ATRP polymerization to grow polystyrene chains, they converted the Br atom at the chain end to a dithiobenzoate moiety by reacting the hairy NPs with PBD (Scheme 1.3A) under the ATRP conditions in the absence of monomer. Chain extension of the grafted polymer with styrene was then conducted via RAFT polymerization. Benicewitz et al. reported on the immobilization of a RAFT-silane agent (Scheme 1.3B) onto silica nanoparticles for the SI-RAFT polymerization to grow polystyrene and poly(*n*-butyl acrylate) polymer chains.[10] More recently, Perrier et al. reported the use of a triethoxysilane-functionalized RAFT CTA (Scheme 1.3C) to modify monodisperse silica nanoparticles for SI-RAFT polymerization of styrene.[11]

1.1.1.3 Synthesis of Well-Defined Multicomponent Polymer Brush-Grafted Nanoparticles by Surface-Initiated "Living"/Controlled Polymerization

Multicomponent polymer brushes contain two or more different polymers in the brush layer. Examples include block copolymer brushes and mixed polymer brushes. These brushes can undergo self-reorganization in response to environmental changes and exhibit different microstructures under different conditions.[12-15] One early example of the synthesis of diblock copolymer brush-grafted NPs was reported by Matyjaszewski et al. using SI-ATRP through a two-step process.[5] A series of silica NPs grafted with well-defined diblock copolymer brushes, such as polystyrene-*b*-poly(*n*-butyl acrylate) and poly(methyl methacrylate) - *b* - poly (*n*-butyl acrylate), were successfully synthesized.[5]

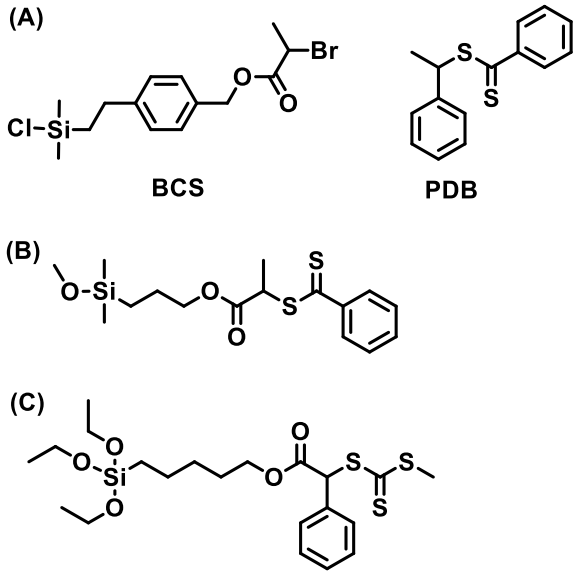

Scheme 1.3. Various Functionalized Chain Transfer Agents (CTA) For Surface-Initiated RAFT Polymerization.[9-11]

Our group has studied both mixed polymer brush and block copolymer brush-grafted nanoparticle systems. A difunctional initiator-terminated monochlorosilane containing an initiating moiety for ATRP and an initiating group for NMRP was synthesized and used to functionalize silica NPs. Well-defined binary mixed homopolymer brushes were prepared by sequential SI-ATRP of *t*-butyl acrylate, conducted at a lower temperature (75 °C) and SI-NMRP of styrene, at a higher temperature (120 °C). Subsequent removal of *t*- butyl groups of poly(*t*-butyl acrylate) produced amphiphilic mixed poly(acrylic acid)/polystyrene brush-grafted silica NPs (Scheme 1.4).[4] The successful synthesis of well-defined mixed homopolymer brushes on silica particles allowed for the study of their responsive behavior. More recently, silica NPs grafted with diblock copolymer brushes composed of a thermoresponsive block and a charged block were made by SI-ATRP and subsequent post-polymerization modification.[16] Above a critical concentration, aqueous dispersions of these diblock copolymer brush-grafted NPs have been shown to undergo thermally induced sol-gel transitions.

1.1.2 Nanoparticles as Oil Lubricant Additives for Friction and Wear Reduction

1.1.2.1 Nanolubricants Made by Use of Dispersant (Surfactant) or Surface Modification with Small Molecule Alkoxysilanes

Increasing the energy efficiency and lifetime of machinery has long been a challenge. Nanolubricants, which are a class of lubricants that capitalizes on the use of NPs for friction and wear reduction applications, have shown great promise.[17-22] Many different types of NPs, such as metals, metal oxides, metal sulfides, etc., have been shown to increase the lubrication properties when added into a base oil. Although large friction and wear

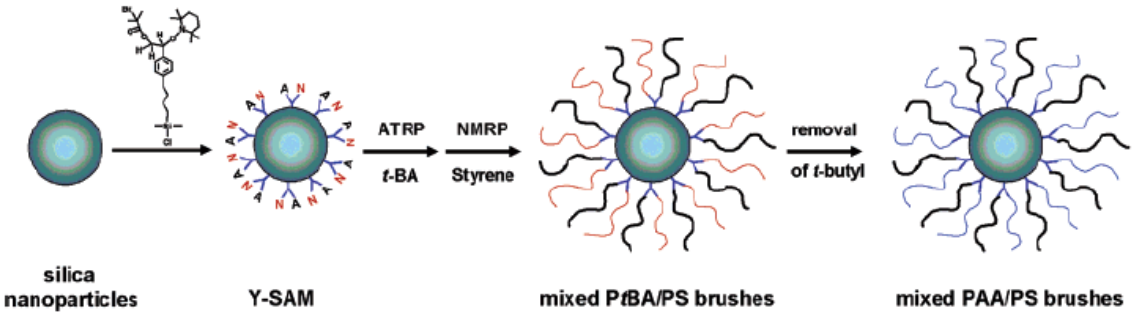

Scheme 1.4. Synthesis of Amphiphilic Mixed Poly(Acrylic Acid)/polystyrene Brushes on Silica Nanoparticles.[4] (Reproduced from Ref. 4 with permission from the American Chemical Society)

reduction has been reported, the dispersibility and stability of these NPs in hydrophobic oils have remained a challenge.[19,20] Commonly, the mixture of NPs and oil is sonicated or shaken to form a dispersion before adding onto a metal surface for testing of their lubrication properties.[21,22] NPs have a strong tendency to undergo aggregation in the lubricating base oil due to their relatively small size and high surface energy. In order to realize the full potential of nanolubricants, stable dispersions must be achieved.

To solubilize NPs in lubricating base oils, researchers have used two methods: formulation of NPs with dispersants and surface modification of NPs to increase the oil solubility. Many dispersants were tested, including aliquot 336, oleic acid, and sorbitol monostearate, to name a few, but in some cases they were found to reduce the performance of NPs and none of the NP dispersions displayed long term stability (> 2 weeks).[23-26] The mechanism of dispersant-stabilization of NPs was the absorption of amphiphilic dispersant molecules onto the surface of NPs. Another common approach to dispersing and stabilizing NPs in oils is a surface modification of NPs with various alkoxysilanes. Silanization is applicable to substrates bearing surface hydroxyl groups. This method requires the use of organic compounds containing a functional group capable of reacting with the NP surface and a long alkyl group for stabilization.[27] Often, this is accomplished through a two-step process, in which an alkoxysilane, for example, (3-aminopropyl)triethoxysilane is first tethered to the surface and a long alkyl acid, such as lauric or stearic acid, is then reacted with the amine group, yielding a long alkyl stabilizer on the surface.[28,29] Although many attempts have been made, it remains a great challenge to achieve dispersions of NPs in lubricating base oils over a large temperature range (e.g, -20 °C to 100 °C).

1.1.2.2 Polymer Brush-Grafted NPs as Lubricant Additives

A promising approach to preparing oil-soluble NPs is the use of polymer brushes synthesized by surface-initiated "living"/controlled radical polymerization. Our group pioneered the synthesis of oil-soluble polymer brush-grafted NPs by SI-ATRP of lauryl methacrylate from initiator-functionalized silica and titania NPs.[30] The effect of the molecular weight of polymer brushes on the tribological performance of hairy NPs in PAO was studied, and it was found that as molecular weight decreased the friction reduction performance of hairy NPs increased at a concentration of 1 wt% (Figure 1.2). This is likely due to the relative amount of core NPs present in a 1 wt% dispersion increased as the polymer molecular weight decreased. Stability tests were performed for 55 days at -20 °C, 22 °C, and 100 °C for poly(lauryl methacrylate) (PLMA) brush grafted silica NPs with a molecular weight of 4.1 kDa (HNP-SiO_2-4.1k) and PLMA-grafted titania NPs with a $M_{n,SEC}$ of 16.2 kDa (HNP-TiO_2-16.2k).[30] These hairy NPs showed excellent dispersibility and stability, and only slight discoloration at 100 °C was observed for hairy TiO_2 NPs (Figure 1.3). The superior dispersibility and stability of hairy NPs in oil results from the favorable enthalpic interactions between PLMA brushes and PAO and the entropic steric repulsion between hairy NPs.

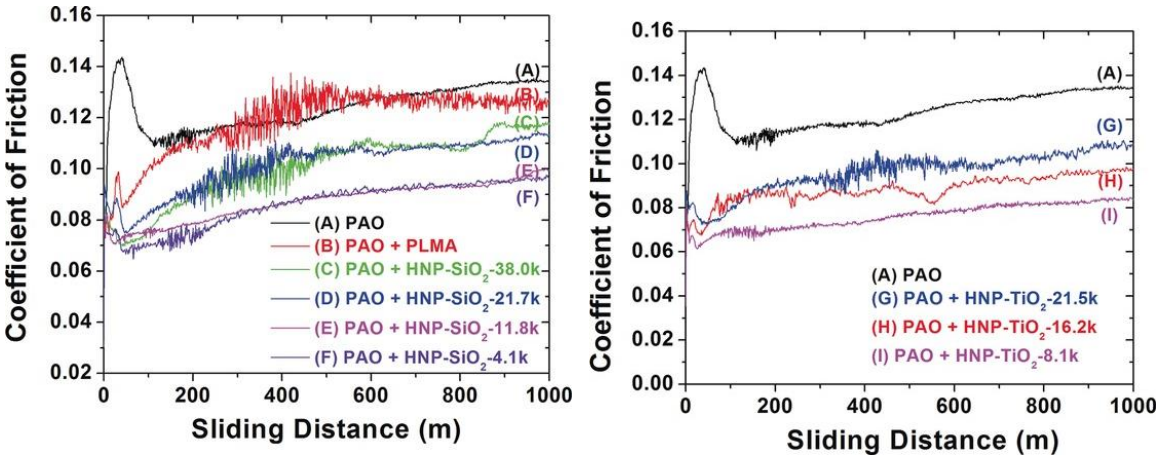

Figure 1.2. Friction curves of PAO (A), free PLMA-38.0k (B), HNP-SiO_2-38.0k (C), HNP-SiO_2-21.7k (D), HNP-SiO_2-11.8k (E), HNP-SiO_2-4.1k (F), HNP-TiO_2-21.5k (G), HNP-TiO_2-16.2k (H), and HNP-TiO_2-8.1k (I).[30] All dispersions are 1 wt% in PAO. (Adapted from Ref. 30 with permission from Angewandte Chemie)

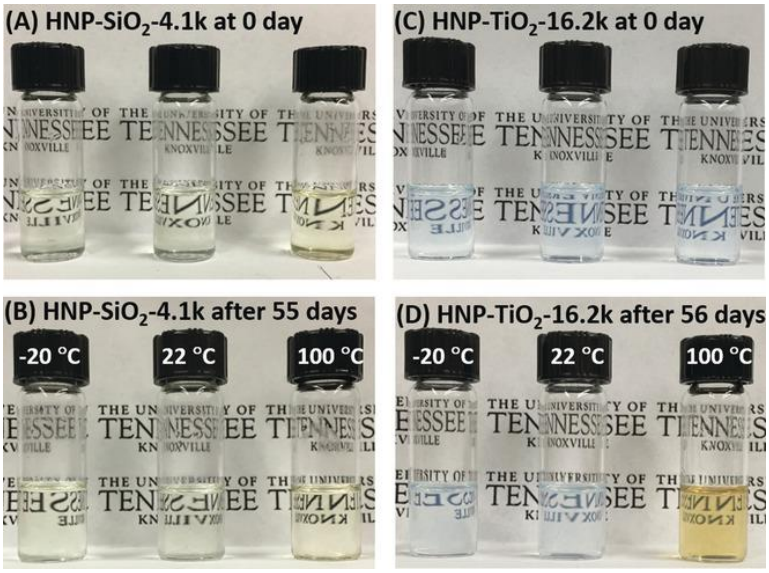

Figure 1.3. Optical images of 1 wt % dispersions of HNP-SiO_2-4.1k in PAO before (A) and after being kept at −20, 22, 100 °C for 55 days (B), and 1 wt % dispersions of HNP-TiO_2-16.2k in PAO before (C) and after being kept at −20, 22, and 100 °C for 56 days (D).[30] (Reproduced from Ref. 30 with permission from Angewandte Chemie)

1.2 Dissertation Overview

This dissertation work is focused on the synthesis of polymer brush-grafted silica NPs and their application as oil additives for friction and wear reduction. The second chapter explores how the alkyl pendant group length of the monomer affects the dispersibility and performance of hairy NPs. The third chapter presents the synthesis of functional hairy NPs with the incorporation of phosphonate groups into the brushes. The fourth chapter describes the mixing of oil-soluble hairy NPs and an oil-miscible ionic liquid and the enhanced friction reduction performance when combined. The fifth chapter reports on the synthesis of polyethers with monosulfone-containing pendant groups of varying lengths for potential use as electrocaloric materials. The final chapter provides a summary of my research and potential ideas for future work.

Nanolubricants that display high colloidal stability are of particular interest for practical applications. For this reason, polymer brush-grafted nanoparticles have potential in the field of nanolubricants. Chapter 2 focuses on the synthesis of a set of hairy silica NPs composed of poly(alkyl methacrylate) brushes with varying pendant group lengths. SI-RAFT polymerization was employed for the synthesis of hairy NPs from trithiocarbonate CTA-functionalized, 23 nm silica NPs. A corresponding CTA was added into the polymerization mixtures to facilitate the characterization by SEC. Hairy NPs prepared from alkyl methacrylates with shorter alkyl pendant groups (6 and 8 carbon atoms) were found to be cloudy in PAO at room temperature, while those prepared from monomers with longer alkyl pendant groups (12, 13, and 16 carbons atoms) were found to form homogenous dispersions. Significant friction reductions were achieved with the use of

homogenous dispersions of hairy NPs compared with the PAO base oil. We found that the primary function of the grafted polymer chains is to stabilize the silica particles in oil.

The work described in Chapter 3 aims to increase the function of polymer brushes in hairy NPs with the incorporation of triboactive element phosphorus into the brushes. The hairy NPs were prepared by SI-RAFT copolymerization of a long alkyl methacrylate (13 or 16 carbon atoms in the pendant) and a phosphonate-functionalized monomer at feed molar ratios of 95 : 5, 90 : 10, 85 : 15, and 80 : 20. Three phosphonate-functionalized monomers were designed and synthesized: diethyl (4-vinylbenzyl)phosphonate, 11-(diethoxyphosphoryl)undecyl methacrylate, and 2-(diethoxyphosphoryl) ethyl methacrylate. SI-RAFT copolymerization of hexadecyl methacrylate and MAC2P from CTA-functionalized silica NPs afforded hairy NPs with the best dispersibility, likely due to the better shielding of phosphonate groups by the hexadecyl pendant groups.

Chapter 4 presents a study on the combination of oil-soluble hairy NPs and an oil-miscible ionic liquid (IL) as additives for PAO for friction and wear reduction. We found that the lubricating performance was improved significantly when the two promising additives are mixed at certain ratios. A PLMA brush-grafted silica NP sample was synthesized by SI-RAFT polymerization and mixed with a phosphonium-phosphate IL at various mass ratios. At a total concentration of 2 wt% and sufficiently high individual concentrations, tribological tests showed that significant decreases in friction were achieved compared with the 2 wt% hairy NPs alone and 2 wt% IL alone. Scanning electron microscopy-energy dispersive X-ray spectroscopy (SEM-EDS) indicated the presence of

both Si and P in the tribofilm, suggesting that both hairy silica NPs and the IL participated in the tribo-chemical reaction.

Chapter 5 describes the synthesis of isotactic and atactic polyethers with monosulfone-containing pendant groups by the reaction of isotactic and atactic polyepichlorohydrins with various *n*-alkanethiols and the subsequent oxidation of the thioether groups. ^{13}C NMR spectroscopy analysis confirmed the formation of isotactic poly((*R*)-epichlorohydrin) by ring-opening polymerization of (*R*)-(-)-epichlorohydrin using a commercial methylaluminoxane (MAO) catalyst. ^{1}H NMR spectroscopy showed that the substitution reaction of atactic and isotactic polyepichlorohydrin with *n*-alkane thiols were complete. The structures of these polymers are being characterized by our collaborators.

References

1. Zhu, M.-Q.; Wang, L.-Q.; Exarhos, G. J.; Li, A. D. Q. Thermosensitive Gold Nanoparticles. *J. Am. Chem. Soc.* **2004,** *126* (9), 2656-2657.
2. Chiu, J. J.; Kim, B. J.; Kramer, E. J.; Pine, D. J. Control of Nanoparticle Location in Block Copolymers. *J. Am. Chem. Soc.* **2005,** *127* (14), 5036-5037.
3. Prucker, O.; Rühe, J. Synthesis of Poly(styrene) Monolayers Attached to High Surface Area Silica Gels through Self-Assembled Monolayers of Azo Initiators. *Macromolecules* **1998,** *31* (3), 592-601.
4. Li, D.; Sheng, X.; Zhao, B. Environmentally Responsive "Hairy" Nanoparticles: Mixed Homopolymer Brushes on Silica Nanoparticles Synthesized by Living Radical Polymerization Techniques. *J. Am. Chem. Soc.* **2005,** *127* (17), 6248-6256.
5. Pyun, J.; Jia, S.; Kowalewski, T.; Patterson, G. D.; Matyjaszewski, K. Synthesis and characterization of organic/inorganic hybrid nanoparticles: Kinetics of surface-initiated atom transfer radical polymerization and morphology of hybrid nanoparticle ultrathin films. *Macromolecules* **2003,** *36* (14), 5094-5104.
6. Ohno, K.; Morinaga, T.; Koh, K.; Tsujii, Y.; Fukuda, T. Synthesis of Monodisperse Silica Particles Coated with Well-Defined, High-Density Polymer Brushes by Surface-Initiated Atom Transfer Radical Polymerization. *Macromolecules* **2005,** *38* (6), 2137-2142.
7. Li, D.; Jones, G. L.; Dunlap, J. R.; Hua, F.; Zhao, B. Thermosensitive Hairy Hybrid Nanoparticles Synthesized by Surface-Initiated Atom Transfer Radical Polymerization. *Langmuir* **2006,** *22* (7), 3344-3351.

8. Husseman, M.; Malmström, E. E.; McNamara, M.; Mate, M.; Mecerreyes, D.; Benoit, D. G.; Hedrick, J. L.; Mansky, P.; Huang, E.; Russell, T. P.; Hawker, C. J. Controlled Synthesis of Polymer Brushes by "Living" Free Radical Polymerization Techniques. *Macromolecules* **1999,** *32* (5), 1424-1431.

9. Tsujii, Y.; Ejaz, M.; Sato, K.; Goto, A.; Fukuda, T. Mechanism and Kinetics of RAFT-Mediated Graft Polymerization of Styrene on a Solid Surface. 1. Experimental Evidence of Surface Radical Migration. *Macromolecules* **2001,** *34* (26), 8872-8878.

10. Li, C.; Benicewicz, B. C. Synthesis of Well-Defined Polymer Brushes Grafted onto Silica Nanoparticles via Surface Reversible Addition-Fragmentation Chain Transfer Polymerization. *Macromolecules* **2005,** *38* (14), 5929-5936.

11. Ohno, K.; Ma, Y.; Huang, Y.; Mori, C.; Yahata, Y.; Tsujii, Y.; Maschmeyer, T.; Moraes, J.; Perrier, S. Surface-Initiated Reversible Addition-Fragmentation Chain Transfer (RAFT) Polymerization from Fine Particles Functionalized with Trithiocarbonates. *Macromolecules* **2011,** *44* (22), 8944-8953.

12. Feng, J.; Haasch, R. T.; Dyer, D. J. Photoinitiated Synthesis of Mixed Polymer Brushes of Polystyrene and Poly(methyl methacrylate). *Macromolecules* **2004,** *37* (25), 9525-9537.

13. Ionov, L.; Sidorenko, A.; Stamm, M.; Minko, S.; Zdyrko, B.; Klep, V.; Luzinov, I. Gradient Mixed Brushes: "Grafting To" Approach. *Macromolecules* **2004,** *37* (19), 7421-7423.

14. LeMieux, M. C.; Julthongpiput, D.; Bergman, K. N.; Cuong, P. D.; Ahn, H.-S.; Lin, Y.-H.; Tsukruk, V. V. Ultrathin Binary Grafted Polymer Layers with Switchable Morphology. *Langmuir* **2004,** *20* (23), 10046-10054.
15. Zhao, B.; He, T. Synthesis of Well-Defined Mixed Poly(methyl methacrylate)/Polystyrene Brushes from an Asymmetric Difunctional Initiator-Terminated Self-Assembled Monolayer. *Macromolecules* **2003,** *36* (23), 8599-8602.
16. Wright, R. A. E.; Hu, B.; Henn, D. M.; Zhao, B. Reversible sol-gel transitions of aqueous dispersions of silica nanoparticles grafted with diblock copolymer brushes composed of a thermosensitive inner block and a charged outer block. *Soft Matter* **2015,** *11* (34), 6808-6820.
17. Chen, Y.; Renner, P.; Liang, H. Dispersion of Nanoparticles in Lubricating Oil: A Critical Review. *Lubricants* **2019,** *7* (1), 7.
18. Chiñas-Castillo, F.; Spikes, H. A. Mechanism of Action of Colloidal Solid Dispersions. *J. Tribol.* **2003,** *125* (3), 552-557.
19. Dai, W.; Kheireddin, B.; Gao, H.; Liang, H. Roles of nanoparticles in oil lubrication. *Tribol. Int.* **2016,** *102*, 88-98.
20. Gulzar, M.; Masjuki, H. H.; Kalam, M. A.; Varman, M.; Zulkifli, N. W. M.; Mufti, R. A.; Zahid, R. Tribological performance of nanoparticles as lubricating oil additives. *J. Nanopart. Res.* **2016,** *18* (8), 223.
21. Kalin, M.; Kogovšek, J.; Remškar, M. Mechanisms and improvements in the friction and wear behavior using MoS_2 nanotubes as potential oil additives. *Wear* **2012,** *280-281*, 36-45.

22. Rabaso, P.; Ville, F.; Dassenoy, F.; Diaby, M.; Afanasiev, P.; Cavoret, J.; Vacher, B.; Le Mogne, T. Boundary lubrication: Influence of the size and structure of inorganic fullerene-like MoS_2 nanoparticles on friction and wear reduction. *Wear* **2014,** *320*, 161-178.

23. Bogunovic, L.; Zuenkeler, S.; Toensing, K.; Anselmetti, D. An Oil-Based Lubrication System Based on Nanoparticular TiO_2 with Superior Friction and Wear Properties. *Tribol. Lett.* **2015,** *59* (2), 29.

24. Hu, Z. S.; Dong, J. X.; Chen, G. X. Study on antiwear and reducing friction additive of nanometer ferric oxide. *Tribol. Int.* **1998,** *31* (7), 355-360.

25. Qiu, S.; Zhou, Z.; Dong, J.; Chen, G. Preparation of Ni Nanoparticles and Evaluation of Their Tribological Performance as Potential Additives in Oils. *J. Tribol.* **1999,** *123* (3), 441-443.

26. Rabaso, P.; Dassenoy, F.; Ville, F.; Diaby, M.; Vacher, B.; Le Mogne, T.; Belin, M.; Cavoret, J. An Investigation on the Reduced Ability of IF-MoS_2 Nanoparticles to Reduce Friction and Wear in the Presence of Dispersants. *Tribol. Lett.* **2014,** *55* (3), 503-516.

27. Sui, T.; Song, B.; Wen, Y.-h.; Zhang, F. Bifunctional hairy silica nanoparticles as high-performance additives for lubricant. *Sci. Rep.* **2016,** *6*, 22696.

28. López, T. D.-F.; González, A. F.; Del Reguero, Á.; Matos, M.; Díaz-García, M. E.; Badía-Laíño, R. Engineered silica nanoparticles as additives in lubricant oils. *Sci. Technol. Adv. Mater.* **2015,** *16* (5), 055005.

29. Yu, B.; Qian, L.; Yu, J.; Zhou, Z. Effects of Tail Group and Chain Length on the Tribological Behaviors of Self-Assembled Dual-Layer Films in Atmosphere and in Vacuum. *Tribol. Lett.* **2008,** *34* (1), 1.

30. Wright, R. A. E.; Wang, K.; Qu, J.; Zhao, B. Oil-Soluble Polymer Brush Grafted Nanoparticles as Effective Lubricant Additives for Friction and Wear Reduction. *Angew. Chem., Int. Ed.* **2016,** *55* (30), 8656-8660.

Chapter 2. Poly(alkyl methacrylate) Brush-Grafted Silica Nanoparticles as Oil Lubricant Additives: Effects of Alkyl Pendant Group on Oil Dispersibility, Stability, and Lubrication Property

Abstract

This chapter describes the synthesis of a series of poly(alkyl methacrylate) brush-grafted, 23 nm silica nanoparticles (hairy NPs) and the study of the effect of alkyl pendant length on their use as oil lubricant additives for friction and wear reduction. The hairy NPs were prepared by surface-initiated reversible addition-fragmentation chain transfer polymerization from trithiocarbonate chain transfer agent (CTA)-functionalized silica NPs in the presence of a free CTA. We found that hairy NPs with sufficiently long alkyl pendant groups (containing > 8 carbon atoms, such as 12, 13, and 16 in this study) could be readily dispersed in poly(alphaolefin) (PAO), forming clear, homogeneous dispersions, and exhibited excellent stability at low and high temperatures as revealed by visual inspection and dynamic light scattering studies. While poly(*n*-hexyl methacrylate) hairy NPs cannot be dispersed in PAO at ambient conditions or at 80 °C, interestingly, poly(2-ethylhexyl methacrylate) hairy NPs can be dispersed in PAO at 80 °C, but not at room temperature, with a reversible clear-to-cloudy transition observed upon cooling. High contact stress ball-on-flat reciprocating sliding tribological tests at 100 °C showed significant reductions in both coefficient of friction (up to 38%) and wear volume (up to 90% for iron flat) for transparent, homogeneous dispersions of hairy NPs in PAO at a concentration of 1.0 wt% compared with neat PAO. The formation of a load-bearing tribofilm at the rubbing interface was confirmed using scanning electron microscopy coupled with energy dispersive X-ray spectroscopy.

2.1. Introduction

Lubrication is vitally important for numerous mechanical systems,[1-4] with examples including pumps, gears, vehicles, trains, and aircrafts. Not only can lubricants extend the lifetime of individual components and entire systems, thus improving durability and reliability, but also boost energy conversion efficiency, an issue that has received widespread attention in recent years. As such, lubricants with increased performance are being continuously sought, and significant progress has been made in the past decades. For automotive engines, fully formulated lubricants contain a variety of additives such as antioxidants, detergents, anti-wear agents, friction reducers, and viscosity index improvers,[1] which have distinct functions during engine operation. Zinc dialkyldithiophosphates (ZDDPs) have been widely used as anti-wear additives[1-6] due to their low cost and relatively rapid formation of protective tribofilms at the rubbing interfaces.[5-8] However, the presence of significant levels of both sulfur and phosphorus are troublesome for exhaust treatment, and it has been reported that ZDDPs can poison catalysts in catalytic converters.[9] Consequently, a limit has been imposed by regulations on the amount of ZDDP that can be added into engine lubricants. Therefore, the pursuit of additives capable of partially or wholly replacing ZDDP has generated much interest,[10-12] and among many possible candidates, nanoparticles (NPs) have been suggested as a promising class.[12]

The use of NPs as additives is particularly intriguing because of their potential to exhibit desired interactions with surface asperities, as afforded by their small size, large surface area, tunability of surface chemistry, etc.[12-26] NP-additized lubricants, sometimes

dubbed “nanolubricants”,[12] have been demonstrated to impart relatively strong boundary films (i.e., tribofilms) formed from complex mechano-chemical reactions at rubbing interfaces involving NPs under harsh conditions of high local pressure and temperature.[12,13] Desired tribological properties have been observed for NPs based on metals as well as so-called inorganic fullerenes such as MoS_2.[14-19] Both types of NPs can effectively form protective layers at the material surfaces, typically through thermo-mechanically induced melting and delamination, respectively. Metal oxide NPs, including titanium, silicon, copper, and zinc oxides, have also been shown to exhibit anti-wear and anti-friction properties.[20-24] The application of NPs as lubricant additives, however, is almost always impeded in some way by their tendency towards aggregation in hydrocarbon solvents because of the high surface area associated with their small size, relatively high surface energy, and van der Waals attractive interactions. When aggregation occurs, the effective particle size increases, resulting in a rapid decrease in diffusion into contact areas and thus an increase in interfacial friction and material wear. Therefore, the colloidal stability of individually dispersed NPs is paramount for the effective utilization of essentially all nanolubricants. As such, nanolubricants are typically formulated with surfactants or are surface modified with appropriate organic compounds to stabilize the NP-oil interface.[12-26] Despite the progress that has been made, it remains a great challenge to achieve stable, homogeneous dispersions of NPs in base oils (e.g., polyalphaolefin (PAO)) that exhibit long-term colloidal stability in a temperature range from the extreme cold in winter (e.g., -20 °C) to typical engine operating conditions (~100 °C) and to realize the full potential of NPs as lubricant additives for friction and wear reduction.

Polymer brush-grafted NPs (i.e., hairy NPs) consists of a layer of polymer chains densely tethered at one end to the surface of core NPs.[27-30] These nanostructured hybrid NPs exhibit remarkable dispersibility and superior stability in good solvents because of the solvation forces from the favorable enthalpic interactions between the brushes and solvents and the entropic, steric repulsions between hairy NPs, which effectively prevent NPs from undergoing irreversible aggregation.[27-34] Our lab recently reported the synthesis of oil-soluble poly(lauryl methacrylate) (PLMA or PC12) brush-grafted 23.8 nm silica and 15 nm (nominal) titania NPs by surface-initiated atom transfer radical polymerization (SI-ATRP) and the use of these hairy NPs as lubricant additives for friction and wear reduction.[35] These hairy NPs can be readily dispersed in PAO base oil, forming transparent homogeneous dispersions that exhibited long-term stability at -20, ambient temperature, and 100 °C. Tribological analysis at 100 °C showed that addition of 1.0 wt% of PC12 hairy NPs with either silica or titania core led to significant reductions in friction (up to ~ 40%) and wear volume. At a 1.0 wt% concentration of hairy NPs, it was observed that friction reduction increased with decreasing brush molecular weight, which was attributed to the increased number of NPs in PAO.[35] In addition, our lab found that the coefficient of friction decreased with increasing hairy NP concentration from 0.25 to 1, 2 and 4 wt%, although the improvement was small when the concentration was above 2 wt%.

In this work, we focused on the effects of alkyl pendant group of poly(alkyl methacrylate) brushes on dispersibility, stability, and lubrication property of hairy NPs. A series of poly(alkyl methacrylate) brush-grafted, 23 nm silica NPs with various alkyl pendant lengths (Scheme 2.1) were synthesized by surface-initiated reversible addition-

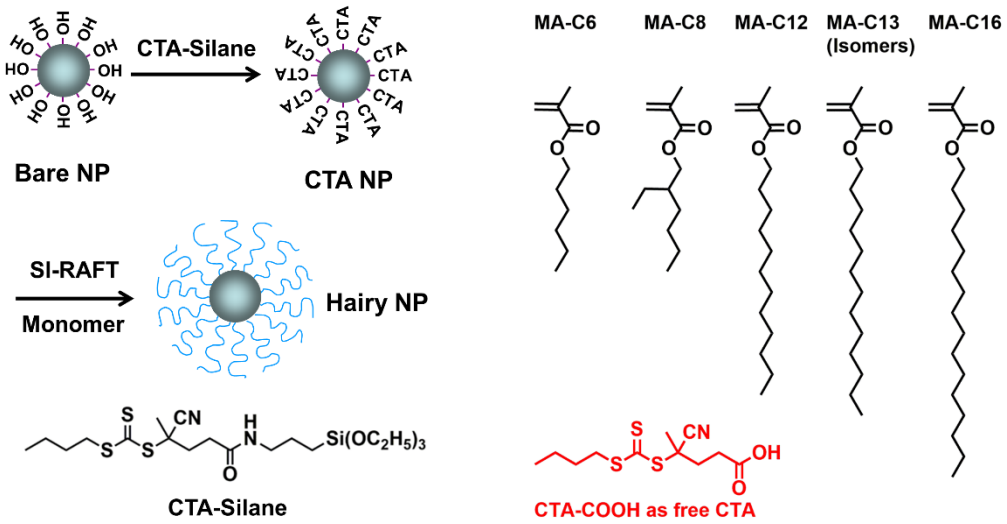

Scheme 2.1. Synthesis of Various Poly(alkyl methacrylate) Brush-Grafted, 23 nm Silica Nanoparticles by Surface-Initiated Reversible Addition-Fragmentation Chain Transfer (RAFT) Polymerization and Chemical Structures of Monomers and RAFT Chain Transfer Agents (CTAs).

fragmentation chain transfer (SI-RAFT)[36-42] polymerization from silica NPs surface functionalized with a chain transfer agent (CTA) in the presence of a free CTA. RAFT polymerization allows for the synthesis of well-defined polymers with desired molecular weights and relatively low dispersities.[43,44] We found that the alkyl pendant length must be longer than 8 carbon atoms for the hairy NPs to be easily dispersed in PAO at room temperature to form stable homogeneous systems. All readily dispersible hairy NPs showed significant friction and wear reductions when added into PAO at a concentration of 1.0 wt%. While the results reported here demonstrate the effectiveness of poly(alkyl methacrylate) brush-grafted silica NPs with sufficiently long alkyl pendants in particular as lubricant additives, we believe that this exploration of the effect of polymer's chemical composition on hairy NP's stability and lubrication performance will provide a guideline for design of polymer brush-grafted inorganic or metallic NPs as effective nanolubricants in general.

2.2. Experimental Section

2.2.1. Materials

Silica nanoparticles (NPs) with a size of 10–15 nm, according to the manufacturer, were obtained from Nissan Chemical as a dispersion in methyl isobutyl ketone (MIBK) at a concentration of 30-31 wt% SiO_2 (MIBK-ST). *n*-Hexyl methacrylate (MA-C6, 97%, TCI), 2-ethylhexyl methacrylate (MA-C8, >99.0 %, TCI), lauryl methacrylate (MA-C12, 97%, Acros), tridecyl methacrylate (MA-C13, mixture of branched-chain isomers, TCI), and hexadecyl methacrylate (MA-C16, Wake Chemicals USA) were passed through a

column of silica gel (bottom)/activated basic aluminum oxide (top) (2/1, v/v) to remove the inhibitor. Monomers were stored in a refrigerator prior to use. Toluene and THF were dried with sodium/benzophenone, distilled under a nitrogen atmosphere, and used immediately. 1-Butanethiol (98%, Acros), carbon disulfide (>99%, Fisher), 4,4'-azobis(4-cyanopentanoic acid) (98%, Alfa Aesar), iodine (pure, Acros), *N*,*N*′-dicyclohexylcarbodiimide (DCC, 99%, Acros), *N*-hydroxysuccinimide (NHS, >98%, Acros), and (3-aminopropyl)triethoxysilane (APTES, 99%, Acros) were used without further purification. Azobisisobutyronitrile (AIBN, 98%, Aldrich) was recrystallized from ethanol and dried under vacuum before use. The polyalphaolefin (PAO) used in this work was SpectraSyn^{TM} 4 PAO fluid obtained from ExxonMobil, with kinematic viscosities of 19.0 cSt and 4.1 cSt at 40 and 100 °C respectively. Its pour point was – 87 °C. All other chemical reagents were purchased from either Aldrich or Fisher and used without further purification.

2.2.2. Characterization

Size exclusion chromatography (SEC) of the free polymers formed in the synthesis poly(alkyl methacrylate) brush-grafted silica NPs was performed using a PL-GPC 20 (an integrated SEC system from Polymer Laboratories, Inc.) equipped with a refractive index detector, one PLgel 5 μm guard column (50 × 7.5 mm), and two PLgel 5 μm mixed-C columns (each 300 × 7.5 mm, linear range of molecular weight from 200 to 2 000 000 Da). THF was the mobile phase, and the flow rate for analysis was set at 1.0 mL/min. The SEC system was calibrated with polystyrene standards, and the data were processed using Cirrus GPC/SEC software (Polymer Laboratories, Inc.). ^{1}H and ^{13}C NMR spectra were recorded

on a Varian VNMRS 500 MHz spectrometer or Mercury 300 MHz, and the residual solvent proton signal was used as the internal reference. Thermogravimetric analysis (TGA) was carried out in N_2 at a heating rate of 20 °C/min from room temperature to 800 °C using TA Discovery TGA-MS or TA Q-series Q50. Scanning transmission electron microscopy (STEM) was performed using a Zeiss Auriga equipped with a scanning transmission electron detector at an accelerating voltage of 30 keV. The STEM samples of poly(alkyl methacrylate) brush-grafted silica NPs were prepared by drop-casting their THF dispersions with a concentration of 2 mg/mL onto carbon-coated, copper TEM grids. Scanning electron microscopy and energy dispersive x-ray spectroscopy (SEM-EDS) analysis of the wear track was performed using a Zeiss EVO MA15, equipped with an XFlash 6|30 silicon drift detector. An accelerating voltage of 20 kV was used, and topographic images were obtained using a secondary electron detector. The high-resolution mass spectroscopy (HRMS) experiment was performed using a JEOL Model JMS-T100LC (AccuTOF) orthogonal time-of-flight (TOF) mass spectrometer (Peabody, MA) with an IonSense (Danvers, MA) DART source. The HRMS sample of CTA-Silane was prepared in methanol with a concentration of 4.3 mg/g.

2.2.3. Synthesis of 4-(((Butylthio)carbonothioyl)thio)-4-cyanopentanoic Acid (CTA-COOH)

CTA-COOH was synthesized according to a literature procedure with slight modifications (1-butanethiol was used instead of 1-dodecanethiol).[44] Sodium hydride (5.858 g of 60% dispersion in mineral oil, corresponding to 3.515 g of NaH, 146.5 mmol) was added into a 250 mL 3-necked flask that contained diethyl ether (100 mL) under a

nitrogen atmosphere, followed by gradual addition of *n*-butanethiol (12.665 g, 140.44 mmol) through an addition funnel. Carbon disulfide (11.162 g, 146.60 mmol) was then added dropwise, and a yellow precipitate appeared. After the reaction proceeded at room temperature for 1 h, the solid precipitate was collected by vacuum filtration and re-suspended in diethyl ether (100 mL) in a 250 mL 3-necked flask. Solid iodine (15.653 g, 61.675 mmol) was then added piecewise into the flask, and the mixture was stirred at room temperature overnight. The solid was removed by filtration, and the dark brown filtrate was washed three times with a saturated, aqueous sodium thiosulfate solution, with no color observed in the aqueous layer upon the final wash. The organic layer was further washed once with water, collected, and dried over anhydrous sodium sulfate. The volatiles were removed using a rotary evaporator, yielding a dark, red-orange oil, which was further dried under high vacuum.

The obtained bis(*n*-butylsulfanylthiocarbonyl) disulfide (5.146 g, 15.56 mmol), 4,4-azobis(4-cyanovaleric acid) (5.440 g, 19.41 mmol), and ethyl acetate (100 mL) were added into a 250 mL 3-necked flask. The mixture was stirred under a nitrogen atmosphere to form a homogeneous solution. The flask was then placed in an oil bath and refluxed at 75 °C overnight, and then the solvent was removed by a rotary evaporator. The crude product was purified by silica gel column chromatography using a mixture of hexanes and ethyl acetate (3 : 2, v/v). An orange oil was obtained after drying under high vacuum (4.051 g, 89.3%). ^{1}H NMR δ (ppm, $CDCl_3$): 3.34 (t, $CH_3CH_2CH_2CH_2S$-, 2H), 2.69-2.67 (m, -CCH_2CH_2CO-, 2H), 2.57-2.36 (m, -CCH_2CH_2CO- ,2H) 1.88 (s, -CH_3, 3H), 1.71-1.65 (m,

$CH_3CH_2CH_2CH_2S$-, 2H), 1.47-1.39 (m, $CH_3CH_2CH_2CH_2S$-, 2H), 0.92 (t, $CH_3CH_2CH_2CH_2S$-, 3H).

2.2.4. Synthesis of *n*-Butyl (2-Cyano-5-oxo-5-((3-(triethoxysilyl)propyl)amino) pentan-2-yl) carbonotrithioate (CTA-Silane)

4-(((Butylthio)carbonothioyl)thio)-4-cyanopentanoic acid (CTA-COOH, 4.051 g, 13.90 mmol) was dissolved in dichloromethane (40 mL) in a 250 mL three-necked flask, followed by the addition of *N*-hydroxysuccinimide (NHS, 2.472 g, 21.49 mmol). The reaction vessel was placed in an ice/water bath, and the mixture was stirred with a magnetic stir bar under an N_2 atmosphere. *N*,*N*′-Dicyclohexylcarbodiimide (DCC, 3.953 g, 19.16 mmol) was dissolved in dichloromethane (40 mL), and the solution was added dropwise into the flask via an addition funnel. After the reaction mixture was stirred at room temperature overnight, the solid was removed by gravity filtration. The filtrate was concentrated using a rotary evaporator and then dissolved in dichloromethane (100 mL). (3-Aminopropyl)triethoxysilane (APTES, 3.002 g, 13.56 mmol), dissolved in dichloromethane (10 mL), was added dropwise to the solution; the reaction mixture was stirred at room temperature overnight, with little to no discoloration being observed. The white precipitate present in the reaction mixture was removed by filtration, and the solution was then concentrated by using a rotary evaporator. The product was purified by silica gel column chromatography, initially using pure hexane as eluent and slowly transitioning to a mixture of hexane and ethyl acetate (1 : 1, v/v), yielding an orange viscous liquid (2.537 g, 36.9 %). ^{1}H NMR δ (ppm, $CDCl_3$): 5.93 (br s, -N*H*, 1H), 3.84-3.80 (m, -O(CH_2CH_3)$_3$, 6H), 3.33 (t, $CH_3CH_2CH_2CH_2S$-, 2H), 3.26-3.24 (m, -NH$CH_2CH_2CH_2Si$-, 2H), 2.54-2.32

(m, -CC*H*$_2$C*H*$_2$CO-, 4H), 1.88 (s, -C(CN)C*H*$_3$, 3H), 1.69-1.63 (m, CH$_3$CH$_2$C*H*$_2$CH$_2$S- and -NHCH$_2$C*H*$_2$CH$_2$Si-, 4H), 1.46-1.39 (m, CH$_3$C*H*$_2$CH$_2$CH$_2$S-, 2H), 1.23 (t, -O(CH$_2$C*H*$_3$)$_3$, 9H), 0.93 (t, C*H*$_3$CH$_2$CH$_2$CH$_2$S-, 3H), 0.63 (t, -NHCH$_2$CH$_2$C*H*$_2$Si-, 2H). ^{13}C NMR δ (ppm, CDCl$_3$): 217.23 (-S(*C*=S)S-), 170.05 (-CH$_2$(*C*O)NH-), 119.21 (-*C*N), 58.50 (-O(*C*H$_2$CH$_3$)$_3$), 46.72 (-NH*C*H$_2$CH$_2$CH$_2$Si-), 41.98 (-S*C*(CH$_3$)(CN)CH$_2$-), 36.70 (CH$_3$CH$_2$CH$_2$*C*H$_2$S-), 34.54 (-*C*H$_2$CH$_2$CO-), 31.87 (CH$_3$CH$_2$*C*H$_2$CH$_2$S-), 29.71 (-CH$_2$*C*H$_2$CONH-), 25.00 (-CH$_2$*C*H$_2$CH$_2$Si-), 22.74 (CH$_3$*C*H$_2$CH$_2$CH$_2$S-), 22.06 (-SC(*C*H$_3$)(CN)CH$_2$-), 18.29 (-Si(OCH$_2$*C*H$_3$)$_3$), 13.55 (*C*H$_3$CH$_2$CH$_2$CH$_2$S-), 7.80 (-CH$_2$CH$_2$*C*H$_2$Si-). HRMS (DART-TOF): m/z calc C$_{20}$H$_{38}$N$_2$O$_4$S$_3$Si [M+H]$^+$: 495.18412; found: 495.18252; mass error: 3.23 ppm.

2.2.5. Synthesis of CTA-Functionalized Silica NPs (CTA-NPs)

Three batches of CTA-NPs used in the present work denoted as CTA-NPs-B1, -B2, and -B3, were prepared by similar procedures. The following is the description for the preparation of CTA-NPs-B3. MIBK-ST (3.348 g of dispersion with a concentration of 30 wt%, corresponding to 1.004 g of bare SiO_2 NPs) was weighed into a 100 mL three-necked flask and diluted with anhydrous THF (50 mL), followed by slow addition of CTA-Silane (0.995 g, 2.009 mmol) through an addition funnel. The reaction mixture was stirred with a magnetic stir bar and refluxed in a 75 °C thermostated oil bath. The reaction was carried out for two days, after which the mixture changed from yellow to dark orange but remained transparent. The CTA NPs were isolated by ultracentrifugation (Beckman Optima L-90K Ultracentrifuge with type 60 Ti rotor, 35000 rpm, 60 min, 4°C), re-dispersed in THF, and separated by ultracentrifugation again. This dispersion-ultracentrifugation washing cycle

was repeated for a total of four times. The purified CTA-NPs-B3 (0.805 g), a dark orange solid, was dispersed in THF and stored as a dispersion with a concentration of 64.1 mg/g in the fridge.

2.2.6. Synthesis of Poly(Alkyl Methacrylate) Brush-Grafted Silica NPs

Poly(alkyl methacrylate) brush-grafted silica NPs (hairy NPs) were synthesized by surface-initiated reversible addition-fragmentation chain transfer (SI-RAFT) polymerization from CTA-NPs. Described below is the synthesis of poly(tridecyl methacrylate) (PC13) brush-grafted silica NPs, denoted as PC13-NP3-7.2k, where PC13 is the grafted polymer, NP3 refers to hairy NPs made from CTA-NPs-B3, and 7.2k is the $M_{n,SEC}$ of the corresponding free polymer. Other hairy NPs were prepared following a similar procedure and named using the same method. Tridecyl methacrylate (MA-C13, mixture of branched-chain isomers, 0.901 g, 3.356 mmol), CTA-COOH (30.2 mg, 0.104 mmol), AIBN (2.578 mg, 0.0157 mmol, from 0.188 g of a stock solution in THF with a concentration of 13.7 mg/g), and a dispersion of CTA-NPs-B3 in THF with a concentration of 64.1 mg/g (3.126 g, corresponding to 200.4 mg of CTA-NPs) were added into a 25 mL two-necked flask, followed by the addition of *N*,*N*-dimethylformamide (DMF, 0.0632 g) used as internal standard. After the reaction mixture was degassed by three freeze–pump–thaw cycles, the flask was placed in an oil bath with a preset temperature of 70 °C. After 18 h, the polymerization was stopped by removing the flask from the oil bath, exposing the reaction mixture to air, and diluting with THF (5 mL). The final monomer conversion was found to be 97.6%, as determined by ^{1}H NMR spectroscopy analysis by comparing the average of the vinyl peaks at 6.08 and 5.52 ppm against the peak at 2.87 ppm from internal

standard DMF for initial 0 min and final sample. The DP was 25, calculated using the monomer conversion and the molar ratio of monomer MA-C13 to the sum of free and grafted CTA as detailed in a publication from our lab[45] and also in the appendix (A.1. Calculation of Degree of Polymerization and Grafting Density of PC13 Brushes in PC13-NP3-7.2k). The PC13 brush-grafted silica NPs (i.e., PC13-NP3-7.2k) were separated by ultracentrifugation (35000 RPM, 60 min, 4°C), re-dispersed in THF, and centrifuged again. This purification cycle was repeated for a total of five times. The hairy NPs were dispersed in THF and stored as a dispersion with a concentration of 19.0 mg/g. The supernatant liquid from the first centrifuge cycle was precipitated in methanol to isolate the free polymer PC13, which was further purified by dissolving in THF and precipitating in methanol again. SEC analysis of the purified free homopolymer PC13 showed that the $M_{n,SEC}$ value was 7.2 kDa with a Đ of 1.16 relative to polystyrene standards.

2.2.7. Preparation and Stability Study of 1.0 wt% Dispersions of Poly(Alkyl Methacrylate) Brush-Grafted Silica NPs in PAO

The following is the preparation of a 1.0 wt% dispersion of PC13-NP1-9.7k in PAO. Other samples were prepared using a similar procedure. PAO (7.451 g) was weighed in a 20 mL scintillation vial followed by the addition of a dispersion of PC13-NP1-9.7k in THF with a concentration of 19.0 mg/g (3.896 g, corresponding to 74.0 mg of hairy NPs). The resultant mixture was ultrasonicated using Fisher Scientific FS6 for 5 min until a homogeneous dispersion was achieved. THF was initially removed by a gentle stream of nitrogen, and the dispersion was further dried under high vacuum to ensure that THF was completely removed.

To test the stability of the dispersions of hairy NPs in PAO, aliquots of each sample were quiescently stored in a freezer (–15 °C), at ambient condition (18 °C), and in a 100 °C oil bath, with digital photographs being taken periodically to record the state of the hairy NP dispersions. While PC12-NP1-9.5k, PC13-NP1-9.7k, PC13-NP3-7.2k, and PC16-NP2-8.3k formed clear and stable dispersions in PAO (Figure A1), the 1.0 wt% suspensions of PC6-NP1-7.0k and PC8-NP1-7.8k in PAO were found to be cloudy and unstable at room temperature. Interestingly, the PAO dispersion of PC8-NP1-7.8k became clear and homogeneous at elevated temperatures, while the dispersion of PC6-NP1-7.0k showed no visible change upon heating but stayed cloudy. The clear PAO dispersion of PC8 brush-grafted silica NPs with a concentration of 1.0 wt% was cooled from an elevated temperature at an interval of 1 °C in an Isotemp (Fisher Scientific) and equilibrated at each temperature for 5 min. The temperature at which a dispersion turned cloudy was recorded as cloud point.

Dynamic light scattering (DLS) measurements were performed to further study the stability of PC13-NP1-9.7k in PAO using a Malvern Zetasizer Nano ZS instrument equipped with a He-Ne 633 nm laser and a temperature controller at a scattering angle of 173°. Three 1.0 wt% dispersions of PC13-NP1-9.7k in PAO were prepared and kept at –15 °C, ambient temperature (18 °C), and 100 °C, respectively, for 60 days. Aliquots were removed and diluted with pure PAO to a concentration of 0.1 mg/g, and the hydrodynamic sizes of hairy NPs were measured at 23 °C by DLS. The viscosity of PAO at 23 °C, 27.6 cP, was calculated from the kinematic viscosity (34.5 cSt) from the literature and its density at 23 °C (0.80 g/mL).[10]

2.2.8. Tribological Testing

To investigate the effect of polymer brush composition on the tribological properties of hairy silica NPs in PAO, high contact stress, ball-on-flat tests were performed using a Phoenix Tribology Plint TE 77 tribo-tester. In each test, an AISI 52100 steel ball was reciprocally slid against a stationary CL35 cast iron flat, both of which were submerged in the lubricant. A sliding stroke of 10 mm and an oscillation frequency of 10 Hz were used. The tribological tests were conducted at 100 °C for a total sliding distance of 1000 m under a point contact load of 100 N. The friction force was measured in situ by a piezoelectric load cell and the friction coefficient was calculated through normalization by the load. For each hairy NP lubricant sample, at least two runs were conducted and the average was used. After testing, the iron flat and steel ball, as well as their respective wear scars, were cleaned thoroughly with acetone and isopropanol for wear measurements and SEM/EDS characterization. Material wear volumes of the resultant testing scars on both the iron flat and steel ball were measured using optical surface profilometry (Wyko NT9100).

When characterizing the tribological properties of PC6-NP1-7.0kDa and PC8-NP1-7.8kDa in PAO, 1.0 wt% dispersions of these two NP samples were heated to 80 °C and stirred for 30 min prior to loading onto the iron flat that had been preheated to 100 °C. In the case of PC8-NP1-7.8k-additized PAO, the applied dispersion was transparent and homogeneous, whereas the PC6-NP1-7.0k-additized PAO remained cloudy at the elevated temperature. The lubricant was then allowed to thermally equilibrate for 10 min before tribological testing was carried out. To investigate the effect of the inherent instability of these hairy particles, PC6-NP1-7.0k- and PC8-NP1-7.8k-additized PAO lubricants were

subjected to a quiescent period of seven days at room temperature, during which the NPs appeared to have finished settling out of the PAO. In both cases, oil was removed from the top, NP-poor portion of the dispersion and applied directly to the iron flat at ambient temperature prior to tribological testing.

2.2.9. Removal of RAFT CTA Chain End Group of PC13-NP3-7.2k by Treatment with AIBN

PC13-NP3-7.2k (73.3 mg) was dispersed in toluene (1.020 g) in a 25 mL two-necked flask via ultrasonication (Fisher Scientific FS6) to form a clear, homogeneous dispersion. After AIBN (21.0 mg, 0.128 mmol) was added into the flask, the mixture was degassed by three freeze-pump-thaw cycles. The reaction mixture was then heated to 80 °C in an oil bath and stirred overnight to ensure complete chain-end saturation. The mixture was then diluted with THF. The hairy NPs were isolated by ultracentrifugation (Beckman Optima L-90K Ultracentrifuge with type 60 Ti rotor, 35000 RPM, 60 min, 4 °C), redispersed in THF, and centrifuged again. This purification cycle was repeated for a total of three times. The AIBN-treated hairy NPs were isolated, dried under vacuum to yield a sticky, white solid (PC13-NP3-7.2k-AIBN, 59.6 mg), and characterized by TGA and ^{1}H NMR spectroscopy analysis for comparison with PC13-NP3-7.2k.

To confirm the removal of RAFT CTA trithiocarbonate end groups of hairy NPs by treatment with AIBN at 80 °C, a similar reaction using the free PC13 homopolymer with a $M_{n,SEC}$ of 7.2 kDa and a DP of 25 (135 mg, 0.0219 mmol) was carried out with AIBN (55 mg, 0.33 mmol) and toluene (3.013 g) at 80 °C for 4 h. The polymer was then purified by precipitation in methanol three times, dried under high vacuum, and analyzed by ^{1}H NMR

spectroscopy. The trithiocarbonate end groups were completely removed for both hairy NPs PC13-NP3-7.2k and free polymer PC13 as evidenced by the disappearance of the peak at 3.23 ppm (-S(C=S)SCH_2CH$_2$CH$_2$CH$_3$) (see Figure A2). A color change of the polymer and hairy NPs from yellow to white after AIBN treatment was also observed.

2.2.10. Synthesis of Free Polymer Poly(tridecyl methacrylate) with a $M_{n,SEC}$ of 20.8 k (PC13-20.8k) by ATRP

Copper(I) bromide (13.0 mg, 0.0906 mmol) and copper(II) bromide (4.1 mg, 0.018 mmol) were added to a 25 mL two-necked flask alongside ethyl 2-bromoisobutyrate (EBiB, 5.1 mg, 0.026 mmol) and tridecyl methacrylate (MA-C13, 0.946 g, 3.52 mmol). *N*,*N*,*N*′,*N*′′,*N*′′-Pentamethyldiethylenetriamine (PMDETA, 20.0 mg, 0.115 mmol) was added to the mixture immediately before freezing and degassing by three freeze–pump–thaw cycles. The polymerization was carried out at 55 °C for 135 min, achieving a monomer conversion of 53.5 % before being halted by exposure to air and dilution in THF. The degree of polymerization (DP) was calculated to be 72, and $M_{n,SEC}$ of 20.8 kDa and a Đ of 1.15 (Figure A3) as determined by SEC analysis.

2.3. Results and Discussion

2.3.1. Synthesis of RAFT CTA-Functionalized 23 nm Silica NPs

To study the effect of alkyl pendant length on oil dispersibility, stability, and lubrication property of poly(alkyl methacrylate) brush-grafted NPs as engine lubricant additives, SI-RAFT polymerization was chosen to grow poly(alkyl methacrylate) brushes from silica NPs because RAFT allows for readily achieving high monomer conversions and obtaining

desired degrees of polymerization (DPs) while maintaining relatively low dispersities. To this end, a triethoxysilane-functionalized chain transfer agent (CTA), CTA-Silane, was designed and synthesized (Scheme 2.2); we used *n*-butyl instead of the more popular *n*-dodecyl as the Z group in order to avoid possible steric hindrance during the RAFT chain transfer process on the surface of silica NPs. 4-(((Butylthio)carbonothioyl)thio)-4-cyanopentanoic acid (CTA-COOH) was prepared using a procedure adapted from the literature.[44] Briefly, sodium *n*-butyl trithiocarbonate was synthesized from sodium 1-butanethiolate and carbon disulfide, followed by oxidization with iodine to yield bis(*n*-butylsulfanylthiocarbonyl) disulfide. CTA-COOH was obtained by reaction of the disulfide with 4,4′-azobis(4-cyanovaleric acid) in ethyl acetate at 80 °C and purified by silica gel column chromatography. To mitigate possible aminolysis of the trithiocarbonate moiety of CTA-COOH in the reaction with (3-aminopropyl)triethoxysilane (APTES), *N*-hydroxysuccinimide (NHS) was used to activate the carboxylic acid of CTA-COOH in the presence of *N*,*N*′-dicyclohexylcarbodiimide in dichloromethane. The triethoxysilane group was then introduced onto the CTA by slow addition of APTES to the solution of NHS ester; the characteristic yellow color of the CTA remained strong throughout the reaction. The final product, CTA-Silane, was purified by column chromatography and obtained as an orange viscous liquid. The molecular structure of CTA-Silane was confirmed by ^{1}H and ^{13}C NMR spectroscopy as well as high-resolution mass spectrometry. Figure 2.1A shows its ^{1}H NMR spectrum in $CDCl_3$ with peak assignments. The integrals of the peaks were in agreement with the molecular structure.

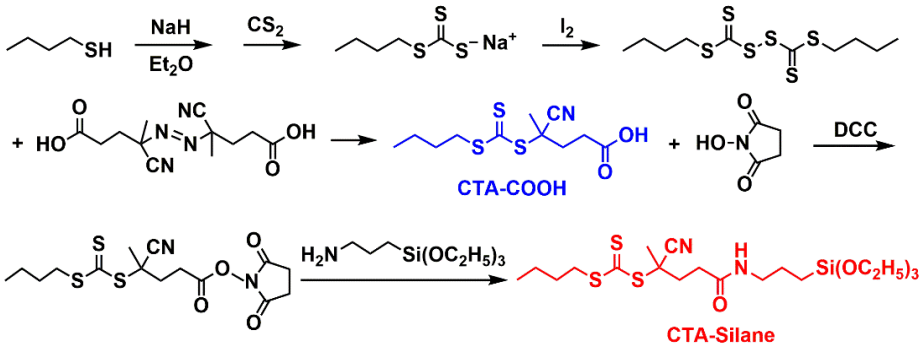

Scheme 2.2. Synthesis of Triethoxysilane-Functionalized Trithiocarbonate CTA (CTA-Silane).

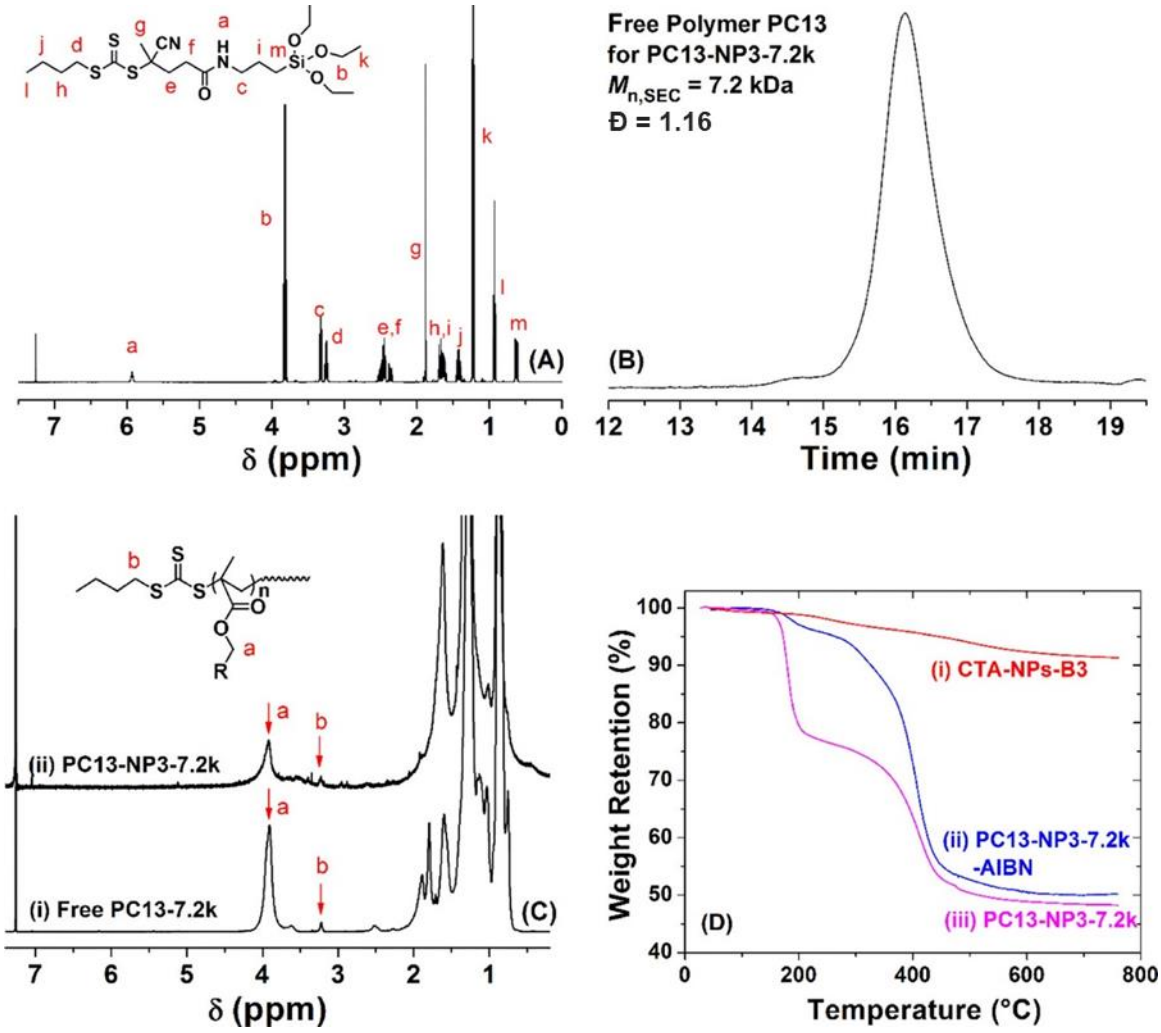

Figure 2.1. (A) ^{1}H NMR spectrum of CTA-Silane in $CDCl_3$. (B) SEC trace of free polymer with a $M_{n,SEC}$ of 7.2k (PC13-7.2k) formed from free CTA, CTA-COOH, in the synthesis of PC13-NP3-7.2k. (C) ^{1}H NMR spectra of free polymer PC13-7.2k and PC13-NP3-7.2k hairy NPs in $CDCl_3$. (D) Thermogravimetric analysis (TGA) of (i) CTA-NPs-B3, (ii) PC13-NP3-7.2k after treatment with AIBN, and (iii) PC13-NP3-7.2k. The TGA was carried out in N_2 at a heating rate of 20 °C/min.

CTA-Silane was then immobilized onto the surface of bare silica NPs. The dispersion of silica NPs in methyl isobutyl ketone (MIBK) with a concentration of 30% (MIBK-ST from Nissan Chemical) was first diluted with anhydrous THF, followed by the addition of CTA-Silane at a mass ratio of 1 : 1 with respect to bare silica NPs. The surface functionalization reaction was carried out at 75 °C in a nitrogen atmosphere under stirring conditions for two days. The trithiocarbonate CTA-functionalized silica NPs (CTA-NPs) were isolated and purified by multiple rounds of ultracentrifugation/re-dispersion in THF. The obtained CTA-NPs, distinctly orange in color, were stored as a dispersion in THF. Three batches of CTA-NPs were made from the same bottle of MIBK-ST using similar procedures and denoted as CTA-NPs-B1, -B2, and -B3. These CTA-NPs were used to make various poly(alkyl methacrylate) brush-grafted silica NPs, and scanning transmission electron microscopy (STEM) analysis of hairy NPs yielded an average size of 23 nm for core silica NPs.

2.3.2. Synthesis of Poly(alkyl methacrylate) Brushes with Various Alkyl Pendant Groups on Silica NPs by SI-RAFT

Five methacrylate monomers with various alkyl pendant groups (MA-C6, -C8, -C12, -C13, and -C16 in Scheme 2.1) were selected for a systematic study of the effects of alkyl pendant length on the dispersibility and stability of poly(alkyl methacrylate) brush-grafted NPs in PAO and the tribological property of hairy NPs as lubricant additives for friction and wear reduction. The surface-initiated RAFT polymerizations of alkyl methacrylates from CTA-NPs were carried out at 70 °C using azobisisobutyronitrile (AIBN) as an initiator. A suitable amount of CTA-COOH was added to the polymerization mixture as

free CTA to achieve better control of surface-initiated RAFT polymerization and to facilitate the characterization of the grafted polymer chains through the generation of a corresponding analogous free polymer. It has been well established that the molecular weights and molecular weight distributions of polymer brushes grafted on NPs synthesized by surface-initiated "living"/controlled radical polymerization are essentially identical to those of the corresponding free polymer formed from the free initiator/CTA.[32-34,42,45,46] After the polymerization proceeded overnight (≥ 18 h), a high monomer conversion, in the range of 92.1 to 98.5 %, was achieved. The reaction was then halted by exposure to air and diluted with THF, and the hairy NPs were separated from the free polymer and purified by multiple cycles of ultracentrifugation/redispersion in THF. The obtained hairy NPs appeared yellow, indicating the retention of the trithiocarbonate end group. The DP of the polymer was calculated from the final monomer conversion and the molar ratio of the monomer to the sum of free and surface CTA, as detailed in Appendix A for one sample.

A total of 6 hairy silica NP samples with comparable DPs (~ 30, varying from 25 to 38) were synthesized, one sample each of MA-C6, -C8, -C12, -C16 and two samples from MA-C13. The hairy NP samples were named by the following method using poly(tridecyl methacrylate) or poly(MA-C13) (PC13) brush-grafted silica NPs with a $M_{n,SEC}$ of 7.2k synthesized from CTA-NPs-B3 as an example. This sample was denoted as PC13-NP3-7.2k, where PC13 is the grafted polymer, NP3 refers to CTA-NPs-B3 used to make hairy NPs, and 7.2k is the $M_{n,SEC}$ of the corresponding free polymer. Size exclusion chromatography (SEC) analysis confirmed that all of the polymerizations were controlled as indicated by the unimodal SEC peaks with narrow dispersities (≤ 1.25) relative to PS

standards. Figure 2.1B shows the SEC trace of the free polymer PC13 formed from CTA-COOH in the synthesis of PC13-NP3-7.2k; other SEC curves can be found in Appendix A (Figures A4-A8). The grafted polymer chains on silica NPs can be "seen" from the ^{1}H NMR spectra of hairy NPs in $CDCl_3$, a good solvent for the free polymers, as shown in Figure 2.1C for PC13-NP3-7.2k and the corresponding free polymer PC13. The peak located at 3.92 ppm, which was from the –COOC*H*$_2$- of PC13, appears in the ^{1}H NMR spectra of both hairy NPs and free polymer PC13; interestingly, the peak from the RAFT CTA end group $CH_3(CH_2)_2CH_2S(C=S)S$- can also be clearly seen at 3.23 ppm. All these suggest that the grafted polymer on the NPs possess a high degree of freedom or mobility in a good solvent, which is crucial for the dispersibility and stability in PAO.

Thermogravimetric analysis (TGA) was employed to characterize the polymer content in each hairy NP sample. For all six hairy NP samples, there was a large drop in weight retention at 800 °C compared with CTA-NPs (Figure 2.1D shows the TGA of PC13-NP3-7.2k); a closer inspection showed that, for hairy NPs with DPs of 25 to 38, the weight retention at 800 °C was around 50%, ranging from 44.2 to 51.6% (see Appendix A Figures A4-A8), except the sample made from MA-C16 (PC16-NP2-8.3k) that had a slightly higher weight retention of 62.3%. A noticeable feature seen in the TGA thermograms of these hairy NPs is the pronounced two-step decomposition, with the first one occurring at ~ 180 °C. Since this was not observed in PC12 brush-grafted silica NPs synthesized by SI-ATRP[35], we suspected that the first fast weight loss was caused by the thermolysis of the trithiocarbonate end group, which generated free radicals triggering the decomposition of polymer chains. The trithiocarbonate end group can be observed both visually, as the

samples display a characteristic yellow color, and by ^{1}H NMR spectroscopy, as shown in Figure 2.1C for both free PC13-7.2k and PC13-NP3-7.2k. To test this hypothesis, we treated PC13-NP3-7.2k with a large excess of AIBN at 80 °C overnight to remove the trithiocarbonate end group,[47,48] and ^{1}H NMR spectroscopy analysis showed that the peak at 3.23 ppm in Figure 2.1C from $CH_3(CH_2)_2CH_2S(C=S)S$- disappeared (see Appendix A Figure A2). The characteristic yellow color of hairy NPs disappeared and the NPs appeared white. A control experiment using free polymer PC13 revealed that 4 h is sufficient to completely remove the trithiocarbonate end group. As shown in Figure 2.1D, the AIBN-treated, white PC13-NP3-7.2k exhibited a normal, one-step decomposition curve. We note here that a similar but less pronounced phenomenon was also reported for the polymers containing a trithiocarbonate end group in the TGA analysis.[49]

To visualize poly(alkyl methacrylate) brush-grafted silica NPs, hairy NPs were cast onto carbon-coated TEM grids from their dispersions in THF, a good solvent for all poly(alkyl methacrylate) polymers studied here, with a concentration of 2 mg/mL and characterized by STEM. As shown in Figure 2.2, hairy silica NPs self-assembled to some degree into a close-packed pattern in accordance with the presence of grafted polymer chains. By using DP, TGA data, and the size of silica NPs (23 nm) determined from STEM micrographs in Figure 2.2, we calculated the grafting density of polymer brushes for each sample. The results are summarized in Table 2.1 along with other characterization data. For hairy NP samples synthesized from the same batch of CTA-NPs, there appears a general trend that the grafting density is lower for the polymer brushes with a larger alkyl pendant group, which is likely due to the increased steric hindrance.

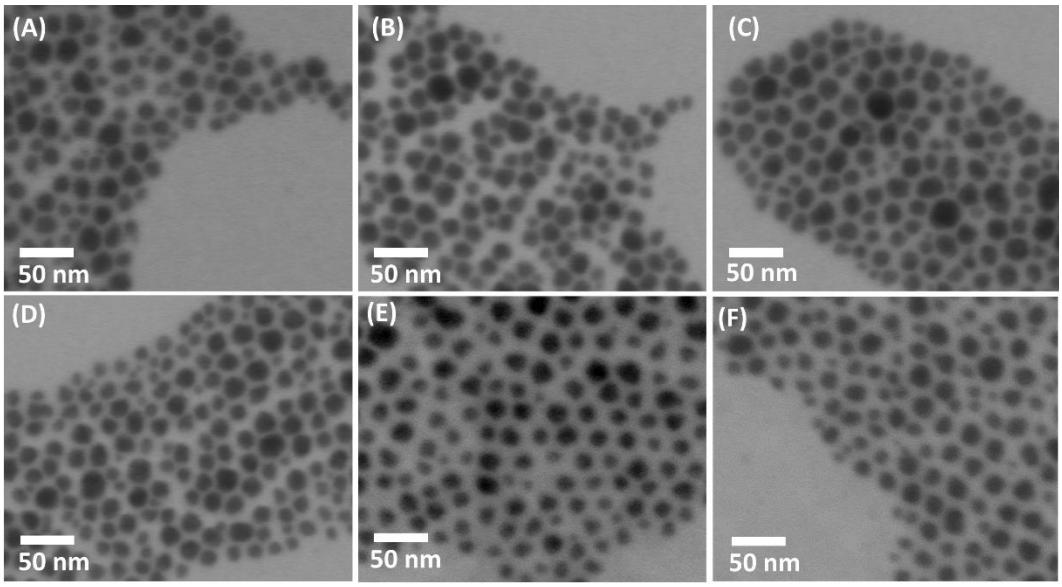

Figure 2.2. Bright field scanning transmission electron microscopy (STEM) micrographs of (A) PC6-NP1-7.0k, (B) PC8-NP1-7.8k, (C) PC12-NP1-9.5k, (D) PC13-NP1-9.7k, (E) PC13-NP3-7.2k, and (F) PC16-NP2-8.3k cast onto carbon-coated, copper TEM grids from 2 mg/mL dispersions of hairy silica NPs in THF.

Table 2.1. Characterization Data for Hairy Silica NPs and Corresponding Free Polymers

Hairy NPs	CTA-NPs [a]	Monomer [a]	$M_{n,SEC}$ [b] (kDa)	Đ [b]	DP [c]	σ [d] (chains/nm^2)
PC6-NP1-7.0k	CTA-NPs-B1	MA-C6	7.0	1.25	32	0.72
PC8-NP1-7.8k	CTA-NPs-B1	MA-C8	7.8	1.23	38	0.57
PC12-NP1-9.5k	CTA-NPs-B1	MA-C12	9.5	1.24	29	0.52
PC13-NP1-9.7k	CTA-NPs-B1	MA-C13	9.7	1.20	32	0.62
PC13-NP3-7.2k	CTA-NPs-B3	MA-C13	7.2	1.16	25	0.69
PC16-NP2-8.3k	CTA-NPs-B2	MA-C16	8.3	1.14	27	0.28

[a] The batch of CTA-NPs used for the preparation of respective hairy NP sample. [b] Number average molecular weight ($M_{n,SEC}$) and dispersity (Đ) of the corresponding free polymer were determined by size exclusion chromatography (SEC) relative to polystyrene standards using THF as solvent. [c] Degree of polymerization (DP) was calculated from the monomer conversion and the molar ratio of monomer to the sum of free CTA and surface-grafted CTA. [d] Grafting density (σ) was calculated using the size of silica NPs (23 nm), DP, and TGA data.

2.3.3. Effect of Alkyl Pendant Group of Poly(alkyl methacrylate) on Dispersibility and Stability of Hairy Silica NPs in PAO

To study the dispersibility and stability of the obtained hairy silica NPs in PAO base oil, 1.0 wt% dispersions in PAO were prepared by the following procedure. A dispersion of a hairy NP sample in THF was diluted with PAO and ultrasonicated to ensure complete mixing, after which THF was removed using a gentle stream of nitrogen followed by high vacuum. All hairy NPs, except PC6- and PC8-grafted silica NPs, were found to be fully dispersed in PAO at room temperature, forming homogeneous, transparent dispersions (Figure 2.3A and Figure A1 in Appendix A). It should be noted here that the use of THF to prepare 1.0 wt% dispersions of hairy NPs in PAO is convenient but not necessarily required as the readily dispersible hairy NPs could be dispersed directly in PAO by ultrasonication or vortex mixing. We also note here that the unmodified silica NPs from MIBK-ST are not stable in the base oil and precipitation occurs at ambient conditions.

To examine the colloidal stability of hairy NPs in PAO, 1.0 wt% dispersions of PC13-NP1-9.7k in PAO were concurrently stored at -15 °C, ambient conditions (18 °C), and 100 °C. All three samples remained clear and homogeneous after 60 days, as shown in Figure 2.3A, and no visible changes were observed. Dynamic light scattering (DLS) was carried out at 23 °C to measure the size distribution of hairy NPs in these three dispersions and compare them to a freshly prepared dispersion of PC13-NP1-9.7k in PAO. The DLS samples were prepared by diluting the original dispersions with neat PAO to a concentration of 0.1 mg/mL. The intensity-weighted hydrodynamic size was 56.2 nm for the freshly prepared sample. This value was essentially unchanged for the samples stored

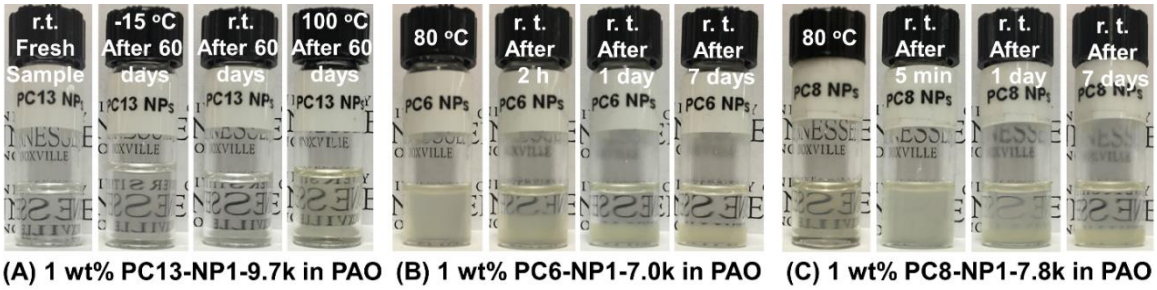

Figure 2.3. Optical photos of (A) a freshly prepared 1.0 wt% dispersion and three 1.0 wt% dispersions of PC13-NP1-9.7k in PAO after storage for 60 days at -15 °C, room temperature (r.t.), and 100 °C; (B) a 1.0 wt% dispersion of PC6-NP1-7.0k in PAO at 80 °C and sitting at r.t. for 2 h, 24 h, and 7 days after removal from a 80 °C oil bath; (C) a 1.0 wt% dispersion of PC8-NP1-7.8k in PAO at 80 °C and sitting at r.t. for 5 min, 1 day, and 7 days after removal from a 80 °C oil bath.

at -15, 18, and 100 °C for 60 days, with an average size of 54.4 nm, 57.5 nm, and 58.9 nm, respectively (Figure 2.4). This confirmed the robustness of polymer brush-grafted silica NPs and the high stability of these hairy NPs in PAO.

As mentioned earlier, PC6- and PC8-grafted silica NPs cannot be dispersed in PAO to form a homogenous and clear dispersion at a concentration of 1.0 wt% at room temperature. This observation is expected for PC6-NP1-7.0k because PC6 free polymer itself is insoluble in PAO, as also reported in the literature.[50] Physical mixing and ultrasonication of PC6-NP1-7.0k in PAO at ambient temperature yielded an unstable suspension, which underwent nearly complete separation in less than two hours. Heating the mixture to 80 °C resulted in no visual change, and the NPs settled out quickly upon sitting quiescently at room temperature (Figure 2.3B). Interestingly, the 1.0 wt% heterogeneous suspension of PC8-NP1-7.8k in PAO became clear and homogeneous upon heating at 80 °C (Figure 2.3C). This cloudy-to-clear transition was reversible; upon cooling at room temperature, the clear dispersion turned cloudy. By cooling the clear, 1.0 wt% dispersion of PC8-NP1-7.8k in PAO from an elevated temperature in 1 °C steps, the cloud point was found to be 54 °C by visual inspection.

This clouding transition is particularly interesting as PC8 free polymer is soluble in PAO even at 0 °C. Apparently, the transition is caused by the presence of core silica NPs, very likely due to the unfavorable enthalpic interactions between PAO and silica NPs and the van der Waals attractive forces between hairy NPs; the combination of the two appears to be comparable to the favorable brush solvation forces for PC8-NP1-7.8k. If we increase

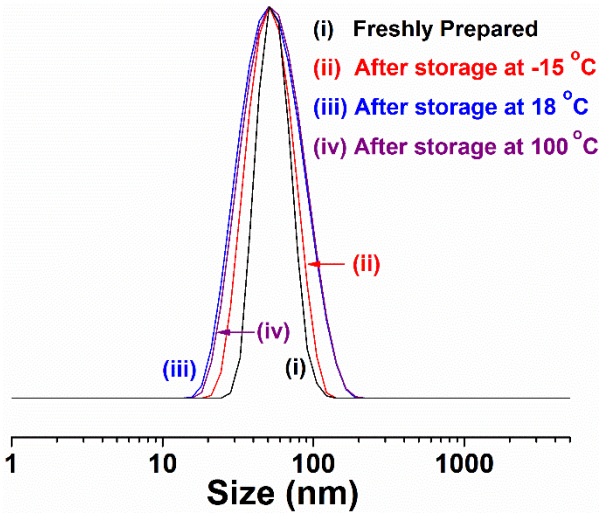

Figure 2.4. Hydrodynamic size distributions of PC13-NP1-9.7k in a freshly prepared dispersion in PAO (i) and in PAO dispersions after being stored for 60 days at -15 °C (ii), room temperature (18 °C) (iii), and 100 °C (iv). The DLS measurements were conducted at 23 °C with a hairy NP concentration of 0.1 mg/g.

the brush chain length and thus the favorable PAO-brush interactions, the cloud point should decrease.

2.3.4. Effect of Alkyl Pendant Group of Poly(alkyl methacrylate) Brushes on Lubrication Property of Hairy NP-Additized PAO

The effectiveness of poly(alkyl methacrylate) brush-grafted silica NPs with various alkyl pendant groups as additives for lubricating base oil, PAO, to reduce friction and wear was investigated at a concentration of 1.0 wt% using a Plint TE-77 tribo-tester at 100 °C. A ball-on-flat reciprocating configuration was employed using a CL35 cast iron flat and an AISI 52100 steel ball with a diameter of 9.525 mm, with the rubbing interface completely submerged in the lubricating oil. A normal force of 100 N and an oscillation frequency of 10 Hz with 10 mm stroke were used, and the total sliding distance was 1000 m. At least two tests were performed for each hairy NP sample, and the results were averaged. For comparison, we also prepared a lubricant by dissolving a free polymer of MA-C13 with a DP of 72, a $M_{n,SEC}$ of 20.8 kDa, and a Đ of 1.15 (PC13-20.8k) in PAO to form a 1.0 wt% solution. The synthesis of this polymer is included in the experimental section. As shown in Figure 2.5A, for 1.0 wt% of PC13-20.8k in PAO, while the coefficient of friction (COF) was reduced to some degree in the second half of the sliding compared with the PAO, the sharp increase of COF, a signature of scuffing failure, observed at the beginning of the test was neither prevented nor reduced, indicating a minimal effect of poly(alkyl methacrylate) itself in wear or scuffing protection. This corroborated our previous observation for the effect of free polymer poly(lauryl methacrylate).[35]

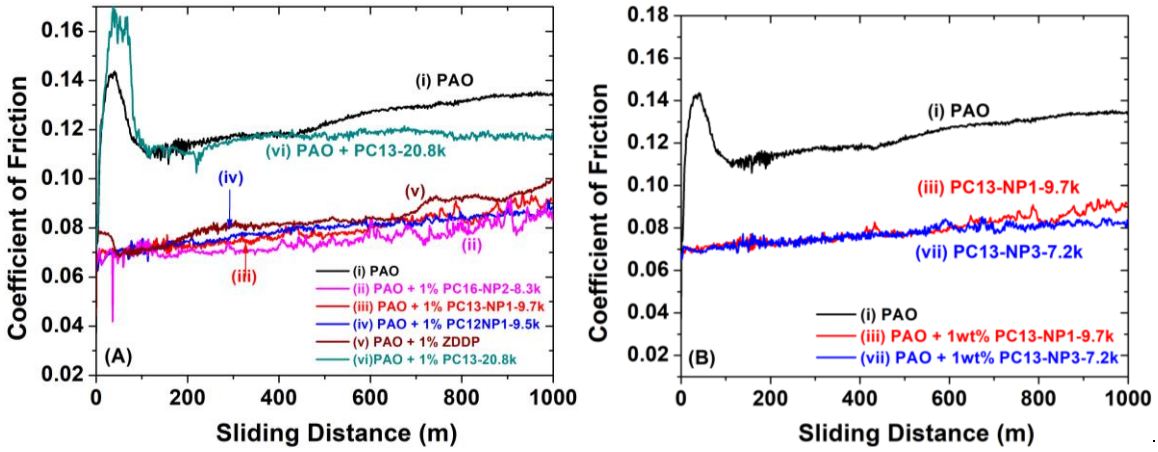

Figure 2.5. (A) Friction curves for PAO SpectraSyn^{TM} 4 (i), PAO additized with 1.0 wt% PC16-NP2-8.3k (ii), PC13-NP1-9.7k (iii), PC12-NP1-9.5k (iv), ZDDP (v), and PC13-20.8k free polymer (vi). (B) Friction curves for PAO additized with 1.0 wt% PC13-NP3-7.2k (vii) as well as neat PAO (i) and PAO additized with 1.0 wt% PC13-NP1-9.7k (iii) for comparison. The tribological tests were performed using a Plint TE-77 tribo-tester at 100 °C under a point contact load of 100 N for a sliding distance of 1000 m. The curves for (i) PAO and (v) PAO additized with 1.0 wt% ZDDP were from the literature for comparison.[35]

In contrast, for all hairy NPs that readily formed homogeneous transparent dispersions in PAO at room temperature, namely PC12-, PC13-, and PC16- grafted NPs, the COF exhibited a smooth start without scuffing and a much lower steady-state value relative to PAO throughout the sliding process (Figure 2.5). The friction coefficient values were between 0.08 and 0.1 at 1000 m, with PC16-NP2-8.3k exhibiting the largest friction reduction (38%) relative to the base oil. As a matter of fact, the COF traces of PC12-NP1-9.5k, PC13-NP1-9.7k, and PC16-NP2-8.3k were all below that of PAO containing 1.0 wt% ZDDP (Figure 2.5A), which implied better frictional behavior for these hairy NPs than the ZDDP at the same concentration. Note that compared with ZDDP, the sulfur content of hairy NPs from the CTA end group is significantly lower or negligible. Figure 2.5B shows that two PC13-grafted NP samples performed very similarly; their friction curves essentially overlapped until ~ 600 m, after which PC13-NP3-7.2k exhibited slightly lower COF values. Considering the limited contribution to the friction reduction from the polymer alone, the somewhat similar tribological performances of four hairy NP samples with different alkyl pendant groups highlighted the importance of the core silica NPs in the effectiveness of hairy NPs as additives. Although there was no single trend discernable in the entire sliding process for the three different poly(alkyl methacrylate) brushes, a closer look at the four friction curves showed that PC16-NP2-8.3k performed slightly better than other three samples over the entire sliding process while the traces of PC12- and PC13-NPs were very similar. While these hairy NPs had different chemical compositions, DPs, and grafting densities (Table 2.1), a brief look at TGA data revealed that PC16-NP2-8.3k had noticeably higher weight retention at 800 °C (62.3% PC16-NP2-8.3k, 44.2% for PC13-

NP1-9.7k, 48.2% for PC13-NP3-7.2k, and 51.6% for PC12-NP1-9.5k). Higher weight retention at 800 °C means that there are more silica NPs present in PAO at a concentration of 1.0 wt%, which would result in a larger friction reduction. Our group previously observed that a higher concentration of PC12 hairy NPs typically produced lower COFs.[35] Thus, the slightly better performance of PC16-NP2-8.3k can be attributed to more NPs at the same concentration. The slightly lower COF values of PC13-NP3-7.2k compared with PC13-NP1-9.7k in the second half of the sliding process might also result from more NPs present in the system because the weight retention at 800 °C was 44.2% for PC13-NP1-9.7k and 48.2% for PC13-NP3-7.2k. It appears that the foremost function of the grafted polymer brushes is to provide the colloidal stability for silica core NPs in base oil PAO. Once a homogeneous dispersion is achieved, the number density of NPs in the lubricant is likely to be a primary factor in tribological performance.

Material wear volumes were measured by optical surface profilometry of the wear scars formed on the iron flats and, to a lesser extent, on the steel balls during each tribological test and are shown in Table 2.2. The wear volumes of the iron flats for PC13-NP1-9.7k, PC13-NP3-7.2k, PC12-NP1-9.5k, and PC16-NP2-8.3k were found to have similar magnitudes and ranged from 11.7 to 23 × 10^7 μm^3, which were significantly smaller (by 5 to 10 times, or reduced by 80 – 90%) than that for neat PAO (113.0 × 10^7 μm^3). However, these values were slightly higher than that for the ZDDP-additized oil (7.9 × 10^7 μm^3). The wear volumes of the steel balls for these hairy NPs, ranging from 0.019 to 0.048 × 10^7 μm^3,

Table 2.2. Wear Volumes for Balls and Flats from Tribological Tests

Lubricant Sample	Flat Wear Volume ($\times 10^7$ μm^3)	Ball Wear Volume ($\times 10^7$ μm^3)
PAO	113.0 ± 35.9	0.786 ± 0.193
PAO + 1.0% PC6-NP1-7.0k	1.5 ± 0.3[a]	0.024 ± 0.018
PAO + 1.0% PC8-NP1-7.8k	17.5 ± 2.5	0.028 ± 0.00005
PAO + 1.0% PC12-NP1-9.5k	11.7 ± 1.4	0.025 ± 0.0003
PAO + 1.0% PC13-NP1-9.7k	16.0 ± 0.8	0.019 ± 0.015
PAO + 1.0% PC13-NP3-7.2k	23.0 ± 1.7	0.048 ± 0.017
PAO + 1.0% PC16-NP2-8.3k	18.0 ± 1.3	0.019 ± 0.006
PAO + 1.0% ZDDP	7.9 ± 3.1	0.047 ± 0.020
PAO + 1.0% PC6-NP1-7.0k-Settled	50.9 ± 10.3	-0.097 ± 0.054[b]
PAO + 1.0% PC8-NP1-7.8 k-Settled	19.4 ± 0.3	0.129 ± 0.074

[a] Measurement likely skewed due to the non-circulatory nature of oil during testing; PC6-NP1-7.0k settled directly onto flat after loading, effectively coating the substrate. [b] Value is negative as additional material adhered to the ball, likely a result of scuffing.

were reduced by >95% compared with that for the base oil (0.786×10^7 μm^3), and were similar to the value for the ZDDP.

As described earlier, PC6- and PC8-grafted silica NPs were unable to form clear, homogeneous dispersions in PAO at a concentration of 1.0 wt% under ambient conditions. Upon heating, while the 1.0 wt% suspension of PC6-NP1-7.0k in PAO stayed cloudy, PC8-NP1-7.8k was found to be fully dispersed in PAO forming a transparent and stable system. To characterize the tribological property of the fully dispersed PC8-NP1-7.8k, PAO additized with 1.0 wt% PC8-NP1-7.8k was heated to 80 °C and stirred for 30 min to achieve a clear NP dispersion. A 1.0 wt% PC6-NP1-7.0k-additized PAO lubricant was also prepared using the same conditions to form a visually uniform suspension. These two NP-containing lubricants were then added onto the iron flats preheated to 100 °C and subjected to the same tribological testing described earlier; the results are presented in Figure 2.6. Interestingly, PC8-NP1-7.8k performed similarly to those more easily dispersed hairy NPs (Figure 2.6A); the COF curve essentially overlapped with that of PC13-NP3-7.2k. Note that the weight retentions of these two hairy NPs at 800 °C were very similar, 49.1% for PC8-NP1-7.8k and 48.2% for PC13-NP3-7.2k, which once again indicated the importance of the mass of the core NPs or number of NPs at a hairy NP concentration of 1.0 wt% in tribological performance. The addition of 1.0 wt% PC6-NP1-7.0k into PAO, even if not dispersed, also exhibited a significant reduction in friction compared with the base oil PAO, but performed noticeably worse than those more easily dispersed hairy NPs, e.g., PC13-NP3-7.2k as shown in Figure 2.6B. The end value of the COF at 1000 m for PC6-NP1-7.0k was higher by 0.02 than that of PC13-NP3-7.2k. Following the testing of PC6-NP1-

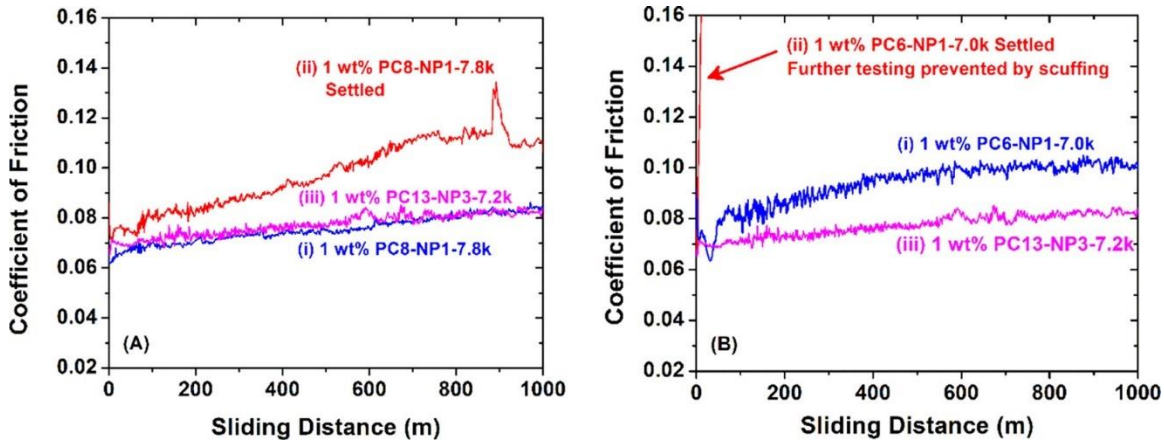

Figure 2.6. (A) Friction curves for PAO additized with 1.0 wt% PC8-NP1-7.8k (i) preheated and stirred at 80 °C to achieve a uniform state and (ii) after sitting quiescently at room temperature for 7 days. (B) Friction curves for PAO containing 1.0 wt% PC6-NP1-7.0k (i) preheated and stirred at 80 °C to achieve a uniform state and (ii) after sitting quiescently at room temperature for 7 days. The curve for PAO containing 1.0 wt% PC13-NP3-7.2k (iii) was included for comparison in both (A) and (B). The tribological tests were performed using a Plint TE-77 tribo-tester at 100 °C under a load of 100 N.

7.0k, a noticeable amount of NPs settled onto the flat, likely explaining the anomalously low wear observed for this sample (Table 2.1). It should be noted that any substrate the protection provided in this manner would almost certainly be voided upon oil circulation due to effective lowering of hairy NP concentration.

To test the effect of the inherent instability of PC6-NP1-7.0k and PC8-NP1-7.8k in PAO at room temperature on lubrication performance, both samples were subjected to a quiescent period of 7 days, after which the particles appeared to have completely settled (Figure 2.3B and 2.3C). Tribological testing was then performed on the top, clear portion of the oil. PC6-NP1-7.0k underwent early-onset scuffing in a manner similar to the base oil, but the friction exceeded the testing threshold and halted further testing (Figure 2.6B). The average material wear volume on the iron flat reached 50.9×10^7 μm^3 in its brief testing time, suggesting no benefit beyond the base PAO. PC8-NP1-7.8k, in contrast, showed some degree of friction reduction relative to pure PAO, but lubrication performance was significantly decreased compared with that of the homogeneous dispersion formed at elevated temperature (Figure 2.6A). The wear volume on the iron flat averaged at 19.4×10^7 μm^3, was slightly higher than that for the transparent homogeneous dispersion and still in line with other hairy NP-additized lubricants. As shown in Figure 2.3, the rate of hairy NP settling appeared to be slower for PC8-NP1-7.8k than for PC6-NP1-7.0k, and, due to its higher affinity for PAO, it is likely that a small amount of PC8-NP1-7.8k persisted in the oil and provided protection at the rubbing interface.

2.3.5. SEM-EDS Analysis of Wear Scar Formed During Tribological Testing

The increased tribological performance of oil-soluble polymer brush-grafted NP-additized PAO originated from the function of hairy NPs in the interfacial zone between two sliding surfaces and the formation of a protective tribofilm assisted by NPs. As a result of the intricate mechanical and chemical processes at the rubbing interfaces under rather harsh conditions, substrate-shielding tribolayers have been observed for various lubricating additives, including ZDDP and ionic liquids,[5-11] and are typically elementally enriched according to the additive composition. Using the focused ion beam (FIB) technique and transmission electron microscopy, our group previously observed a 200–400 nm tribofilm on the wear track formed during the tribological testing of hairy silica NP-additized PAO, and the film was enriched in silicon.[35] Here we used energy dispersive X-ray spectroscopy (EDS) analysis coupled with scanning electron microscopy (SEM) to confirm the presence of a tribofilm at the wear scar's surface. A scanning electron micrograph of a wear scar formed during the testing of PC13-NP3-7.2k is shown in Figure 2.7A along with two EDS spectra taken from inside and outside the wear track, respectively (Figure 2.7B). A marked increase in both silicon and oxygen content inside the scar relative to the unblemished iron flat was observed. Elemental mapping of iron, oxygen, and silicon at the end of wear track (Figure 2.7C-E, respectively) shows a clear increase in oxygen and silicon in the scar, whereas the scar is nearly indistinguishable from the pristine iron flat in the elemental mapping of iron. These observations indicate the formation of a tribofilm on the surface of the wear track, which involved and likely was assisted by polymer brush-grafted silica NPs,

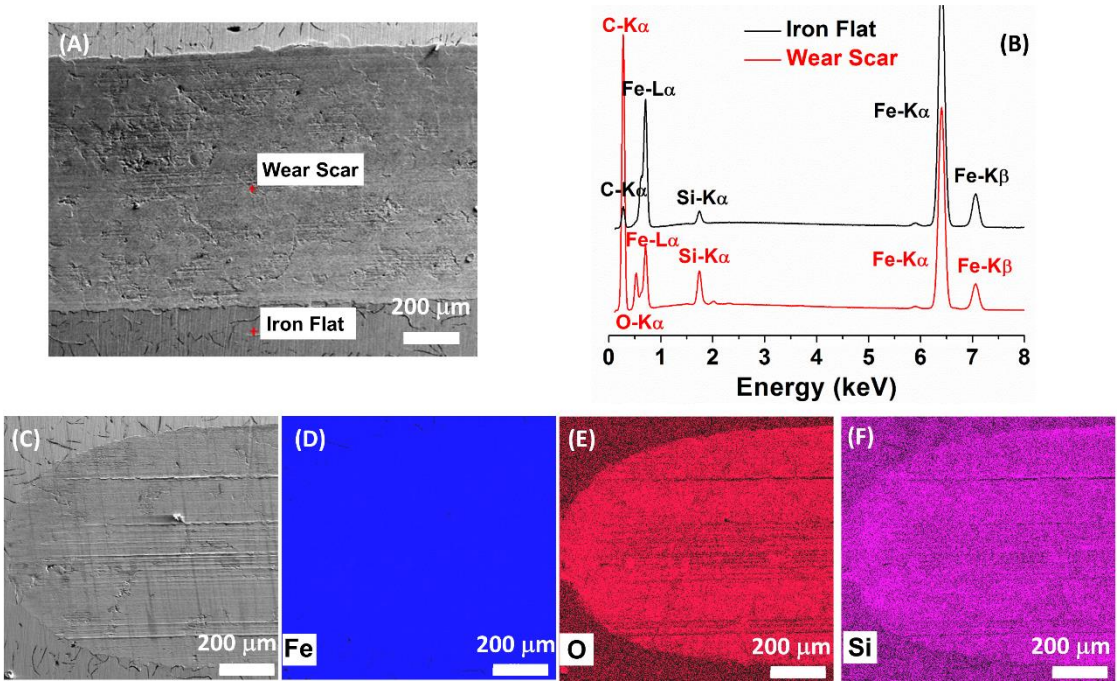

Figure 2.7. (A) SEM micrograph of a wear scar formed on the iron flat during the tribological testing of PAO additized with 1.0 wt% PC13-NP3-7.2k, (B) EDS spectra recorded inside and outside the wear scar (at locations marked in (A)), and SEM micrograph (C) and elemental mapping of Fe (D), O (E), and Si (F) at the end of the wear track.

providing protection for the substrate underneath and thus preventing scuffing and reducing friction and wear.

2.4. Conclusions

A series of poly(alkyl methacrylate) brush-grafted silica NPs of varying alkyl pendant length were synthesized by SI-RAFT polymerization from CTA-functionalized, 23 nm silica NPs, and their dispersibility and stability in PAO and lubrication property were investigated.[51] PC12-, PC13-, and PC16- grafted silica NPs were readily and fully dispersed in PAO upon ultrasonication, producing transparent, homogeneous dispersions that possessed exceptional colloidal stability at high and low temperatures as observed both visually and by DLS. Neither PC6-NP1-7.0k nor PC8-NP1-7.8k formed a homogeneous, stable dispersion in PAO at ambient temperature at a concentration of 1.0 wt%, although PC8-grafted NPs were found to be fully dispersed in PAO at elevated temperatures and exhibited a reversible clear-to-cloudy transition upon cooling. Tribological testing using a ball-on-flat reciprocating configuration showed a significant reduction in both coefficient of friction (up to ~ 38%) and wear volume (up to ~ 90% for the iron flat) when 1.0 wt% homogeneous transparent dispersions of hairy NPs in PAO were used as lubricants compared with neat PAO. The poor colloidal stability and NP settling in PAO dispersions of PC6- and PC8-grafted silica NPs greatly hindered lubrication performance, highlighting the need for homogeneous and stable dispersions of NP additives in PAO. The tribofilm formed at the rubbing interface during tribological testing was confirmed by SEM-EDS and found to be enriched with silicon and oxygen relative to the unmarred iron flat. Note

that in this work, 23 nm silica NPs were employed to synthesize hairy NPs; the core NP size is believed to affect the lubrication performance of hairy NPs. The excellent colloidal stability along with significant friction and wear reduction for PAO additized with poly(alkyl methacrylate) brush-grafted 23 nm silica NPs containing sufficiently long alkyl pendants, observed in this study, is encouraging in the pursuit of more effective and more environmentally-friendly additives for the formulation of advanced engine lubricants.

References

1. *Engine Oils and Automotive Lubrication*; Bartz, W. J., Ed.; Marcel Dekker: New York, 1993.
2. *Synthetic Lubricants and High-Performance Functional Fluids*, 2nd ed; Rudnick, L. R., Shubkin, R. L., Eds.; Marcel Dekker: New York, 1999.
3. *Lubricant Additives: Chemistry and Applications*, 2nd ed; Rudnick, L. R., Ed.; CRC Press: Boca Raton, FL, 2009.
4. *Synthetics, Mineral Oils, and Bio-Based Lubricants: Chemistry and Technology*, 2nd ed; Rudnick, L. R., Ed.; CRC Press: Boca Raton, FL, 2013.
5. Spikes, H. The History and Mechanisms of ZDDP. *Tribol. Lett.* **2004**, *17*, 469 –489.
6. Barnes, A. M.; Bartle, K. D.; Thibo, V. R. A. A Review of Zinc Dialkyldithiophosphates (ZDDPS): Characterisation and Role in the Lubricating Oil. *Tribol. Int.* **2001**, *34*, 389-395.
7. Spikes, H. Low- and Zero-Sulphated Ash, Phosphorus and Sulphur Anti-Wear Additives for Engine Oils. *Lubr. Sci.* **2008**, *20*, 103-136.
8. Zhang, J.; Spikes, H. On the Mechanism of ZDDP Antiwear Film Formation. *Tribol. Lett.* **2016**, *63*, 24.
9. Demydov, D.; Adhvaryu, A.; McCluskey, P.; Malshe, A. P. In *Nanoscale Materials in Chemistry: Environmental Applications, ACS Symposium Series, Vol. 1045*; Erickson, L. E.; Koodali, R. T.; Richards, R. M., Eds.; American Chemical Society: Washington, DC, 2010; Chapter 8, pp 137–163.

10. Qu, J.; Bansal, D. G.; Yu, B.; Howe, J. Y.; Luo, H.; Dai, S.; Li, H. Q.; Blau, P. J.; Bunting, B. G.; Mordukhovich, G.; Smolenski, D. J. Antiwear Performance and Mechanism of an Oil-Miscible Ionic Liquid as a Lubricant Additive. *ACS Appl. Mater. Interfaces* **2012**, *4*, 997–1002.
11. Qu, J.; Barnhill, W. C.; Luo, H.; Meyer III, H. M.; Leonard, D. N.; Landauer, A. K.; Kheireddin, B.; Gao, H.; Papke, B. L.; Dai, S. Synergistic Effects Between Phosphonium-Alkylphosphate Ionic Liquids and Zinc Dialkyldithiophosphate (ZDDP) as Lubricant Additives. *Adv. Mater.* **2015**, *27*, 4767-4774.
12. Martin, J. M.; Ohmae, N. *Nanolubricants*. John Wiley & Sons: Chichester, England, 2008.
13. Gulzar, M.; Masjuki, H. H.; Kalam, M. A.; Varman, M.; Zulkifli, N. W. M.; Mufti, R. A.; Zahid, R. Tribological Performance of Nanoparticles as Lubricating Oil Additives. *J. Nanopart. Res.*, **2016**, *18*, 223.
14. Qiu, S.; Zhou, Z.; Dong, J.; Chen, G. Preparation of Ni Nanoparticles and Evaluation of Their Tribological Performance as Potential Additives in Oils. *J. Tribol.* **1999**, *123*, 441–443.
15. Tarasov, S.; Kolubaev, A.; Belyaev, S.; Lerner, M.; Tepper, F. Study of Friction Reduction by Nanocopper Additives to Motor Oil. *Wear* **2002**, *252*, 63–69.
16. Padgurskas, J.; Rukuiza, R.; Prosyčevas, I.; Kreivaitis, R. Tribological Properties of Lubricant Additives of Fe, Cu and Co Nanoparticles. *Tribol. Int.* **2013**, *60*, 224 –232.

17. Joly-Pottuz, L.; Dassenoy, F.; Belin, M.; Vacher, B.; Martin, J. M.; Fleischer, N. Ultralow-Friction and Wear Properties of IF-WS_2 under Boundary Lubrication. *Tribol. Lett.* **2005**, *18*, 477-485.

18. Rabaso, P.; Ville, F.; Dassenoy, F.; Diaby, M.; Afanasiev, P.; Cavoret, J.; Vacher, B.; Le-Mogne, T. Boundary lubrication: Influence of the Size and Structure of Inorganic Fullerene-like MoS_2 Nanoparticles on Friction and Wear Reduction. *Wear* **2014**, *320*, 161-178.

19. Rapoport, L.; Lvovsky, M.; Lapsker, I.; Leshchinsky, V.; Volovik, Y.; Feldman, Y.; Margolin, A.; Rosentsveig, R.; Tenne, R. Slow Release of Fullerene-like WS_2 Nanoparticles from Fe−Ni Graphite Matrix: A Self-Lubricating Nanocomposite. *Nano Lett.* **2001**, *1*, 137–140.

20. Xue, Q.; Liu, W.; Zhang, Z. Friction and Wear Properties of a Surface-Modified TiO_2 Nanoparticle as an Additive in Liquid Paraffin. *Wear* **1997**, *213*, 29–32.

21. Battez, A. H.; Rico, J. E. F.; Arias, A. N.; Rodriguez, J. L. V.; Rodriguez, R. C.; Fernandez, J. M. D. The Tribological Behaviour of ZnO Nanoparticles as an Additive to PAO6. *Wear* **2006**, *261*, 256 –263.

22. Kim, D.; Archer, L. A. Nanoscale Organic-Inorganic Hybrid Lubricants. *Langmuir* **2011**, *27*, 3083–3094.

23. Li, D. D.; Xie, Y. C.; Yong, H. S.; Sun, D. Z. Surfactant-Assisted Preparation of Y_2O_3-Stabilized ZrO_2 Nanoparticles and Their Tribological Performance in Mineral and Commercial Lubricating Oils. *RSC Adv.* **2017**, *7*, 3727 –3735.

24. Li, B.; Wang, X.; Liu, W.; Xue, Q. Tribochemistry and Antiwear Mechanism of Organic-Inorganic Nanoparticles as Lubricant Additives. *Tribol. Lett.* **2006**, *22*, 79–84.

25. Wu, Y. Y.; Tsui, W. C.; Liu, T. C. Experimental Analysis of Tribological Properties of Lubricating Oils with Nanoparticle Additives. *Wear* **2007**, *262*, 819–825.

26. Spikes, H. Friction Modifier Additives. *Tribol. Lett.* **2015**, *60*, 5.

27. Pyun, J.; Matyjaszewski, K. Synthesis of Nanocomposite Organic/Inorganic Hybrid Materials Using Controlled/"Living" Radical Polymerization. *Chem. Mater.* **2001**, *13*, 3436–3448.

28. Zhao, B.; Zhu, L. Mixed Polymer Brush-Grafted Particles: A New Class of Environmentally Responsive Nanostructured Materials. *Macromolecules* **2009**, *42*, 9369-9383.

29. Barbey, R.; Lavanant, L.; Paripovic, D.; Schuwer, N.; Sugnaux, C.; Tugulu, S.; Klok, H. A. Polymer Brushes via Surface-Initiated Controlled Radical Polymerization: Synthesis, Characterization, Properties, and Applications. *Chem. Rev.* **2009**, *109*, 5437–5527.

30. Bao, C. H.; Horton, J. M.; Bai, Z. F.; Li, D. J.; Lodge, T. P.; Zhao, B. Stimuli-Triggered Phase Transfer of Polymer-Inorganic Hybrid Hairy Particles between Two Immiscible Liquid Phases. *J. Polym. Sci. Part B: Polym. Phys.* **2014**, *52*, 1600-1619.

31. von Werne, T.; Patten, T. E. Preparation of Structurally Well-Defined Polymer−Nanoparticle Hybrids with Controlled/Living Radical Polymerizations. *J. Am. Chem. Soc.* **1999**, *121*, 7409–7410.

32. Li, D. J.; Sheng, X.; Zhao, B. Environmentally Responsive "Hairy" Nanoparticles: Mixed Homopolymer Brushes on Silica Nanoparticles Synthesized by Living Radical Polymerization Techniques. *J. Am. Chem. Soc.* **2005**, *127*, 6248-6256.

33. Ohno, K.; Koh, K.; Tsujii, Y.; Fukuda, T. Fabrication of Ordered Arrays of Gold Nanoparticles Coated with High-Density Polymer Brushes. *Angew. Chem. Int. Ed.* **2003**, *42*, 2751–2754.

34. Husseman, M.; Malmstrom, E. E.; McNamara, M.; Mate, M.; Mecerreyes, D.; Benoit, D. G.; Hedrick, J. L.; Mansky, P.; Huang, E.; Russell, T. P.; Hawker, C. J. Controlled Synthesis of Polymer Brushes by "Living" Free Radical Polymerization Techniques. *Macromolecules* **1999**, *32*, 1424-1431.

35. Wright, R. A. E.; Wang, K. W.; Qu, J.; Zhao, B. Oil-Soluble Polymer Brush-Grafted Nanoparticles as Effective Lubricant Additives for Friction and Wear Reduction. *Angew. Chem. Int. Ed.* **2016**, *55*, 8656-8660.

36. Skaff, H.; Emrick, T. Reversible Addition-Fragmentation Chain Transfer (RAFT) Polymerization from Unprotected Cadmium Selenide Nanoparticles. *Angew. Chem., Int. Ed.* **2004**, *43*, 5383-5386.

37. Li, C.; Benicewicz, B. C. Synthesis of Well-Defined Polymer Brushes Grafted onto Silica Nanoparticles via Surface Reversible Addition-Fragmentation Chain Transfer Polymerization. *Macromolecules* **2005**, *38*, 5929-5936.

38. Li, C.; Han, J.; Ryu, C. Y.; Benicewicz, B. C. A Versatile Method To Prepare RAFT Agent Anchored Substrates and the Preparation of PMMA Grafted Nanoparticles. *Macromolecules* **2006**, *39*, 3175-3183.

39. Peng, Q.; Lai, D. M. Y.; Kang, E. T.; Neoh, K. G. Preparation of Polymer-Silicon(100) Hybrids via Interface-Initiated Reversible Addition-Fragmentation Chain Transfer (RAFT) Polymerization. *Macromolecules* **2006**, *39*, 5577-5582

40. Zhao, Y.; Perrier, S. Reversible Addition-Fragmentation Chain Transfer Graft Polymerization Mediated by Fumed Silica Supported Chain Transfer Agents. *Macromolecules* **2007**, *40*, 9116-9124.

41. Li, Y.; Benicewicz, B. C. Functionalization of Silica Nanoparticles via the Combination of Surface-Initiated RAFT Polymerization and Click Reactions. *Macromolecules* **2008**, *41*, 7986–7992.

42. Ohno, K.; Ma, Y.; Huang, Y.; Mori, C.; Yahata, Y.; Tsujii, Y.; Maschmeyer, T.; Moraes, J.; Perrier, S. Surface-Initiated Reversible Addition-Fragmentation Chain Transfer (RAFT) Polymerization from Fine Particles Functionalized with Trithiocarbonates. *Macromolecules* **2011**, *44*, 8944–8953.

43. Chiefari, J.; Chong, Y. K.; Ercole, F.; Kristina, J.; Jeffery, J.; Le, T. P. T.; Mayadunne, R. T. A.; Meijs, G. F.; Moad, C. L.; Moad, G.; Rizzardo, E.; Thang, S. H. Living Free-Radical Polymerization by Reversible Addition-Fragmentation Chain Transfer: The RAFT Process. *Macromolecules* **1998**, *31*, 5559-5562.

44. Moad, G.; Chong, Y. K.; Postma, A.; Rizzardo, E.; Thang, S. H. Advances in RAFT Polymerization: the Synthesis of Polymers with Defined End-Groups. *Polymer* **2005,** *46*, 8458-8468.

45. Wright, R. A. E.; Hu, B.; Henn, D. M.; Zhao, B. Reversible Sol-Gel Transitions of Aqueous Dispersions of Silica Nanoparticles Grafted with Diblock Copolymer

Brushes Composed of a Thermosensitive Inner Block and a Charged Outer Block. *Soft Matter* **2015**, *11*, 6808-6820.

46. Wright, R. A. E.; Henn, D. M.; Zhao, B. Thermally Reversible Physically Crosslinked Hybrid Network Hydrogels Formed by Thermosensitive Hairy NPs. *J. Phys. Chem. B* **2016**, *120*, 8036-8045.
47. Willcock, H.; O'Reilly, R. K., End Group Removal and Modification of RAFT polymers. *Polym. Chem.* **2010,** *1*, 149-157.
48. Perrier, S.; Takolpuckdee, P.; Mars, C. A., Reversible Addition-Fragmentation Chain Transfer Polymerization: End Group Modification for Functionalized Polymers and Chain Transfer Agent Recovery. *Macromolecules* **2005,** *38*, 2033-2036.
49. Postma, A.; Davis, T. P.; Moad, G.; O'Shea, M. S., Thermolysis of RAFT-Synthesized Polymers. A Convenient Method for Trithiocarbonate Group Elimination. *Macromolecules* **2005,** *38*, 5371-5374.
50. Bielecki, R. M.; Benetti, E. M.; Kumar, D.; Spencer, N. D. Lubrication with Oil-Compatible Polymer Brushes. *Tribol. Lett.* **2012**, *45*, 477–487.
51. The work presented in this chapter has been published as an article. Seymour, B. T.; Wright, R. A. E.; Parrot, A. C.; Gao, H.; Martini, A.; Qu, J.; Dai, S.; Zhao, B. Poly(alkyl methacrylate) Brush-Grafted Silica Nanoparticles as Oil Lubricant Additives: Effects of Alkyl Pendant Groups on Oil Dispersibility, Stability, and Lubrication Property. *ACS Appl. Mater. Interfaces*, **2017**, *9* (29), 25038–25048.

Appendix A

for

Chapter 2. Poly(alkyl methacrylate) Brush-Grafted Silica Nanoparticles as Oil Lubricant Additives: Effects of Alkyl Pendant Group on Oil Dispersibility, Stability, and Lubrication Property

A.1. Calculation of Degree of Polymerization and Grafting Density of Polymer Brushes in PC13-NP3-7.2k

The degree of polymerization (DP) of the grafted polymer in PC13-HNP3-7.2k was calculated from the monomer conversion and the molar ratio of monomer to the sum of free and surface CTA. The amount of surface CTA grafted on silica NPs that successfully initiated RAFT polymerization was determined from the monomer conversion and the TGA of PC13 brush-grafted silica NPs, PC13-NP3-7.2k, and CTA-NPs-B3. To account for the difference in weight retentions of CTA-NPs-B3 and PC13-NP3-7.2k at 100 °C, which is assumed to be from moisture/absorbed small molecules, the TGA curve of CTA-NP3-B3 was shifted upward by 0.38% so that the weight retentions of two curves at 100 °C are identical. Thus, the weight retention of CTA-NP3 at 800 °C was changed from 91.22 % to 91.60%. The mass ratio of volatile to nonvolatile components, i.e., silica, at 800 °C is 9.17 : 100 for CTA-NP3-B3 and 107.3 : 100 for PC13-NP3-7.2k. As the mass of the CTA-NPs used in the polymerization was 0.2004 g, the total mass of the grafted polymer is [(107.3-9.17)/(100 + 9.17)] × 0.2004 g = 0.180 g. The total monomer in the reaction mixture (0.901 g) was multiplied by monomer conversion (97.6 %) to give a total polymer mass of 0.879 g. Using the ratio of total polymer to free polymer (0.879 g/ (0.879 g – 0.180 g)) as the ratio of total CTA to free CTA (30.2 mg, 0.104 mmol), the total amount of CTA in the polymerization system was calculated to be 0.131 mmol, yielding a surface-bound CTA content of 0.135 mmol/ g CTA-NPs, a monomer-to-CTA ratio of 25.6:1, and a DP of 25.

For the calculation of grafting density of PC13 brushes in PC13-NP3-7.2k, assuming that the silica NPs are spherical and has a density of 2.07 g/cm^3, the mass of a single NP with a diameter of 23 nm is 1.32×10^{-17} g. Using the polymer to silica ratio described above [(107.3-9.17)/100 = 98.1/100), the amount of the grafted PC13 homopolymer on one silica NP in PC13-NP3-7.2k is 1.29×10^{-17} g. The molecular weight of PC13 polymer in PC13-NP3-7.2k calculated from the DP is 6700 g/mol. Thus, the number of the grafted PC13 chains on one silica NP in PC13-NP3-7.2k is (1.28×10^{-17} g/6700 g/mol) × (6.022×10^{23} mol^{-1}) = 1150 chains. The surface area of one bare silica NP ($\pi \times 23^2$) = 1662 nm^2. Thus, the grafting density of PC13 brushes on silica NPs in PC13-NP3-7.2k is 0.69 chains/nm^2.

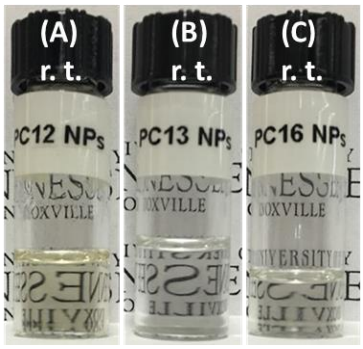

Figure A1. Optical photos of PC12-NP1-9.5k, PC13-NP1-9.7k, and PC16-NP2-8.3k in PAO with a concentration of 1.0 wt% at room temperature.

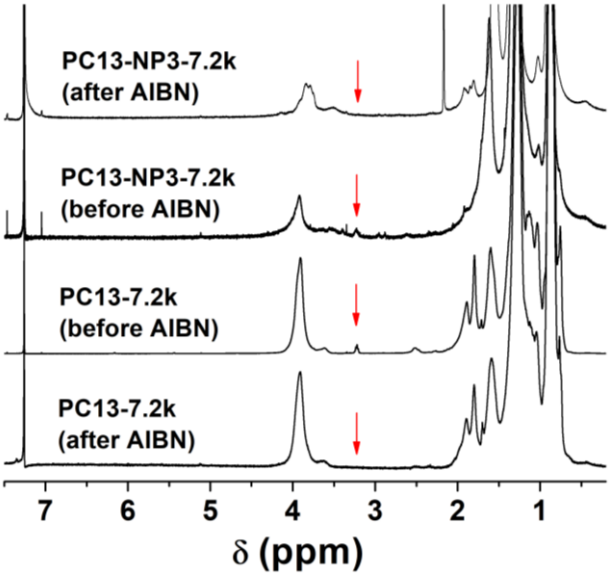

Figure A2. ^{1}H NMR spectra of PC13-NP3-7.2k and free polymer PC13-7.2k before and after AIBN treatment at 80 °C in $CDCl_3$.

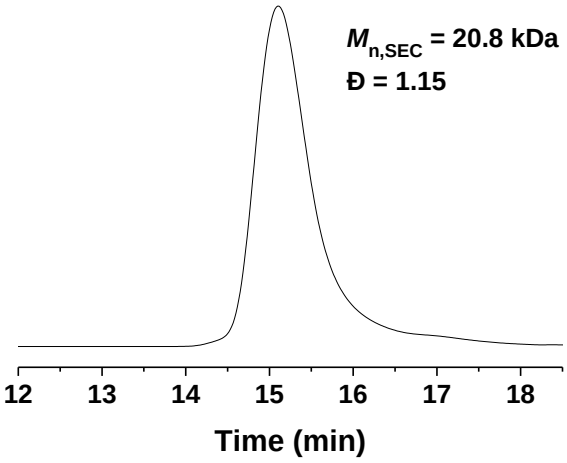

Figure A3. SEC trace of poly(tridecyl methacrylate) with a $M_{n,SEC}$ of 20.8 kDa (PC13-20.8k) synthesized by ATRP.

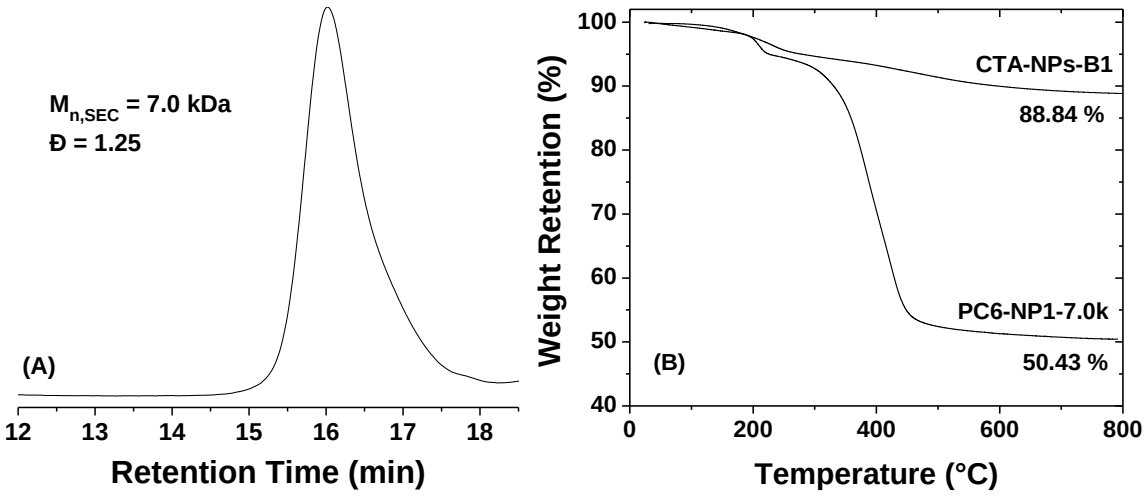

Figure A4. (A) SEC trace of free polymer poly(*n*-hexyl methacrylate) (PC6) formed from free CTA-COOH in the synthesis of PC6 brush-grafted silica NPs (PC6-NP1-7.0k) by surface-initiated RAFT polymerization of MA-C6 from CTA-functionalized silica NPs (CTA-NPs-B1). (B) Thermogravimetric analysis of CTA-NPs-B1 and PC6-NP1-7.0k. The TGA was carried out in N_2 at a heating rate of 20 °C/min.

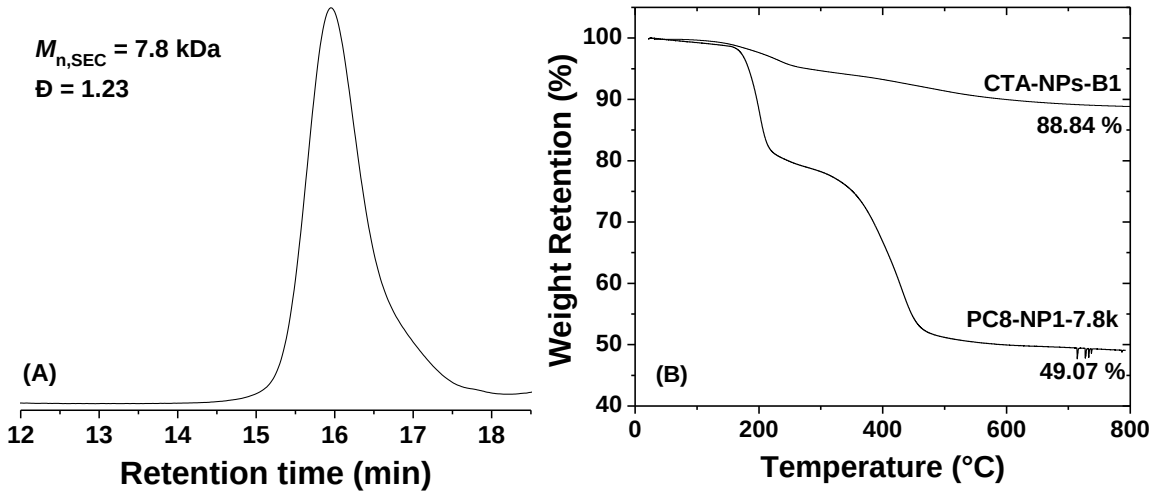

Figure A5. (A) SEC trace of free polymer poly(2-ethylhexyl methacrylate) (PC8) formed from free CTA-COOH in the synthesis of PC8-NP1-7.8k hairy NPs by surface-initiated RAFT polymerization of MA-C8 from CTA-NPs-B1. (B) Thermogravimetric analysis of CTA-NPs-B1 and PC8-NP1-7.8k. The TGA was carried out in N_2 at a heating rate of 20 °C/min.

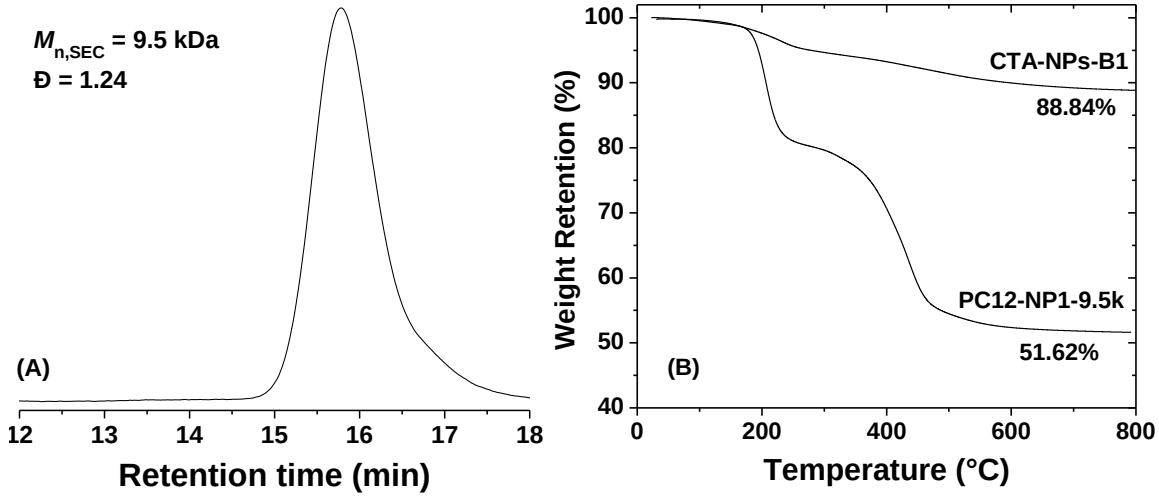

Figure A6. (A) SEC trace of free polymer poly(lauryl methacrylate) (PC12) formed from free CTA-COOH in the synthesis of PC12-NP1-9.5k hairy NPs by surface-initiated RAFT polymerization of MA-C12 from CTA- NPs-B1. (B) Thermogravimetric analysis of CTA-NPs-B1 and PC12-NP1-9.5 kDa. The TGA was carried out in N_2 at a heating rate of 20 °C/min.

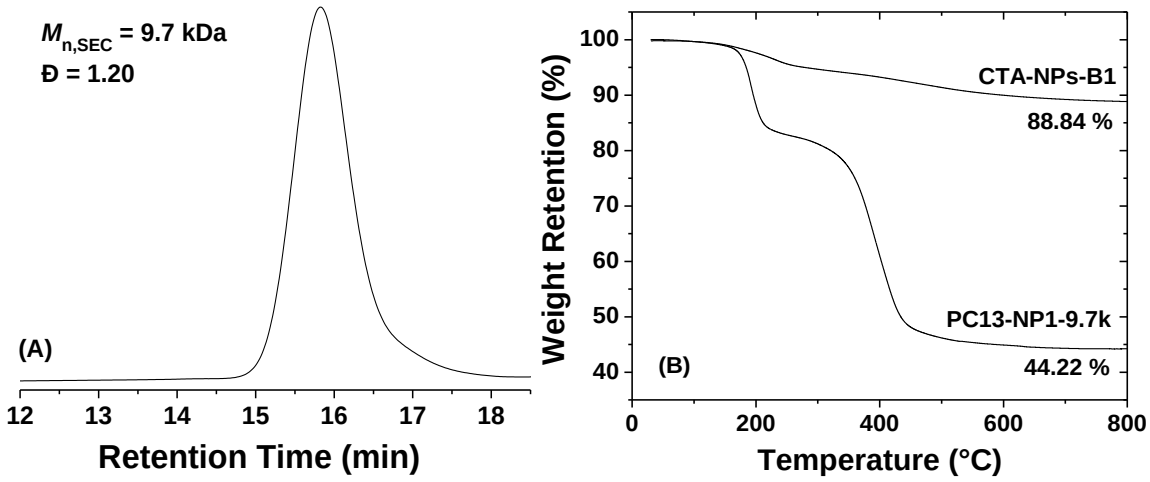

Figure A7. (A) SEC trace of free polymer poly(tridecyl methacrylate) (PC13) formed from free CTA-COOH in the synthesis of PC13-NP1-9.7k hairy NPs by surface-initiated RAFT polymerization of MA-C13 from CTA-NPs-B1. (B) Thermogravimetric analysis of CTA-NPs-B1 and PC13-NP1-9.7k. The TGA was carried out in N_2 at a heating rate of 20 °C/min.

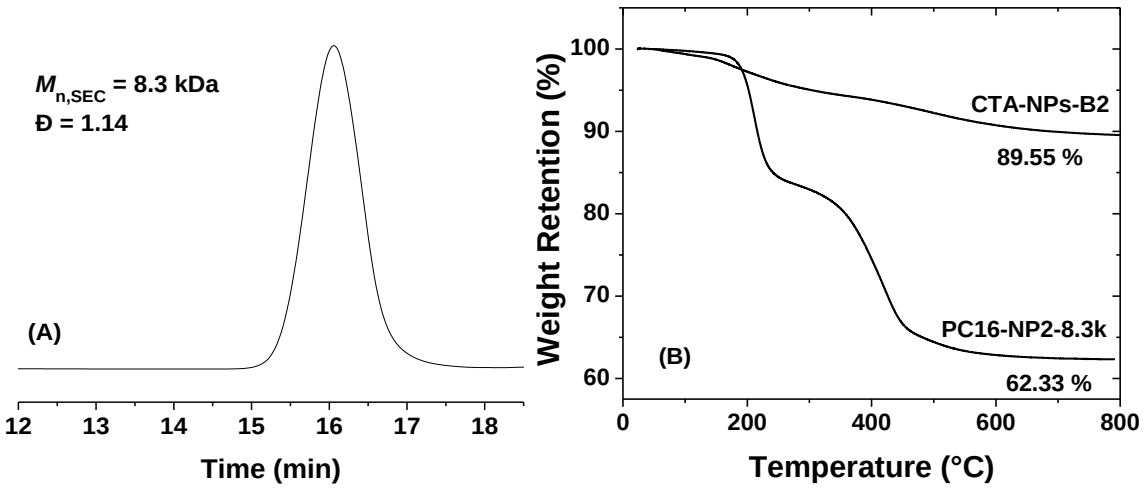

Figure A8. (A) SEC trace of free polymer poly(hexadecyl methacrylate) (PC16) formed from free CTA-COOH in the synthesis of PC16-NP2-8.3k hairy NPs by surface-initiated RAFT polymerization of MA-C16 from CTA-NPs-B2. (B) Thermogravimetric analysis of CTA-NPs-B2 and PC16-NP2-8.3 kDa. The TGA was carried out in N_2 at a heating rate of 20 °C/min.

Chapter 3. Synthesis of Phosphonate-Functionalized Polymer Brush-Grafted Silica Nanoparticles as Oil Lubricant Additive for Friction and Wear Reduction

Abstract

This chapter presents the synthesis of phosphonate-functionalized polymer brush-grafted, 23 nm silica nanoparticles (hairy NPs) for potential use as an oil lubricant additive and the study of their dispersibility and stability in PAO. The work in Chapter 2 showed that the primary role of poly(alkyl methacrylate) brushes of oil-soluble hairy NPs is the suspension of silica NPs in hydrophobic lubricating oil polyalphaolefin (PAO). To increase the function of hairy NPs, we introduced a triboactive element, phosphorus, into the brushes by surface-initiated RAFT copolymerization of a methacrylate monomer with a long alkyl pendant group and a phosphonate-containing monomer in this work. Three phosphonate-functionalized monomers were prepared, and they are diethyl (4-vinylbenzyl)phosphonate (StP), 11-(diethoxyphosphoryl)undecyl methacrylate (MAC11P), and 2-(diethoxyphosphoryl)ethyl methacrylate (MAC2P). Tridecyl methacrylate (MA-C13) was used for the copolymerization with StP and MAC11P, while hexadecyl methacrylate (MA-C16) was employed for the copolymerization with MAC2P. For each set of hairy NPs, various molar ratios of the comonomer and the phosphonate-functionalized monomer were used, including 95 : 5, 90 : 10, 85 : 15, and 80 : 20. To test the dispersibility of hairy NPs, 1 wt% dispersions in PAO were prepared. It was found that the molar content of StP units in the brushes can be up to 15% without comprising the dispersibility of hairy NPs in PAO. Surprisingly, all of MAC11P-containing hairy NPs were unstable in PAO at room temperature. On the other hand, all of MAC2P hairy NPs can be dispersed and are stable in PAO.

3.1. Introduction

Nanoparticles (NPs) or "nanolubricants" offer great promise for friction and wear reduction applications,[1-9] but the most challenging aspect of developing new nanolubricants remains to be particle suspension.[1] Friction coefficient reductions of ~ 70% have been reported for nanolubricants, however the strong tendency of NPs to undergo aggregation in oils has been a major issue.[2,3] Often, ultrasonication is used to disperse NPs in oil before tribological testing.[4,5] There are two common methods for achieving stable nanolubricant dispersions: formulation with dispersants and surface modification of NPs.[3,6-10] The most common surface modification is achieved by using alkoxysilanes. Despite many attempts, forming homogenous NP dispersions in a base oil, such as polyalphaolefin (PAO), that are stable over a large temperature range from -15 °C to 100 °C remains challenging.

Polymer brush-grafted NPs (hairy NPs),[11-13] which consist of a layer of polymer chains end-tethered to the NP core, exhibit superior dispersibility and stability in good solvents due to the favorable enthalpic interactions between the polymer and solvent and the entropic steric repulsions between the hairy NPs.[14] Our group recently reported the synthesis of oil-soluble poly(lauryl methacrylate) brush-grafted silica and titania NPs by surface-initiated atom transfer radical polymerization (SI-ATRP) and studied their lubricating properties in PAO.[15] These hairy NPs were very stable in PAO in the temperature range from -20 °C to 100 °C. The addition of 1 wt% hairy NPs decreased the friction by up to 40% and the wear by up to 90%. In Chapter 2, we investigated the effect of the alkyl pendant group of methacrylate monomer on the dispersibility of hairy NPs in

oil and found that hairy NPs with longer pendant groups (> 8 carbon atoms) in the brushes were readily dispersed in PAO.[16] Tribological testing of 1 wt% homogeneous dispersions of various hairy NPs in PAO revealed little difference in lubrication performance. This observation suggested that the main function of the grafted polymer chains was the stabilization of silica NPs in oil.

In an attempt to further improve the performance of hairy NPs, we aimed to increase the function of hairy NPs by incorporating a triboactive element, phosphorus, into the polymer brushes without compromising solubility in the base oil. Three phosphonate-functionalized monomers were design and synthesized (Scheme 3.1): diethyl (4-vinylbenzyl)phosphonate (StP), 11-(diethoxyphosphoryl)undecyl methacrylate (MAC11P), and 2-(diethoxyphosphoryl)ethyl methacrylate (MAC2P). Three sets of phosphonate-functionalized hairy NPs were synthesized by surface-initiated reversible addition-fragmentation chain transfer (SI-RAFT) copolymerizations of MA-C13 with either StP or MAC11P and MA-C16 with MAC2P from 23 nm CTA-functionalized silica NPs (Scheme 3.1). The molar ratios of two monomers were varied from 95 : 5, 90 :10, 85: 15, and 80 : 20, with the lower molar content being the phosphonate-functionalized monomer. CTA-COOH was used as free CTA in the polymerizations to assist with characterization by forming analogous free copolymers. The dispersibility of the obtained hairy NPs in PAO was investigated. We found that the hairy NPs synthesized by copolymerization of MA-C16 and MAC2P exhibited better dispersibility at higher molar contents in PAO than the two sets of hairy NPs. The oil-soluble phosphonate-functionalized hairy NPs are promising, and we plan to conduct tribological studies on all

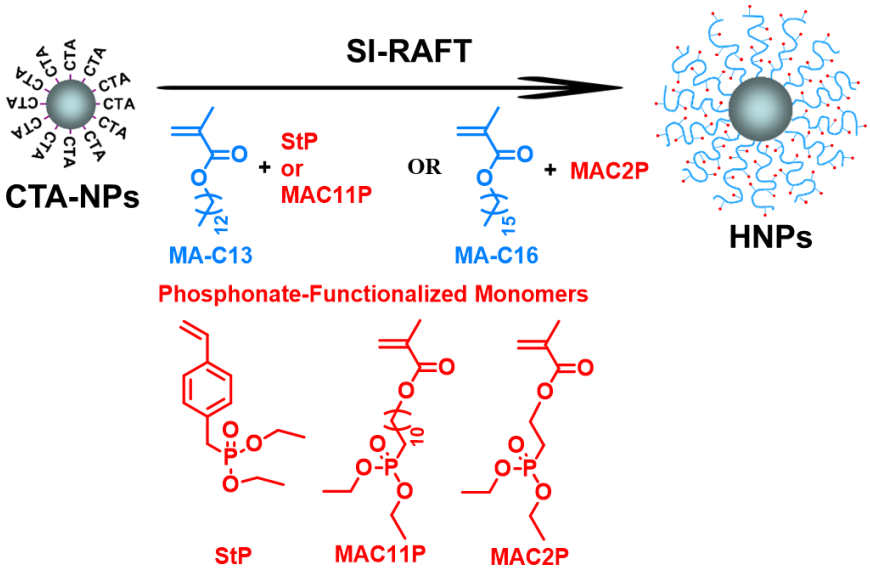

Scheme 3.1. Synthesis of Phosphonate-Functionalized Polymer Brush-Grafted Silica Nanoparticles by Surface-Initiated Reversible Addition-Fragmentation Chain Transfer (SI-RAFT) Copolymerization of Tridecyl Methacrylate (MA-C13) with StP or MAC11P, or of Hexadecyl Methacrylate (MA-C16) with MAC2P.

homogenous dispersions of functionalized NPs.

3.2. Experimental Section

3.2.1. Materials

Silica nanoparticles in methyl isobutyl ketone (MIBK) with a nominal size of 10-15 nm were obtained from Nissan Chemical as a dispersion with a concentration of 30-31 wt% SiO_2 (MIBK-ST). Tridecyl methacrylate (MA-C13, mixture of branched-chain isomers, TCI) and hexadecyl methacrylate (MA-C16, Wake Chemicals USA) were passed through a basic alumina column to remove inhibitor (hydroquinone monomethyl ether). Triethyl phosphite (98%, Alfa Aesar), 4-vinylbenzyl chloride (90%, ACROS Organics), 11-bromoundecan-1-ol (97%, Ark Pharm), 3,4-dihydro-2H-pyran (99%, Alfa Aesar), methacryloyl chloride (stabilized, 97%, Alfa Aesar), triethylamine (99%, Alfa Aesar), and benzyl 2-bromoethyl ether (97%, TCI) were used as received without purification. Amberlyst™ 15 (Alfa Aesar) and palladium catalyst (10% on carbon, Type 487, Alfa Aesar) were used as received. The polyalphaolefin (PAO) base oil used in this work was Spectrasyn™ 4 PAO oil obtained from ExxonMobil, with kinematic viscosities of 19.0 cSt at 40 °C and 4.1 cSt at 100 °C. 4-(((Butylthio)carbonothioyl)thio)-4-cyanopentanoic acid (CTA-COOH) was prepared using a procedure adapted from the literature and used as free chain transfer agent (CTA) in the synthesis of hairy NPs.[17] *n*-Butyl (2-cyano-5-oxo-5-((3-(triethoxysilyl)propyl)amino)pentan-2-yl)carbonotrithioate (CTA-silane) was synthesized according to a previously described procedure.[16] Azobisisobutyronitrile (AIBN) (98%, Aldrich) was recrystallized from ethanol and dried under high vacuum before use. All other

chemical reagents were purchased from Sigma Aldrich or Fisher and used without further purification.

3.2.2. Characterization

Size exclusion chromatography (SEC) of the free polymers formed from the free CTA in the synthesis of phosphonate-functionalized polymer brush-grafted silica NPs was performed using a PL-GPC 20 (an integrated SEC system from Polymer Laboratories, Inc.) equipped with a refractive index detector, a PLgel 5 μm guard column (50 × 7.5 mm), and two PLgel 5 μm mixed-C columns (each 300 × 7.5 mm, linear range of molecular weight from 200 to 2,000,000 Da). THF was used as the mobile phase with a set flow rate of 1.0 mL/min. The system was calibrated with narrow dispersity polystyrene standards, and the data was processed using Cirrus GPC/SEC software (Polymer Laboratories, Inc.). ^{1}H, ^{13}C, and ^{31}P NMR spectra were recorded on a Varian Mercury Vx 300 MHz or Varian VNMRS 500 MHz, and the residual solvent peak was used as the internal reference. Thermogravimetric analysis (TGA) was performed in N_2 at a heating rate of 20 °C/min from room temperature to 800 °C using TA Q-series Q50.

3.2.3. Synthesis of Diethyl (4-Vinylbenzyl)phosphonate (StP)

4-Vinylbenzyl chloride (3.019 g, 19.78 mmol), triethyl phosphite (6.676 g, 40.18 mmol), and hydroquinone (0.129 g) were added to a 50 mL 2-necked round bottom flask with a stir bar. The sealed reaction flask was degassed by three cycles of freeze-pump-thaw before being placed in a 100 °C oil bath for 30 h. The unreacted triethyl phosphite was distilled out of the reaction flask under high vacuum at 100 °C. The crude mixture left in the distillation flask was diluted with methylene chloride at room temperature, transferred

to a separatory funnel, and washed three times with 1 M NaOH solution to remove hydroquinone inhibitor. The organic layer was dried over anhydrous $NaSO_4$ and then separated by gravity filtration. The filtered organic solution was concentrated by rotary evaporation, and the crude product was further purified by silica gel column chromatography using a mixture of hexanes and ethyl acetate (1 : 1, v/v) as eluent. A slightly yellow viscous liquid was obtained after drying under high vacuum (1.777 g, 35.3%). ^{1}H NMR δ (ppm, $CDCl_3$): 7.37-7.23 (m, aromatic, 4H), 6.72-6.65 (m, CH_2CH-, 1H), 5.72 (d, C*H*H'CH-, 1H), 5.22 (d, CH*H'*CH-, 1H), 4.07-3.95 (m, -P(OC*H*$_2$CH$_3$)$_2$, 4H), 3.14 (d, -C*H*$_2$P-, 2H), 1.24 (t, -P(OCH$_2$C*H*$_3$)$_2$, 6H). ^{13}C NMR δ (ppm, $CDCl_3$): 136.41 (CH_2*C*H-), 136.21 (CH_2CH*C*-), 131.18 (-*C*CH_2P-), 129.91 (aromatic), 126.35 (aromatic), 113.66 (*C*H_2CH-), 62.14 (-P(O*C*H$_2$CH$_3$)$_2$), 32.99 (-C*C*H$_2$P-), 16.38 (-P(OCH$_2$*C*H$_3$)$_2$).

3.2.4. Synthesis of 11-(Diethoxyphosphoryl)undecyl Methacrylate (MAC11P)

The multi-step synthesis of MAC11P began with the synthesis of a THP-protected alkyl bromide (THPC11Br). 3,4-Dihydro-2H-pyran (5.156 g, 61.30 mmol) and 11-bromo-1-undecanol (13.601 g, 54.14 mmol) were added to a 100 mL 3-necked round bottom flask and diluted with freshly distilled THF (40 mL). The reaction flask was placed in an N_2 environment. Hydrochloric acid with a concentration of 36.5 wt% (0.421 g, 11.55 mmol) was added to a scintillation vial and diluted with dry THF (10 mL). The HCl solution was then transferred to an addition funnel equipped at the top of the reaction flask and added dropwise. The reaction was allowed to proceed at room temperature for 25 h. The mixture was concentrated using rotary evaporation, diluted with methylene chloride, and transferred to a separatory funnel. The mixture was then washed three times with a

saturated NaCl solution. The organic layer was collected and dried over anhydrous sodium sulfate. The sodium sulfate was then removed by gravity filtration, and the solution was concentrated. The crude product was purified by column chromatography using ethyl acetate as eluent. A clear liquid was obtained after drying under high vacuum (17.896 g, 93.6% yield). ^{1}H NMR δ (ppm, $CDCl_3$): 4.58-4.52 (m, -OC*H*O-, 1H), 3.90-3.80 (m,-OCHOC*H*H'- (ring), 1H), 3.75-3.65 (m, -C*H*H'OCHO- (linear), 1H), 3.53-3.42 (m, -OCHOCH*H'*- (ring), 1H), 3.42-3.30 (m, BrC$H_2$$CH_2$-, -CH*H'*OCHO- (linear), 3H), 1.90-1.20 (m, $BrCH_2C$*H*$_2C$*H*$_2C$*H*$_2C$*H*$_2C$*H*$_2C$*H*$_2C$*H*$_2C$*H*$_2C$*H*$_2CH_2OCHOCH_2C$*H*$_2C$*H*$_2C$*H*$_2$, 24H). ^{13}C NMR δ (ppm, $CDCl_3$): 98.75 (-O*C*HO-), 67.58 (-OCHO*C*H_2), 62.23 (-*C*H_2OCHO-), 33.90 (Br*C*H_2-), 32.76 ($BrCH_2$*C*H_2-), 30.72 (-OCH*C*H_2CH_2-), 29.68 (-*C*H_2CH_2OCHO-), 29.45 ($BrCH_2CH_2CH_2CH_2$*C*H_2-), 29.39 ($BrCH_2CH_2CH_2CH_2CH_2$*C*H_2-), 29.37 (-*C*$H_2CH_2CH_2CH_2CH_2O$-), 29.34 (-*C*$H_2CH_2CH_2CH_2O$-), 28.68 (-*C*$H_2CH_2CH_2O$-), 28.10 ($BrCH_2CH_2CH_2$*C*H_2-), 26.16 ($BrCH_2CH_2$*C*H_2-), 25.45 (-$OCHOCH_2$*C*$H_2CH_2CH_2$-), 19.63 (-$OCHOCH_2CH_2$*C*H_2CH_2-).

The second step of the synthesis was the Arbuzov reaction to substitute the Br with a phosphonate functional group. THPC11Br (3.566 g, 10.09 mmol) and triethyl phosphite (2.715 g, 16.34 mmol) were added to a 25 mL 2-necked round bottom flask equipped with a stir bar. The reaction flask was placed in an N_2 environment, and the mixture was stirred at 150 °C for 20 h. Excess triethyl phosphite was removed by distillation under high vacuum at 100 °C. The crude mixture was then purified by silica gel column chromatography using a mixture of hexanes and ethyl acetate (2 : 1, v/v) as eluent initially and then a mixture of ethyl acetate and methanol (1 : 1, v/v) to increase the polarity. A

slightly yellow viscous liquid was obtained after drying under high vacuum (3.081 g, 67.4%). This product was designated THPC11P. ^{1}H NMR δ (ppm, $CDCl_3$): 4.57 (t, -OC*H*O-, 1H), 4.20-3.99 (m, -P(OC*H*$_2$CH$_3$)$_2$, 4H), 3.91-3.82 (m, -OCHOC*H*H'- (ring), 1H), 3.77-3.67 (m, -C*H*H'OCHO- (linear), 1H), 3.54-3.44 (m, -OCHOCH*H'*- (ring) , 1H), 3.43-3.33 (m, -CH*H'*OCHO- (linear), 1H), 1.91-1.22 (m, (OCH$_2$C*H*$_3$)$_2$PC*H*$_2$C*H*$_2$C*H*$_2$C*H*$_2$C*H*$_2$C*H*$_2$C*H*$_2$C*H*$_2$ C*H*$_2$C*H*$_2$CH$_2$OCHOCH$_2$C*H*$_2$C*H*$_2$C*H*$_2$, 32H) ^{13}C NMR δ (ppm, $CDCl_3$): 98.72 (-O*C*HO-), 67.55 (-OCHO*C*H$_2$ (ring)-), 62.21 (-*C*H$_2$OCHO (linear)-), 61.59 (-P(O*C*H$_2$CH$_3$)$_2$), 32.78 (-P*C*H$_2$-), 30.72 (-PCH$_2$CH$_2$*C*H$_2$-), 29.68 (-OCH*C*H$_2$-), 29.46 (-*C*H$_2$CH$_2$O-), 29.41 (-PCH$_2$CH$_2$CH$_2$CH$_2$*C*H$_2$-), 29.35 (-PCH$_2$CH$_2$CH$_2$CH$_2$CH$_2$*C*H$_2$-), 29.30 (-*C*H$_2$CH$_2$CH$_2$CH$_2$CH$_2$O-), 29.24 (-*C*H$_2$CH$_2$CH$_2$CH$_2$O-), 29.17 (-PCH$_2$CH$_2$CH$_2$*C*H$_2$-), 29.01 (-*C*H$_2$CH$_2$CH$_2$O-), 26.17 (-PCH$_2$*C*H$_2$-), 25.44 (-OCHOCH$_2$*C*H$_2$CH$_2$CH$_2$), 19.61 (-OCHOCH$_2$CH$_2$*C*H$_2$CH$_2$), 16.34 (-P(OCH$_2$*C*H$_3$)$_2$).

The third step of the synthetic route was the deprotection of THP using an acidic ion-exchange resin. THPC11P (3.081 g), methanol (3.130 g), and Amberlyst® 15 (2.000 g) were added to a 25 mL 2-necked round bottom flask equipped with a stir bar. The flask was placed in an N_2 environment and set in a 45 °C oil bath while stirring for 5 days. The deprotection was monitored throughout the reaction using ^{1}H NMR spectroscopy by observing the disappearance of the THP's CH peak at 4.50 ppm. Once the peak was completely removed, gravity filtration was used to separate the Amberlyst resin. The filtrate was then concentrated and purified by column chromatography using a mixture of methylene chloride and methanol (95 : 5 v/v) as eluent. A viscous yellow liquid was

obtained after drying under high vacuum (1.723 g, 71.2% yield). This product was designated HOC11P. ^{1}H NMR δ (ppm, $CDCl_3$): 4.14-4.01 (m, -P(OC*H*$_2$CH$_3$)$_2$, 4H), 3.62 (t, -CH$_2$C*H*$_2$OH, 2H), 1.75-1.23 (m, (OCH$_2$C*H*$_3$)$_2$PC*H*$_2$C*H*$_2$C*H*$_2$C*H*$_2$C*H*$_2$C*H*$_2$C*H*$_2$C*H*$_2$C*H*$_2$C*H*$_2$C*H*$_2$CH$_2$O, 26H). ^{13}C NMR δ (ppm, $CDCl_3$): 70.58 (HO*C*H$_2$-), 61.59 (-P(O*C*H$_2$CH$_3$)$_2$), 33.78 (HOCH$_2$*C*H$_2$-), 32.63 (-P*C*H$_2$-), 32.24 (-PCH$_2$CH$_2$*C*H$_2$-), 29.23 (-PCH$_2$CH$_2$CH$_2$*C*H$_2$-), 28.56 (-PCH$_2$CH$_2$CH$_2$CH$_2$*C*H$_2$-) 27.96 (-PCH$_2$CH$_2$CH$_2$CH$_2$CH$_2$*C*H$_2$-), 25.98 (HOCH$_2$CH$_2$CH$_2$CH$_2$*C*H$_2$-), 25.58 (HOCH$_2$CH$_2$CH$_2$*C*H$_2$-), 19.39 (-PCH$_2$*C*H$_2$-), 18.24 (HOCH$_2$CH$_2$*C*H$_2$-), 16.16 (-P(OCH-$_2$*C*H$_3$)$_2$).

The final step of the monomer synthesis was accomplished through a reaction with methacryloyl chloride to yield monomer MAC11P. HOC11P (1.723 g, 5.590 mmol) and triethylamine (0.772 g, 7.483 mmol) were added to a 25mL 2-necked round bottom flask equipped with a stir bar along with methylene chloride (5 mL). Methacryloyl chloride (0.772 g, 7.483 mmol) was added to a vial and diluted with methylene chloride (5 mL) before being transferred to an addition funnel attached to the reaction flask. The flask was placed in an N_2 environment and placed in an ice/water bath for 15 min before the dropwise addition of the methacryloyl chloride solution. The reaction mixture was stirred at room temperature for 27 h. A white precipitate was observed during the reaction, which was removed by partitioning with an aqueous phase. The crude mixture was then diluted with methylene chloride (50 mL), transferred to a separatory funnel, and washed twice with 1 M NaOH solution. The organic layer was dried over anhydrous sodium sulfate and then separated by gravity filtration. The organic layer was concentrated using a rotary

evaporator, and the product was purified by silica gel column chromatography using methylene chloride as eluent initially and then changing to a mixture of methylene chloride and methanol (1 : 1 v/v). A yellow liquid was obtained after drying under high vacuum (1.523 g, 72.4% yield). ^{1}H NMR δ (ppm, $CDCl_3$): 6.09 (s, -C=C*H*H', 1H), 5.54 (s, -C=CH*H'*, 1H), 4.18-3.99 (m, -P(OC*H*$_2$CH$_3$)$_2$, -CH$_2$C*H*$_2$O-, 6H), 1.94 (s, -CC*H*$_3$, 3H), 1.79-1.50 (m, -PC*H*$_2$CH$_2$CH$_2$CH$_2$ CH$_2$CH$_2$CH$_2$CH$_2$C*H*$_2$C*H*$_2$CH$_2$O-, 6H), 1.42-1.23 (m, -PCH$_2$C*H*$_2$C*H*$_2$C*H*$_2$C*H*$_2$C*H*$_2$C*H*$_2$C*H*$_2$C*H*$_2$ CH$_2$CH$_2$CH$_2$O-, -P(OCH$_2$C*H*$_3$)$_2$, 20H). ^{13}C NMR δ (ppm, $CDCl_3$): 167.50 (-*C*=O), 136.52 (-*C*=CH$_2$), 125.07 (-C=*C*H$_2$), 64.77 (-CH$_2$*C*H$_2$O-), 61.27 (-P(O*C*H$_2$CH$_3$)$_2$), 30.68 (-P*C*H$_2$-), 30.46 (-PCH$_2$CH$_2$*C*H$_2$-), 29.42 (-PCH$_2$CH$_2$CH$_2$CH$_2$*C*H$_2$-), 29.30 (-PCH$_2$CH$_2$CH$_2$CH$_2$CH$_2$*C*H$_2$-), 29.04 (-*C*H$_2$CH$_2$CH$_2$CH$_2$CH$_2$O-), 28.57 (-PCH$_2$CH$_2$CH$_2$*C*H$_2$-), 26.60 (-*C*H$_2$CH$_2$CH$_2$CH$_2$CH$_2$O-), 25.93 (-*C*H$_2$CH$_2$O-), 24.74 (-PCH$_2$*C*H$_2$-), 22.33 (-*C*H$_2$CH$_2$CH$_2$O-), 18.29 (-C*C*H$_3$), 16.49 (-P(OCH$_2$*C*H$_3$)$_2$).

3.2.5. Synthesis of 2-(Diethoxyphosphoryl)ethyl Methacrylate (MAC2P)

The multi-step synthesis of MAC2P began with the preparation of a benzyl-protected phosphonate (BnC2P). Triethyl phosphite (6.014 g, 36.19 mmol) and benzyl 2-bromoethyl ether (4.489 g, 20.87 mmol) were added to a 25 mL 2-necked round bottom flask equipped with a stir bar. The mixture was refluxed at 200 °C for 4 h. The reflux condenser was removed every 30 min to allow the escape of ethyl bromide. The crude mixture was then purified by silica gel column chromatography using a mixture of methylene chloride and acetone (9 : 1 v/v) as eluent. A clear liquid was obtained after drying under high vacuum (3.955 g, 69.8%). ^{1}H NMR δ (ppm, $CDCl_3$): 7.36-7.23 (m, aromatic, 5H), 4.51 (s, -OC*H*$_2$C-

, 2H), 4.17-3.98 (m, -P(OC*H*$_2$CH$_3$)$_2$, 4H), 3.79-3.65 (m, -OC*H*$_2$CH$_2$P-, 2H), 2.20-2.05 (m, -OCH$_2$C*H*$_2$P-, 2H), 1.28 (t, -P(OCH$_2$C*H*$_3$)$_2$, 6H). ^{13}C NMR δ (ppm, CDCl$_3$): 137.76 (aromatic), 128.28 (aromatic), 127.60 (aromatic), 72.89 (-O*C*H$_2$C-), 64.11 (-P(O*C*H$_2$CH-$_3$)$_2$), 61.46 (-O*C*H$_2$CH$_2$P-), 27.90 (-OCH$_2$*C*H$_2$P-), 16.33 (-P(OCH$_2$*C*H$_3$)$_2$).

The next step in the reaction was the removal of the benzyl protecting group. BnC2P (3.901 g, 11.69 mmol) and 10% palladium on carbon (0.309 g) were added to a 100 mL 3-necked round bottom flask and diluted with ethanol (40 mL). The flask was placed under an N_2 environment for 30 min before an H_2 balloon was attached through a syringe penetrating one of the reaction flask rubber septa. The N_2 was turned off and the mixture was bubbled with H_2 for 1 h via a needle. The air bleed was then removed and the system was left under H_2 environment for 3 d. The reaction mixture was passed through Celite® filtering agent to the remove palladium carbon catalyst and rinsed with methanol. The methanol was removed from the filtered solution, which was then diluted with DI H_2O and extracted 3 times with hexanes. The water layer was concentrated, and the product was purified by silica gel column chromatography by first using a mixture of hexane and methylene chloride (1 : 1 v/v) as eluent and later switching to a mixture of methylene chloride and methanol (1 : 1 v/v). After drying under high vacuum a yellow liquid was obtained (0.923 g, 35.3%). This product is designated HOC2P. ^{1}H NMR δ (ppm, CDCl$_3$): 4.20-4.06 (m, -P(OC*H*$_2$CH$_3$)$_2$, 4H), 3.95-3.85 (m, HOC*H*$_2$CH$_2$-, 2H), 2.61 (b, *H*O-, 1H), 2.11-2.00 (m, HOCH$_2$C*H*$_2$-, 2H), 1.34 (t, -P(OCH$_2$C*H*$_3$)$_2$, 6H). ^{13}C NMR δ (ppm, CDCl$_3$): 61.83 (-P(O*C*H$_2$CH$_3$)$_2$), 56.83 (HO*C*H$_2$CH$_2$P-), 29.59 (HOCH$_2$*C*H$_2$P-), 16.39 (-P(OCH$_2$*C*H$_3$)$_2$).

The last step in the synthesis of MAC2P was a reaction involving the alcohol group of HOC2P and methacryloyl chloride. HOC2P (0.854 g, 4.69 mmol) and triethylamine (0.689 g, 6.81 mmol) were added to a 50 mL 2-necked round bottom flask and diluted with methylene chloride (5 mL). The reaction flask was placed in an ice/water bath under an N_2 environment. Methacryloyl chloride (0.690 g, 6.69 mmol) was added to a vial and diluted with methylene chloride (5 mL). This solution was then transferred to an addition funnel equipped to the reaction flask and added dropwise to the stirring mixture. The reaction was allowed to proceed at room temperature for 20 h and monitored by ^{1}H NMR spectroscopy. The mixture was then further diluted with methylene chloride (15 mL), transferred to a separatory funnel, and washed with a saturated sodium bicarbonate solution three times. The organic layer was collected and dried over anhydrous sodium sulfate. Sodium sulfate was removed by gravity filtration, and the filtrate was concentrated by rotary evaporation. The crude mixture was purified by silica gel column chromatography using a mixture of ethyl acetate and hexanes (1 : 1 v/v) as eluent initially and later changing to pure ethyl acetate. Pure product was obtained as a yellow liquid after drying under high vacuum (0.696 g, 59.3 %). ^{1}H NMR δ (ppm, $CDCl_3$): 6.12 (s, $CH_3C=C\mathit{H}H'$-, 1H), 5.58 (s, $CH_3C=CH\mathit{H'}$-, 1H), 4.41-4.34 (m, -$OC\mathit{H}_2CH_2P$-, 2H) 4.17-4.06 (m, -$P(OC\mathit{H}_2CH_3)_2$, 4H), 2.24-2.15 (m, -$OCH_2\mathit{C}H_2P$-, 2H), 1.93 (s, $C\mathit{H}_3CC$=O-, 3H), 1.32 (t, -$P(OCH_2C\mathit{H}_3)_2$, 6H). ^{13}C NMR δ (ppm, $CDCl_3$): 167.02 ($CH_3C\mathit{C}$=O-), 136.00 ($CH_3\mathit{C}=CH_2$-), 125.90 ($CH_3C=\mathit{C}H_2$-), 61.83 (-$P(O\mathit{C}H_2CH_3)_2$), 58.90 (-$O\mathit{C}H_2CH_2P$-), 26.59 (-$OCH_2\mathit{C}H_2P$-), 18.21 ($\mathit{C}H_3C=CH_2$-), 16.37 (-$P(OCH_2\mathit{C}H_3)_2$).

3.2.6. Synthesis of CTA-Functionalized Silica Nanoparticles (CTA-NPs)

Two batches of CTA-NPs were prepared using similar procedures and are denoted CTA-NP-I and CTA-NP-II. The following procedure describes the synthesis of CTA-NP-I. MIBK-ST (3.469 g of a dispersion in MIBK with a concentration of 30 wt %, corresponding to 1.041 g of bare SiO_2 NPs) and CTA-silane (1.014 g, 2.048 mmol) was added to a 100 mL three-necked round bottom flask, followed by the addition of freshly distilled THF (40 mL). The flask was placed in a 70 °C thermostated oil bath and stirred for 90 h. A slight color change from yellow to dark orange was observed, but the solution remained transparent. The CTA-NPs were purified by four rounds of ultracentrifugation (Beckman Optima L-90K Ultracentrifuge with type 60 Ti rotor, 35k rpm, 1 h, 4 °C) and redispersion in THF. The obtained CTA-NPs (CTA-NP-I, 0.852 g) were dispersed in freshly distilled THF with a concentration of 90.1 mg/g and stored in the refrigerator prior to use.

3.2.7. Synthesis of Phosphonate-Functionalized Polymer Brush-Grafted Silica NPs

Two series of polymer brush-grafted, 23 nm silica NPs were synthesized by surface-initiated RAFT copolymerizations of MA-C13 with a phosphonate monomer, either StP or MAC11P, with molar feed ratios of 95:5, 90:10, 85:15, and 80:20. The hairy NPs were designated as PC13S or PC13C11P, where the S and C11P identify the phosphonate monomer used and the number following is the feed molar fraction. Similarly, a set of hairy silica NPs were prepared by SI-RAFT copolymerization of MA-C16 and MAC2P with molar ratios of 95:5, 90:10, 85:15, and 80:20 and were named in a similar fashion. The following describes the procedure used for the synthesis of PC13S-0.05 HNPs. All other

hairy NP samples were synthesized according to a similar procedure. MA-C13 (0.854 g, 3.18 mmol), StP (0.042 g, 0.165 mmol), CTA-COOH (0.031 g, 0.106 mmol), dimethylformamide (0.065 g), AIBN (0.272 g of a 10.4 mg/g AIBN stock solution in THF, corresponding to 2.83 mg, 0.017 mmol AIBN), and CTA-NP-I (1.107 g of a 90.1 mg/g CTA-NP-I stock solution in THF, corresponding to 99.7 mg of CTA-NP-I) were added to a 25 mL 2-necked round bottom flask and capped with a glass septum. The polymerization mixture was degassed by three rounds of freeze-pump-thaw and then stirred in a 70 °C oil bath for 20 h under an N_2 atmosphere. The polymerization was monitored by ^{1}H NMR spectroscopy. Note that most polymerizations went to ~100% conversion in 24 h. The flask was removed from the oil bath, and the mixture was diluted with THF (5 mL). The hairy NPs were isolated and purified by five rounds of ultracentrifugation (35k rpm, 1 h, 4 °C) and redispersion in THF. The decanted solution from the first round of ultracentrifugation contained the majority of the analogous free polymer. This free polymer solution was concentrated using a rotary evaporator and purified by three rounds of precipitation in methanol and redissolving in methylene chloride. The purified free polymer was analyzed by SEC to determine $M_{n,SEC}$ and Đ, and ^{1}H NMR spectroscopy was used to determine the actual content of phosphonate groups. For this sample, $M_{n,SEC}$ = 9.3 kDa and Đ = 1.67 (relative to PS standards), and the actual molar content of StP in the copolymer = 5.0 %. The purified HNPs were analyzed by TGA to determine the DP and the grafting density. This sample was found to have a grafting density = 0.46 chains/nm^2. The dispersions of this HNP sample in PAO with a concentration of 1 wt% HNP was prepared and found to be clear and stable at room temperature.

3.2.8. Preparation of 1.0 wt% Dispersions of Phosphonate-Functionalized Polymer Brush-Grafted Silica NPs in PAO

To test the dispersibility and stability of phosphonate-functionalized polymer brush-grafted silica NPs with varying compositions, 1 wt% HNP dispersions were prepared in PAO. The following procedure was used for the preparation of PC13S-0.05 NPs, all other HNP dispersions were prepared using similar procedures. PAO (1.043 g) was weighed in a vial, followed by the addition of a PC13S-0.05 NPs dispersion in THF (1.059 g, with a concentration of 9.8 mg/g, corresponding to 10.4 mg of HNPs). The PAO dispersion was thoroughly mixed before removing THF under an air stream initially and later under high vacuum to ensure complete removal of THF. The stability of HNPs in PAO at different temperatures was inspected visually, and optical photographs were taken of the dispersions at different temperatures.

3.3. Results and Discussion

3.3.1. Synthesis of Phosphonate-Functionalized Hairy NPs by SI-RAFT Copolymerization of MA-C13 with StP and Their Dispersibility in PAO

3.3.1.1 Synthesis of Phosphonate-Functionalized Monomer StP

To increase the function of oil-soluble polymer brush-grafted NPs, we aimed to introduce triboactive element phosphorus into the brushes of hairy NPs. For this purpose, we synthesized three different monomers that contain a phosphonate group and incorporated them into the polymer brushes by surface-initiated RAFT copolymerization with a methacrylate monomer containing a long alkyl pendant group, either MA-C13 or

MA-C16. The three phosphonate-functionalized monomers are diethyl (4-vinylbenzyl)phosphonate (StP), 11-(diethoxyphosphoryl)undecyl methacrylate (MAC11P), and 2-(diethoxyphosphoryl)ethyl methacrylate (MAC2P); their molecular structures are shown in Scheme 3.1. Monomer StP was synthesized through an Arbuzov reaction between 4-vinylbenzyl chloride and triethyl phosphite (Scheme 3.2). The monomer was purified by silica gel column chromatography using a mixture of hexanes and ethyl acetate (1 : 1, v/v) as eluent. The molecular structure was confirmed by ^{1}H and ^{13}C NMR spectroscopy, and the spectra are shown in Figure 3.1.

3.3.1.2. Synthesis of Phosphonate-Functionalized Hairy NPs by SI-RAFT Copolymerization of MA-C13 and StP

To study the effect of phosphonate content on the dispersibility in PAO and the tribological property of phosphonate-functionalized hairy NPs, SI-RAFT polymerization was employed to grow copolymer brushes of MA-C13 and StP from 23 nm silica nanoparticles at various molar ratios of the two monomers in the feed. The phosphonate group is highly polar, and the incorporation of StP into the brushes is expected to decrease the dispersibility of hairy NPs in PAO. For this reason, we chose to copolymerize StP with MA-C13. Note that poly(MA-C13) brush-grafted, 23 nm silica NPs (PC13 HNPs) have previously been shown to exhibit excellent dispersibility and long-term stability in PAO.[18] The molar feed ratio of MA-C13 and StP was varied from 95 : 5, 90 : 10, 85 : 15, and 80 : 20, and the corresponding hairy NPs are named as PC13S-0.05, -0.10, -0.15, and -0.20, where 0.05, 0.10, 0.15, 0.20 represent the StP molar contents in the feeds. A PC13 HNP sample was also synthesized from the same batch of CTA-NPs (CTA-NP-I) for

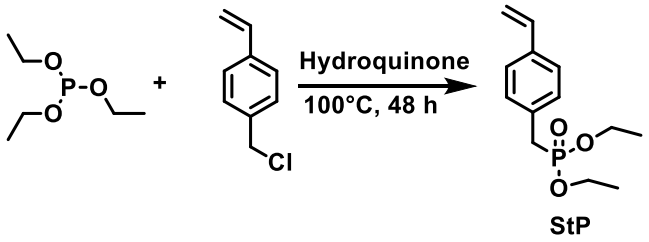

Scheme 3.2. Synthesis of Diethyl (4-Vinylbenzyl)phosphonate (StP).

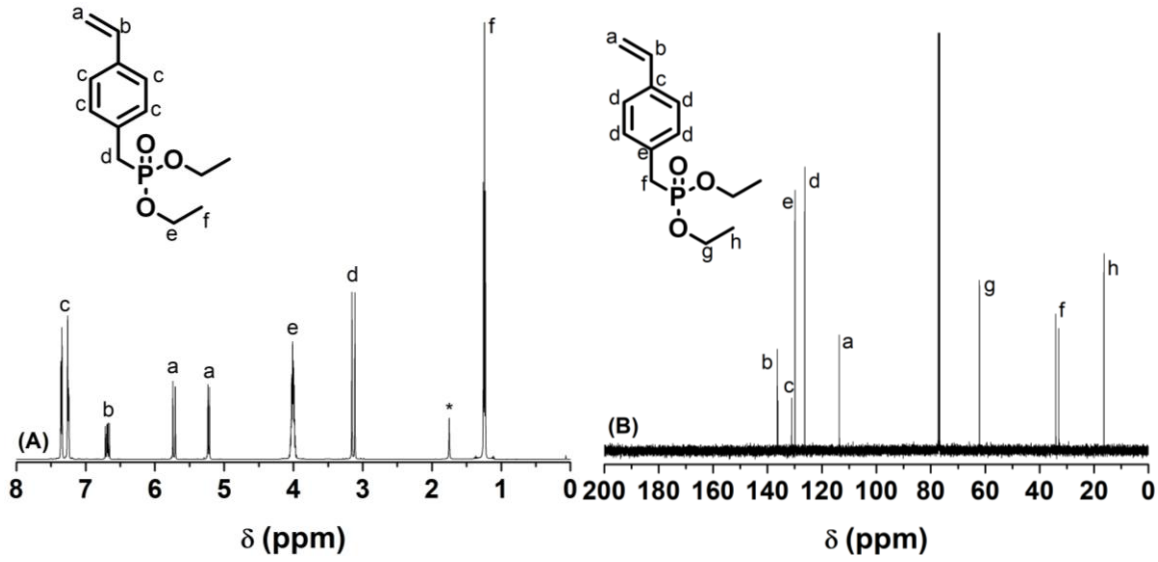

Figure 3.1. ^{1}H (A) and ^{13}C (B) NMR spectra of StP in $CDCl_3$.

comparison. We anticipated that a higher content of phosphonate would result in a better tribological property, but lead to decreased dispersibility and stability in the PAO base oil. Two batches of CTA-NPs were used in the synthesis of hairy NPs in the work presented in this chapter, but all StP-containing hairy NPs were synthesized from the same batch of CTA-NPs (CTA-NP-I). CTA-COOH was added into the polymerization mixtures as a free CTA to facilitate the characterization of polymer molecular weights and dispersities by creating analogous free polymers during the synthesis of hairy NPs. The polymerizations were monitored by ^{1}H NMR spectroscopy through the analysis of the vinyl peaks at 6.10 and 5.54 ppm for MA-C13 and 5.76, 5.70, 5.25, and 5.20 ppm for StP with the DMF (-N(CH_3)$_2$) peaks at 2.96 and 2.88 ppm as internal standard; all of the polymerizations went to about 100% conversion for both monomers in 20 h. The free polymer formed in the synthesis of PC13 HNPs was characterized by ^{1}H NMR spectroscopy (Figure 3.2A). The free copolymers of MA-C13 and StP formed during the synthesis of phosphonate-functionalized HNPs were separated by ultracentrifugation and purified by three rounds of precipitation in methanol. The purified free copolymers were characterized by ^{1}H NMR spectroscopy, and an increase in the intensity of the benzyl CH_2 peak at 3.06 ppm from StP monomer units was observed as the phosphonate content in the feed increased (Figures 3.3A, 3.4A, 3.5A, and 3.6A). The actual contents of StP monomer units in the copolymers were calculated from the ^{1}H NMR spectra of the purified free copolymers by using the peak at 3.18-2.99 ppm (-CCH_2P-) and the peaks at 4.24-3.52 ppm (-COOCH_2 of MA-C13 and -P(OCH_2CH$_3$)$_2$ from StP). The free polymers were all analyzed by size exclusion chromatography (SEC) using THF as eluent (Figures 3.2B, 3.3B, 3.4B, 3.5B, and 3.6B).

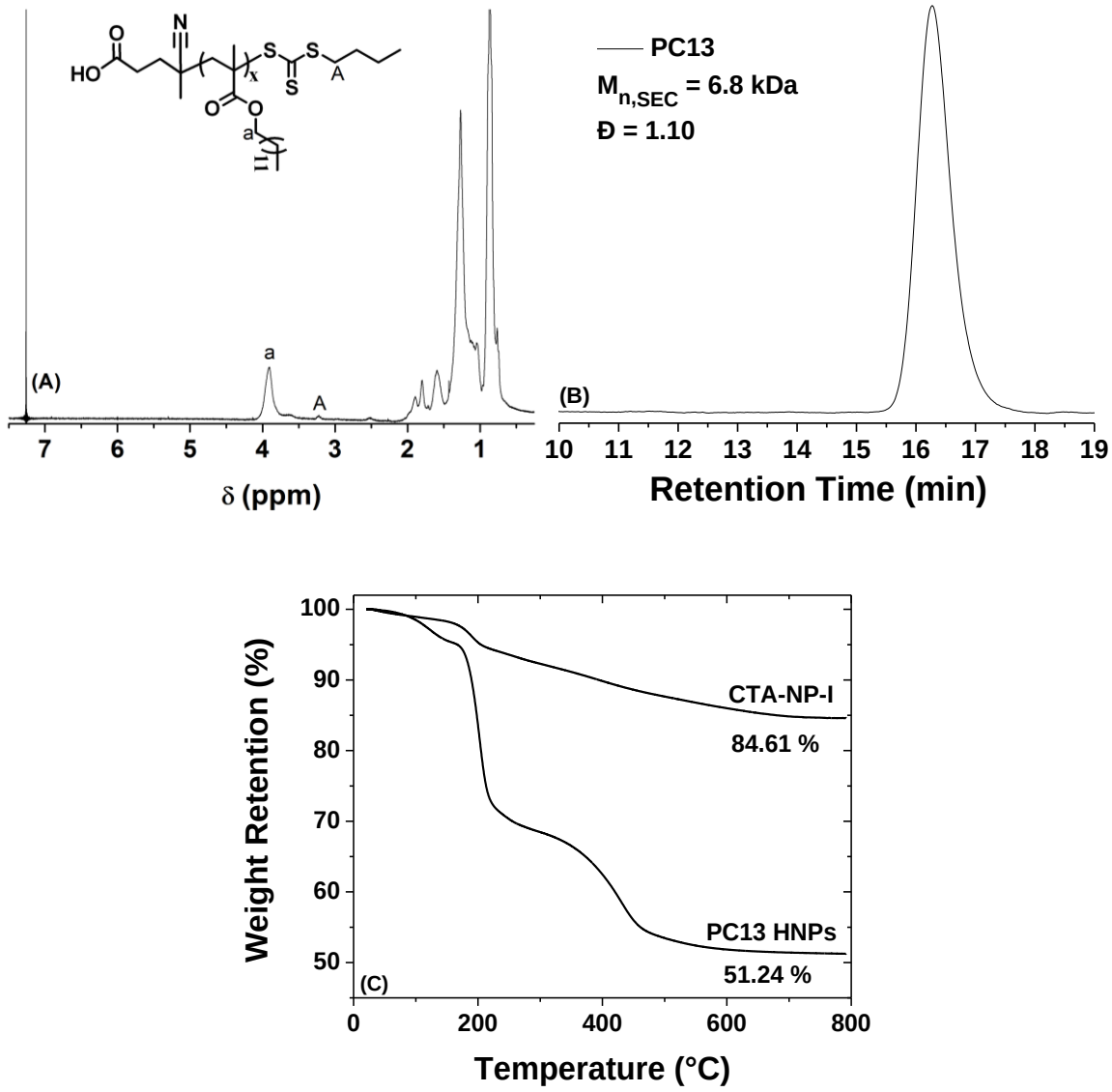

Figure 3.2. [1]H NMR spectrum of PC13 free polymer (A), SEC trace of PC13 free polymer (B), and TGA analysis of PC13 HNPs and CTA-NP-I (C).

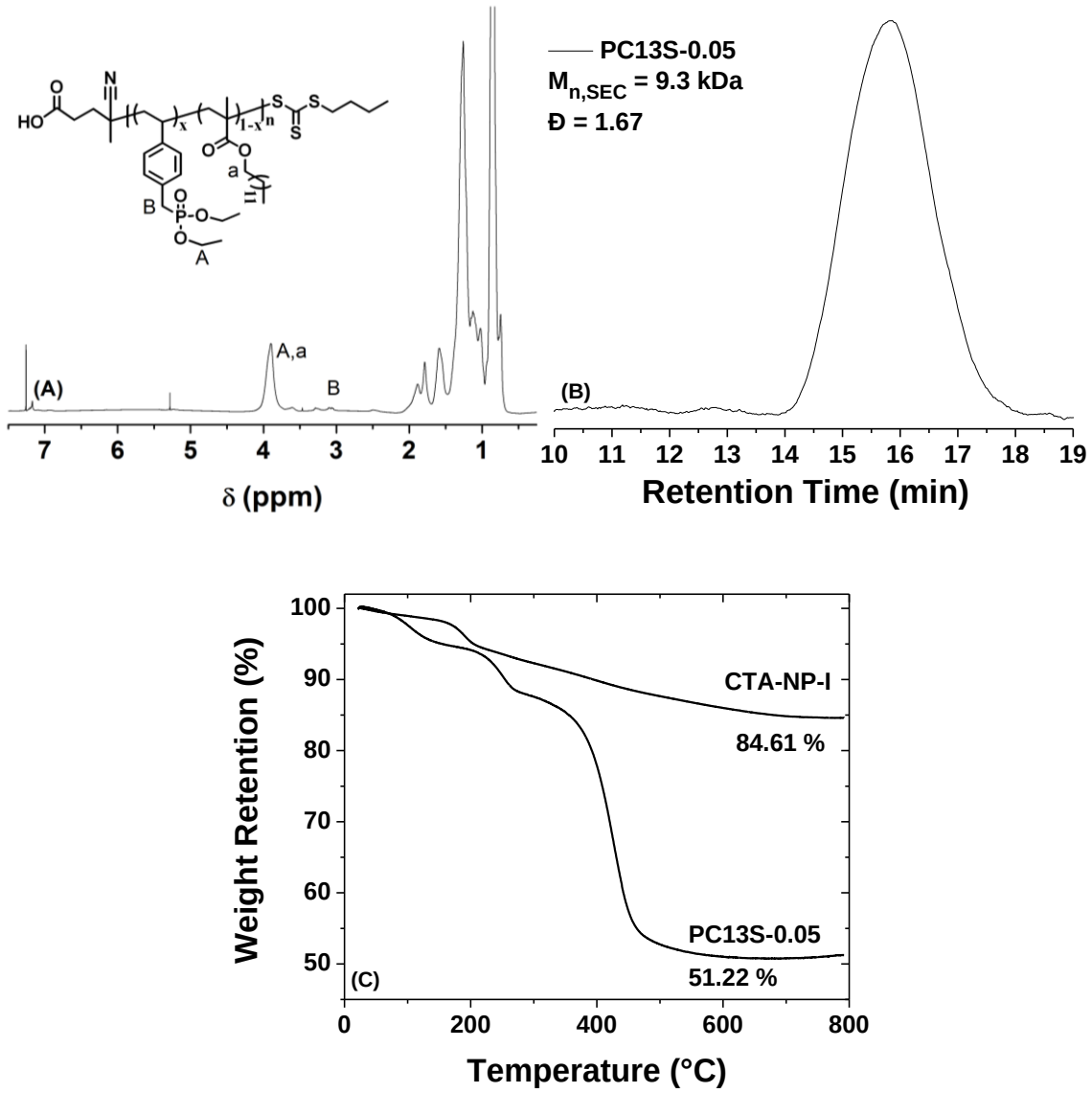

Figure 3.3. ^{1}H NMR spectrum of PC13S-0.05 free polymer (A), SEC trace of PC13S-0.05 free copolymer (B), and TGA analysis of PC13S-0.05 HNPs and CTA-NP-I (C).

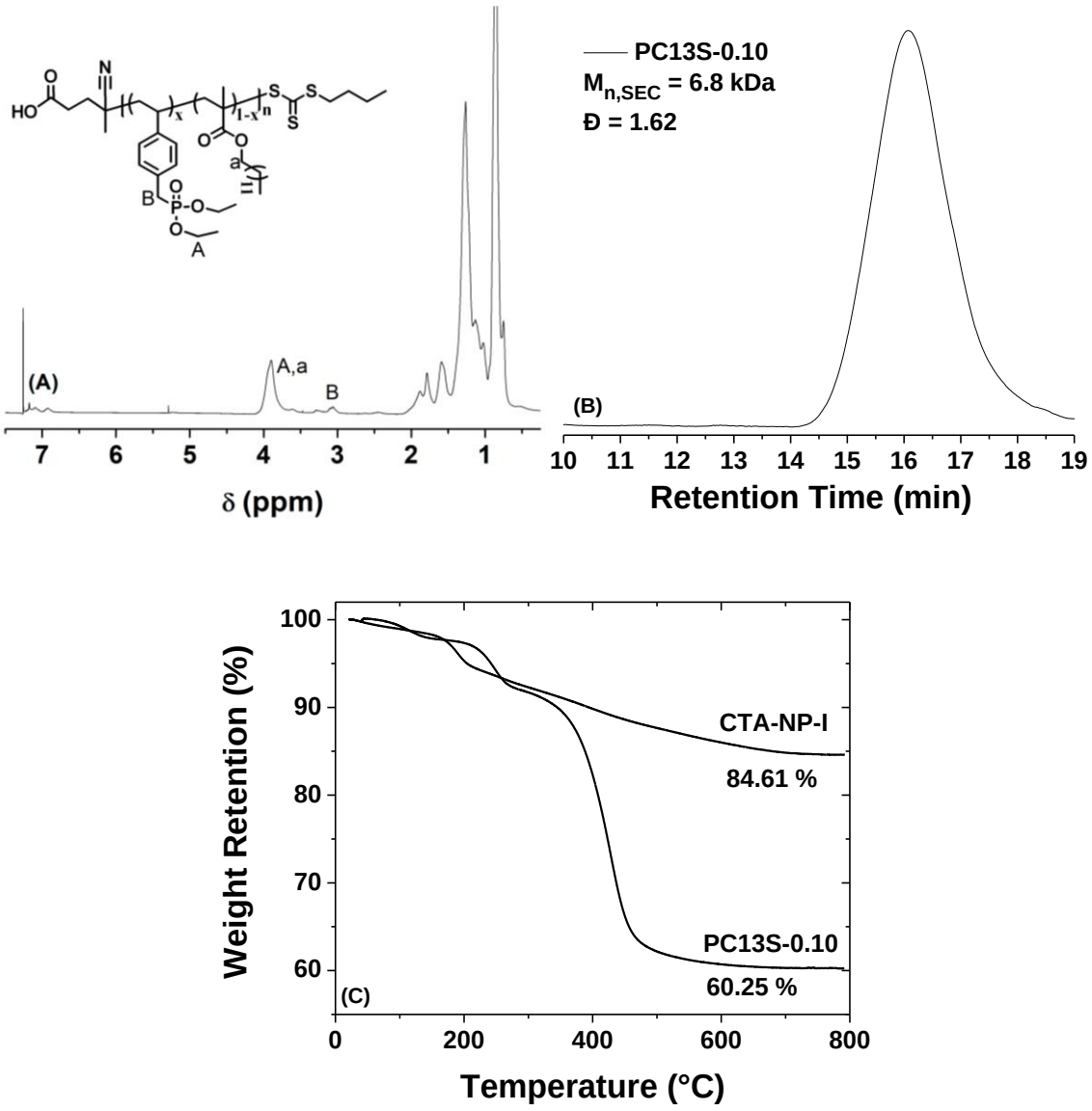

Figure 3.4. ^{1}H NMR spectrum of PC13S-0.10 free polymer (A), SEC trace of PC13S-0.10 free polymer (B), and TGA analysis of PC13S-0.10 HNPs and CTA-NP-I (C).

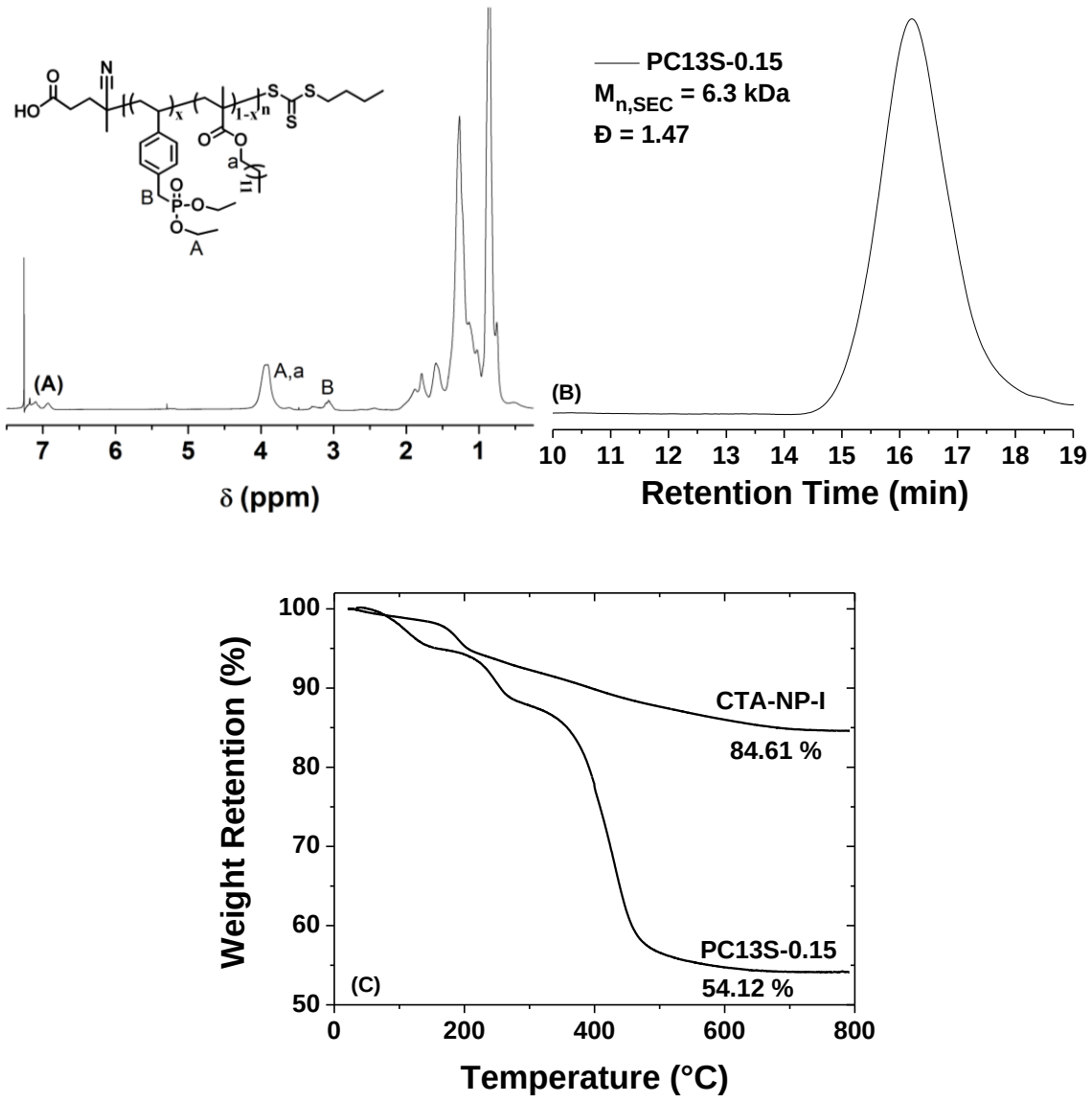

Figure 3.5. ^{1}H NMR spectrum of PC13S-0.15 free polymer (A), SEC trace of PC13S-0.15 free polymer (B), and TGA analysis of PC13S-0.15 HNPs and CTA-NP-I (C).

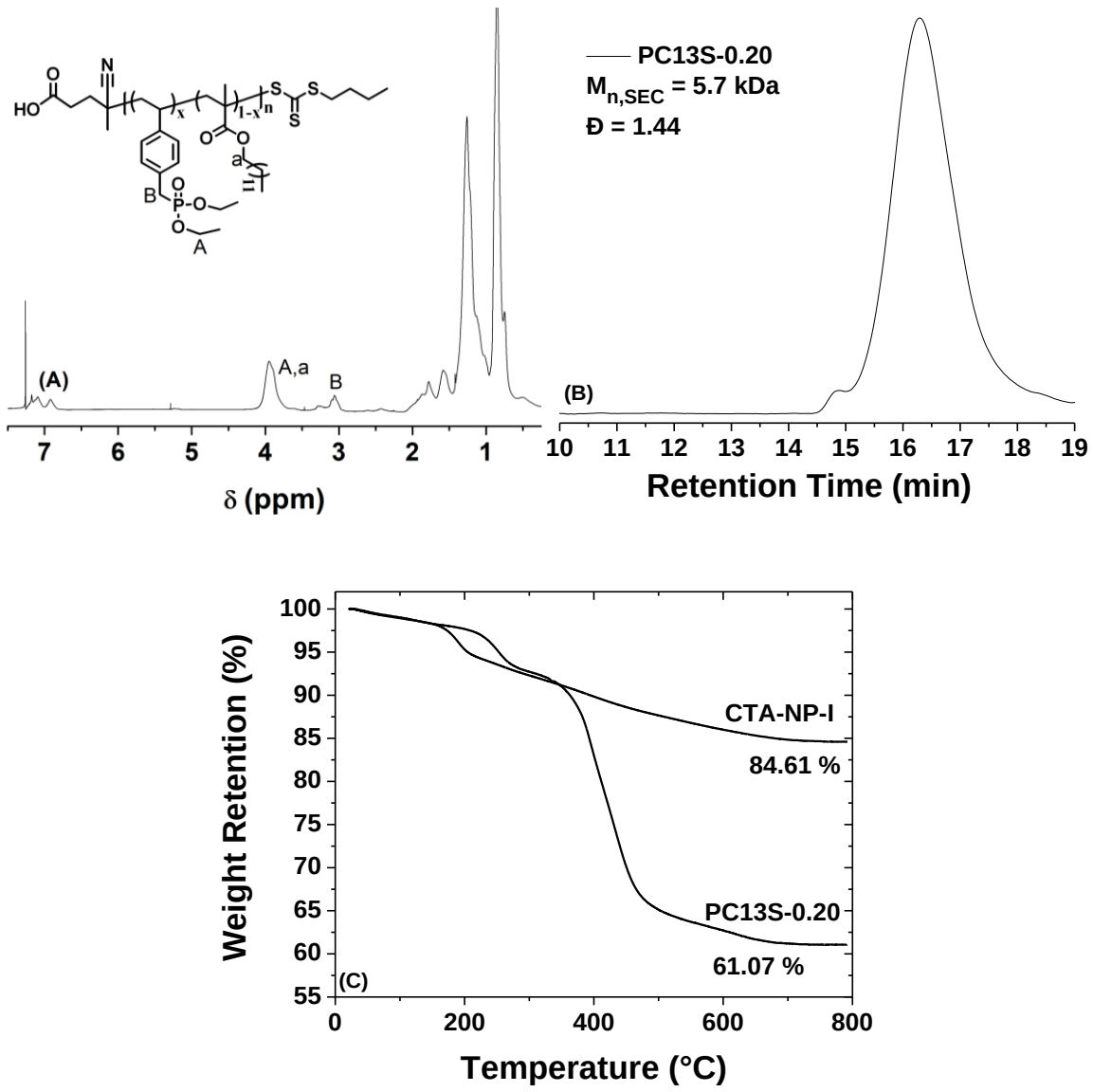

Figure 3.6. [1]H NMR spectrum of PC13S-0.20 free polymer (A), SEC trace of PC13S-0.20 free polymer (B), and TGA analysis of PC13S-0.20 HNPs and CTA-NP-I (C).

The molecular weights were found to be in the range of 5.7–9.3 kDa, with dispersities in the range of 1.44-1.67. High dispersities obtained in these copolymerizations were likely due to the electron withdrawing nature of phosphonate groups, which destabilizes the resulting StP radical. Lastly, the hairy NPs were characterized by thermogravimetric analysis (TGA) to determine the polymer brush contents (Figures 3.2C, 3.3C, 3.4C, 3.5C, and 3.6C). To calculate the DP and the grafting density of polymer brushes in each hairy NP sample, we assumed that the RAFT polymerization was controlled. The number of repeat units of each monomer in the copolymer was estimated by using the corresponding monomer conversion and the molar ratio of the monomer to the sum of free CTA and effective surface CTA as described in Chapter 2. By using the TGA data, the size of silica NPs (23 nm), and the actual molecular weight of the copolymer, the grafting density was calculated. The results are summarized in Table 3.1 along with other characterization data for all hairy NP samples and free copolymers.

3.3.1.3. Dispersibility and Stability of PC13S HNPs in PAO

To study the dispersibility and stability of PC13S HNPs in PAO, 1 wt% dispersions were prepared by adding calculated amounts of PAO and a dispersion of an HNP sample in THF into a 20 mL scintillation vial, mixing them thoroughly, and removing THF initially by air stream and then under high vacuum. All of the hairy NP samples except PC13S-0.20 were found to be dispersible at room temperature in PAO, forming clear and homogenous dispersions (Figure 3.7A). The mixture of PC13S-0.20 in PAO was cloudy at room temperature but became completely homogenous and clear upon heating to 80 °C. However, after being allowed to cool to room temperature, the dispersion turned cloudy

Table 3.1. Summary of Characterization Data for PC13S Hairy Silica NPs and Free Copolymers

Sample	Molar Content of StP in Feed (%)	StP Content in Copolymer by NMR (%)	StP Conversion (%)	MA-C13 Conversion (%)	$\overline{n}_{StP}$	$\overline{n}_{MA\text{-}C13}$	DP_{total}	Grafting Density (chains/nm^2)	$M_{n,SEC}$ (kDa)	Đ
PC13	N/A	N/A	N/A	99.8	N/A	30.2	30	0.44	6.8	1.10
PC13S-0.05	4.9	4.1	~100	~100	1.45	27.9	29	0.44	9.3	1.67
PC13S-0.10	10.0	9.6	~100	~100	3.07	27.6	31	0.28	6.8	1.62
PC13S-0.15	15.6	15.3	~100	~100	4.68	25.5	30	0.38	6.3	1.47
PC13S-0.20	20.8	21.3	~100	~100	6.57	25.1	32	0.26	5.7	1.44

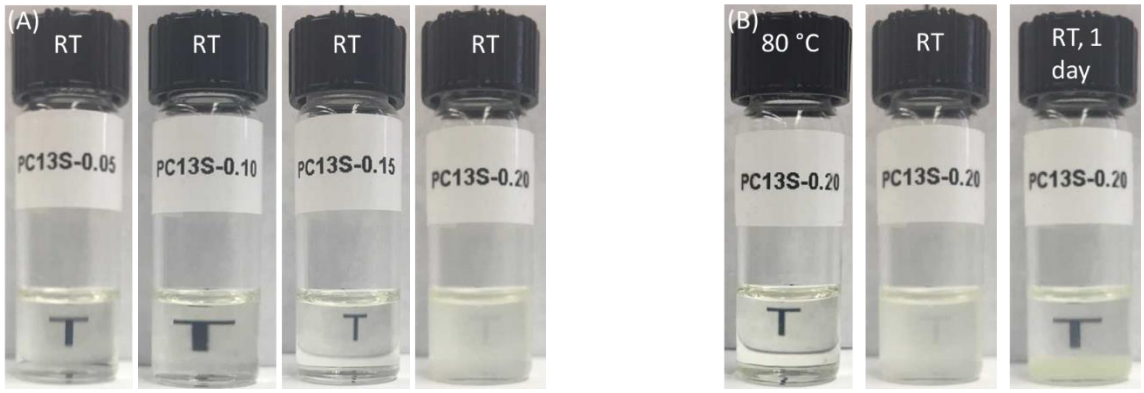

Figure 3.7. Optical images of dispersions of phosphonate-functionalized hairy NPs, PC13S-0.05, -0.10, -0.15, and -0.20, in PAO at room temperature (A), and the mixture of 1 wt% PC13S-0.20 in PAO at 80 °C, room temperature (RT), and after standing at room temperature for 1 day (B).

again, and the NPs precipitated out to the bottom of the vial after one day (Figure 3.7B). We plan to do tribological testing of the homogenous dispersions of PC13S HNPs in PAO to investigate the potential of these hybrid NPs as oil additives for friction and wear reduction.

3.3.2. Synthesis of Phosphonate-Functionalized Hairy NPs by SI-RAFT Copolymerization of MA-C13 with MAC11P and Their Dispersibility in PAO

3.3.2.1 Synthesis of Phosphonate-Functionalized Monomer MAC11P

The second monomer, MAC11P (Scheme 3.1), contained a long alkyl spacer between the C=C bond and the phosphonate group, which was designed to increase the hydrophobicity and thus possibly the dispersibility of hairy NPs in PAO. MAC11P is a methacrylate-type monomer, which is more suitable for copolymerization with MA-C13, a methacrylate, than StP, a styrenic monomer. The synthesis of MAC11P consists of four steps (Scheme 3.3), which started with the THP protection of 11-bromoundecan-1-ol, yielding THPC11Br. The THP protection of the alcohol group was necessary to minimize the side reaction of the alcohol group with triethyl phosphite in the Arbuzov reaction. The product from the Arbuzov reaction was purified and designated as THPC11P. The THP-protecting group was then removed using an acidic ion exchange resin, Amberlyst 15, in methanol, yielding HOC11P. The last step in the synthesis of this monomer is the reaction of HOC11P with methacryloyl chloride. The final product was purified by silica gel column chromatography using a mixture of methylene chloride and methanol (1 : 1 v/v) as eluent. ^{1}H and ^{13}C NMR spectra for MAC11P are shown in Figure 3.8, and the NMR spectra of intermediate products can be found in Appendix B (Figures B.1-B.3).

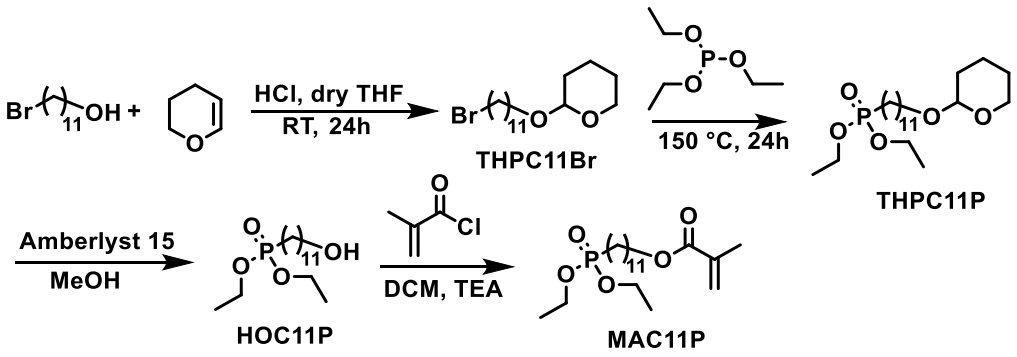

Scheme 3.3. Synthesis of 11-(Diethoxyphophoryl)undecyl Methacrylate (MAC11P).

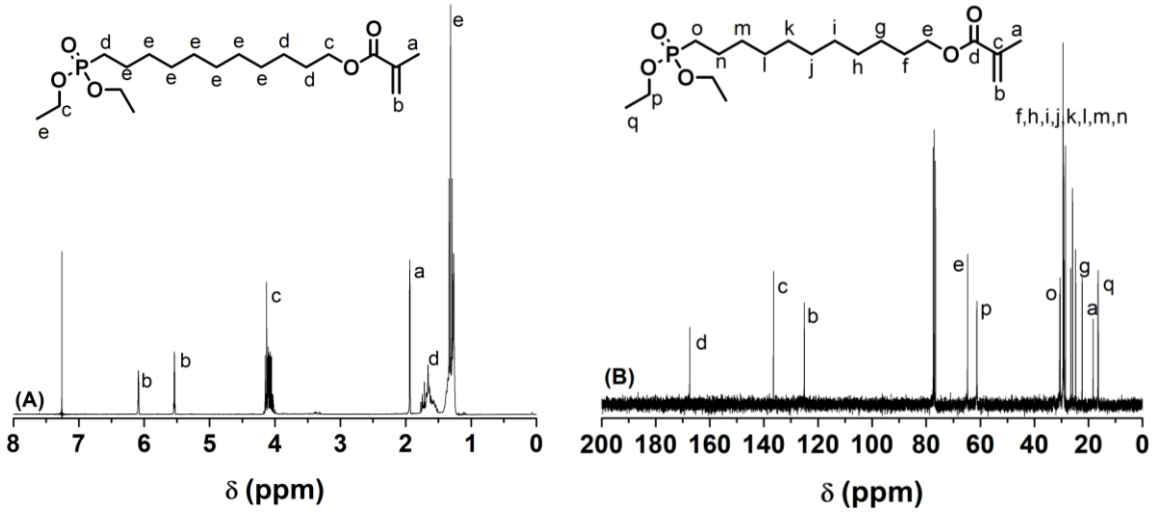

Figure 3.8. ^{1}H (A) and ^{13}C (B) NMR spectra of MAC11P in $CDCl_3$.

3.3.2.2. Synthesis of Phosphonate-Functionalized HNPs by SI-RAFT Copolymerization of MA-C13 and MAC11P

A series of hairy silica NPs were synthesized by using SI-RAFT copolymerization of MA-C13 and MAC11P with feed molar ratios of 95 : 5, 90 : 10, 85 : 15, and 80 : 20, which are designated as PC13C11P-0.05, -0.10, -0.15, and -0.20, respectively, similar to the naming of PC13S hairy NPs. All of these hairy NPs were prepared from the second batch CTA-NPs (CTA-NP-II). The polymerizations were monitored by ^{1}H NMR spectroscopy using the average integrals of vinyl peaks at 6.10 and 5.59 ppm relative to the average integral of the DMF peaks at 2.96 and 2.88 ppm (internal standard). Due to the vinyl peaks of the two monomers used in the copolymerizations being in the same position, the individual conversion for each monomer cannot be calculated separately; therefore the same conversion is assumed for both monomers. All polymerizations went to high conversions in 20 h. After the separation of hairy NPs and free polymer by ultracentrifugation, the free polymers were purified by precipitation in methanol and redissolving in methylene chloride three times. The purified free copolymers were analyzed by ^{1}H NMR spectroscopy (Figures 3.9A, 3.10A, 3.11A, and 3.12A), and an increase in the intensity of the ethoxy peaks from MAC11P monomer units can be seen with the increasing content of phosphonate in the feed. The actual contents of MAC11P monomer units in the copolymers were calculated from the ^{1}H NMR spectra of the purified free copolymers by using the peak at 4.15-4.04 ppm (-P(OCH_2CH$_3$)$_2$) and the peaks at 4.03-3.53 ppm (-COOCH_2 of MA-C13 and MAC11P). The purified free copolymers also were characterized by SEC (Figures 3.9B, 3.10B, 3.11B, and 3.12B), revealing similar molecular

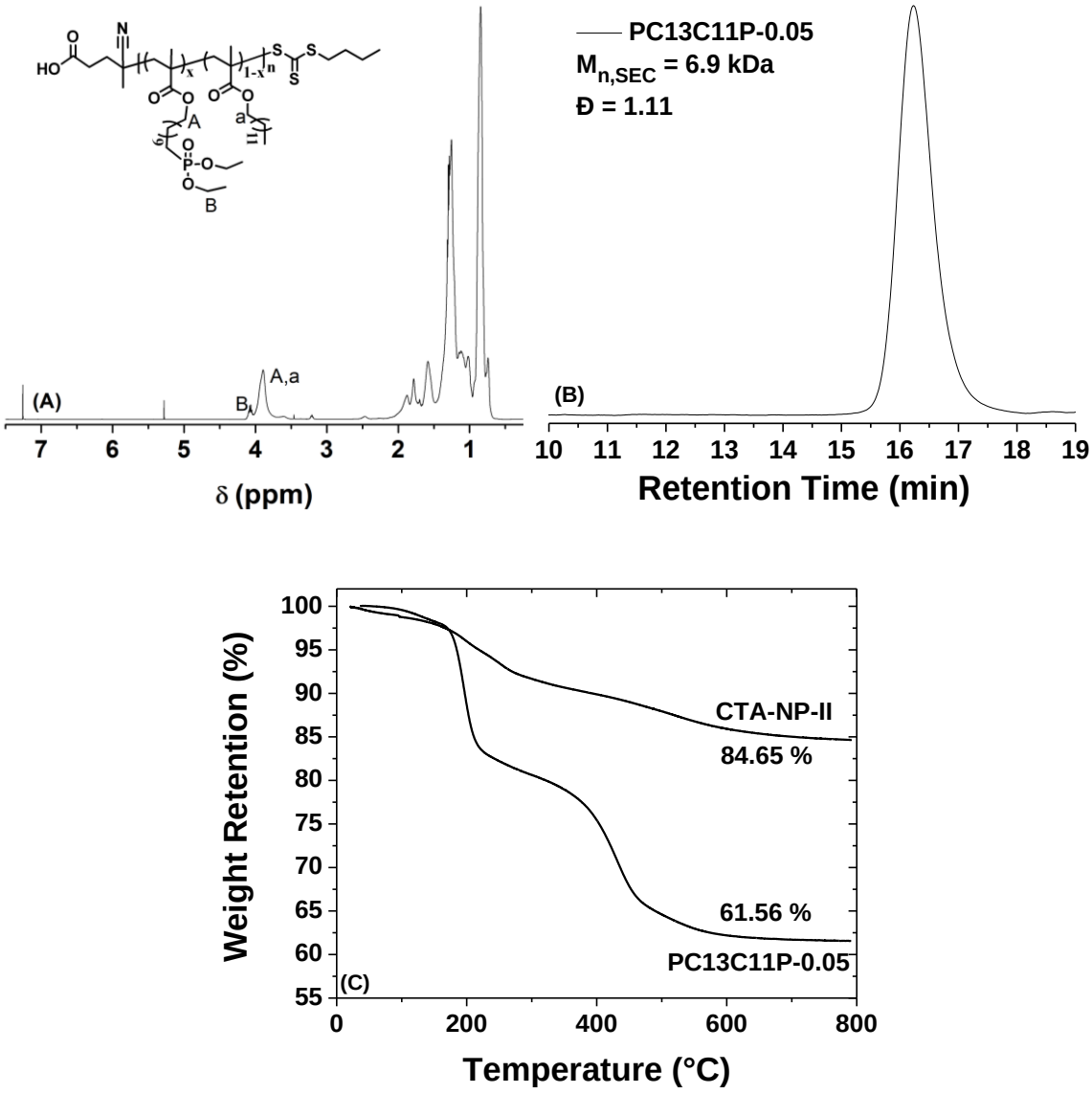

Figure 3.9. (A) ^{1}H NMR spectrum of PC13C11P-0.05 free polymer, (B) GPC trace of PC13C11P-0.05 free polymer using THF as eluent, and (C) TGA of PC13C11P-0.05 HNPs

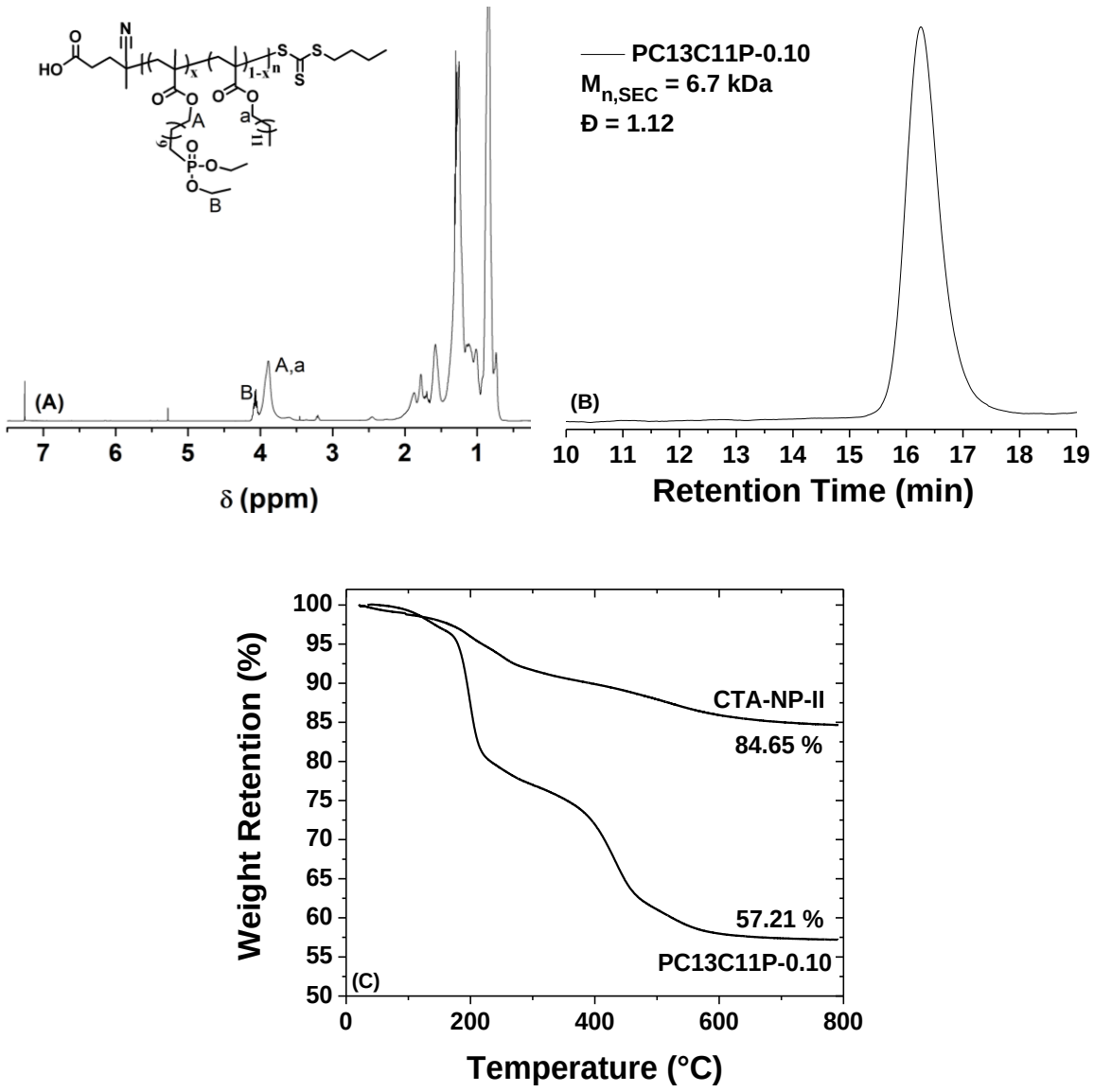

Figure 3.10. (A) ^{1}H NMR spectrum of PC13C11P-0.10 free polymer, (B) GPC trace of PC13C11P-0.10 free polymer using THF as eluent, and (C) TGA of PC13C11P-0.10 HNPs.

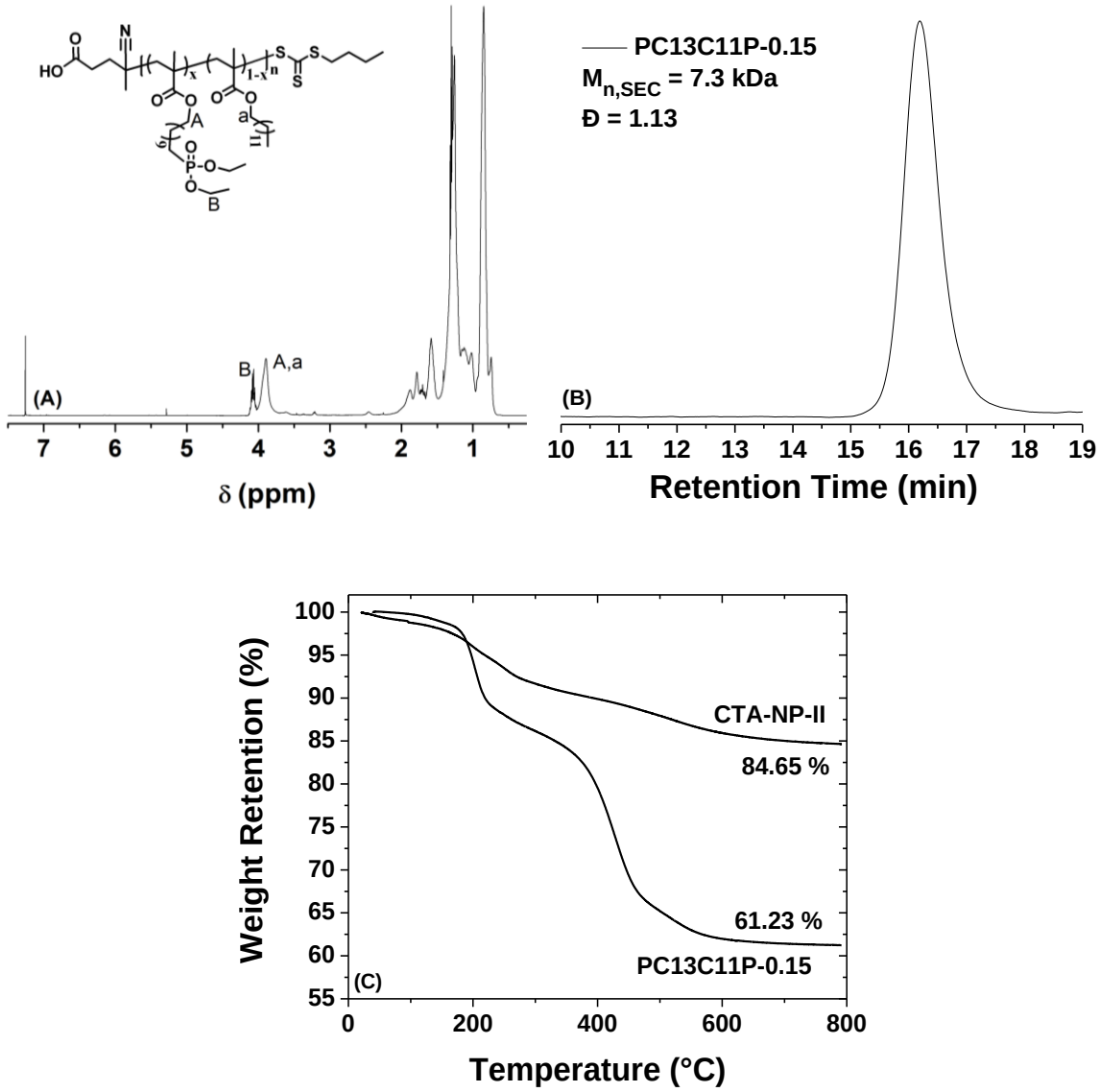

Figure 3.11. (A) ^{1}H NMR spectrum of PC13C11P-0.15 free polymer, (B) GPC trace of PC13C11P-0.15 free polymer, and (C) TGA of PC13C11P-0.15 HNPs.

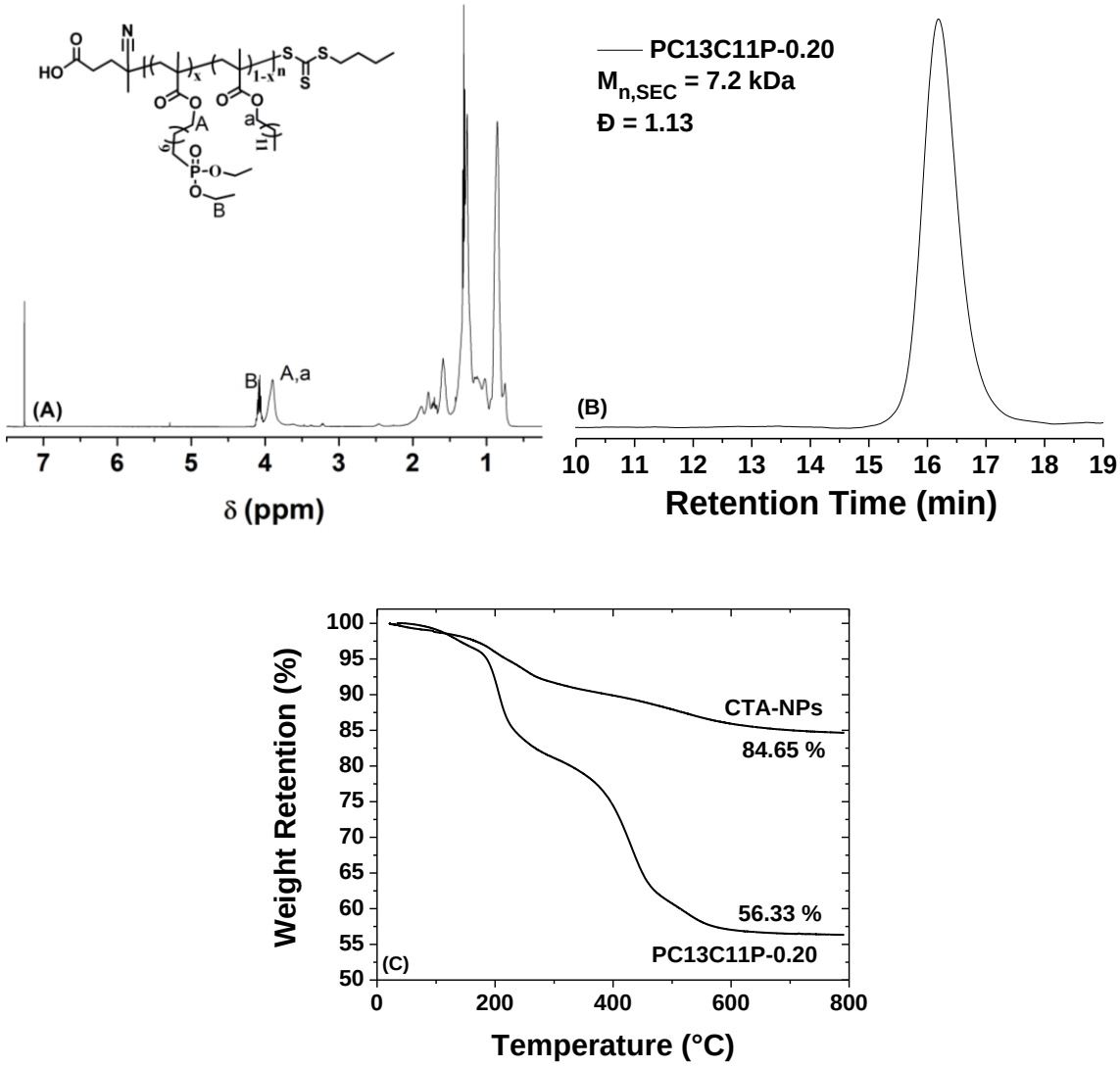

Figure 3.12. (A) ^{1}H NMR spectrum of PC13C11P-0.20 free polymer, (B) GPC trace of PC13C11P-0.20 free polymer, and (C) TGA of PC13C11P-0.20 HNPs.

weights in the range of 6.7-7.3 kDa and narrows dispersities of 1.11-1.13. The purified PC13C11P HNPs were analyzed by TGA (Figures 3.9C, 3.10C, 3.11C, and 3.12C), and the grafting densities were found to be similar in the range of 0.25 - 0.33 chains/nm^2, and DPs were 30 or 31 for all samples. All characterization data for PC13C11P HNPs and free copolymers are summarized in Table 3.2.

3.3.2.3. Dispersibility and Stability Studies of PC13C11P HNPs

Dispersions of PC13C11P HNPs in PAO with a concentration of 1 wt% were prepared using the same procedure as described for PC13S HNPs. Surprisingly, all of the PC13C11P dispersions were found to be cloudy at room temperature to varying degrees (Figure 3.13A). After storage at room temperature for one day, all of the hairy NPs precipitated out (Figure 3.13B). Even with heating to 80 °C, none of these hairy NPs samples formed a homogenous dispersion. These observations are totally different from our original design of incorporating a longer alkyl spacer to increase the dispersibility of hairy NPs in PAO. Likely this is because a longer spacer made the phosphonate group more exposed, leading to stronger interactions between phosphonate groups. As such, we further designed and synthesized MAC2P, which has a much shorter alkyl spacer. The phosphonate groups are expected to be better shielded from each other by the longer alkyl pendant group of the comonomer in the brushes of hairy NPs.

Table 3.2. Summary of Characterization Data for PC13C11P Hairy Silica NPs and Free Copolymers

Sample	Molar Content of MAC11P in Feed (%)	MAC11P Content in Copolymer by NMR (%)	MAC11P Conversion (%)	MA-C13 Conversion (%)	$\overline{n}_{MAC11P}$	$\overline{n}_{MA-C13}$	DP_{total}	Grafting Density (chains/nm^2)	$M_{n,SEC}$ (kDa)	Đ
PC13C11P-0.05	5.4	5.0	98.6	98.6	1.67	29.5	31	0.25	6.9	1.11
PC13C11P-0.10	10.3	10.0	95.6	95.6	3.07	26.8	30	0.33	6.7	1.12
PC13C11P-0.15	14.5	14.9	~100	~100	4.54	26.8	31	0.25	7.3	1.13
PC13C11P-0.20	21.0	20.2	98.7	98.7	6.55	24.7	31	0.32	7.2	1.13

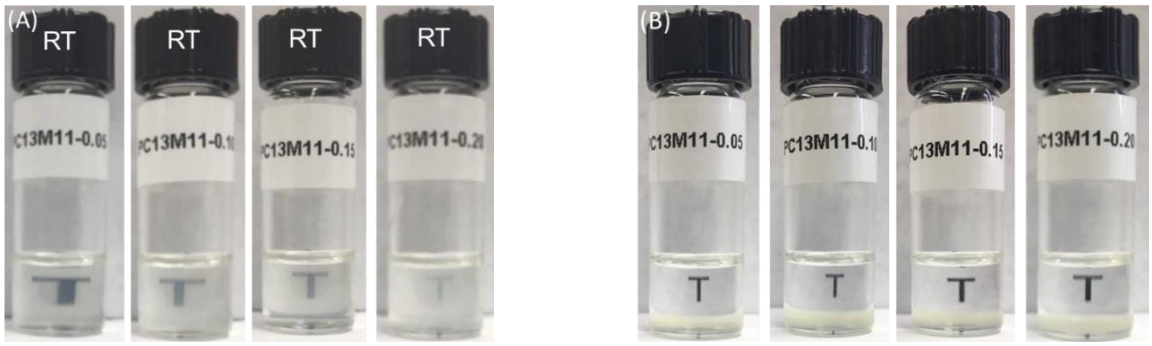

Figure 3.13. Optical images of PC13M11P hairy NPs in PAO with a concentration of 1 wt% at room temperature (A) and after standing at room temperature for one day (B).

3.3.3. Synthesis of Phosphonate-Functionalized HNPs by SI-RAFT Copolymerization of C16MA with MAC11P and Their Dispersibility in PAO

3.3.3.1 Synthesis of Phosphonate-Functionalized Monomer MAC2P

The third monomer, MAC2P, is also a methacrylate-type monomer but with a shorter alkyl spacer (2 methylene groups) between the vinyl group and the phosphonate group. As discussed in the preceding section, the much shorter spacer likely would increase the dispersibility of hairy NPs in PAO due to the increased shielding of phosphonate groups. The synthesis of MAC2P was also a multiple-step process (Scheme 3.4), which began with an Arbuzov reaction between benzyl 2-bromoethyl ether and triethyl phosphite, yielding BnC2P. The next step is the removal of the benzyl group of BnC2P using H_2 (g) with a palladium catalyst to yield HOC2P. The final step of the synthesis of MAC2P is the reaction of HOC2P with methacryloyl chloride. The product, MAC2P, was purified by column chromatography using a mixture of ethyl acetate and hexanes (1 : 1 v/v) as eluent and the molecular structure was confirmed by ^{1}H and ^{13}C NMR spectroscopy (Figure 3.14). The NMR spectroscopy data of the intermediate compounds can be found in Appendix B (Figures B.4 and B.5).

3.3.3.2. Synthesis of Phosphonate-Functionalized Hairy NPs by SI-RAFT Copolymerization of MA-C16 with MAC2P

The third set of phosphonate-functionalized hairy NPs were synthesized by SI-RAFT copolymerization of MA-C16 and MAC2P with molar ratios of 95 : 5, 90 : 10, 85 : 15, 80 : 20 in the feeds. The HNP samples were denoted as PC16C2P-0.05, -0.10, -0.15, and -0.20, where 0.05, 0.10, 0.15, and 0.20 are the molar ratios of MAC2P used in the

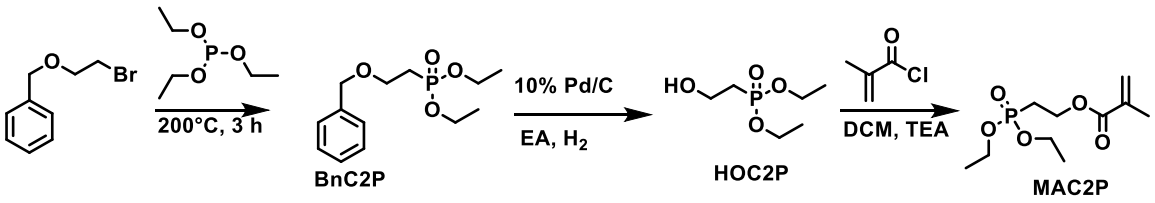

Scheme 3.4. Synthesis of 2-(Diethoxyphosphoryl)ethyl Methacrylate (MAC2P).

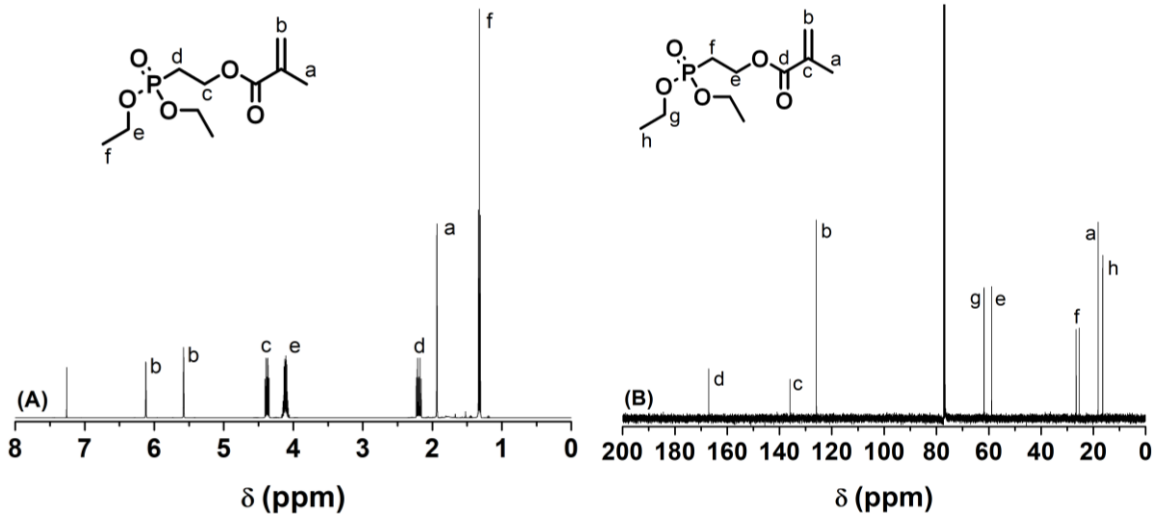

Figure 3.14. ^{1}H (A) and ^{13}C (B) NMR spectra of MAC2P in $CDCl_3$.

polymerization. A poly(MA-C16) homopolymer (PC16) brush-grafted NP sample was also synthesized for comparison. For this set of hairy NPs, we used MA-C16, which has a longer alkyl pendant than MA-C13, in an attempt to further shield phosphonate groups for each other. Similar to the synthesis of other phosphonate-functionalized HNPs described above, CTA-COOH was added into the polymerization mixtures as a free CTA to form an analogous free polymer. The monomer conversions were monitored by ^{1}H NMR spectroscopy using the average integral of the vinyl peaks located at 6.13 and 5.59 ppm for MAC2P and 6.10 and 5.54 ppm for MA-C16 relative to the DMF peaks at 2.96 and 2.8 ppm (added as internal standard). All polymerizations went to high conversions for both monomers (90.3 - ~100%) in 20 h. The resulting free polymers and HNPs were separated by ultracentrifugation. An attempt to purify the free copolymers by precipitation in methanol was unsuccessful, so the actual phosphonate content was calculated from the molar feed ratio used in the copolymerization. The free copolymers were characterized by SEC (Figures 3.15A, 3.16A, 3.17A, 3.18A, 3.19A) and similar molecular weights in the range of 8.3-9.5 kDa and narrow dispersities of 1.11-1.15 were observed. The purified hairy NPs were analyzed by TGA (Figures 3.15B, 3.16B, 3.17B, 3.18B, and 3.19B). The number of repeat units of each monomer in the copolymer and the grafting density were calculated as described earlier. The grafting densities of PC16C2P-0.05, PC16C2P-0.10, and PC16C2P-0.15 were found to be in the range of 0.31-0.36 chains/nm^2, while PC16C2P-0.20 had a lower grafting density (0.17 chains/nm^2). The total DPs for all free polymers were similar and in the range of 28-31. The characterization data for PC16 and PC16C2P hairy NPs and free copolymers are summarized in Table 3.3.

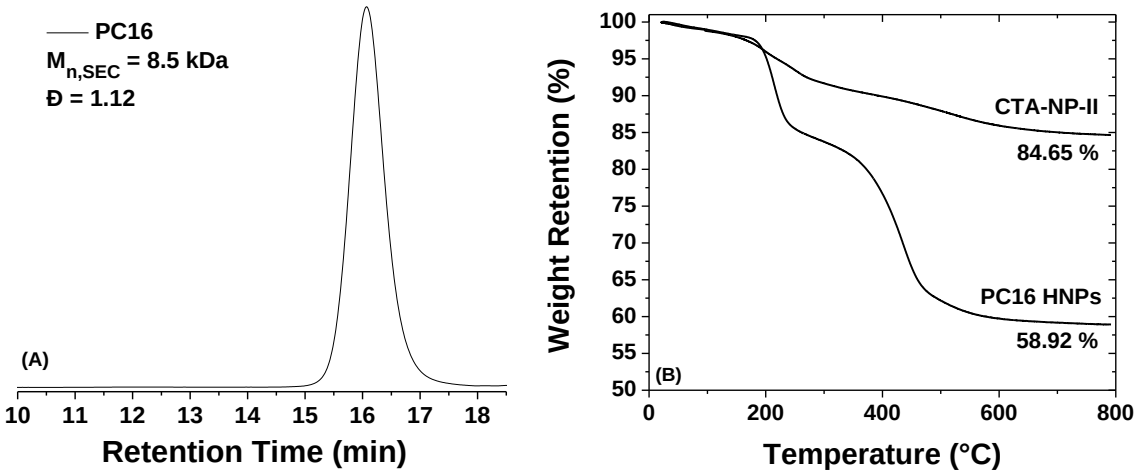

Figure 3.15. (A) GPC trace of PC16 free polymer and (B) TGA of PC16 HNPs.

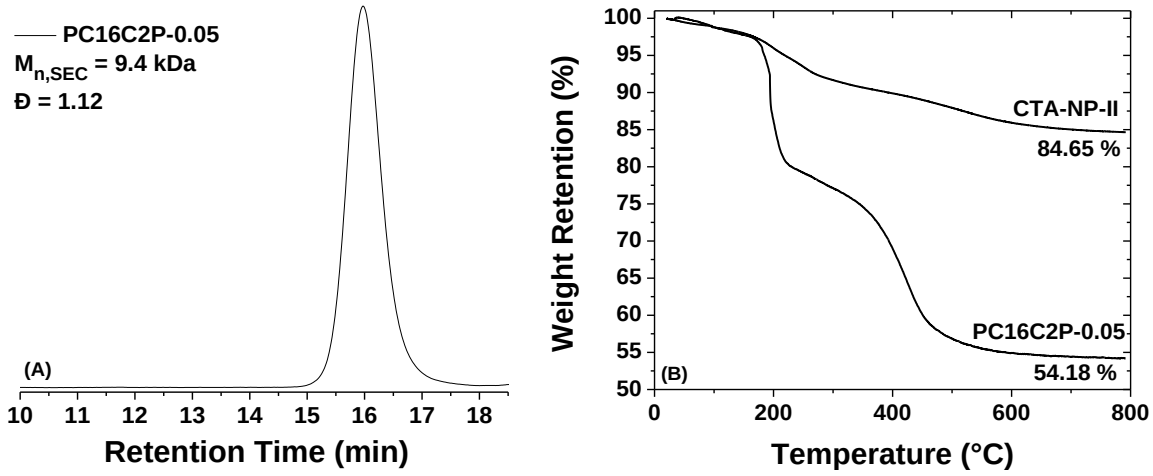

Figure 3.16. (A) GPC trace of PC16C2P-0.05 free polymer and (B) TGA of PC16C2P-0.05 HNPs.

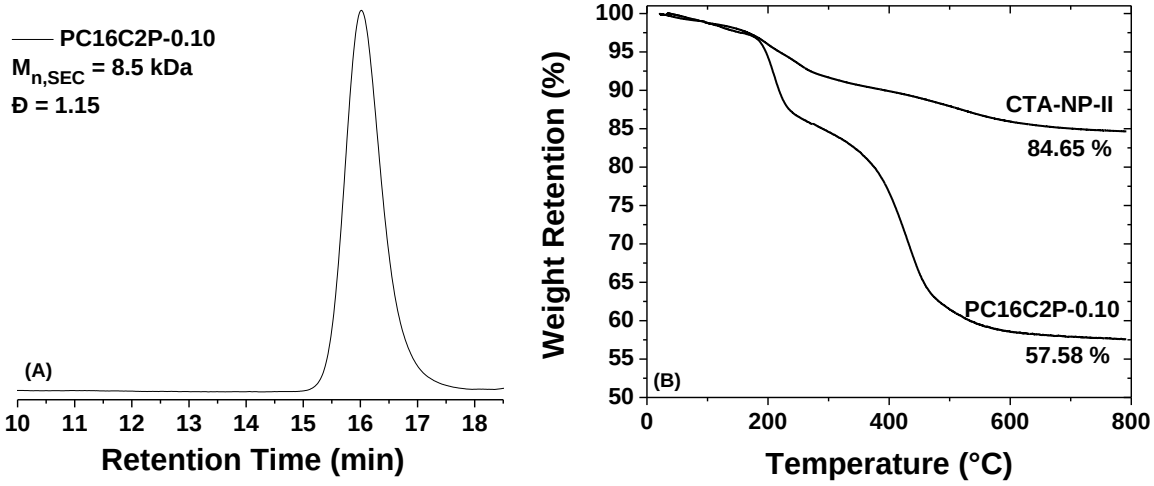

Figure 3.17. (A) GPC trace of PC16C2P-0.10 free polymer and (B) TGA of PC16C2P-0.10 HNPs.

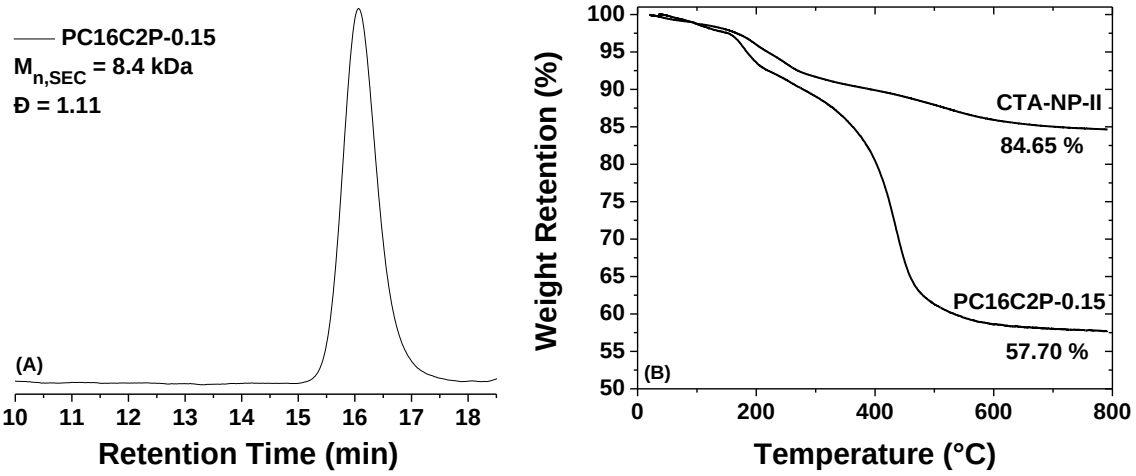

Figure 3.18. (A) GPC trace of PC16C2P-0.15 free polymer and (B) TGA of PC16C2P-0.15 HNPs.

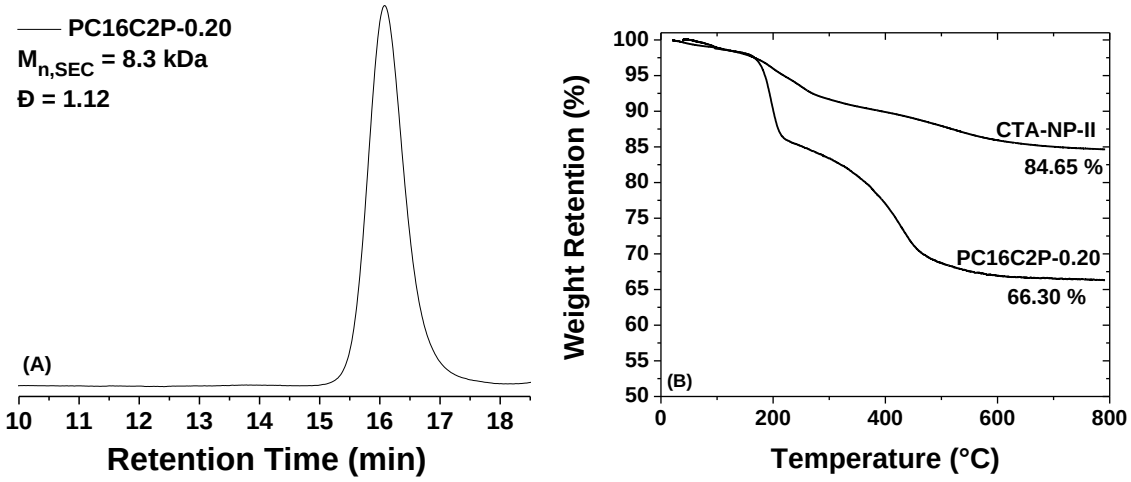

Figure 3.19. (A) GPC trace of PC16C2P-0.20 free polymer and (B) TGA of PC16C2P-0.20 HNPs.

Table 3.3. Summary of Characterization Data for PC16C2P Hairy Silica NPs and Free Copolymers

Sample	Molar Content of MAC2P in Feed (%)	MAC2P Conversion (%)	MA-C16 Conversion (%)	$\bar{n}_{MAC2P}$	$\bar{n}_{MA\text{-}C16}$	DP_{total}	Grafting Density (chains/nm^2)	$M_{n,SEC}$ (kDa)	Đ
PC16	N/A	N/A	97.7	N/A	29.4	29	0.28	8.5	1.12
PC16C2P-0.05	5.5	~100	98.2	1.61	27.0	29	0.36	9.4	1.12
PC16C2P-0.10	10.1	94.8	94.5	2.91	25.7	29	0.31	8.5	1.15
PC16C2P-0.15	15.5	92.4	90.3	4.40	23.4	28	0.32	8.4	1.11
PC16C2P-0.20	20.9	98.0	96.4	6.49	24.3	31	0.17	8.3	1.12

3.3.3.3. Dispersibility and Stability Studies of PC16C2P HNPs in PAO

To test the dispersibility of PC16C2P HNPs in PAO, 1 wt% dispersions of PC16C2P-0.05, -0.10, -0.15, and -0.20 were prepared using a procedure similar to those for other phosphonate-functionalized HNPs described earlier. Unlike the other two sets of phosphonate-functionalized hairy NPs, all of the four PC16C2P HNP samples were fully dispersed and stable at room temperature (Figure 3.20). From these observations, it appears that more MAC2P can be copolymerized into the brushes while keeping HNPs dispersible and stable in PAO. We will study the lubricating properties of these functionalized hairy silica NPs.

3.4. Conclusions

Three sets of phosphonate-containing hairy silica NPs were synthesized from CTA-functionalized, 23 nm silica NPs by SI-RAFT copolymerization of a methacrylate with a long alkyl pendant with either StP, MAC11P, or MAC2P. For StP and MAC11P copolymerization, MA-C13 was used as the comonomer, while MA-C16 was used for the copolymerization with MAC2P. For each set of hairy NPs, the molar ratio of the comonomer and the phosphonate-functionalized monomer was varied from 100 : 0, 95 : 5, 90 : 10, 85 :15, and 80 : 20. For PC13S HNPs, when the StP molar content was 15% or below, the hairy NPs can be dispersed in PAO at room temperature and formed homogenous, clear dispersions. When the StP molar content was 20%, the hairy NPs formed a cloudy mixture with PAO at room temperature. Surprisingly, all of the PC13C11P

Figure 3.20. Optical images of dispersions of PC16C2P-0.05, -0.10, 0-.15, and -0.20 in PAO at a concentration of 1 wt% at room temperature.

hairy NPs formed cloudy mixtures with PAO at a concentration of 1 wt%, likely because a longer alkyl spacer made the phosphonate groups more exposed and thus enhanced their interactions. For this reason, we further synthesized a methacrylate monomer, MAC2P, with a shorter alkyl spacer and copolymerized it with MA-C16. All of PC16C2P hairy NPs were dispersible in PAO at 1 wt% at room temperature. These results are promising. We will study the lubricating properties of these phosphonate-functionalized hairy NPs in the future.

References

1. Chen, Y.; Renner, P.; Liang, H. Dispersion of Nanoparticles in Lubricating Oil: A Critical Review. *Lubricants* **2019,** 7(1), 7.
2. Dai, W.; Kheireddin, B.; Gao, H.; Liang, H. Roles of nanoparticles in oil lubrication. *Tribol. Int.* **2016,** *102*, 88-98.
3. Gulzar, M.; Masjuki, H. H.; Kalam, M. A.; Varman, M.; Zulkifli, N. W. M.; Mufti, R. A.; Zahid, R. Tribological performance of nanoparticles as lubricating oil additives. *J. Nanopart. Res.* **2016,** *18* (8), 223.
4. Kalin, M.; Kogovšek, J.; Remškar, M. Mechanisms and improvements in the friction and wear behavior using MoS_2 nanotubes as potential oil additives. *Wear* **2012,** *280-281*, 36-45.
5. Rabaso, P.; Ville, F.; Dassenoy, F.; Diaby, M.; Afanasiev, P.; Cavoret, J.; Vacher, B.; Le Mogne, T. Boundary lubrication: Influence of the size and structure of inorganic fullerene-like MoS_2 nanoparticles on friction and wear reduction. *Wear* **2014,** *320*, 161-178.
6. Kim, D.; Archer, L. A. Nanoscale Organic-Inorganic Hybrid Lubricants. *Langmuir* **2011,** *27* (6), 3083-3094.
7. Li, B.; Wang, X.; Liu, W.; Xue, Q. Tribochemistry and antiwear mechanism of organic-inorganic nanoparticles as lubricant additives. *Tribol. Lett.* **2006,** *22* (1), 79-84.
8. Li, D.; Xie, Y.; Yong, H.; Sun, D. Surfactant-assisted preparation of Y2O3-stabilized ZrO_2 nanoparticles and their tribological performance in mineral and commercial lubricating oils. *RSC Adv.* **2017,** *7* (7), 3727-3735.

9. Spikes, H. Friction Modifier Additives. *Tribol. Lett.* **2015,** *60* (1), 5.
10. Wu, Y. Y.; Tsui, W. C.; Liu, T. C. Experimental analysis of tribological properties of lubricating oils with nanoparticle additives. *Wear* **2007,** *262* (7), 819-825.
11. Bao, C.; Horton, J. M.; Bai, Z.; Li, D.; Lodge, T. P.; Zhao, B. Stimuli-triggered phase transfer of polymer-inorganic hybrid hairy particles between two immiscible liquid phases. *J. Polym. Sci., Part B: Polym. Phys.* **2014,** *52* (24), 1600-1619.
12. Barbey, R.; Lavanant, L.; Paripovic, D.; Schüwer, N.; Sugnaux, C.; Tugulu, S.; Klok, H.-A. Polymer Brushes via Surface-Initiated Controlled Radical Polymerization: Synthesis, Characterization, Properties, and Applications. *Chem. Rev.* **2009,** *109* (11), 5437-5527.
13. Pyun, J.; Matyjaszewski, K. Synthesis of Nanocomposite Organic/Inorganic Hybrid Materials Using Controlled/"Living" Radical Polymerization. *Chem. of Mater.* **2001,** *13* (10), 3436-3448.
14. Li, D.; Sheng, X.; Zhao, B. Environmentally Responsive "Hairy" Nanoparticles: Mixed Homopolymer Brushes on Silica Nanoparticles Synthesized by Living Radical Polymerization Techniques. *J. Am. Chem. Soc.* **2005,** *127* (17), 6248-6256.
15. Wright, R. A. E.; Wang, K.; Qu, J.; Zhao, B. Oil-Soluble Polymer Brush Grafted Nanoparticles as Effective Lubricant Additives for Friction and Wear Reduction. *Angew. Chem., Int. Ed.* **2016,** *55* (30), 8656-8660.
16. Seymour, B. T.; Wright, R. A. E.; Parrott, A. C.; Gao, H.; Martini, A.; Qu, J.; Dai, S.; Zhao, B. Poly(alkyl methacrylate) Brush-Grafted Silica Nanoparticles as Oil Lubricant

Additives: Effects of Alkyl Pendant Groups on Oil Dispersibility, Stability, and Lubrication Property. *ACS Appl. Mater. Interfaces* **2017,** *9* (29), 25038-25048.

17. Moad, G.; Chong, Y. K.; Postma, A.; Rizzardo, E.; Thang, S. H. Advances in RAFT polymerization: the synthesis of polymers with defined end-groups. *Polymer* **2005,** *46* (19), 8458-8468.
18. Seymour, B. T.; Fu, W.; Wright, R. A. E.; Luo, H.; Qu, J.; Dai, S.; Zhao, B. Improved Lubricating Performance by Combining Oil-Soluble Hairy Silica Nanoparticles and an Ionic Liquid as an Additive for a Synthetic Base Oil. *ACS Appl. Mater. Interfaces* **2018,** *10* (17), 15129-15139.

Appendix B

for

Chapter 3. Synthesis of Phosphonate-Functionalized Polymer Brush-Grafted Silica Nanoparticles as Oil Lubricant Additive for Friction and Wear Reduction

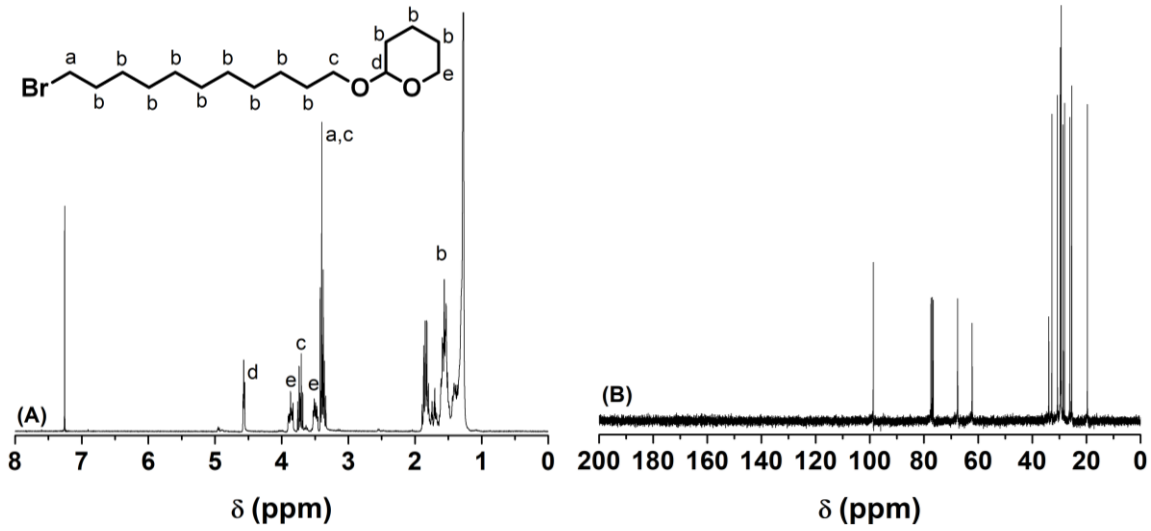

Figure B1. ^{1}H (A) and ^{13}C (B) NMR spectra of THPC11Br in $CDCl_3$.

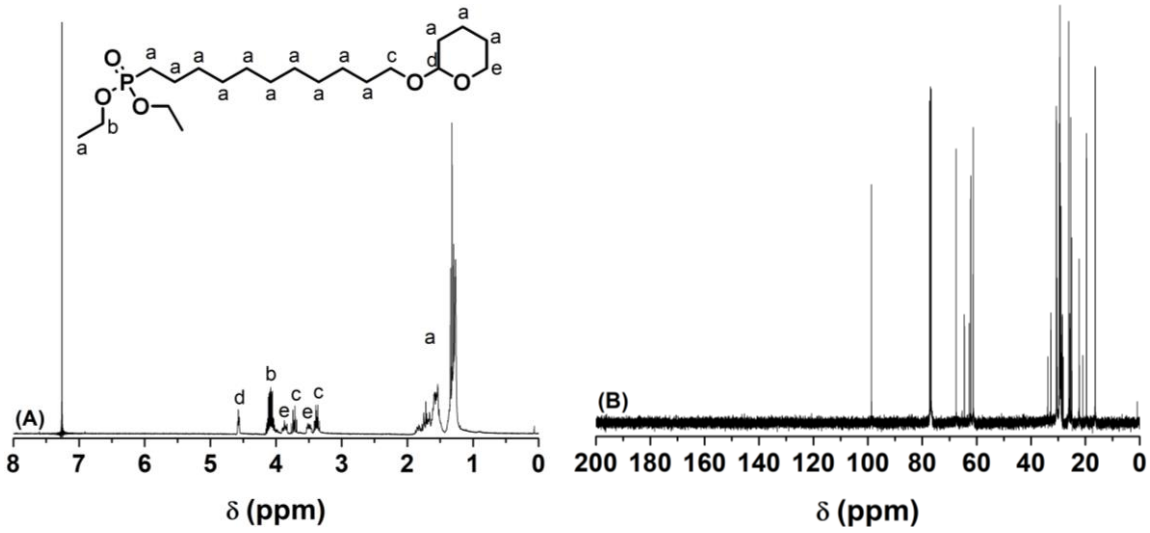

Figure B2. ^{1}H (A) and ^{13}C (B) NMR spectra of THPC11P in $CDCl_3$.

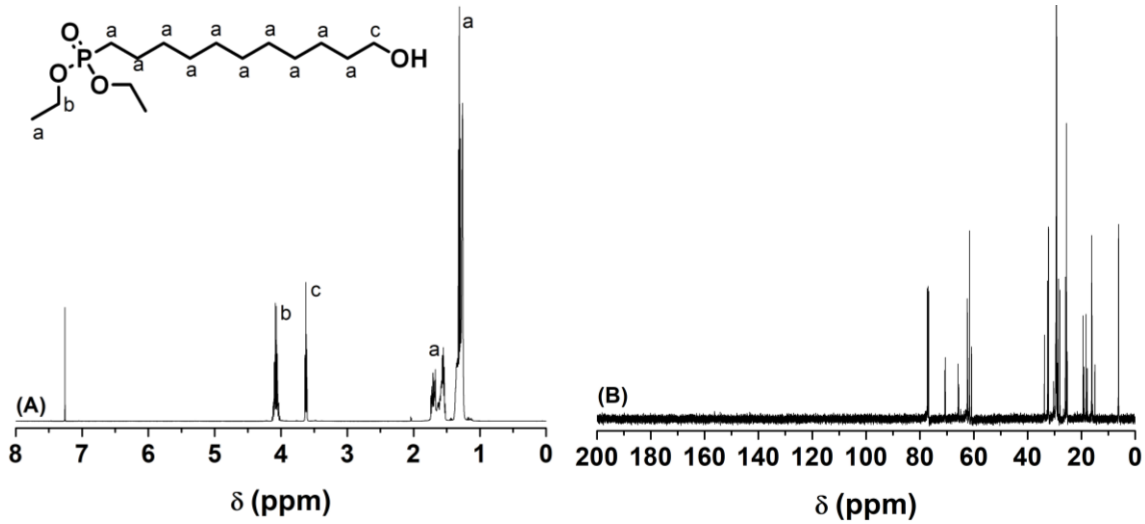

Figure B3. ^{1}H (A) and ^{13}C (B) NMR spectra of HOC11P in $CDCl_3$.

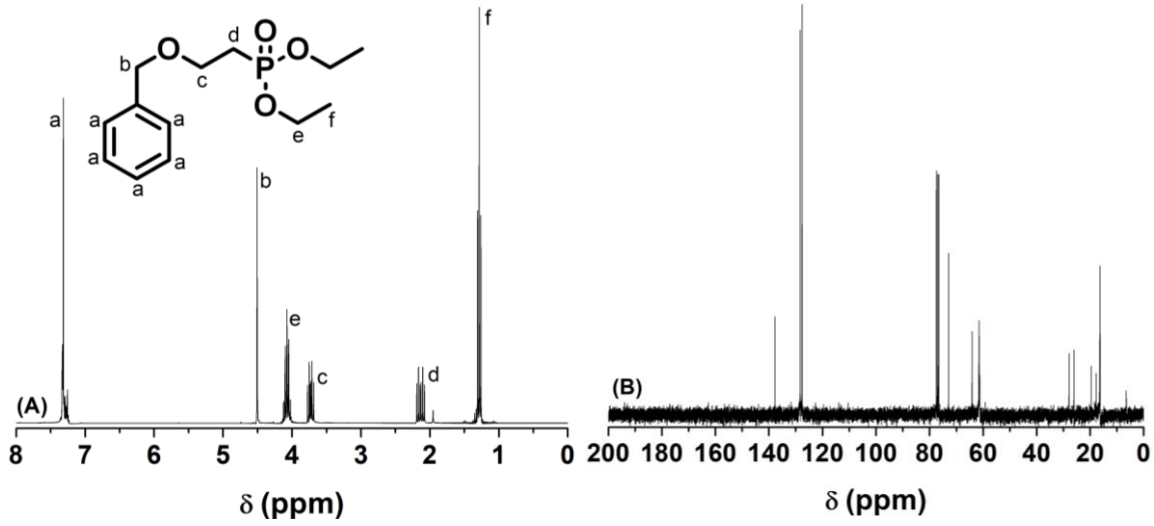

Figure B4. ^{1}H (A) and ^{13}C (B) NMR spectra of BnC2P in $CDCl_3$.

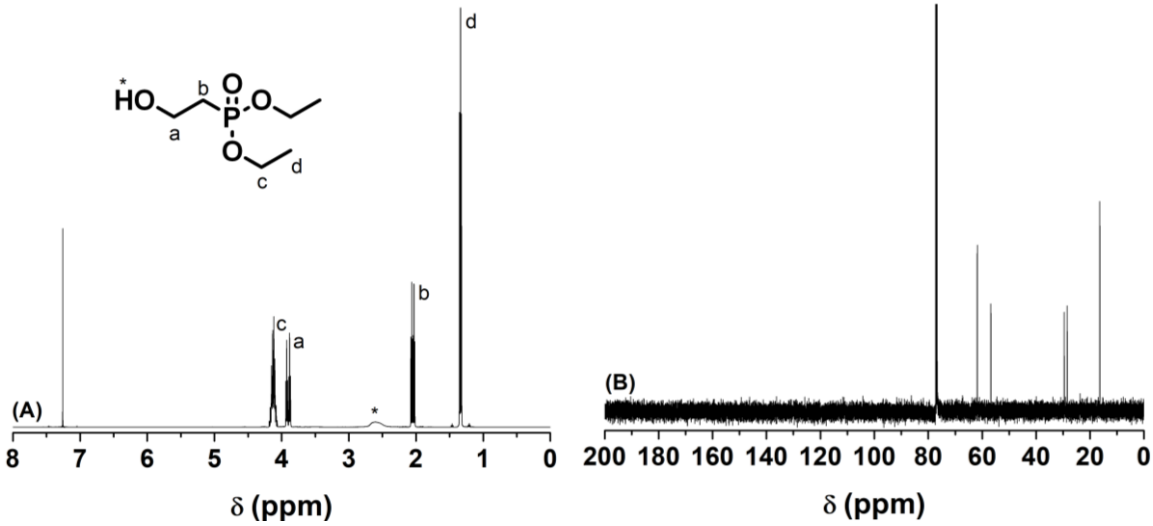

Figure B5. ^{1}H (A) and ^{13}C (B) NMR spectra of HOC2P in $CDCl_3$.

Chapter 4. Improved Lubricating Performance by Combining Oil-Soluble Hairy Silica Nanoparticles and an Ionic Liquid as an Additive for a Synthetic Base Oil

Abstract

This chapter presents a finding of improved lubricating performance by combining oil-soluble poly(lauryl methacrylate) brush-grafted silica nanoparticles (hairy NPs or HNP) and an oil-miscible phosphonium-phosphate ionic liquid (IL) as a friction reducing additive for a polyalphaolefin (PAO) oil. The HNP was synthesized by surface-initiated reversible addition-fragmentation chain transfer polymerization. At a total concentration of 2 wt% and sufficiently high individual concentrations for HNP and IL in PAO, high contact stress, ball-on-flat reciprocating tribological tests showed that the friction decreased by up to 23% compared with 2% HNP alone in PAO and by up to 35% compared to the PAO mixed with 2% IL. Scanning electron microscopy-energy dispersive X-ray spectroscopy (SEM-EDS) and X-ray photoelectron spectroscopy (XPS) analysis revealed that the tribofilm formed from the PAO containing 1% HNP + 1% IL was enriched with both Si and P, indicating that both hairy NPs and IL were involved in the tribo-chemical reactions. In addition, the O 1s and Si 2p peaks in the core-level XPS spectra exhibited significant shifts for the mixture of 1% HNP + 1% IL compared to those for 2% HNP, suggesting the possible formation of new covalent bonds. These results indicated that hairy silica NPs and IL reacted with each other and also with the metal substrate during the rubbing process, which likely strengthened the tribofilm and its bonding with the substrate and thus further improved the lubrication.

4.1. Introduction

Lubrication plays an indispensable role in machinery, for it not only improves mechanical systems' durability by reducing friction and wear but also increases energy efficiency.[1-6] An example is the lubrication of wind turbines. Generally, there are three lubrication regimes for mechanical systems: boundary regime where the asperities of two rubbing surfaces come into contact and collide with each other, hydrodynamic/elastohydrodynamic regime where sliding surfaces are fully separated by a continuous lubricating oil film, and mixed regime, an intermediate regime between boundary and hydrodynamic where only the tallest asperities from opposing surfaces occasionally make contact.[1-4] A lubricant usually is composed of base oil and multiple additives with different functionalities, including anti-oxidant, viscosity modifier, anti-wear, friction modifier, detergent, dispersant, anti-foam, etc.[5-9]

Ionic liquids (ILs),[10-15] particularly oil-miscible ionic liquids,[7,13-15] and nanoparticles (NPs)[16-29] are two promising classes of additives for friction reduction and wear protection that have been intensively studied in recent years. ILs are molten salts with relatively low melting points, often below room temperatures, due to the large ions involved.[11,15,30] They possess many intriguing characteristics, such as no or extremely low volatility, high thermal and chemical stability, wide electrochemical window, etc.[30] Since Ye et al. first explored the use of ILs as lubricants,[10] extensive studies have been conducted on the tribological properties of various ILs.[10-15] In particular, oil-miscible phosphonium-phosphate ILs,[13-15] have shown effective anti-scuffing and anti-wear characteristics in addition to significant friction reduction, which was attributed to the physical adsorption

of anions and the tribofilm formation on metallic surfaces. For example, addition of 1.04% tetraoctylphosphonium bis(2-ethylhexyl) phosphate ([P8888][DEHP]) into a low viscosity gas-to-liquid 4 cSt (GTL 4) base oil prevented scuffing and resulted in a decrease in total wear volume by 91.5% and a reduction of the average steady-state friction coefficient by ~ 10% compared to GTL 4 when tested in a ball-on-flat reciprocating configuration at 100 °C under a normal load of 100 N.[13]

NPs are another class of promising oil additives for friction and wear reduction because of their potential to exhibit desired interactions with substrates and their readily tunable size, composition, and surface functionality.[16-29] A variety of NPs, including metals,[18-20] metal oxides,[21-26] and metal sulfides,[27,28] have been shown to possess excellent abilities to form protective tribofilms on the surface of rubbing materials when employed as lubricant additives. However, one major issue with the use of NPs is their high tendency to undergo aggregation in nonpolar oils, for example, synthetic lubricating base oil polyalphaolefin (PAO), due to the large difference in chemical composition between the oil and NPs and the high van der Waals attractive forces between NPs.[17] If NPs become aggregated and unstable in oil, their tribological benefits will be lost. Our group recently reported a class of oil-soluble polymer brush-grafted silica and titania NPs (hairy silica and titania NPs) that exhibited excellent dispersibility and remarkable stability in PAO at both low (– 20 °C) and high temperature (100 °C).[31,32] It is worth noting that hairy NPs, consisting of a layer of polymer chains densely grafted on the surface of core NPs, have received considerable interest in recent years due to a variety of potential applications.[31-38] The superior dispersibility and stability of hairy NPs in PAO was attributed to the favorable

enthalpic interactions between polymer brushes and PAO molecules and sterically repulsive interactions between hairy NPs. With the use of oil-soluble hairy NPs, significant friction (up to ~ 40%) and wear reductions (up to ~ 90%) were achieved at a concentration of 1 wt% compared with PAO base oil.[31,32]

As discussed, oil-soluble ILs and hairy NPs are two distinct types of potential lubricant additives, with vastly different sizes and chemical compositions.[11,15,31,32] The tribofilms, which are enriched with triboactive elements from additives and are responsible for wear protection and friction reduction, are formed from drastically different mechanochemical reactions under harsh conditions of local high pressures and high temperatures. The typical tribofilm thickness was previously observed to be 10 – 400 nm for oil-miscible ILs[13,39] and 200 – 400 nm for hairy silica NPs.[31] Note that iron (poly)phosphates have been identified in the tribofilms from phosphonium-phosphate ILs.[13] While phosphate anions of ILs adsorb onto the substrate surfaces, the electrically neutral hairy silica NPs unlikely have any interactions with metallic surfaces before the rubbing begins. On the other hand, phosphate anions can react with silica/silicate to form covalent linkages, which have been utilized to improve bonding strength.[40-42] On the basis of these considerations, we hypothesized that the combination of hairy NPs and phosphonium-phosphate ILs as a lubricant additive could lead to a further improvement in the lubricating performance. The complex reactions between phosphate anions, silica, and metal surface during the rubbing process likely will enhance the tribofilm formation, strengthen the protective tribofilms, and improve the bonding of the tribofilm to the metallic substrate. To explore this hypothesis, we synthesized poly(lauryl methacrylate) brush-grafted, 23 nm silica NPs (Scheme 4.1) by

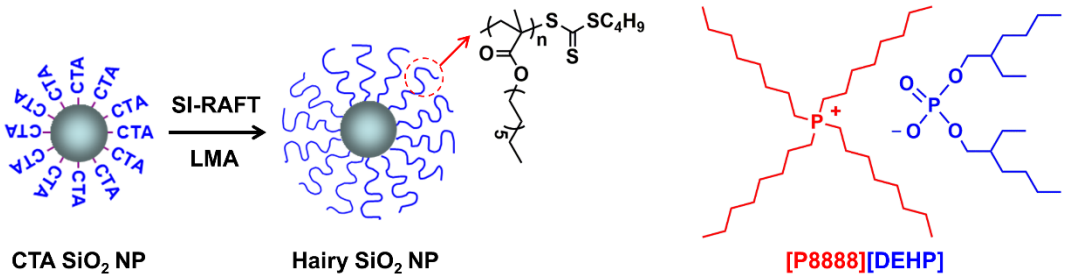

Scheme 4.1. Schematic Illustration of Poly(lauryl methacrylate) (PLMA) Brush-Grafted, 23 nm Silica Nanoparticles (Hairy NPs) and Molecular Structures of PLMA Brushes and [P8888][DEHP].

using surface-initiated reversible addition-fragmentation chain transfer (SI-RAFT) polymerization. The IL used in this work was [P8888][DEHP] (Scheme 4.1).[13] A series of PAO-based lubricants containing both hairy silica NPs and [P8888][DEHP] with a total concentration of 2 wt% but various ratios were prepared and tested in boundary lubrication. We found that at certain individual concentrations the lubrication performance was improved significantly compared to the PAO mixed with either hairy NPs or [P8888][DEHP] alone.

4.2. Experimental Section

4.2.1. Materials

The silica NPs used in the present work was obtained from Nissan Chemical as a dispersion in methyl isobutyl ketone (MIBK-ST) with an NP concentration of 30-31wt%. The average NP size was 10–15 nm according to the manufacturer. Lauryl methacrylate (LMA) (97%, Acros) was passed through a column of activated basic aluminum oxide (top) and silica gel (bottom) (2/1, v/v) to remove the inhibitor and stored in a refrigerator prior to use. Tetrahydrofuran (THF) was dried with sodium/benzophenone, distilled under nitrogen atmosphere, and used immediately. 4-(((Butylthio)carbonothioyl)thio)-4-cyanopentanoic acid (CTA-COOH), used as the free chain transfer agent (CTA) in the synthesis of hairy NPs, and *n*-butyl (2-cyano-5-oxo-5-((3-(triethoxysilyl)propyl)amino)pentan-2-yl) carbonotrithioate (CTA-Silane), were synthesized according to the procedures described previously.[32] Azobisisobutyronitrile (AIBN) (98%, Aldrich) was recrystallized from ethanol and dried under high vacuum

before use. The PAO fluid used in the present work was SpectraSyn^{TM} 4 PAO oil (ExxonMobil). The kinematic viscosities of this PAO are 19.0 cSt and 4.1 cSt at 40 and 100 °C respectively, and its pour point is – 87 °C. [P8888][DEHP] was synthesized by following the procedure in the literature,[7,13] and the purity was confirmed by ^{1}H NMR spectroscopy. All other chemical reagents were purchased from either Aldrich or Fisher and used as received.

4.2.2.Characterization

Size exclusion chromatography (SEC) of poly(lauryl methacrylate) (PLMA), the free polymer formed from the free CTA in the synthesis of PLMA hairy silica NPs (HNP), was performed using a PL-GPC 20 (an integrated SEC system from Polymer Laboratories, Inc.) equipped with a refractive index detector, one PLgel 5 μm guard column (50 × 7.5 mm), and two PLgel 5 μm mixed-C columns (each 300 × 7.5 mm, linear molecular weight range of 200 to 2 000 000 Da). THF was used as the mobile phase, and the flow rate was set at 1.0 mL/min for the analysis. The SEC system was calibrated with narrow disperse polystyrene standards, and the data were processed using Cirrus GPC/SEC software (Polymer Laboratories, Inc.). ^{1}H NMR spectra were recorded on a Varian VNMRS 500 MHz spectrometer, and the residual solvent proton signal was used as the internal reference. Thermogravimetric analysis (TGA) of CTA-functionalized silica NPs and PLMA hairy NPs was carried out in N_2 at a heating rate of 20 °C/min from room temperature to 800 °C using TA Discovery TGA-MS. Scanning transmission electron microscopy (STEM) was performed using a Zeiss Auriga equipped with a scanning transmission electron detector at an accelerating voltage of 30 keV. The STEM sample of

PLMA hairy NPs was prepared by drop casting of a 2 mg/mL dispersion in THF onto copper TEM grids coated with a carbon film. Scanning electron microscopy (SEM) and energy dispersive X-ray spectroscopy (EDS) analysis of the wear scars formed on cast iron flats from the tribological tests was performed using a Zeiss EVO MA15 equipped with an XFlash 6|30 silicon drift detector at an accelerating voltage of 20 kV. The topographic SEM images were obtained using a secondary electron detector.

A Thermo Scientific K-Alpha XPS was used for the X-ray photoelectron spectroscopy (XPS) analysis of the tribofilms formed on wear tracks from the tribological tests of 2% IL, 2% HNP, and a mixture of 1% HNP + 1% IL. The tested flats were ultrasonicated sequentially in ethanol, acetone, and hexanes, each for five minutes, wiped with Kimwipes and then blown clean with a nitrogen gun to remove possible particulate or other contaminants. All of the flats were rinsed thoroughly with isopropanol again before being placed in the sample chamber of the XPS instrument. The X-ray used in XPS analysis was monochromatic Al-Kα photons and the photons emitted from the samples were analyzed with a hemispherical energy analyzer. The spot size in the XPS analysis was 400 μm. Survey (0-1350 eV range, 1 eV steps, pass energy 200 eV) and core-level (20 eV range, pass energy 150 eV, snapshot mode) spectra of each scar were obtained after 30 s of ion sputtering with an argon-ion sputter gun at 1 keV to remove any possible surface contaminants. For each sample, the core-level spectra of C 1s, O 1s, Si 2p, and P 2pwere collected. Composition depth profiling of the tribo-films was obtained using an argon-ion sputter gun (2 keV, mid current, 1.4 mm raster, sputter rate = 1.51 nm/sec relative to Ta_2O_5) to etch the surface. The atomic compositions were calculated by measuring the peak areas

of all elements present and then normalizing them using tabulated sensitivity values. The software used in the XPS data analysis was Thermo Avantage software (v5.98, Thermo Fisher Scientific).

4.2.3. Synthesis of CTA-Functionalized Silica NPs (CTA-NPs)

MIBK-ST (5.010 g of dispersion in MIBK with a concentration of 30 wt%, corresponding to 1.503 g of bare SiO_2 NPs) and CTA-Silane (2.042 g, 4.132 mmol) were weighed into a 50 mL two-necked flask, followed by the addition of dried, freshly distilled THF (11 mL). The flask was placed in a 70 °C thermostated oil bath. The reaction mixture was stirred with a magnetic stir bar and refluxed for 68 h; a slight color change from yellow to dark orange was observed, but the solution remained transparent. The NPs were then purified by four rounds of ultracentrifugation (Beckman Optima L-90K Ultracentrifuge with type 60 Ti rotor, 35000 rpm, 60 min, 4 °C) and redispersion in THF. The CTA-NPs (1.156 g) were dispersed in freshly distilled THF, producing an orange dispersion with a concentration of 168 mg/g, which was stored in a refrigerator prior to use.

4.2.4. Synthesis of PLMA Hairy Silica NPs

LMA (2.499 g, 9.823 mmol), CTA-COOH as free CTA (89.0 mg, 0.305 mmol), AIBN (7.61 mg, 0.0463 mmol), and CTA-NPs (3.168 g dispersion in THF with a concentration of 168 mg/g, corresponding to 532 mg of CTA-NPs) were added into a 25 mL two-necked flask, followed by the addition of *N*,*N*-dimethylformamide (DMF, 68.4 mg) used as internal standard. The flask was then degassed by three cycles of freeze–pump–thaw and placed in a 70 °C oil bath. The reaction was monitored by ^{1}H NMR spectroscopy. After 18 h, the polymerization was stopped by removing the flask from the oil bath, exposing the

reaction mixture to air, and diluting with THF (5 mL). The final monomer conversion was 90.6 %, which was determined by comparing the average of the integrals of the vinyl peaks at 6.08 and 5.52 ppm against the peaks of internal standard DMF at 2.97-2.85 ppm for the initial 0 min and final samples. The DP of the PLMA was 25, calculated by using the monomer conversion and the molar ratio of monomer to the sum of free CTA and surface CTA grafted on silica NPs. The hairy NPs were purified by five rounds of ultracentrifugation (35000 rpm, 60 min, 4 °C) and re-dispersion in THF. The purified hairy NPs were stored as a dispersion in THF with a concentration of 61.3 mg/g. The free polymer in the supernatant liquid from the first cycle of ultracentrifuge was characterized by SEC analysis, and the $M_{n,SEC}$ was found to be 6.5 kDa with a dispersity (Đ) of 1.14 relative to polystyrene standards.

4.2.5. Preparation of PAO-Based Lubricants Containing Various Amounts of HNP and IL with a Total Concentration of 2% and Stability Study

To study the effect of combining hairy silica NPs (HNP) and [P8888][DEHP] (IL) on lubrication performance, a series of PAO-based lubricants containing various amounts of HNP and IL with an overall concentration of 2% were prepared. The samples included: (a) 2% IL, (b) 2% HNP, (c) 0.34% HNP + 1.66% IL, (d) 0.66% HNP + 1.34% IL, (e) 1% HNP and 1% IL, (f) 1.34% HNP + 0.66% IL, (g) 1.66% HNP + 0.34% IL, and (h) 1.83% HNP + 0.17% IL. The following is the preparation of a PAO solution of 1% HNP + 1% IL. All other samples were prepared using a similar procedure. PAO (3.016 g) was weighed into a 20 mL scintillation vial followed by the addition of [P8888][DEHP] (31.9 mg) and a dispersion of PLMA hairy silica NPs in THF with a concentration of 61.3 mg/g (0.498 g,

corresponding to 30.5 mg of hairy NPs). The resultant mixture was ultrasonicated using Fisher Scientific FS6 for 5 min until a homogeneous dispersion was achieved. THF was then removed under reduced pressure, which was confirmed by ^{1}H NMR analysis.

Dynamic light scattering (DLS) measurements were performed to study the stability of PLMA hairy silica NPs in PAO in the presence of [P8888][DEHP] using a Malvern Zetasizer Nano ZS instrument equipped with a He-Ne S-9 633 nm laser and a temperature controller at a scattering angle of 173°. A dispersion of 1% HNP in PAO and a solution of the mixture of 1% HNP + 1% IL in PAO were prepared. Aliquots were taken from the samples and diluted with pure PAO to a concentration of 0.1 mg/g for DLS measurements at 23 °C. The viscosity of PAO at 23 °C, 27.6 cP, was calculated from the kinematic viscosity (34.5 cSt) and its density at 23 °C (0.80 g/mL) from the literature.[7] The samples were heated at 100 °C for 10 days along with a PAO solution of 1% IL. Aliquots were withdrawn from the solution of 1% HNP + 1% IL in PAO and used for the DLS measurements of the hydrodynamic size of hairy NPs at 23 °C.

4.2.6. Tribological Testing

High contact stress, ball-on-flat boundary lubrication tests were performed using a Phoenix Tribology Plint TE 77 to study the effect of mixing hairy NPs and [P8888][DEHP] in PAO on tribological performance. In each test, an AISI 52100 steel ball with a diameter of 9.25 mm slid reciprocally under a point contact load of 100 N against a stationary CL35 cast iron flat in the presence of a lubricant typically for a total sliding distance of 1000 m. A sliding stroke of 10 mm and an oscillation frequency of 10 Hz were used, and all tribological tests were conducted at 100 °C. The friction force was recorded in situ by a

piezoelectric load cell, and the coefficient of friction (COF) was obtained by dividing the friction force by the load. For each sample, at least two runs were conducted under the same conditions, and the average of the COF curves was calculated and used. After the tribological testing, the iron flat and steel ball along with their respective wear scars were cleaned thoroughly with acetone and isopropanol for wear measurements using optical surface profilometry (Wyko NT9100). The iron flats with wear scars were further cleaned and characterized by SEM-EDS analysis and XPS as mentioned earlier.

4.3. Results and Discussion

4.3.1. Synthesis and Characterization of PLMA Hairy Silica NPs and IL [P8888][DEHP]

PLMA brush-grafted, 23 nm silica NPs (HNP) were made by SI-RAFT polymerization from chain transfer agent (CTA)-functionalized silica NPs. The CTA-NPs were prepared by immobilizing *n*-butyl (2-cyano-5-oxo-5-((3-(triethoxysilyl)propyl)amino)pentan-2-yl) carbonotrithioate (CTA-Silane),[32] a triethoxysilane-terminated CTA, onto the surface of silica NPs from MIBK-ST in dry THF at 75 °C for 68 h in a nitrogen atmosphere. The CTA-NPs were purified by repetitive ultracentrifugation and then stored as a dispersion in THF.

The SI-RAFT polymerization was then conducted to grow PLMA brushes from CTA-NPs at 70 °C using AIBN as initiator in the presence of a free CTA, CTA-COOH. The free CTA was added to facilitate the control of surface polymerization and the characterization of the grafted polymer. For surface-initiated “living”/controlled radical polymerization

from (nano)particles, it has been reported that the molecular weights and dispersity of the free polymers formed from the free initiators or CTAs are essentially identical to those of the polymer brushes on the particles.[43-45] The reaction was run for 18 h, and the monomer conversion was found to be 90.6 % by ^{1}H NMR spectroscopy analysis. The hairy NPs were purified by five cycles of ultracentrifugation and re-dispersion in THF. SEC analysis of the free polymer isolated from the first round of ultracentrifugation showed that the values of $M_{n,SEC}$ and Đ were 6.5 kDa and 1.14, respectively,[46] which suggests a controlled radical polymerization. The HNP was analyzed by thermogravimetric analysis (TGA) and found to have weight retention of 54.6% at 800 °C (Figure 4.1A). This is significantly lower than that of CTA-NPs (86.5%), indicating the successful growth of PLMA brushes on NPs. The degree of polymerization (DP) of PLMA was calculated to be 25 from the ratio of monomer to the sum of free and surface CTA and the monomer conversion.[46] The HNP was imaged by scanning transmission electron microscopy (STEM), and a representative STEM micrograph is presented in Figure 4.1B. Although the original size of silica NPs was 10-15 nm according to Nissan Chemical, our group found that the average size of core silica NPs was 23 nm,[32] which is likely because smaller NPs were lost in the multiple cycles of ultracentrifugation. Using the NP size, DP of PLMA brushes, and TGA data, we calculated the grafting density of PLMA brushes, and it was 0.51 chains/nm^2.[46] The molecular structure of the IL used in this work, [P8888][DEHP],[6] was confirmed by ^{1}H NMR spectroscopy analysis.[46]

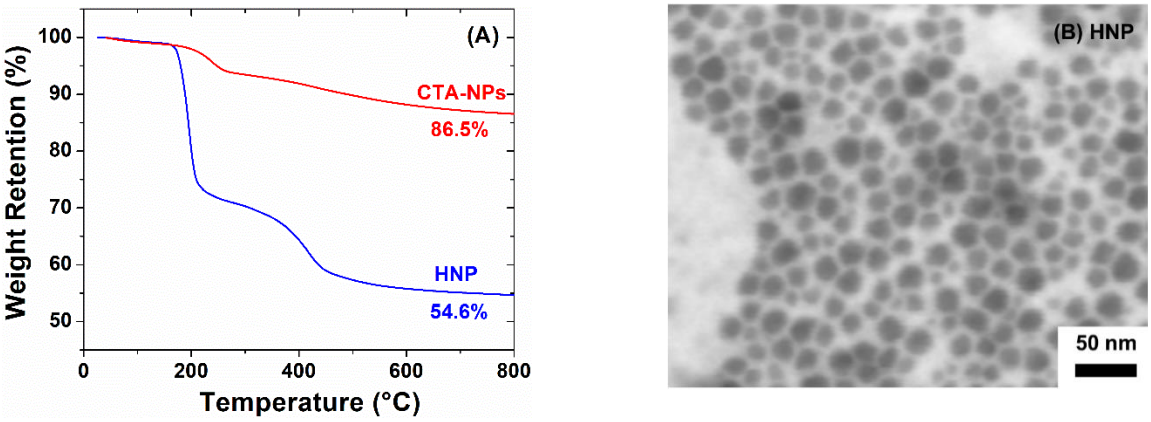

Figure 4.1. (A) Thermogravimetric analysis (TGA) of CTA-functionalized silica NPs (CTA-NPs) and PLMA brush-grafted silica NPs (HNP) made from CTA-NPs and (B) bright field scanning transmission electron microscopy (STEM) micrograph of HNP.

4.3.2. Colloidal Stability of PLMA Hairy Silica NPs in PAO in the Presence of [P8888][DEHP]

Our group previously demonstrated that PLMA brush-grafted, 23 nm silica NPs exhibited superior stability in PAO at both low (-20 °C) and high temperatures (100 °C).[31] To examine if the addition of [P8888][DEHP] affects the colloidal stability of HNP in PAO, we prepared a solution of 1% HNP + 1% IL in PAO and kept it still in a 100 °C oil bath for an extended period of time. For comparison, we also prepared a 1% dispersion of HNP alone in PAO and a 1% solution of the IL in PAO and heated them at 100 °C. Figure 4.2A-C shows the photos of the samples after being kept at 100 °C for 10 days along with freshly prepared solutions of the mixture, HNP alone, and IL alone in PAO. No any aggregation/precipitation was observed except very light yellow coloration for all samples compared with freshly made ones, suggesting that the hairy NPs were stable in PAO in the presence of 1% [P8888][DEHP].

To further study the stability of HNP in the presence of IL in PAO, aliquots were taken from the solution of the mixture after 3 and 10 days and diluted to a concentration of 0.1 mg/g HNP with pure PAO for DLS analysis at 23 °C. Figure 4.2D shows the intensity-weighted hydrodynamic size distributions for HNP from the freshly prepared solution of 1% HNP + 1% IL and the two samples of the mixture after being heated at 100 °C for 3 and 10 days, along with a freshly made HNP dispersion in PAO for comparison. The curves basically overlapped with each other, and the average size was 63.6 nm for HNP alone, 57.7 nm for the freshly prepared mixture of HNP and IL, 59.2 nm and 57.3 nm for the mixture after 3 and 10 days at 100 °C, respectively. Because of the hydrodynamic sizes of

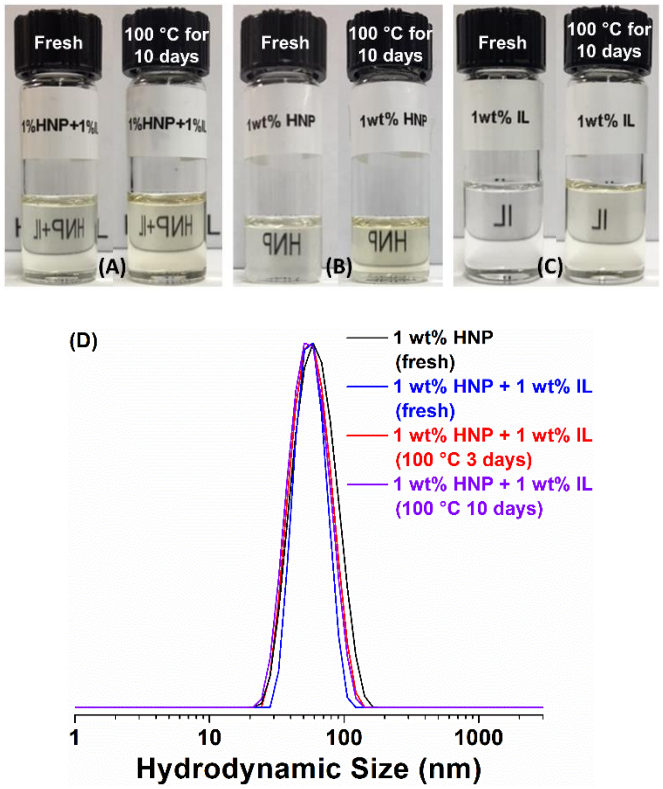

Figure 4.2. Optical photos of PAO solutions containing (A) 1% hairy NPs (HNP) + 1% [P8888][DEHP] (IL), (B) 1% HNP alone, and (C) 1% IL alone, freshly prepared and after thermal treatment at 100 °C for 10 days; (D) intensity-weighted hydrodynamic size distribution, obtained by DLS study, of hairy NPs at a concentration of 0.1 mg/g from the freshly prepared 1% dispersion of HNP alone, a freshly made solution of 1% HNP + 1% IL in PAO, and the PAO solution containing 1% HNP + 1% IL after being heated at 100 °C for 3 and 10 days.

HNP are similar, it indicates that these PLMA brush-grafted silica NPs are stable in PAO in the presence of the IL even at elevated temperatures for an extended period of time. From both visual inspection and DLS measurements, we can conclude that PLMA hairy silica NPs and [P8888][DEHP] are compatible with each other when used as additives for PAO lubricating base oil.

4.3.3. Lubrication Performance of PAO Mixed with HNP, IL, or HNP + IL

To study the possible further friction reduction effect of combining hairy NPs and [P8888][DEHP] as additives, a series of PAO lubricants containing both HNP and IL with a total concentration of 2 wt% but various individual concentrations were prepared. They are: (a) 2% IL, (b) 2% HNP, (c) 0.34% HNP + 1.66% IL, (d) 0.66% HNP + 1.34% IL, (e) 1% HNP and 1% IL, (f) 1.34% HNP + 0.66% IL, (g) 1.66% HNP + 0.34% IL, and (h) 1.83% HNP + 0.17% IL. The tribological properties of these samples were investigated using a Plint TE-77 tribo-tester at 100 °C in a ball-on-flat reciprocating configuration. In all tests, an AISI 52100 steel ball slid back and forth on a CL35 cast iron flat in a lubricant sample at an oscillation frequency of 10 Hz with a 10 mm stroke. The point contact load was 100 N, and the total sliding distance was typically 1000 m. At least two identical tests were performed for each lubricant sample, and the results were averaged.

Figure 4.3 shows the friction curves for all of the aforementioned samples along with pure PAO for comparison. Consistent with the previously reported results,[7,31,32] the PAO mixed with either HNP or IL showed a significant reduction in the coefficient of friction (COF) relative to pure PAO. For both 2% IL and 2% HNP lubricants, the COF started at around 0.07 and increased gradually over the course of sliding and ended at 0.11 for IL and

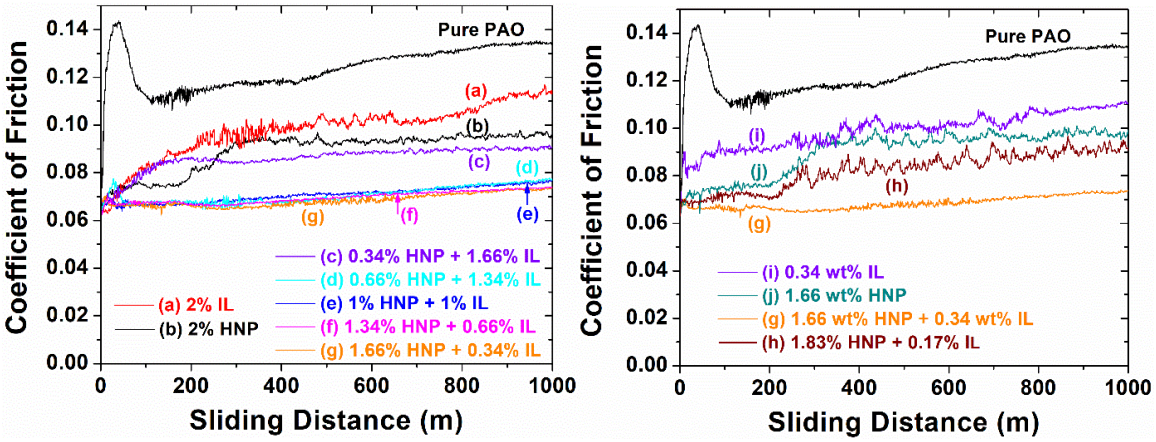

Figure 4.3. Friction curves for the PAO SpectraSyn^{TM} 4 mixed with (a) 2% IL, (b) 2% HNP, (c) 0.34% HNP + 1.66% IL, (d) 0.66% HNP + 1.34% IL, (e) 1% HNP and 1% IL, (f) 1.34% HNP + 0.66% IL, (g) 1.66% HNP + 0.34% IL, (h) 1.83% HNP + 0.17% IL, (i) 0.34% IL, and (j) 1.66% HNP. The tribological tests were performed using a Plint TE-77 tribo-tester at 100 °C under a point contact load of 100 N for a sliding distance of 1000 m.

0.095 for HNP (see curves (a) and (b) in Figure 4.3). Compared with pure PAO, the friction at the 1000 m sliding distance decreased by 16% for IL and 29% for HNP. A distinctive feature of all additive-containing samples is the absence of the sharp peak of scuffing at the beginning of the sliding process observed for pure PAO. Clearly, adding either HNP or IL or both prevented the scuffing from happening. Further reductions in friction were observed for the samples containing both HNP and IL as additives. While the friction curves of (c) 0.34% HNP + 1.66% IL and (h) 1.83% HNP + 0.17% IL were only slightly lower than the 2% HNP curve (b), noticeable decreases in COF values were found for all other samples containing both HNP and IL: (d) 0.66% HNP + 1.34% IL, (e) 1.0% HNP + 1.0% IL, (f) 1.34% HNP + 0.66% IL, and (g) 1.66% HNP + 0.34% IL. Calculations showed that the friction decreased by 20 – 23 % in comparison to the 2% HNP sample and by 32 – 35% relative to the 2% IL at the end of the sliding process. In addition, all four friction curves (curves (d), (e), (f), and (g) in Figure 4.3) were significantly smoother and flatter, testifying that the combination of two compatible additives led to improved lubricating performance. By examining the data in Figure 4.3, one can find that it is necessary to have sufficiently high individual concentrations for both additives; too little HNP (e.g., (c) 0.34% HNP + 1.66% IL) or too little IL (e.g., (h) 1.83% HNP + 0.17% IL) resulted in only a slight improvement in friction reduction.

To confirm the positive effect of combining HNP and IL as additives for PAO, we conducted the tribological tests for the PAO mixed with 0.34% IL alone (curve (i) in Figure 4.3) and 1.66% HNP alone (curve (j) in Figure 4.3). Clearly, both lubricants exhibited higher friction coefficients compared with the mixture of (g) 1.66% HNP + 0.34% in PAO

throughout the sliding process, strongly suggesting a positive effect on the lubrication performance by mixing hairy silica NPs and IL as additives for PAO.

The wear volumes for each lubricant sample were measured by optical surface profilometry of the wear scars formed on the iron flat and the steel ball during the tribological tests. The results are shown in Table 4.1. Compared with pure PAO, the total wear was reduced by ~ 90% for all additive-containing PAO lubricants, with a range from 85.9% (for (i) 0.34 wt% IL alone) to 93.9% (for (c) 0.34% HNP + 1.66% IL). Most of the mixtures with a total concentration of 2% showed lower wear volumes compared with either 2% HNP or 2% IL. For example, the flat wear for (e) 1% HNP + 1% IL was reduced by 33% and 17% compared with 2% HNP and 2% IL, respectively. However, the flat wear volume for (g) 1.66% HNP + 0.34% (13.32×10^7 μm^3) was only slightly smaller than those for 1.66% HNP alone (14.01×10^7 μm^3) and 0.34% IL alone (15.47×10^7 μm^3). Despite this observation, there seems to be a trend that the wear decreased with decreasing the concentration of HNP from 1.83% to 0.34% and simultaneously increasing the IL concentration from 0.17% to 1.66% in the mixture. In summary, the wear protection was improved by combining HNP and IL as additives at certain ratios, but the level of improvement was not as substantial compared with the PAO containing only one additive (either HNP or IL) at the same concentration.

Table 4.1. Wear Volumes for Balls and Flats from Tribological Tests Using Various Lubricants

Lubricant Sample	flat wear volume ($\times 10^7$ μm^3)	ball wear volume ($\times 10^7$ μm^3)
PAO	113.0 ± 35.9	0.786 ± 0.193
(a) PAO + 2% IL	9.90 ± 0.99	0.405 ± 0.120
(b) PAO + 2% HNP	12.26 ± 0.86	0.039 ± 0.026
(c) PAO + 0.34% HNP + 1.66% IL	6.91 ± 0.73	0.067 ± 0.007
(d) PAO + 0.66% HNP + 1.34% IL	7.46 ± 0.33	0.018 ± 0.006
(e) PAO + 1% HNP + 1% IL	8.21 ± 0.17	0.018 ± 0.006
(f) PAO + 1.34% HNP + 0.66% IL	9.77 ± 1.57	0.016 ± 0.010
(g) PAO + 1.66% HNP + 0.34% IL	13.32 ± 1.53	0.012 ± 0.013
(h) PAO + 1.83% HNP + 0.17% IL	12.90 ± 0.63	0.029 ± 0.020
(i) PAO + 0.34% IL	15.47 ± 1.21	0.571 ± 0.293
(j) PAO + 1.66% HNP	14.01 ± 0.44	0.057 ± 0.002

4.3.4. SEM-EDS Analysis of Wear Scars Formed on Iron Flats During Tribological Tests

The improved friction reductions from additive-containing PAO lubricants originate from the formation of tribofilms on rubbing interfaces, which has been reported for various anti-wear additives and friction reducers including ZDDP,[8,9] ionic liquids,[10-15] and hairy NPs.[31,32] The formation of protective tribofilms involves complicated mechano-chemical reactions under high pressures and high temperatures, and the films are usually enriched with respective triboactive elements from additives. For example, our group previously observed by transmission electron microscopy (TEM) a 200-400 nm tribofilm enriched with Si in the wear scar formed from a tribological test with PAO + PLMA brush-grafted silica NPs as lubricant.[31] For phosphonium-phosphate ILs, the tribofilms were typically in the range of 10 – 400 nm and contained P.[13,39]

To study the observed effect of combining HNP and IL as additives for PAO for improved friction reduction, we used scanning electron microscopy coupled with X-ray spectroscopy analysis (SEM-EDS) to confirm the presence of the tribofilms atop of the wear scars formed on iron flats and to characterize the chemical composition of the tribofilms. Three SEM micrographs of the wear scars formed from 2% IL, 2% HNP, and the mixture of 1 % HNP + 1 % IL are shown in Figure 4.4 along with the corresponding elemental maps of Fe, P, O, and Si. While for all three lubricants there was no difference for iron inside and outside the wear scars, a marked increase in oxygen content in the wear scars was observed, suggesting that oxidation was involved in the tribofilm formation during the tribological process. P was found in the wear scar for 2% IL but not for 2%

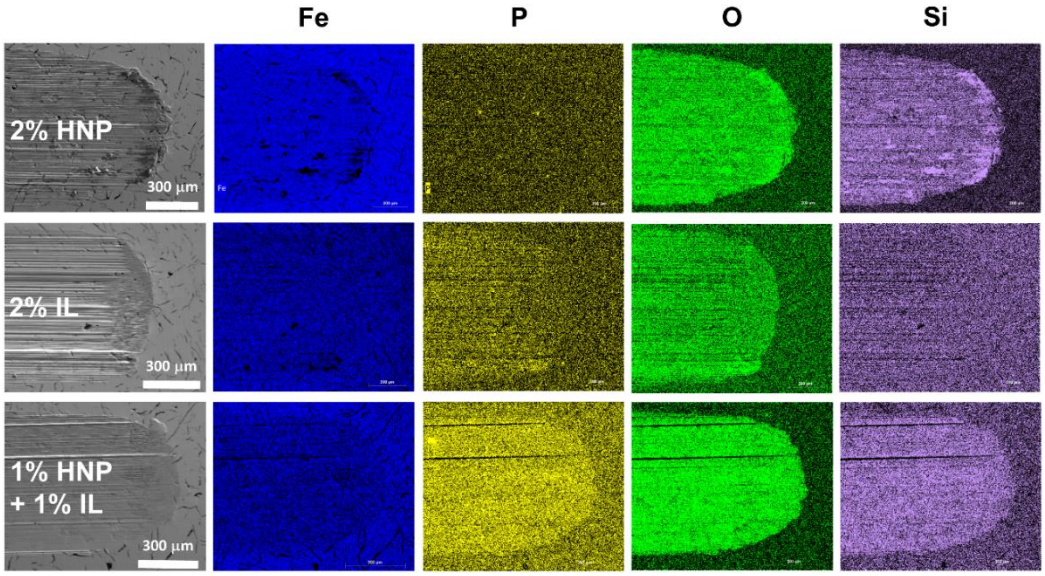

Figure 4.4. SEM micrographs and EDS elemental mapping of Fe, P, O, and Si of the wear scar at the end of wear track formed on the iron flat during the tribological test of the PAO mixed with 2% HNP (top row), 2% IL (middle row), and 1% HNP + 1% IL (bottom row).

HNP, whereas Si was enriched in the wear track for 2% HNP, but not for 2% IL. For the mixture of 1% HNP + 1% IL, both P and Si showed good contrast between the wear scar and the pristine flat. All three EDS spectra are shown in Figure 4.5 (Figure 4.5A for 2% HNP, Figure 4.5B for 2% IL, and Figure 4.5C for the mixture of 1% HNP + 1% IL). The Si Kα peak intensity increased noticeably in the wear scar compared with the pristine flat for both 2% HNP and 1% HNP + 1% IL but not for 2% IL. The P Kα peak appeared in the EDS spectra for 2% IL and 1% HNP + 1% IL but not for 2% HNP. These SEM-EDS data testified that both HNP and IL or their fragments were involved in the mechano-chemical reaction to form the tribofilm for the mixture of 1% HNP + 1% IL. Similar results were obtained for 0.34% IL alone, 1.66% HNP alone, and the mixture of 1.66% HNP + 0.34% IL, as shown in the Appendix.[46]

The atomic compositions of the wear scars for all lubricant samples were obtained from quantitative EDS analysis and are shown in Table 4.2. For both 2% HNP and 1.66% HNP, the P elemental abundance was negligible (0.01%), and the molar ratio of P to Si was extremely small (only 0.002). In contrast, the wear scars formed from the tribological tests of 2% and 0.34% IL contained 0.81% and 0.71% P and 1.34% and 1.03% Si, respectively. The Si is believed to come from the underneath iron substrate as the pristine flat contains 1.87% Si (Table 4.2 and also see EDS spectra in Figure 4.5). Note that the probing depth of EDS is a few micrometers,[47] while the tribofilms are on the order of a few hundreds of nanometers; this means that the chemical composition information underneath the tribofilm was also collected and contributed to the data in Table 4.2. Thus, the molar contents of element P in the tribofilms formed from IL-containing lubricants were underestimated. For

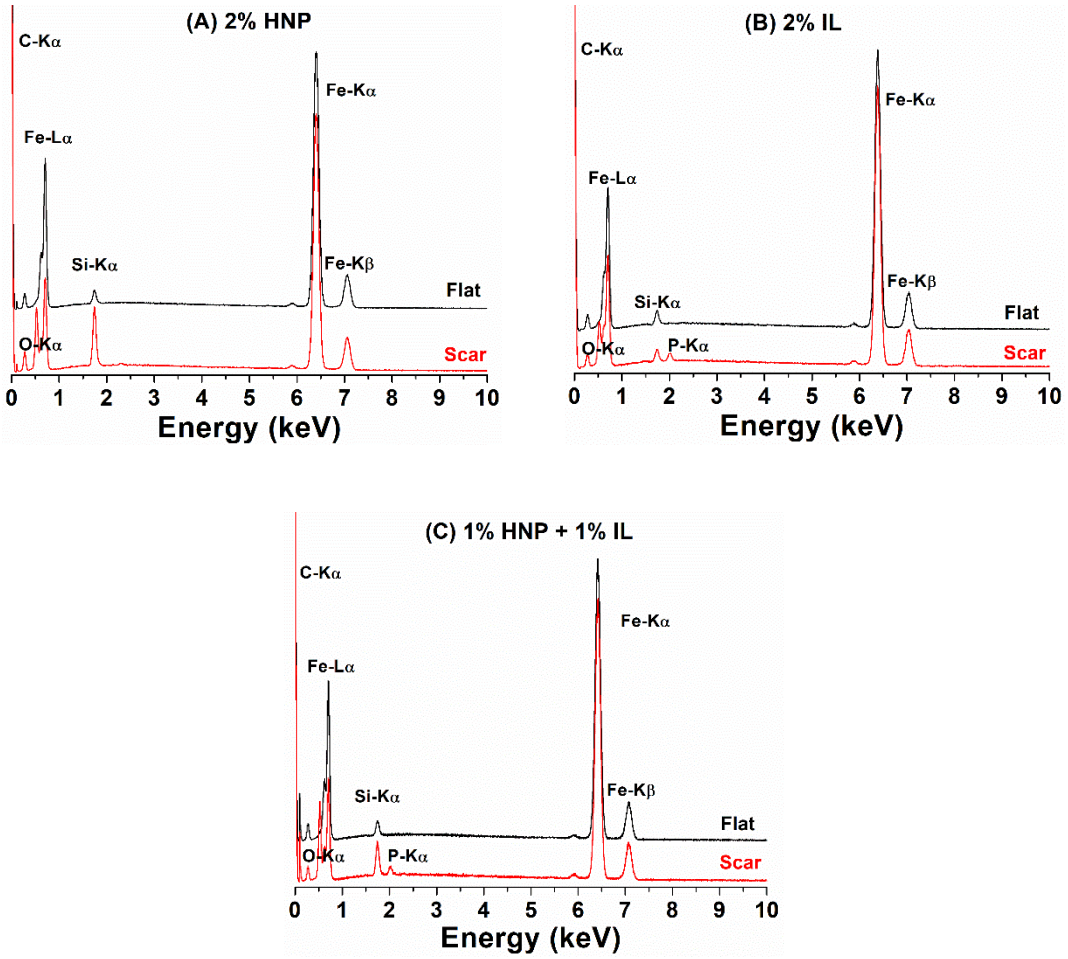

Figure 4.5. Energy dispersive X-ray spectroscopy (EDS) analysis of the pristine flat (outside the wear scar) and the wear scar formed on the flat lubricated by the PAO mixed with (A) 2% HNP, (B) 2% IL, and (C) 1% HNP + 1% IL.

Table 4.2. Atomic Composition of Wear Scars from EDS Analysis and Molar Ratio of P to Si

PAO mixed with	C (%)	O (%)	Fe (%)	Si (%)	P (%)	Mn (%)	P/Si
(a) 2% IL	21.46	14.29	60.65	1.39	0.81	1.39	0.583
(b) 2% HNP	25.45	21.95	46.77	5.36	0.01	0.45	0.002
(c) 0.34% HNP + 1.66% IL	29.63	21.87	44.85	2.12	1.03	0.51	0.486
(d) 0.66% HNP + 1.34% IL	16.68	26.56	52.40	2.99	0.80	0.57	0.268
(e) 1% HNP + 1% IL	21.72	24.26	49.77	2.92	0.76	0.58	0.260
(f) 1.34% HNP + 0.66% IL	22.35	26.56	46.95	3.05	0.66	0.44	0.216
(g) 1.66% HNP + 0.34% IL	24.59	23.81	47.06	3.55	0.55	0.43	0.155
(h) 1.83% HNP + 0.17% IL	21.82	23.18	48.83	5.22	0.42	0.53	0.080
(i) 0.34% IL	27.11	18.67	51.95	1.03	0.71	0.52	0.689
(j) 1.66% HNP	28.01	21.62	44.59	5.25	0.01	0.52	0.002
Pristine Flat	28.84	0.20	68.38	1.87	0.00	0.66	0.00

all lubricant samples containing both HNP and IL, a significant higher P content was observed compared with those containing only HNP, again indicating that IL participated in the tribo-reaction. The P/Si ratio increased with increasing concentration of IL, from 0.080 for (h) 1.83% HNP + 0.17% IL to 0.486 for (c) 0.34% HNP + 1.66% IL. For those mixtures exhibiting a significant improvement in the friction reduction, the P/Si ratios were in the range of 0.16 to 0.27.

4.3.5. Tribofilm Compositions at Different Sliding Distances Using the PAO Mixed with 1% HNP + 1% IL as Lubricant

As mentioned earlier, [P8888][DEHP] can adsorb onto the iron substrate surface via the organophosphate anion, while PLMA hairy silica NPs presumably exhibit no interaction with the metal surface before the rubbing due to the neutral and hydrophobic nature of PLMA brushes. Thus, it would be interesting to see if the IL played a dominant role in the early stage tribochemical reaction and hairy silica NPs entered the reaction later in the tribofilm formation. To investigate this possibility, we conducted three additional tribological tests with the PAO containing 1% HNP + 1% IL and stopped the sliding process at 100 m, 400 m, and 700 m. Figure 4.6 shows the friction curves for these three tests along with the curve for the full sliding process for the same mixture from Figure 4.3. All three shorter friction curves overlapped nicely with the full sliding curve. The wear scars from these three tests were then analyzed with SEM-EDS, and their atomic compositions are summarized in Table 4.3.

While the Si content decreased slightly from 3.53% for the sliding distance of 100 m to 2.92 for 1000 m, the P content stayed about the same, in the range of 0.69 to 0.86. The

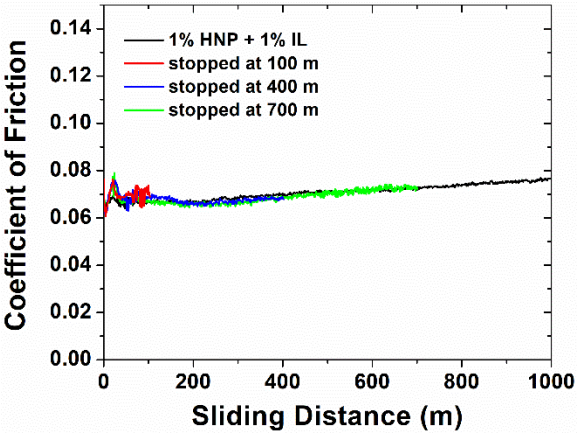

Figure 4.6. Friction curves for the PAO mixed with 1% HNP + 1% IL from tribological tests that were stopped at sliding distances of 100, 400, 700, and 1000 m. The tribological tests were performed using a Plint TE-77 tribo-tester at 100 °C under a point contact load of 100 N.

Table 4.3. Atomic Compositions of Wear Scars Formed on Iron Flats at Different Sliding Distances from EDS analysis Using the PAO Mixed with 1% HNP + 1% IL as Lubricant

Sliding Distance	C (%)	O (%)	Fe (%)	Si (%)	P (%)	Mn (%)	P/Si
100 m	14.32	25.52	55.35	3.53	0.69	0.59	0.195
400 m	16.29	28.57	50.26	3.49	0.86	0.54	0.246
700 m	16.98	25.56	52.83	3.33	0.75	0.56	0.225
1000 m	21.72	24.26	49.77	2.92	0.76	0.58	0.260

P/Si atomic ratio seems to increase slightly, from 0.20 for 100 m to 0.26 for 1000 m, but all of the four values fell into the range of 0.16 to 0.27 previously observed for those mixtures exhibiting significant friction reduction. Despite that the IL molecules adsorb onto the metallic surface first, this experiment suggested that both HNP and IL or their fragments participated in the tribo-reaction in the studied sliding distance range.

4.3.6 XPS Analysis of Tribofilms on Wear Scars

The probing depth of EDS is on the order of a few micrometers,[47] much larger than the typical thicknesses of tribofilms. Therefore, we further characterized the wear scars by X-ray photoelectron spectroscopy (XPS), which has a much smaller probing depth, typically 0.1 to 10 nm.[48] Figure 4.7A shows the survey spectra of the wear scars formed on the iron flats lubricated with 2% HNP, 2% IL, and the mixture of 1% HNP + 1% IL after the surfaces were cleaned by ion sputtering with an Argon-ion gun at 1 keV for 30 s to eliminate possible surface contaminants.

The XPS survey spectrum of the tribofilm formed from 2% HNP clearly showed the presence of Si 2s and 2p peaks at ~ 153 and ~ 102 eV, respectively, and the absence of P 2s and 2p, whereas the wear scar formed by the lubrication with 2% IL contained element P (P 2s at ~ 190 eV and P 2p at ~ 133 eV) and negligible Si. As expected, the 2s and 2p peaks of both Si and P appeared in the XPS spectrum for the mixture of 1% HNP + 1% IL, which confirmed that both HNP and IL were involved in the mechano-chemical reaction for the formation of the outermost layer of the protective tribofilm. All of these are consistent with the observations from SEM-EDS analysis. The atomic compositions from quantitative XPS analysis are summarized in Table 4.4. The molar contents of Si for 2%

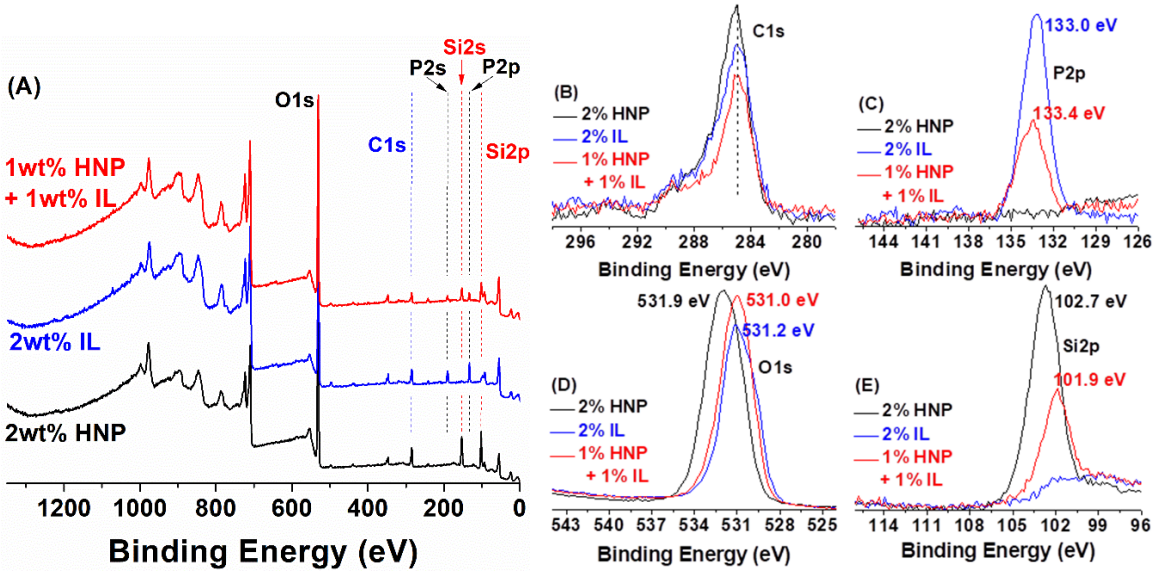

Figure 4.7. (A) XPS survey spectra of the tribofilms formed on iron flats lubricated with the PAO mixed with 2% HNP, 2% IL, and the mixture of 1% HNP + 1% IL and high resolution core level spectra of (B) C 1s, (C) P 2p, (D) O 1s, and (E) Si 2p.

Table 4.4. Atomic Composition of Tribofilms from Quantitative XPS Analysis

PAO containing	C (%)	O (%)	P (%)	Si (%)	Fe (%)	P/Si
2% HNP	13.03	60.41	0.00	18.22	8.34	0.000
2% IL	15.53	63.36	8.43	1.12	11.57	7.527
1% HNP + 1% IL	10.20	65.84	3.71	9.44	10.82	0.393

HNP and the mixture of 1% HNP + 1% IL were 18.22% and 9.44%, respectively, significantly higher than those from EDS (5.36% and 2.92%, respectively). The P content was 8.43% for 2% IL and 3.71% for the mixture, which is also much higher than those from EDS analysis (0.81% and 0.76%, respectively). The molar ratio of P to Si for the mixture was 0.393, again larger than that from the EDS analysis (0.260). As mentioned earlier, these large differences are caused by the different probing depths of EDS and XPS (a few micrometers versus 0.1-10 nm).

The core level spectra of C 1s, P 2p, O 1s, and Si 2p for the three wear scars are shown in Figure 4.7B-D. The phosphorous 2p spectra for 2% IL and the mixture of 1% HNP + 1% IL showed a peak at binding energies of 133.0 and 133.4 eV, respectively, which are attributed to the P-O bond of phosphates[13] (likely iron phosphates for IL and iron and silicate phosphates for the mixture of 1% HNP + 1% IL). No P 2p peak was observed in the tribofilm from 2% HNP. For 2% HNP, the O 1s peak appeared at 531.9 eV, which is attributed to Si-O-Si,[49] while the O 1s signal of Fe-O-Si (530.3 eV)[49] is likely buried inside the main peak. For 2% IL, the O 1s spectrum shows a main peak at the binding energy of 531.2 eV, which is assigned to O-P bond (excluding P-O-Fe),[13] and a shoulder peak at ~ 530.2 eV, which is assigned to Fe-O/Fe-O-P bonds.[13] In contrast, the O 1s spectrum of the wear scar formed from the mixture of 1% HNP + 1% IL exhibits only one peak at 531.0 eV with no visible shoulder peak, which almost enclosed the O 1s peak for 2% IL and overlapped significantly with the O 1s signal for 2% HNP. This might suggest the presence of P-O, Fe-O as well as Si-O bonds. Considering that the O 1s peaks for 2% IL and the mixture of 1% HNP + 1% IL were closer to each other than to the O 1s peak from 2% HNP,

there is a possibility that a portion of Si-O-Si bonds was replaced by new covalent bonds because of the reaction between silica and phosphate anions. The Si 2p signal for the mixture of 1% HNP + 1% IL is found at 101.9 eV, while the Si 2p peak is located at 102.7 eV for 2% HNP. Tanizawa and Suzuki reported that the binding energy of Si 2p was 102.1 eV for silicate-containing apatite, which is almost the same as our observation for the mixture (101.9 eV), and 103.4 eV for silica.[50] Thus, we think that the shift of Si 2P from 102.7 eV for 2% HNP to 101.9 eV for the mixture is likely caused by the formation of new covalent linkages involving Si, O, and P from the reaction between silica core NPs and phosphate anions, despite the fact that the peak shift could be also caused by the changes in local work function or electron density. Note that this shift is also in line with the observation by Hasha et al.[51]

Using argon-ion sputtering to etch the surface, we examined the composition depth profiling of the tribofilm formed from the mixture of 1% HNP + 1% IL. The deconvoluted composition-depth profile is shown in Figure 4.8. The increase of the Fe content with the increase of sputtering time was due to the gradual exposure of the iron substrate. Although obscured by the rising iron signal, the P/Si molar ratio appeared to be similar from the top surface to the interior of the tribofilm, suggesting that both HNP and IL or their fragments were involved throughout the tribochemical reaction. Thus, both EDS and XPS analysis suggested that the organophosphate anion of the IL reacted with silica NPs as well as the cast iron substrate surface in the complex mechano-chemical process, likely enhancing the tribofilm formation and strengthening the protective layer as well as its bonding with the metallic substrate. Consequently, the lubrication performance was improved as observed

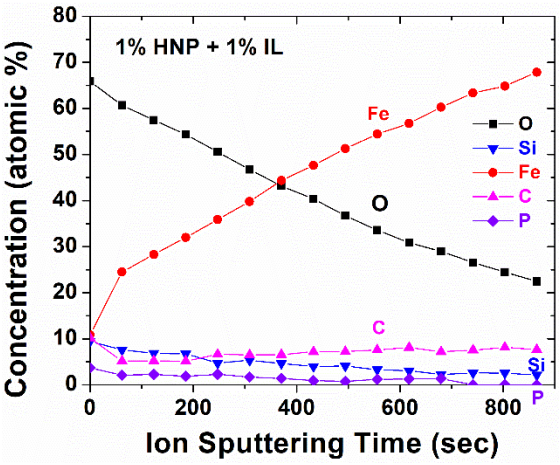

Figure 4.8. XPS composition-depth profile for the tribofilm at top of the wear scar formed on the iron flat surface with the PAO mixed with the mixture of 1% HNP + 1% IL.

for the PAO lubricants containing sufficient amounts of both hairy NPs and IL.

4.4. Conclusions

Oil-soluble polymer brush-grafted silica NPs and phosphonium-phosphate ILs are two different classes of promising lubricant additives for friction and wear reduction. Using high contact stress, ball-on-flat reciprocating tribological testing at 100 °C, we observed significantly improved friction reduction when PLMA hairy NPs and [P8888][DEHP] were used simultaneously as additives.[52] At a total concentration of 2% and sufficiently high individual concentrations, the friction decreased by 20 – 23% in comparison to the 2% HNP sample and by 32 – 35% relative to the 2% IL at the end of the sliding process. SEM-EDS analysis revealed that the wear scars formed on cast iron flats contained both Si and P for PAO + HNP + IL, indicating that both additives were involved in the tribo-chemical reactions. For the mixtures demonstrating significant friction reduction, the P/Si ratio from EDS was found to be in the range of 0.16 to 0.27. XPS characterization showed that the Si 2p peak in the core-level spectra shifted from 102.7 eV for HNP to 101.9 eV for the mixture of 1% HNP + 1% IL, indicating the formation of new covalent bonds from the reactions between HNP and IL. From XPS composition-depth profiling, the molar ratio of P to Si appeared to be similar from the top surface to the interior of the tribofilm. These data suggested that hairy silica NPs and [P8888][DEHP] or their fragments reacted with each other and also with the substrate during the tribological testing, which, we believe, strengthened the tribofilms and their bonding with the iron substrate and consequently improved the friction reduction. The results reported here suggest a new method to further

improve the lubrication performance by combining hairy NPs and ILs as additives for PAO, which may have potential for applications in real-world lubrication.

References

1. Bhushan, B. *Introduction to Tribology*, 2nd ed.; John Wiley & Sons Ltd: 2013.
2. Stachowiak, G. W.; Batchelor, A. W. *Engineering Tribology*, 3rd ed.; Elsevier Butterworth-Heinemann: Burlington, 2005.
3. Rudnick, L. R. *Synthetics, Mineral Oils, and Bio-Based Lubricants: Chemistry and Technology*, 2nd ed.; CRC Press: Boca Raton, 2013.
4. Cai, M. R.; Guo, R. S.; Zhou, F.; Liu, W. M. Lubricating a Bright Future: Lubrication Contribution to Energy Saving and Low Carbon Emission. *Sci. China Tech. Sci.*, **2013**, *56*, 2888-2913.
5. Rudnick, L. R. *Lubricant Additives: Chemistry and Applications*, 2nd ed.; CRC Press: Boca Raton, 2009.
6. Holmberg K.; Andersson P.; Erdemir A. Global Energy Consumption Due to Friction in Passenger Cars. *Tribol. Int.* **2012**, *47*, 221–234.
7. Qu, J.; Bansal, D. G.; Yu, B.; Howe, J. Y.; Luo, H.; Dai, S.; Li, H. Q.; Blau, P. J.; Bunting, B. G.; Mordukhovich, G.; Smolenski, D. J. Antiwear Performance and Mechanism of an Oil-Miscible Ionic Liquid as a Lubricant Additive. *ACS Appl. Mater. Interfaces* **2012**, *4*, 997–1002.
8. Barnes, A. M.; Bartle, K. D.; Thibon, V. R. A. A Review of Zinc Dialkyldithiophosphates (ZDDPS): Characterisation and Role in the Lubricating Oil. *Tribol. Int.* **2001**, *34*, 389-395.
9. Zhang, J.; Spikes, H. On the Mechanism of ZDDP Antiwear Film Formation. *Tribol. Lett.* **2016**, *63*, 1-15.

10. Ye, C.; Liu, W.; Chen, Y.; Yu, L. Room-Temperature Ionic Liquids: a Novel Versatile Lubricant. *Chem. Commun.* **2001**, 2244−2245.

11. Zhou, F.; Liang, Y.; Liu, W. Ionic Liquid Lubricants: Designed Chemistry for Engineering Applications. *Chem. Soc. Rev.* **2009**, *38*, 2590−2599.

12. Cai, M. R.; Liang, Y.; Yao, M.; Xia, Y.; Zhou, F.; Liu, W. Imidazolium Ionic Liquids as Antiwear and Antioxidant Additive in Poly(Ethylene Glycol) for Steel/Steel Contacts. *ACS Appl. Mater. Interfaces* **2010**, *2*, 870−876.

13. Barnhill, W. C.; Qu, J.; Luo, H.; Meyer III, H. M.; Ma, C.; Chi, M.; Papke, B. L. Phosphonium-Organophosphate Ionic Liquids as Lubricant Additives: Effects of Cation Structure on Physicochemical and Tribological Characteristics. *ACS Appl. Mater. Interfaces* **2014**, *6*, 22585–22593.

14. Qu, J.; Barnhill, W. C.; Luo, H.; Meyer III, H. M.; Leonard, D. N.; Landauer, A. K.; Kheireddin, B.; Gao, H.; Papke, B. L.; Dai, S. Synergistic Effects Between Phosphonium-Alkylphosphate Ionic Liquids and Zinc Dialkyldithiophosphate (ZDDP) as Lubricant Additives. *Adv. Mater.* **2015**, *27*, 4767-4774.

15. Zhou, Y.; Qu, J. Ionic Liquids as Lubricant Additives: A Review. *ACS Appl. Mater. Interfaces* **2017**, *9*, 3209-3222.

16. Gulzar, M.; Masjuki, H. H.; Kalam, M. A.; Varman, M.; Zulkifli, N. W. M.; Mufti, R. A.; Zahid, R. Tribological Performance of Nanoparticles as Lubricating Oil Additives. *J. Nanopart. Res.*, **2016**, *18*, 223.

17. Martin, J. M.; Ohmae, N. *Nanolubricants*. John Wiley & Sons: Chichester, 2008.

18. Qiu, S.; Zhou, Z.; Dong, J.; Chen, G. Preparation of Ni Nanoparticles and Evaluation of Their Tribological Performance as Potential Additives in Oils. *J. Tribol.* **1999**, *123*, 441–443.

19. Zhou, J.; Wu, Z.; Zhang, Z.; Liu, W.; Xue, Q. Tribological Behavior and Lubricating Mechanism of Cu Nanoparticles in Oil. *Tribol. Lett.* **2000**, *8*, 213−218.

20. Desanker, M.; Johnson, B.; Seyam, A. M.; Chung, Y.-W.; Bazzi, H. S.; Delferro, M.; Marks, T. J.; Wang, Q. J. Oil-Soluble Silver−Organic Molecule for in Situ Deposition of Lubricious Metallic Silver at High Temperatures. *ACS Appl. Mater. Interfaces* **2016**, *8*, 13637−13645.

21. Xue, Q.; Liu, W.; Zhang, Z. Friction and Wear Properties of a Surface-Modified TiO_2 Nanoparticle as an Additive in Liquid Paraffin. *Wear* **1997**, *213*, 29–32.

22. Li, X.; Cao, Z.; Zhang, Z.; Dang, H. Surface-Modification in situ of Nano-SiO_2 and its Structure and Tribological Properties. *Appl. Surf. Sci.* **2006**, *252*, 7856−7861.

23. Kim, D.; Archer, L. A. Nanoscale Organic−Inorganic Hybrid Lubricants. *Langmuir* **2011**, *27*, 3083–3094.

24. Li, B.; Wang, X.; Liu, W.; Xue, Q. Tribochemistry and Antiwear Mechanism of Organic–Inorganic Nanoparticles as Lubricant Additives. *Tribol. Lett.* **2006**, *22*, 79–84.

25. Ali, M. K., A.; Xianjun, H.; Mai, L.; Qingping, C.; Turkson, R. F.; Bicheng, C. Improving the Tribological Characteristics of Piston Ring Assembly in Automotive Engines Using Al_2O_3 and TiO_2 Nanomaterials as Nano-Lubricant Additives. *Tribol. Int.* **2016**, *103*, 540-554.

26. Battez, A. H.; Rico, J. E. F.; Arias, A. N.; Rodriguez, J. L. V.; Rodriguez, R. C.; Fernandez, J. M. D. The Tribological Behaviour of ZnO Nanoparticles as an Additive to PAO6. *Wear* **2006**, *261*, 256 –263.

27. Rapoport, L.; Fleischer, N.; Tenne, R. Fullerene-like WS_2 Nanoparticles: Superior Lubricants for Harsh Conditions. *Adv. Mater.* **2003**, *15*, 651−655.

28. Joly-Pottuz, L.; Dassenoy, F.; Belin, M.; Vacher, B.; Martin, J. M.; Fleischer, N. Ultralow-Friction and Wear Properties of IF-WS_2 under Boundary Lubrication. *Tribol. Lett.* **2005**, *18*, 477-485.

29. Qi, H.; Guo, Y.; Zhang, L.; Li, G.; Zhang, G.; Wang, T.; Wang, Q. Covalently Attached Mesoporous Silica-Ionic Liquid Hybrid Nanomaterials as Water Lubrication Additives for Polymer-Metal Tribopair. *Tribol. Int.* **2018**, *119*, 721-730.

30. Welton, T. Room-Temperature Ionic Liquids. Solvents for Synthesis and Catalysis. *Chem. Rev.* **1999**, *99*, 2071–2084.

31. Wright, R. A. E.; Wang, K.; Qu, J.; Zhao, B. Oil-Soluble Polymer Brush-Grafted Nanoparticles as Effective Lubricant Additives for Friction and Wear Reduction. *Angew. Chem. Int. Ed.* **2016**, *55*, 8656-8660.

32. Seymour, B. T.; Wright, R. A. E.; Parrott, A. C.; Gao, H. Y.; Martini, A.; Qu, J.; Dai, S.; Zhao, B. Poly(alkyl methacrylate) Brush-Grafted Silica Nanoparticles as Oil Lubricant Additives: Effects of Alkyl Pendant Group on Oil Dispersibility, Stability, and Lubrication Property. *ACS Appl. Mater. Interfaces* **2017**, *9*, 25038–25048.

33. Pyun, J.; Matyjaszewski, K. Synthesis of Nanocomposite Organic/Inorganic Hybrid Materials Using Controlled/"Living" Radical Polymerization. *Chem. Mater.* **2001**, *13*, 3436–3448.

34. Skaff, H.; Emrick, T. Reversible Addition Fragmentation Chain Transfer (RAFT) Polymerization from Unprotected Cadmium Selenide Nanoparticles. *Angew. Chem., Int. Ed.* **2004**, *43*, 5383-5386.

35. Zhao, B.; Zhu, L. Mixed Polymer Brush-Grafted Particles: A New Class of Environmentally Responsive Nanostructured Materials. *Macromolecules* **2009**, *42*, 9369-9383.

36. Bao, C.; Tang, S.; Horton, J. M.; Jiang, X.; Tang, P.; Qiu, F.; Zhu, L.; Zhao, B. Effect of Overall Grafting Density on Microphase Separation of Mixed Homopolymer Brushes Synthesized from Y-Initiator-Functionalized Silica Particles. *Macromolecules* **2012**, *45*, 8027-8036.

37. Wright, R. A. E.; Henn, D. M.; Zhao, B. Thermally Reversible Physically Crosslinked Hybrid Network Hydrogels Formed by Thermosensitive Hairy NPs. *J. Phys. Chem. B* **2016**, *120*, 8036-8045.

38. Liu, G.; Liu, Z.; Li, N.; Wang, X.; Zhou, F.; Liu, W. Hairy Polyelectrolyte Brushes-Grafted Thermosensitive Microgels as Artificial Synovial Fluid for Simultaneous Biomimetic Lubrication and Arthritis Treatment. *ACS Appl. Mater. Interfaces* **2014**, *6*, 20452–20463.

39. Barnhill, W. C.; Luo, H.; Meyer, H. M., III; Ma, C.; Chi, M.; Papke, B. L.; Qu, J. Tertiary and Quaternary Ammonium-Phosphate Ionic Liquids as Lubricant Additives. *Tribol. Lett.* **2016**, *63*, 22.

40 Sango, K.; Sato, S.; Naito, H.; Saeki, T.; Matsushita, T.; Narita, E. Silicon Phosphate as a New Hardener for Alkali Silicate Solutions. *Ind. Eng. Chem. Prod. Res. Dev.*, **1984**, *23*, 315-317.

41. Nurse, R. W.; Welch, J. H.; Gutt, W. High-Temperature Phase Equilibrium in the System Dicalcium Silicate-Tricalcium Phosphate. *J. Chem. Soc.* **1959**, 1077-1083.

42. Iler, R. K. *The Chemistry of Silica: Solubility, Polymerization, Colloid, and Surface Properties, and Biochemistry*; Wiley: New York, 1979.

43. Li, D.; Sheng, X.; Zhao, B. Environmentally Responsive "Hairy" Nanoparticles: Mixed Homopolymer Brushes on Silica Nanoparticles Synthesized by Living Radical Polymerization Techniques. *J. Am. Chem. Soc.* **2005**, *127*, 6248-6256.

44. Husseman, M.; Malmstrom, E. E.; McNamara, M.; Mate, M.; Mecerreyes, D.; Benoit, D. G.; Hedrick, J. L.; Mansky, P.; Huang, E.; Russell, T. P.; Hawker, C. J. Controlled Synthesis of Polymer Brushes by "Living" Free Radical Polymerization Techniques. *Macromolecules* **1999**, *32*, 1424-1431.

45. Wright, R. A. E.; Hu, B.; Henn, D. M.; Zhao, B. Reversible Sol-Gel Transitions of Aqueous Dispersions of Silica Nanoparticles Grafted with Diblock Copolymer Brushes Composed of a Thermosensitive Inner Block and a Charged Outer Block, *Soft Matter*, **2015**, *11*, 6808-6820.

46. Details can be found in Appendix C.

47. Goldstein, J.; Newbury, D. E.; Echlin, P.; Joy, D. C.; Fiori, C.; Lifshin, E. *Scanning Electron Microscopy and X-Ray Microanalysis: A Text for Biologists, Materials Scientists, and Geologists*; Plenum Press: New York and London, 1981.

48. Briggs, D. *Surface Analysis of Polymers by XPS and Static SIMS*; Cambridge University Press: Cambridge, 1998.

49. Amouzou, D.; Fourdrinier, L.; Maseri, F.; Sporken, R. Formation of Me-O-Si Covalent Bonds at the Interface between Polysilazane and Stainless Steel. *Appl. Surface Science*, **2014**, *320*, 519-523.

50. Tanizawa, Y.; Suzuki, T. Effects of Silicate Ions on the Formation and Transformation of Calcium Phosphates in Neutral Aqueous Solutions. *J. Chem. Soc. Faraday Trans.*, **1995**, *91*, 3499-3503.

51. Hasha, D.; Sierra de Saldarriaga, L.; Saldarriaga, C.; Hathaway, P. E.; Cox, D. F.; Davis, M. E. Studies of Silicoaluminophosphates with the Sodalite Structure. *J. Am. Chem. Soc.* **1988**, *110*, 2127-2135.

52. The work presented in this chapter has been published as an article. Seymour, B. T.; Fu, W.; Wright, R. A. E.; Luo, H.; Qu, J.; Dai, S.; Zhao, B. Improved Lubricating Performance by Combining Oil-Soluble Hairy Silica Nanoparticles and an Ionic Liquid as an Additive for a Synthetic Base Oil. *ACS Appl. Mater. Interfaces*, **2018**, *10* (17), 15129–15139.

Appendix C

for

Improved Lubricating Performance by Combining Oil-Soluble Hairy Silica Nanoparticles and an Ionic Liquid as an Additive for a Synthetic Base Oil

C.1. Calculation of Degree of Polymerization and Grafting Density of Polymer Brushes. The degree of polymerization (DP) of the grafted polymer in hairy NPs was calculated from the monomer conversion (90.6%), determined by ^{1}H NMR spectroscopy analysis, and the molar ratio of monomer to the sum of free and surface CTA. The amount of surface CTA grafted on silica NPs that successfully initiated RAFT polymerization was determined from the monomer conversion, the TGA data of CTA-NPs and hairy NPs, and the amount of CTA-NPs used in the polymerization. The weight retentions of CTA-NPs and hairy NPs at 100 °C were 99.18% and 99.34%, respectively. Considering the difference in weight retention at 100 °C, which is believed to be from moisture/absorbed small molecules, the TGA curve of CTA-NPs was shifted upward by 0.16%. The weight retention of CTA-NPs at 800 °C was changed from 86.53 % to 86.69%, and hairy NPs at 800 °C was 54.64%. The mass ratio of volatile to nonvolatile (silica) components at 800 °C is 15.4 : 100 for CTA-NPs and 83.0 : 100 for hairy silica NPs. The amount of the CTA-NPs used in the polymerization was 0.5323 g; the total mass of the grafted polymer is $[(83.0\text{-}15.4)/(100 + 15.4)] \times 0.5323$ g = 0.312 g. The total monomer in the reaction mixture (2.499 g) was multiplied by monomer conversion (90.6 %) to give a total polymer mass of 2.264 g. Using the ratio of total polymer to free polymer (2.264 g/(2.264 g – 0.312 g)) as the molar ratio of total effective CTA to free CTA (89.0 mg, 0.305 mmol), the total amount of CTA in the polymerization system was calculated to be 0.354 mmol, yielding a surface-grafted CTA amount of 0.049 mmol/ g CTA-NPs, a monomer-to-total CTA ratio of 27.7:1, and a DP of 25.

For the calculation of grafting density of polymer brushes, assuming that the silica NPs are spherical and has a density of 2.07 g/cm^3, the mass of a single NP with a diameter of 23 nm is 1.32×10^{-17} g. Using the polymer to silica ratio described above [(83.0-15.4)/100 = 67.6/100], the amount of the grafted polymer on one silica NP is 8.92×10^{-18} g. The molecular weight calculated from the DP is 6400 g/mol, so the number of the grafted polymer chains on one silica NP in PLMA hairy NPs is (8.92×10^{-18} g / 6400 g/mol) × (6.022×10^{23} mol^{-1}) = 840 chains. The surface area of one bare silica NP ($\pi \times 23^2$) = 1662 nm^2. Thus, the grafting density of polymer brushes on silica NPs in PLMA hairy silica NPs is 0.51 chains/nm^2.

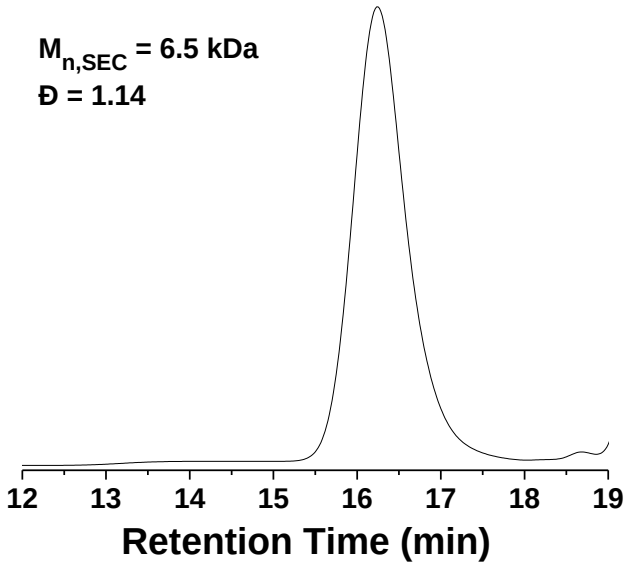

Figure C1. SEC curve of the free polymer poly(lauryl methacrylate) formed in the synthesis of PLMA hairy silica NPs.

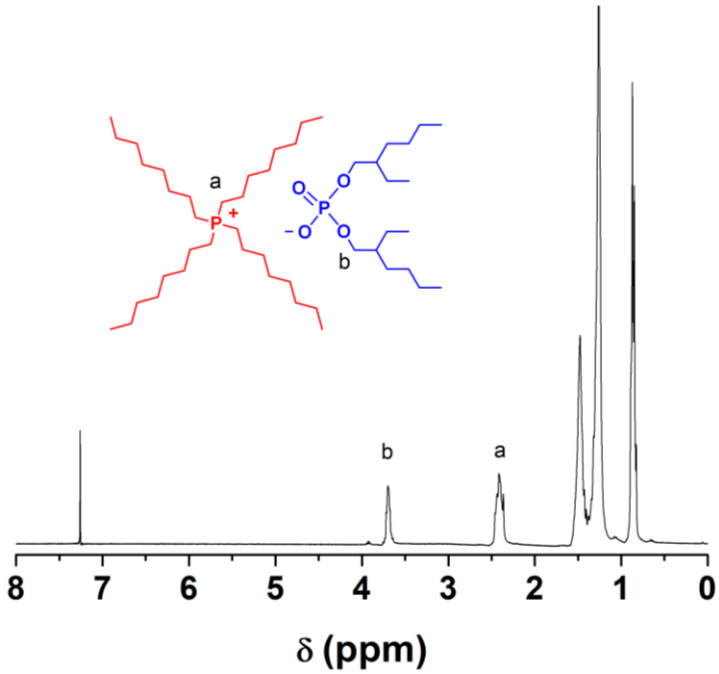

Figure C2. ^{1}H NMR spectrum of oil miscible ionic liquid [P8888][DEHP] in $CDCl_3$.

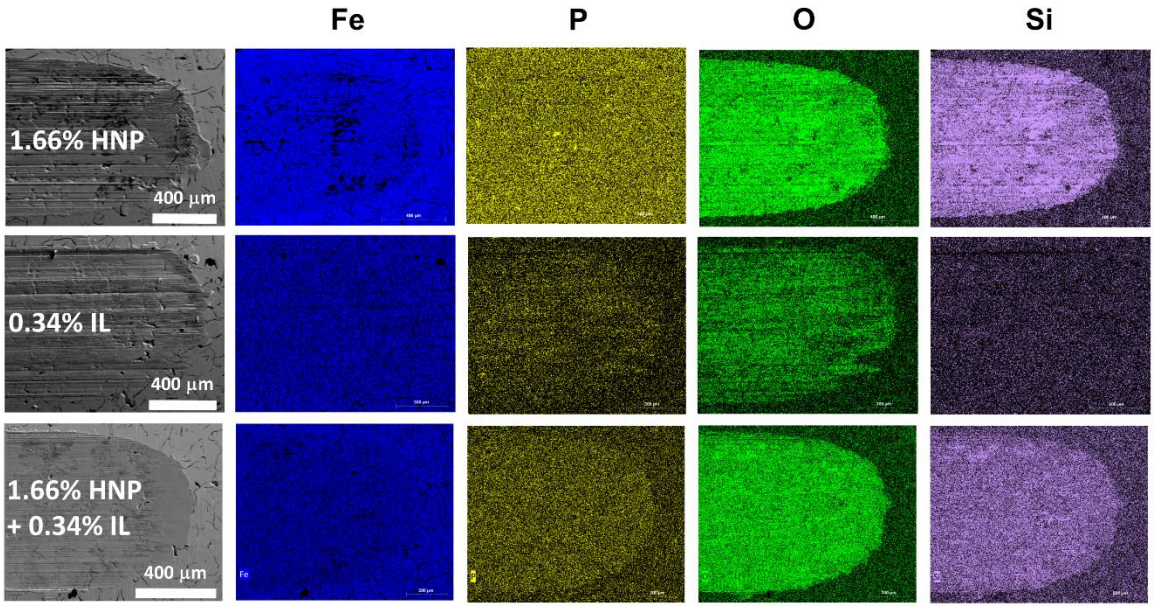

Figure C3. SEM micrograph and EDS elemental mapping of Fe, P, O, and Si of the wear scar at the end of wear track formed on the iron flat during the tribological test of PAO mixed with 1.66% HNP (top row), 0.34% IL (middle row), and 1.66% HNP and 0.34% IL (bottom row).

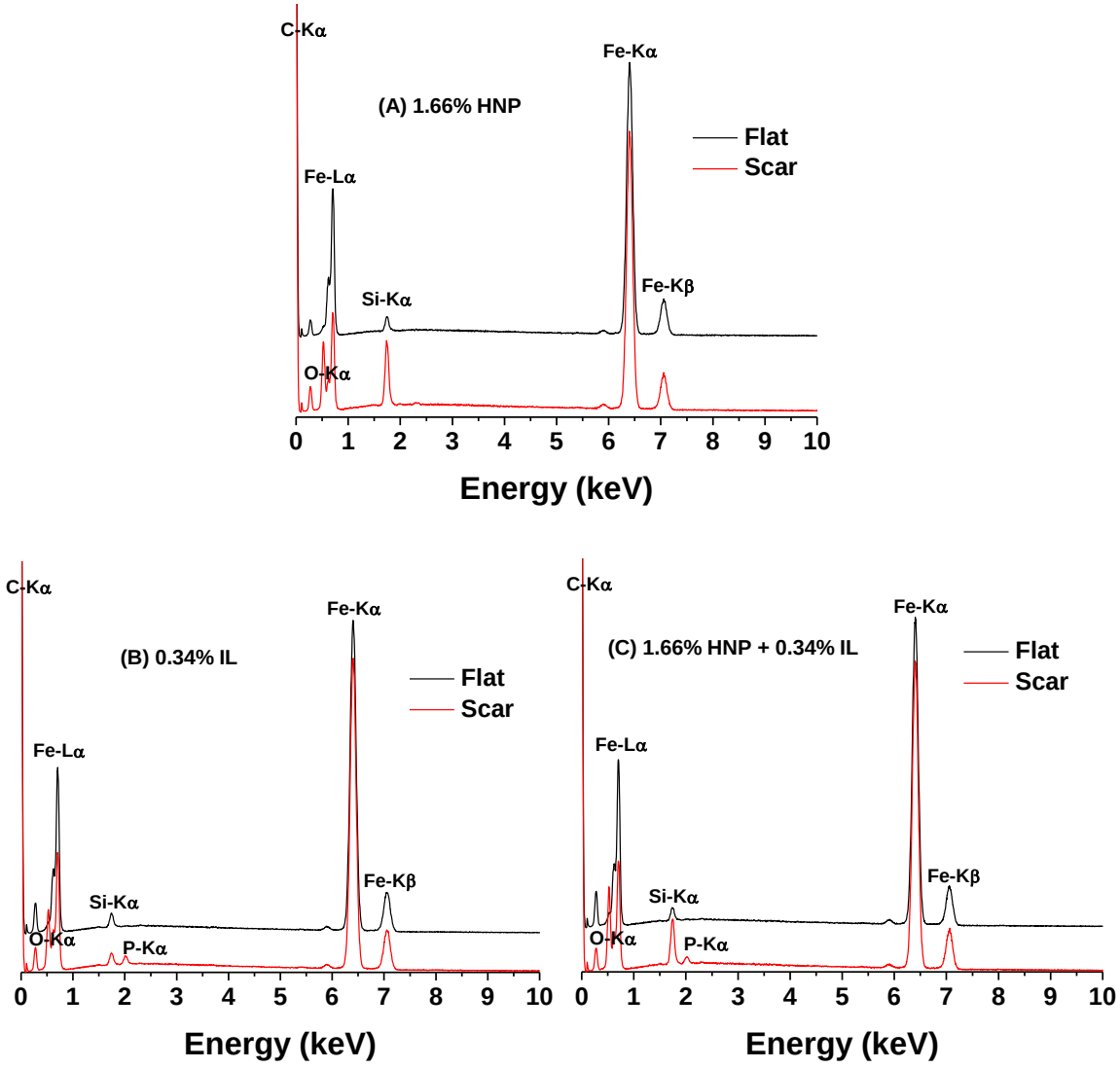

Figure C4. Energy dispersive X-ray spectroscopy analysis of the pristine flat (outside the wear scar) and the wear scar formed on the flat lubricated by the PAO mixed with (A) 1.66% HNP, (B) 0.34% IL, and (C) 1.66% HNP + 0.34% IL.

Chapter 5. Synthesis of Isotactic and Atactic Polyethers with Monosulfone-Containing Pendant Groups

Abstract

As technology advances, new challenges are presented to researchers. One of these challenges is the need for solid-state cooling, which uses more compact and energy efficient materials for on-chip cooling for microelectronic devices. Electrocaloric materials, which have the ability to change temperature in response to application and removal of electrical fields, are promising candidates for efficient on-chip cooling. Ferroelectric crystalline polymers have been reported to exhibit electrocaloric behavior but suffer from various drawbacks such as the need for high driving electric fields and small temperature changes. This chapter presents the synthesis of chiral mesogen-free liquid crystalline polymers, which are expected to exhibit ferroelectric properties and require lower driving electrical fields. The synthesized polymers are polyethers that contain a monosulfone group and have an alkyl tail of varying lengths in the pendant group of every repeat unit. The chiral, isotactic polyethers were synthesized by ring-opening polymerization of *R*-(-)-epichlorohydrin and subsequent post-polymerization modifications. For comparison, atactic poly(epichlorohydrin), purchased from Sigma-Aldrich, was used for the synthesis of atactic polyethers by similar post-polymerization modifications. The thermal stability of the resulting polyethers with monosulfone-containing pendant groups was investigated by thermogravimetric analysis. Our collaborators are currently studying these polymers by differential scanning calorimetry and small and wide angle x-ray scattering.

5.1. Introduction

Electrocaloric materials have the ability to undergo adiabatic thermal changes upon the application and removal of an electrical field. This thermal change is induced by the alignment of polar groups along the applied electrical field and the subsequent randomization of dipoles upon removal of the electrical field.[1] This process is comparable to a vapor compression cooling system, which cools through adiabatic compression and expansion of gases, driven by a mechanical compressor.[2] Although conventional cooling methods, such as vapor compression systems, have the ability to produce a cooling effect, they are often bulky, inefficient, and suffer from short lifetimes due to the breakdown of moving parts. The need for solid-state cooling has prompted researchers to explore the potential of electrocaloric materials.[3,4] When comparing the efficiency of current cooling methods and electrocaloric materials, a term known as the coefficient of performance (COP) is commonly used, which is a measure of heat removed per electrical energy consumed.[5,6] Preliminary studies of electrocaloric materials have shown potential, with a COP of ~3 for ferroelectric ceramics and ~7 for ferroelectric polymers.[5] Current cooling methods such as Peltier coolers, which operates on the basis of the thermoelectric effect, and vapor compression cooling, have reported COPs of 2 - 4.[7]

Electrocaloric ceramics have shown promise due to their low production cost and resistance to breakdown from applied electrical fields, and many recent reports can be found.[8-11] For example, Li et. al studied a $Ba(Hf_xTi_{1-x})O_3$ ferroelectric ceramic, which exhibited an electrocaloric effect of 1.64 K and 1.21 K at 117 °C and 76 °C, respectively.[10] However, electrocaloric polymers hold additional advantages over ceramic materials,

which include processability, relatively lighter weight, and flexibility.[12] Zhang et al. studied crystalline poly(vinylidene fluoride) based copolymers, such as poly(vinylidene fluoride-co-trifluoroethylene) (P(VDF-TrFE)) and poly(vinylidene fluoride-co-trifluoroethylene-co-chlorofluoroethylene) (P(VDF-TrFE-CFE)), which exhibited high COPs and large temperature changes ($\Delta T = 15K$) due to high saturation polarization (50-100 mC/m^2).[1] However, these polymers suffered from high driving electric fields e.g. 307 MV/m near room temperature for the terpolymer P(VDF-TrFE-CFE) for temperature changes of 12 °C. Lin et al. studied similar polymer systems, which also required high driving electrical fields of up to 350 MV/m at room temperature.[13] Despite the large temperature change observed in these copolymers, very high electrical driving fields are needed to align all dipoles properly along the applied electric field due to the densely packed structures of crystalline polymers. High electrical fields ultimately result in a shorter lifetime of materials due to the electrical breakdown.

Liquid crystalline polymers (LCPs) can be used to avoid high driving electrical fields, which have less densely packed structures and require lower electrical driving fields (5-20 MVm^{-1}) to reach saturation polarization.[14] Ferroelectric properties are expected in LCPs in the chiral smectic C (SmC*) phase, which will allow for an entropic cooling effect. Hult et al. synthesized dendritic liquid crystalline polymers with aromatic side chains, which were observed to display ferroelectric SmC* phases.[15] Mesogen-containing ferroelectric LCPs have a relatively low overall dipole density due to bulky rigid aromatic mesogen groups, which limits the polarization.[16] Lee et. al has reported on the synthesis of mesogen-free, achiral, sulfone-containing liquid crystalline polyethers with monosulfone or disulfone-

containing pendant groups (Scheme 5.1.).[17,18] The ordered structure of these polyethers were accredited to the strong dipole-dipole interactions of the polar sulfone groups. In this work, we will synthesize LCPs that have chirality along the polymer backbone in every repeat unit. These LCPs will be chiral polyethers with monosulfone-containing pendant groups, in which we expect to observe the SmC* phase that may require lower electrical driving fields and display large temperature changes in ambient conditions.

In the present work, we introduce chirality into the backbone in every repeat unit of isotactic polyepichlorohydrin (I-PECH) through the ring-opening polymerization of chiral epichlorohydrin. To achieve the desired mesogen-free liquid crystalline polymers, polyethers with side chains containing a monosulfone group and an alkyl tail of varying lengths. Polyethers are chosen as the polymer backbone due to the known flexibility of this type of polymer. A systematic study on how the alkyl tail length affects the polymer's thermal stability will be conducted by comparing thermogravimetric analysis (TGA) results of the polymers with side chains containing a linear alkyl tail of 5 – 12 carbon atoms.

The synthesis of polyethers from epoxides is commonly achieved via an anionic ring-opening polymerization (ROP) route. This is sufficient for the synthesis of low molecular weight, amorphous materials, but anionic ROP of substituted epoxides generally suffers from chain transfer to the monomer. Previous efforts on catalyst development for the synthesis of isotactic, high molecular weight polyethers have proved to be helpful in the understanding of the synthesis of these materials.[19] Ampleman et al. used partially hydrolyzed triethylaluminium ($Al(Et)_3$), one equivalent of $Al(Et)_3$ hydrolyzed with 0.6 equivalents of water in diethyl ether, as catalyst for ROP of *R*-(-)-epichlorhydrin.[20]

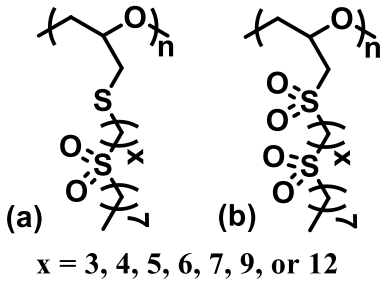

Scheme 5.1. Polyethers with (a) Monosulfone or (b) Disulfone-Containing Pendant Groups.[17,18]

Although this catalyst was slightly different from the Vandenberg catalyst, they were able to synthesize isotactic, high molecular weight chiral polyepichlorohydrin from the chiral monomer. The Vandenberg catalyst is only identified by its preparation: 1 equivalent of trialkyl aluminum, 0.5 equivalent of H_2O, and 0.5 equivalent of acetylacetone.[21] Inspired by the work of Ampleman and Vandenburg, we decided to use commercially available methylaluminoxane (MAO) as the coordination catalyst for the synthesis of I-PECH.

The synthesized I-PECH then underwent post-polymerization modifications to yield isotactic polyethers with monosulfone-containing side chains. The pendant group of I-PECH was first converted to a thioether-containing pendant through a substitution reaction between Cl and *n*-alkanethiols of varying chain lengths in THF using a phase transfer catalyst, tetrabutylammonium bromide (TBAB), and sodium hydride (Scheme 5.2). The obtained thioether-containing polyethers were analyzed by ^{1}H NMR spectroscopy, size exclusion chromatography, and polarimetry after purification. The sulfur in the thioether pendant group was then oxidized into a sulfone group by reacting with 3-chloroperoxybenzoic acid (*m*-CPBA) in chloroform. The resulting polyethers with sulfone-containing pendant groups were analyzed by ^{1}H NMR spectroscopy and TGA after purification. For comparison, atactic polyepichlorohydrin (A-PECH) purchased from Sigma-Aldrich underwent similar modifications. The full synthetic routes starting from A-PECH or I-PECH are outlined in Scheme 5.2.

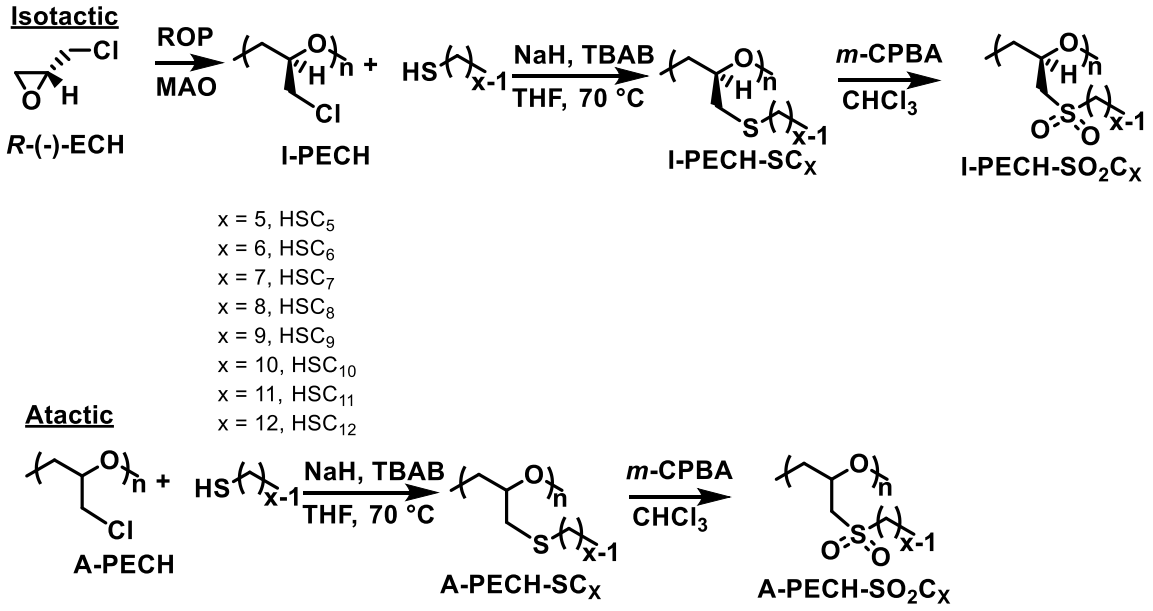

Scheme 5.2. Synthesis of Atactic and Isotactic Polyethers with Monosulfone-Containing Pendant Groups.

5.2. Experimental Section

5.2.1. Materials

The atactic polyepichlorohydrin (A-PECH, with an average M_w of ~700,000 Da by GPC reported by the vendor) used for the synthesis of atactic polyethers that contain monosulfone pendant groups was obtained from Sigma Aldrich. 1-Pentanethiol (HSC5, 98%, TCI), 1-hexanethiol (HSC6, 97%, Alfa Aesar), 1-heptanethiol (HSC7, 98%, Sigma Aldrich), 1-octanethiol (HSC8, 97%, Acros Organics), 1-nonanethiol (HSC9, 98%, Alfa Aesar), 1-decanethiol (HSC10, 96%, Alfa Aesar), 1-undecanethiol (HSC11, 95%, TCI), and 1-dodecanethiol (HSC12, 98%, Acros Organics) were all used as received with no further purification. 3-Chloroperoxybenzoic acid (*m*-CPBA, 70-75% balance 3-chlorobenzoic acid and water, Acros Organics), *n*-tetrabutylammonium bromide (TBAB, 99%, Sigma Aldrich), and sodium hydride (NaH, 60 wt% dispersion in mineral oil, Acros Organics) were used as received. Tetrahydrofuran (THF) was dried with sodium/benzophenone, distilled under a nitrogen atmosphere, and used immediately. *R*-(-)- Epichlorohydrin (*R*-ECH, 98%, Combi-blocks Inc.) and diethyl ether were dried over calcium hydride and distilled before use. Methylaluminoxane (MMAO-12, 7 wt% aluminum in toluene) was purchased from Sigma Aldrich and stored in a nitrogen glove box. All other chemicals and solvents were obtained from either Fisher or Sigma Aldrich and used as received.

5.2.2. Characterization

Size exclusion chromatography (SEC) of polyethers with thioether-containing pendant groups was performed using a PL-GPC 20 (an integrated SEC system from Polymer

Laboratories, Inc.) equipped with a refractive index detector, one PLgel 5 μm guard column (50 × 7.5 mm), and two PLgel 5 μm mixed-C columns (each 300 × 7.5 mm, linear molecular weight range of 200 to 2 000 000 Da). THF was used as the eluent, and the flow rate was set at 1.0 mL/min for the analysis. The SEC system was calibrated with narrow disperse polystyrene standards, and the data were processed using Cirrus GPC/SEC software (Polymer Laboratories, Inc.). ^{1}H NMR spectra were recorded on a Varian Mercury Vx 300 MHz spectrometer and ^{13}C NMR spectra were recorded on a Varian VNMRS 600 MHz spectrometer, and the residual solvent proton signal was used as the internal reference. Thermogravimetric analysis (TGA) of polyethers with monosulfone-containing pendant groups were carried out in N_2 atmosphere at a heating rate of 20 °C/min from room temperature to 700 °C using TA Discovery TGA–MS or TA Instruments Q-50 TGA.

5.2.3. Synthesis of Isotactic Poly((*R*)-(-)-epichlorohydrin) by Ring Opening Polymerization

(*R*)-(-)-Epichlorohydrin (*R*-ECH, 5.0 mL), methylaluminoxane (4.0 mL, 7 wt% aluminum in toluene, corresponding to ~250 mg aluminum), and anhydrous diethyl ether (20 mL) were added to a 50-mL two-necked round bottom flask in a nitrogen glove box. The mixture was stirred with a magnetic stir bar at room temperature, and a white precipitate was gradually formed. After the polymerization proceeded at ambient temperature for 23 h in the glove box, the flask was removed from the glove box and placed under N_2 atmosphere; acetylacetone (10 mL) and methanol (5 mL) were added into the flask and the mixture was stirred for an additional 2 h. The polymerization mixture was

then poured into methanol (75 mL) in an Erlenmeyer flask. After the precipitate settled, the supernatant liquid was decanted. Methanol (75 mL) was then added into the Erlenmeyer flask, and the mixture was stirred for 15 min. The precipitate was left to fully settle, and the supernatant liquid was decanted. The obtained white solid was dried under high vacuum (1.111 g, 18.8% yield). This polymer was used for the synthesis of all isotactic polyethers with monosulfone pendant groups. ^{1}H NMR ($CDCl_3$, 300 MHz), δ (ppm) = 3.80 − 3.52 (m, -C*H*$_2$C*H*(C*H*$_2$Cl)O-, 5H).

5.2.4. Synthesis of Atactic Polyethers with Thioether-Containing Pendant Groups

The following shows the procedure for the synthesis of A-PECH-SC_5 (Scheme 5.2). Similar procedures were used for the synthesis of all other atactic polyethers with thioether-containing pendant groups. A-PECH (0.110 g, 1.19 mmol), tetrabutylammonium bromide (TBAB, 0.073 g, 0.23 mmol), and freshly distilled THF (10 mL) were added to a 50 mL two-necked round bottom flask. The flask was sealed and placed in a 70 °C oil bath, and the mixture was stirred to dissolve the A-PECH. A clear homogeneous solution was observed after about 15 min. The reaction flask was transferred to a fume hood, and HSC5 (0.374 g, 3.59 mmol) was then added into the flask. NaH (60 wt% dispersion in mineral oil, 0.139 g, corresponding to 83.4 mg NaH, 3.48 mmol) was then added to the stirring mixture. After the bubbling ceased, the reaction flask was placed in a 70 °C oil bath, and a reflux condenser was equipped to the reaction flask. After the mixture was stirred and refluxed for 20 h, the polymer was precipitated in deionized H_2O, and centrifugation (Eppendorf Centrifuge 5804, 10k rpm, 10 mins) was used to separate the polymer. The supernatant liquid was decanted, and the polymer was dissolved in methylene chloride.

The polymer was further purified by two rounds of redissolving in methylene chloride and precipitating in methanol. The polymer A-PECH-SC5 was dried under high vacuum and obtained as a clear solid (0.117 g, 61.3% yield). SEC analysis showed that the number average molecular weight ($M_{n,SEC}$) = 182.1 kDa relative to PS standards and dispersity (Đ) = 2.79.

5.2.5. Synthesis of Atactic Polyethers with Monosulfone-Containing Pendant Groups

The obtained A-PECH-SC_5 (0.113 g, 0.705 mmol) was dissolved in chloroform (10 mL) and transferred to a 25 mL two-necked round bottom flask equipped with a magnetic stir bar. The reaction flask was placed under N_2 atmosphere, and *m*-CPBA (0.340 g, 1.97 mmol) was added into the mixture while stirring. After the reaction proceeded at room temperature for 2 h, the mixture was diluted with chloroform (10 mL), transferred to a separatory funnel, and then washed twice with 1 M NaOH solution (10 mL). The organic layer was separated and concentrated by an air stream before precipitation in methanol. The supernatant liquid was decanted, and the precipitated polymer was dried under high vacuum, yielding a white solid (0.072 g, 58.3% yield). All other atactic polyethers with monosulfone-containing pendant groups were synthesized by similar procedures.

5.2.6. Synthesis of Isotactic Polyethers with Thioether-Containing Pendant Groups

The following shows the procedure for the synthesis of I-PECH-SC_5. Similar procedures were used for all other isotactic polyethers with thioether-containing pendant groups. I-PECH (0.079 g, 0.85 mmol), TBAB (0.055 g, 0.17 mmol), and freshly distilled THF (10 mL) were added into a 50 mL two-necked round bottom flask. The flask was sealed and placed in a 70 °C oil bath, and the reaction mixture was stirred. A clear

homogeneous solution/suspension was observed after about 15 min. The reaction flask was moved to a fume hood, and HSC5 (0.270 g, 2.59 mmol) was added into the flask. NaH (60 wt% dispersion in mineral oil, 0.117 g corresponding to 70.2 mg NaH, 2.93 mmol) was then added in the reaction mixture while stirring. After the bubbling stopped the reaction flask was placed in a 70 °C oil bath, and a reflux condenser was equipped on the reaction flask. After the mixture was refluxed under stirring conditions for 20 h, the mixture was poured into deionized H_2O. The precipitate was separated by centrifugation (10k rpm, 10 mins) and the supernatant liquid was decanted. The polymer was redissolved in methylene chloride and precipitated in methanol twice. The polymer was then dried under high vacuum and obtained as a clear solid (0.059 g, 43.4% yield). SEC analysis showed that the $M_{n,SEC}$ = 159.8 kDa relative to PS calibration and Đ = 2.58. Polarimetry revealed that the optical activity was -17.8°.

5.2.7. Synthesis of Isotactic Polyethers Containing Monosulfone Pendant Groups

The obtained I-PECH-SC_5 (0.057 g, 0.36 mmol) was dissolved in chloroform (10 mL) and added to a 25 mL two-necked round bottom flask equipped with a magnetic stir bar. *m*-CPBA (0.173 g, 1.00 mmol) was then added into the flask under N_2 atmosphere while stirring. After the reaction proceeded at room temperature for 2 h, chloroform (10 mL) was added. The mixture was transferred into a separatory funnel and washed twice with 1 M NaOH solution (10 mL). The organic layer was separated, concentrated by an air stream, and precipitated into methanol. After decanting the supernatant liquid, the precipitated polymer was dried under high vacuum and obtained as a white solid (0.060 g, 87.6% yield).

All other isotactic polyethers with monosulfone-containing pendant groups were synthesized by similar procedures.

5.2.8. Optical Activity Measurements of Isotactic Polyethers

The optical activities of polyethers with thioether-containing pendant groups were measured on a PerkinElmer 241 polarimeter using a sodium lamp with a wavelength of 589 nm and an integration time of 1 sec at ambient temperature (~20 °C). The polymers were dissolved in $CHCl_3$ at a concentration of about 10 mg/mL. Three measurements were recorded for each sample, and the average was used as the optical rotation value. The specific rotation was calculated using the equation $[\alpha]_{\lambda}^{T} = \frac{\alpha}{c*l}$; with [α] = specific rotation at a certain temperature (T) and wavelength (λ), α = optical rotation in degrees, c = concentration in g/mL, and l = pathlength in dm. The units of specific rotation are $\frac{\text{deg} * mL}{g*dm}$, which is commonly abbreviated to degrees (°).

5.3. Results and Discussion

5.3.1. Synthesis of Isotactic Poly((*R*)-(-)-epichlorohydrin) by Ring Opening Polymerization

Poly((*R*)-(-)-epichlorohydrin) (I-PECH) was synthesized by ring opening polymerization (ROP) of (*R*)-(-)-epichlorohydrin in diethyl ether using methylaluminoxane (MAO) as the catalyst. The monomer and the solvent were both dried over calcium hydride and distilled to remove any water present before the polymerization. The ROP was conducted at room temperature in an N_2 glove box, and a white precipitate formed gradually after the addition of the catalyst. After the polymerization proceeded for 20 h,

the reaction flask was removed from the glove box and placed under a nitrogen atmosphere. The catalyst residue was extracted from the polymer by adding acetylacetone, which is known to form complexes with the aluminoxane, and stirring for an additional 2 h.[20,22] The mixture was then poured into methanol in an Erlenmeyer flask and stirred for 15 min before allowing the polymer to settle. Once the polymer was fully settled, the supernatant liquid was decanted; fresh methanol was added back into the flask, and the mixture was stirred for an additional 15 min. The polymer was then collected and dried under high vacuum. Figure 5.1 shows the ^{1}H and ^{13}C NMR spectra in $CDCl_3$. Note that the solubility of I-PECH in common organic solvents (such as $CHCl_3$, CH_2Cl_2, THF, DMF, etc.) is rather poor, making characterization by ^{13}C NMR spectroscopy, SEC, and polarimetry challenging. Nevertheless, the ^{13}C NMR spectrum was obtained by collecting the data over an extended period of time (5 h). For comparison, the ^{1}H and ^{13}C spectra of atactic PECH (A-PECH), which was purchased from Sigma-Aldrich and had a nominal molecular weight of 700 kDa, were acquired and are shown in Figure 5.2. From the ^{1}H NMR spectra, there is no noticeable difference in the polymer peak region of 3.76 - 3.56 ppm between I-PECH and A-PECH. Upon further analysis using ^{13}C NMR spectroscopy, we were able to confirm that the obtained I-PECH is highly isotactic as evidenced by a single peak at 69.86 ppm, corresponding to the backbone methylene carbon (Figure 5.1 B). In contrast, the ^{13}C NMR spectrum of A-PECH revealed the backbone methylene carbon peak to be two peaks at 69.67 and 69.39 ppm (Figure 5.2 B), which were consistent with the findings of Ampleman et al. who observed isotactic sequences at 69.30 ppm and racemic sequences at 69.15 and 69.10 ppm, though the peak positions are not identical.[20] This difference could be attributed

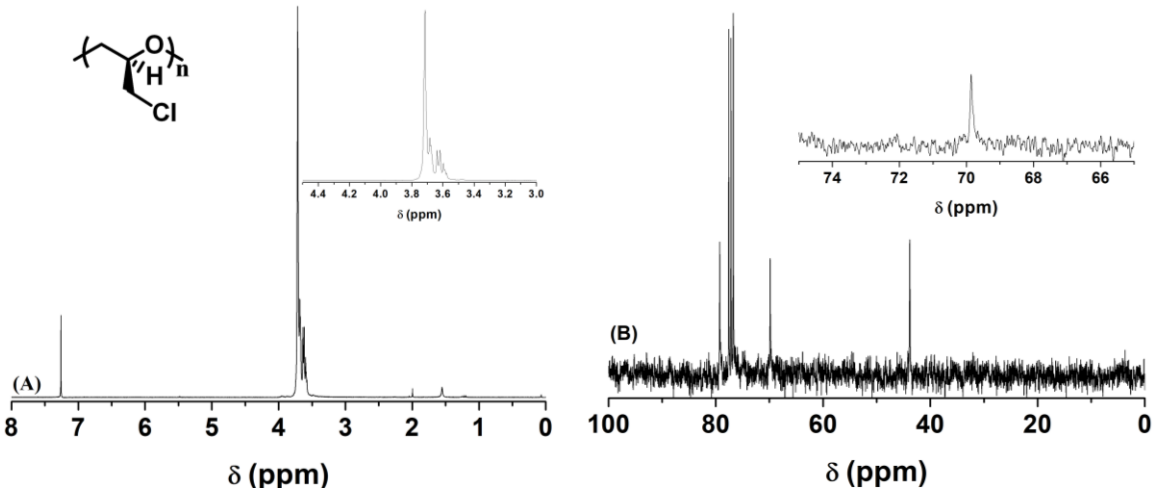

Figure 5.1. (A) ^{1}H and (B) ^{13}C NMR spectrum of I-PECH, synthesized by ring-opening polymerization of (*R*)-(-)-epichlorohydrin with methylaluminoxane as the catalyst, in $CDCl_3$.

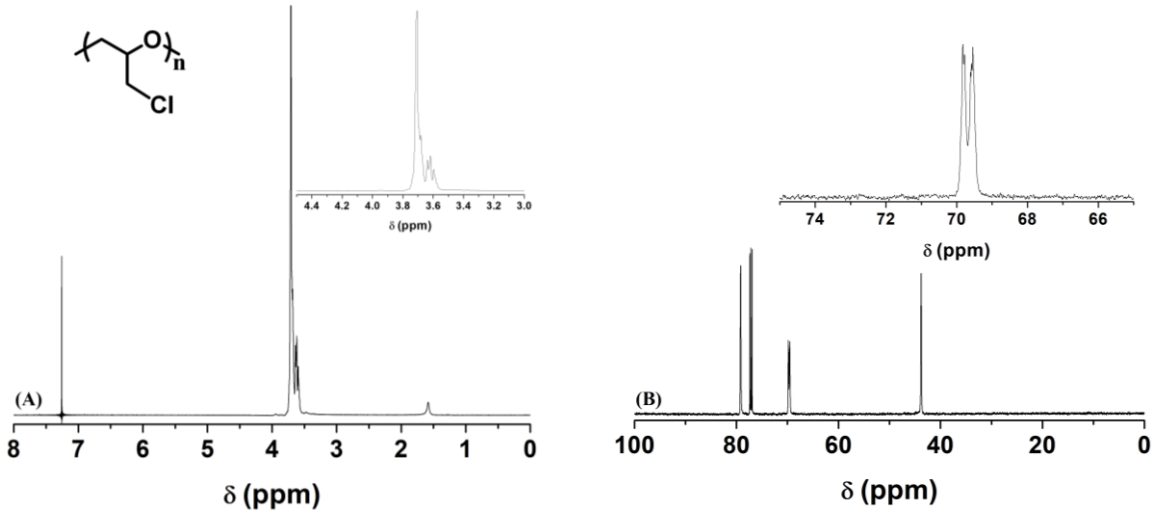

Figure 5.2. (A) ^{1}H and (B) ^{13}C NMR spectrum of A-PECH, purchased from Sigma Aldrich with a molecular weight of 700 kDa, in $CDCl_3$.

to the slight difference in the tacticity of polymer obtained by Ampleman using a catalyst prepared by the in situ hydrolysis of $AlEt_3$ with 0.6 equivalents of water for the ROPs of chiral (*R*)-(-)- epichlorohydrin.[20]

5.3.2. Synthesis of Isotactic and Atactic Polyethers with Thioether-Containing Pendant Groups

To synthesize polyethers with thioether-containing pendant groups, the obtained I-PECH was reacted with linear alkanethiols of varying alkyl lengths, with the number of carbon atoms ranging from 5 to 12, in freshly distilled THF in the presence of sodium hydride. Due to the poor solubility of I-PECH in common organic solvents, I-PECH, THF, and tetrabutylammonium bromide (used as phase transfer catalyst) were first added into a flask and stirred at 70 °C until a homogenous system was formed. After the mixture was cooled to room temperature, an alkanethiol compound was added (in a fume hood), followed by the addition of sodium hydride under stirring conditions. Gas bubbles were observed when sodium hydride was added, and the reaction mixture was kept under N_2 atmosphere at room temperature until the gas bubbling had stopped. The reaction flask was then placed back into an oil bath preheated to 70 °C. The reaction was allowed to proceed under refluxing conditions for 20 h to ensure a maximum degree of substitution to be achieved. The mixture was then precipitated in DI H_2O, and a centrifuge (10k rpm, 10 min) was used to facilitate the separation of the precipitate. After decanting the supernatant liquid, the polymer was redissolved in methylene chloride and precipitated in methanol. This dissolution and precipitation process was repeated an additional two times with methylene chloride and methanol. The polymer was then collected and dried under high

vacuum. The solubility of isotactic samples in common organic solvents was found to increase drastically after the thiol substitution reaction, allowing for characterization by SEC and polarimetry. These polymers are designated as I-PECH-SC_X, where X represents the number of carbon atoms in the thiol compound used to make the polymer. Atactic polyethers with thioether-containing pendant groups were synthesized from the reaction of A-PECH and alkanethiols using a similar procedure as for I-PECH, and are named using the same method as for isotactic polyethers with thioether containing pendant groups. A total of 16 samples (8 isotactic and 8 atactic) were prepared.

Figures 5.3 and 5.4 show the NMR analysis of I-PECH-SC_5 and A-PECH-SC_5. From the ^{1}H NMR spectrum of I-PECH-SC_5 (Figure 5.3A), we observed that the two protons from -C*HCH_2 in the pendant group shifted from 3.75 – 3.57 ppm to 2.80 – 2.48 ppm after the substitution reaction. Quantitative analysis of the integrals of the shifted peaks indicates that the substitution of Cl by the alkanethiol is essentially complete. The ^{13}C NMR spectrum of I-PECH-SC_5 (Figure 5.3B) revealed a single peak at 71.43 ppm. The disappearance of the peak at 69.86 ppm observed in Figure 5.1 B for I-PECH also indicates that the substitution reaction is complete, consistent with the result from the ^{1}H NMR spectroscopy analysis. Figure 5.4 shows the ^{1}H and ^{13}C NMR spectra of A-PECH-SC_5; while similar observations were made for the ^{1}H NMR spectrum, the ^{13}C NMR spectrum showed multiple peaks at 71.39 and 70.65 ppm, which are similar to our findings for A-PECH. However, the peaks are in different positions due to the new chemical environment. Other isotactic and atactic polyethers with thioether-containing pendant groups were also characterized by ^{1}H and ^{13}C NMR spectroscopy, and the spectra are shown in Figures 5.5

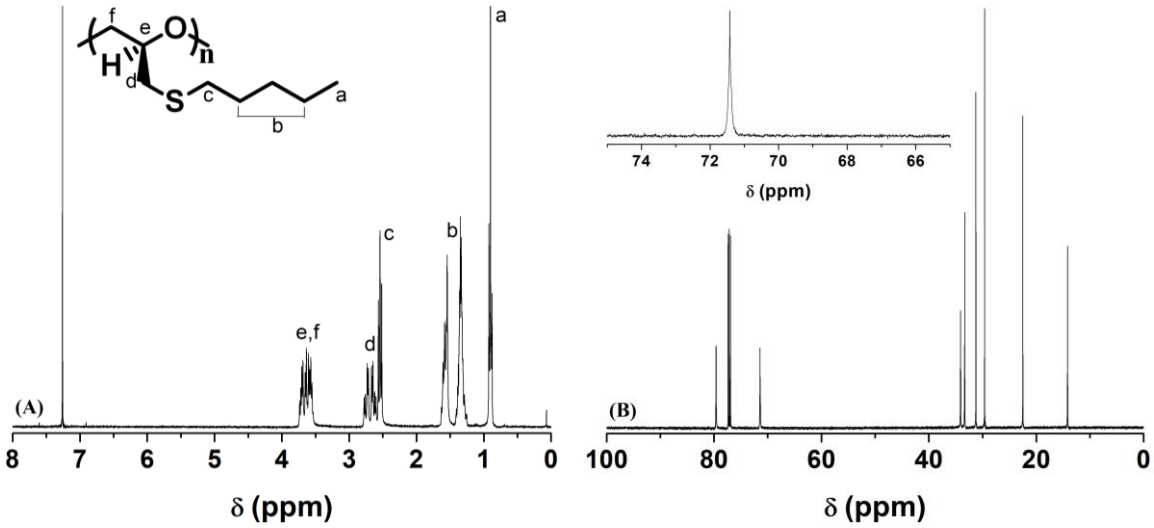

Figure 5.3. (A) ^{1}H and (B) ^{13}C NMR spectrum of I-PECH-SC_5 in $CDCl_3$.

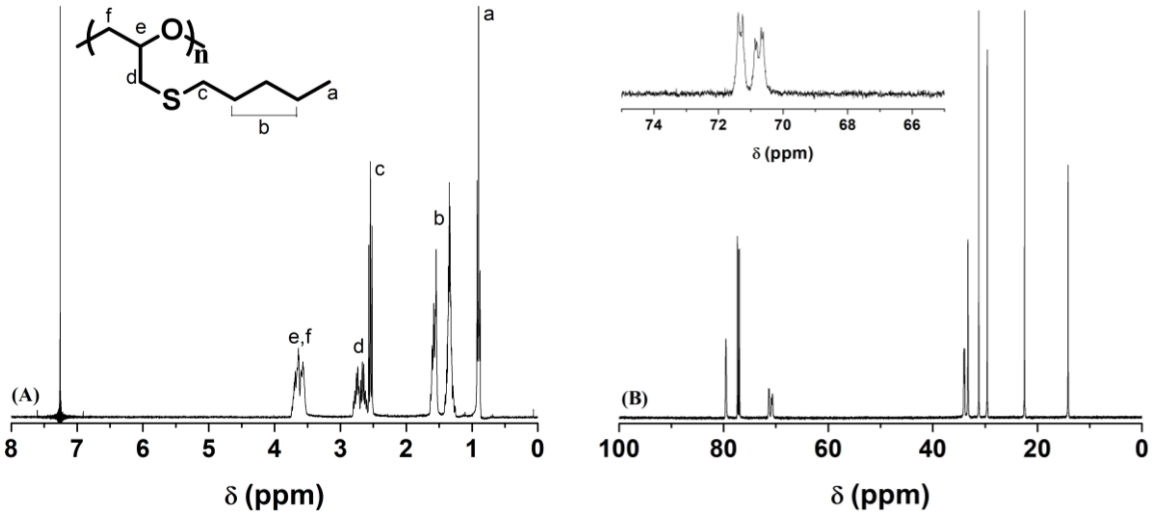

Figure 5.4. (A) ^{1}H and (B) ^{13}C NMR spectrum of A-PECH-SC_5 in $CDCl_3$.

- 5.11. All of the polymers exhibited essentially complete substitution of Cl by linear alkanethiols.

As mentioned earlier, the improved solubility of isotactic polymers after the reaction with thiol compounds allowed for the characterization by size exclusion chromatography (SEC) using THF as eluent. The SEC traces of all polyethers containing thioether pendant groups are shown in Figures 5.12 - 5.15, and the molecular weights and the dispersities (Đ), relative to polystyrene standards, are summarized in Table 5.1. The Đ of all isotactic polyethers with thioether pendant groups are rather large, ranging from 2.5 to 5.5. There appears to be a general trend that the relative number-average molecular weight increased with the increasing length of the thioether pendant group, but some exceptions to this general trend existed. The two peaks observed for I-PECH-SC_{10} is likely due to the total exclusion of the high molecular weight species in the polymer, and thus the $M_{n,SEC}$ value for this polymer is not reliable. These suggested that degradation of the backbone occurred because all of the isotactic samples are made from the same batch of I-PECH.

5.3.3. Optical Activities of Polyethers with Various Thioether-Containing Pendant Groups

Polarimetry is commonly used to measure the optical activity of chiral compounds. These measurements are conducted by passing monochromatic light through a polarizer then the solution containing the compound being analyzed, and an analyzer. The compound is considered optically active if the light is rotated to a measurable degree when the light

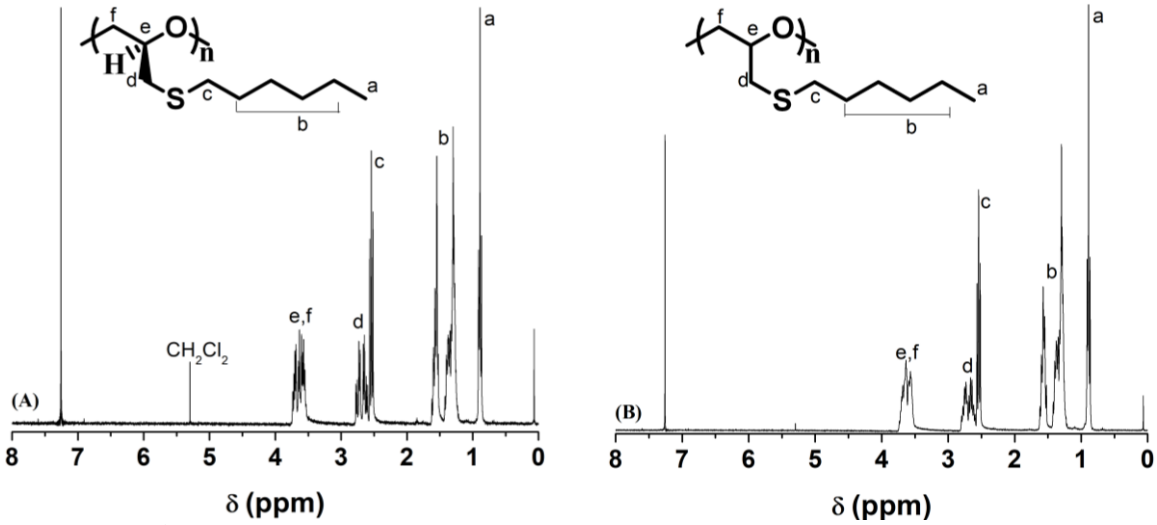

Figure 5.5. ^{1}H NMR spectra of (A) I-PECH-SC_6 and (B) A-PECH-SC_6 in $CDCl_3$.

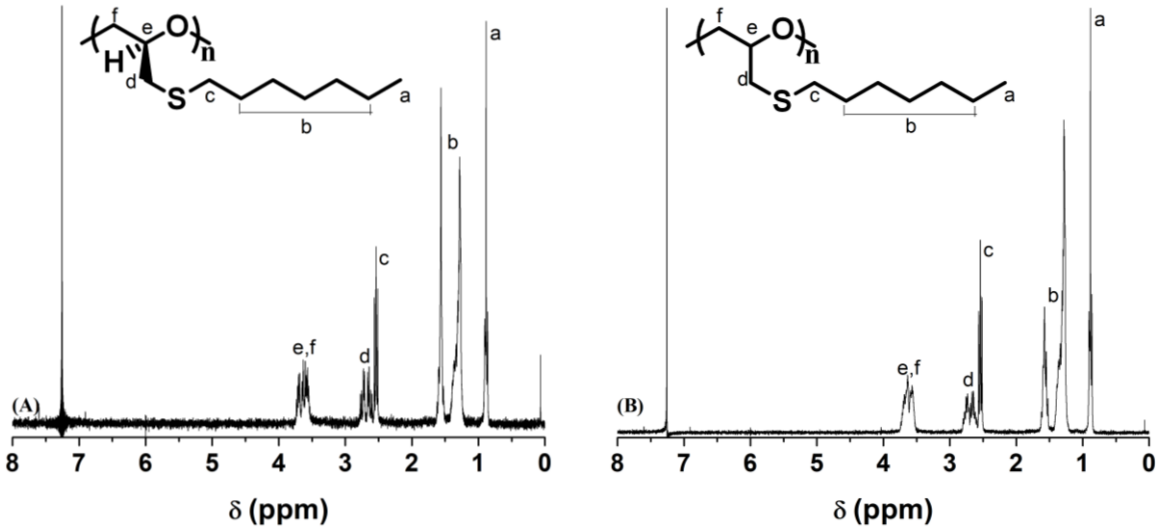

Figure 5.6. ^{1}H NMR spectra of (A) I-PECH-SC_7 and (B) A-PECH-SC_7 in $CDCl_3$.

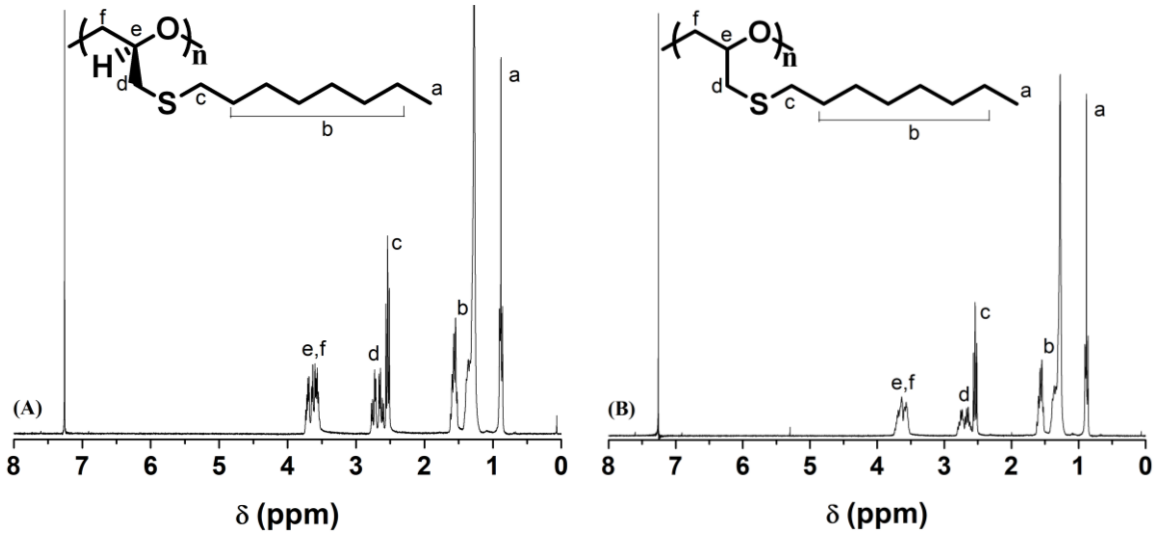

Figure 5.7. ^{1}H NMR spectra of (A) I-PECH-SC_8 and (B) A-PECH-SC_8 in $CDCl_3$.

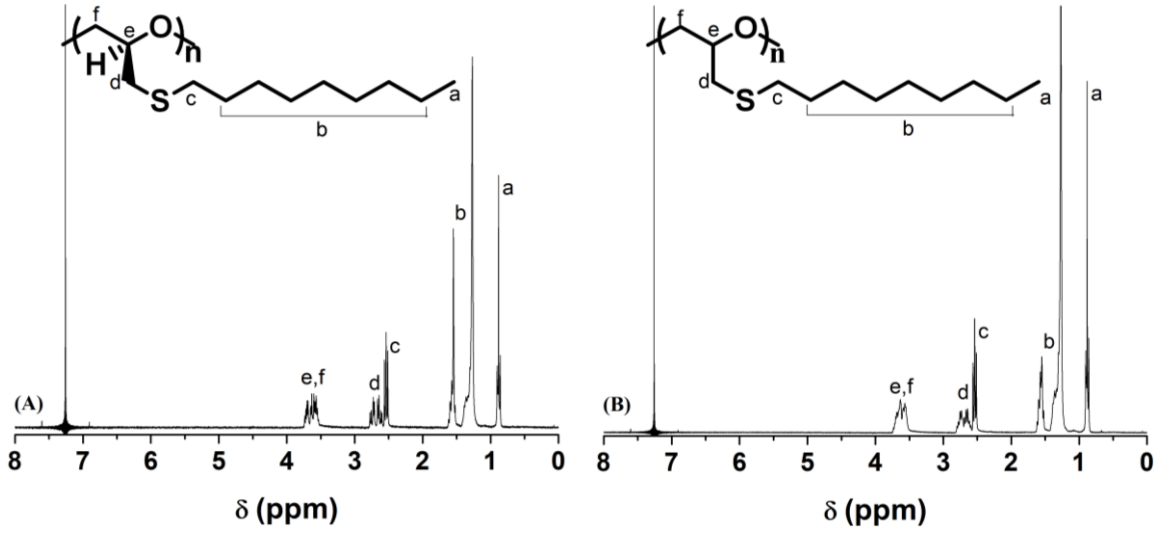

Figure 5.8. ^{1}H NMR spectra of (A) I-PECH-SC_9 and (B) A-PECH-SC_9 in $CDCl_3$.

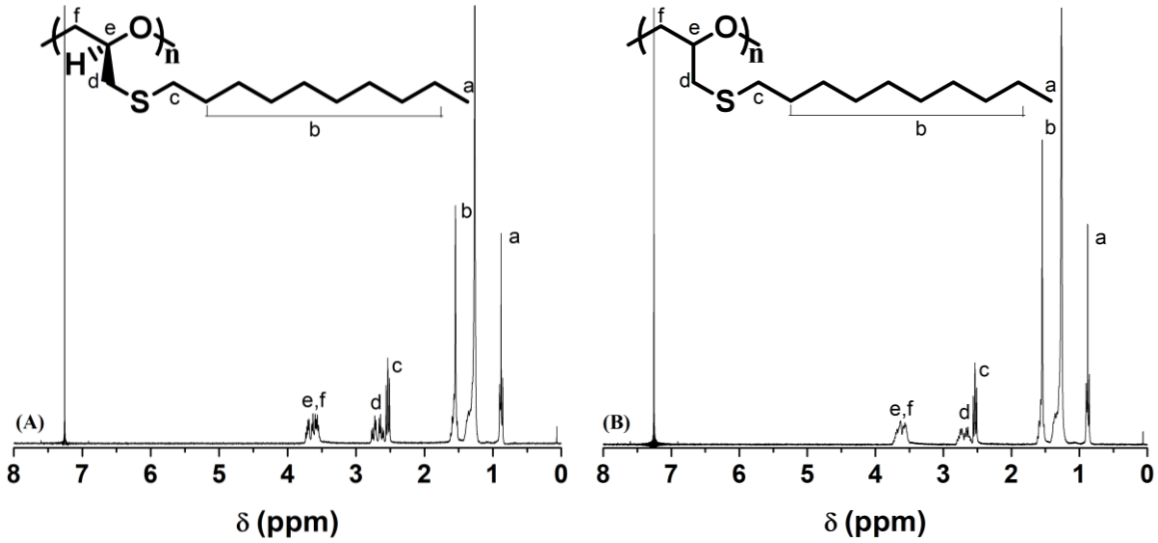

Figure 5.9. ^{1}H NMR spectra of (A) I-PECH-SC_{10} and (B) A-PECH-SC_{10} in $CDCl_3$.

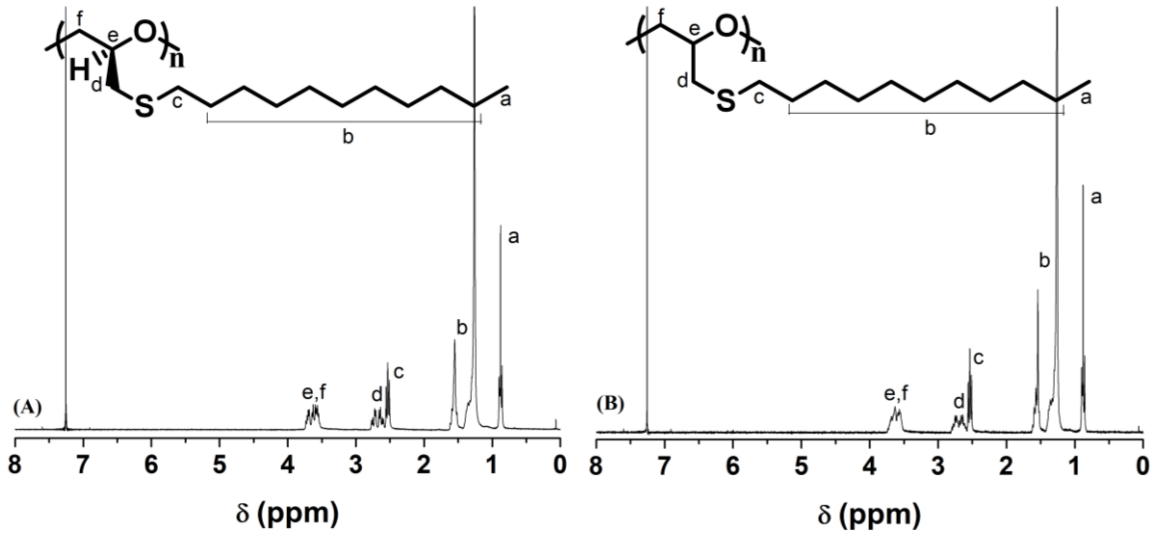

Figure 5.10. ^{1}H NMR spectra of (A) I-PECH-SC_{11} and (B) A-PECH-SC_{11} in $CDCl_3$.

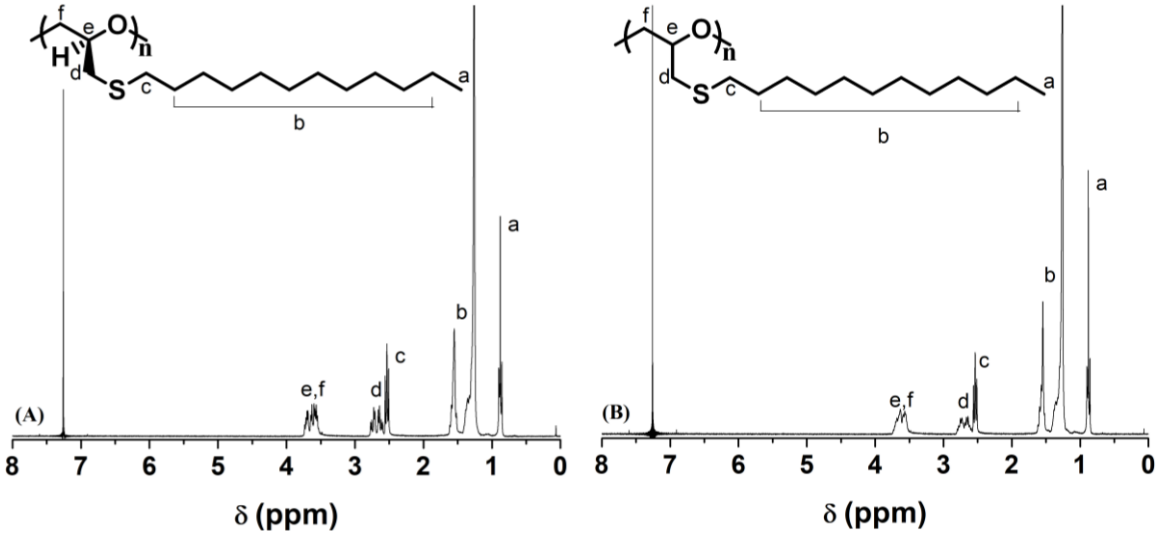

Figure 5.11. ^{1}H NMR spectra of (A) I-PECH-SC_{12} and (B) A-PECH-SC_{12} in $CDCl_3$.

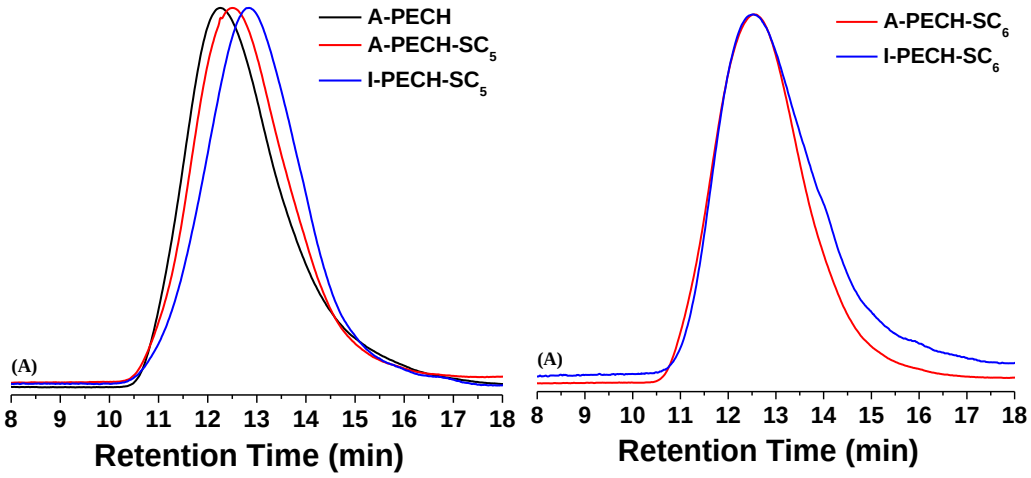

Figure 5.12. SEC traces of (A) A-PECH, A-PECH-SC_5, and I-PECH-SC_5 and (B) A-PECH-SC_6 and I-PECH-SC_6 using THF as eluent.

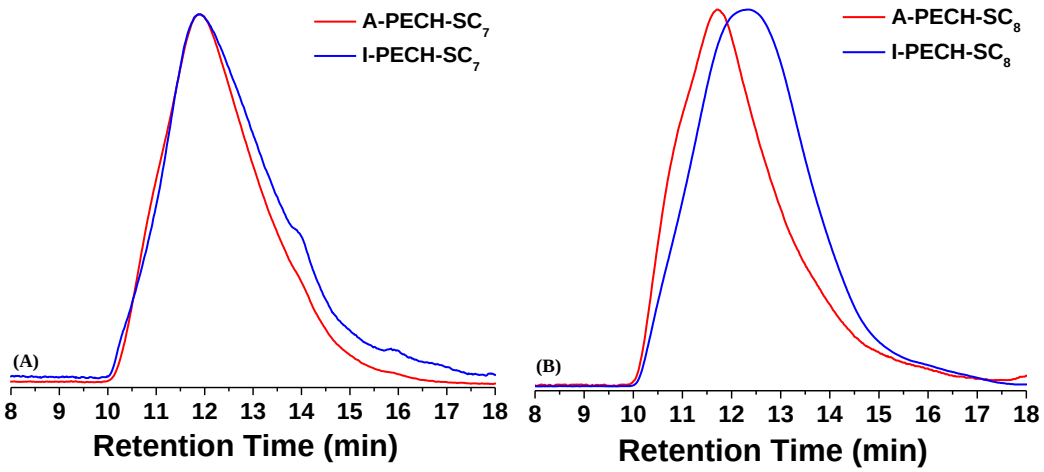

Figure 5.13. SEC traces of (A) A-PECH-SC_7 and I-PECH-SC_7 and (B) A-PECH-SC_8 and I-PECH-SC_8 using THF as eluent.

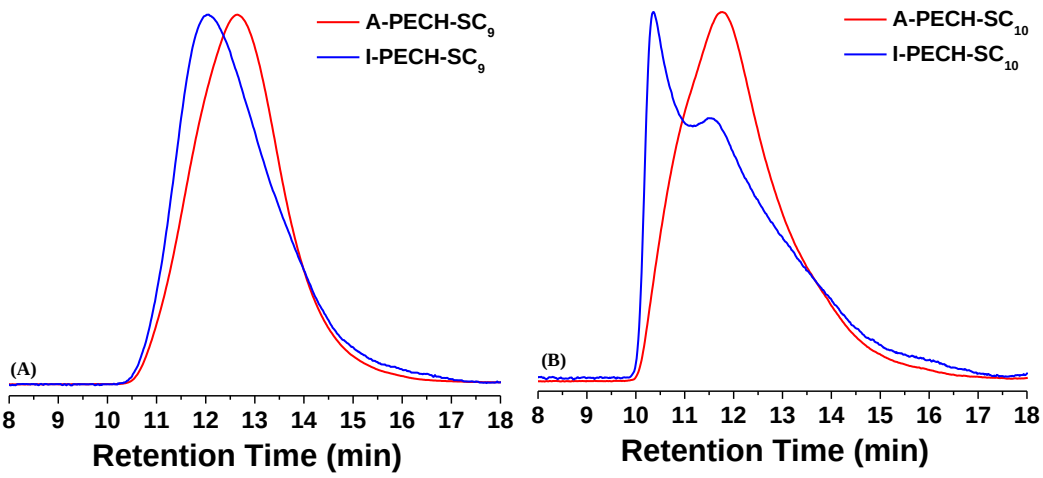

Figure 5.14. SEC traces of (A) A-PECH-SC_9 and I-PECH-SC_9 and (B) A-PECH-SC_{10} and I-PECH-SC_{10} using THF as eluent.

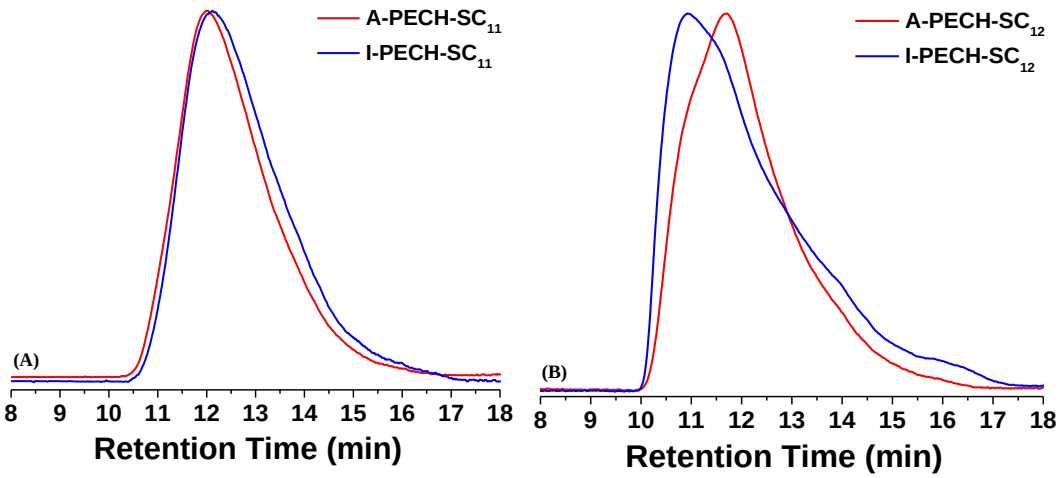

Figure 5.15. SEC traces of (A) A-PECH-SC_{11} and I-PECH-SC_{11} and (B) A-PECH-SC_{12} and I-PECH-SC_{12} using THF as eluent.

Table 5.1. Summary of SEC Characterization data for A-PECH and Polyethers with Thioether Pendant Groups

	$M_{n,SEC}$ (kDa)	$M_{w,SEC}$ (kDa)	Đ
A-PECH	181.8	587.1	3.23
I-PECH	n/a	n/a	n/a
A-PECH-SC_5	182.1	507.4	2.79
I-PECH-SC_5	159.8	412.9	2.58
A-PECH-SC_6	174.5	561.4	3.22
I-PECH-SC_6	136.9	481.3	3.52
A-PECH-SC_7	258.2	1,015.0	3.93
I-PECH-SC_7	289.8	977.7	3.37
A-PECH-SC_8	411.5	1319.5	3.21
I-PECH-SC_8	239.1	903.7	3.78
A-PECH-SC_9	218.0	592.9	2.72
I-PECH-SC_9	298.1	751.3	2.52
A-PECH-SC_{10}	304.6	1,305.8	4.29
I-PECH-SC_{10}	353.4	1,943.4	5.50
A-PECH-SC_{11}	257.1	757.9	2.95
I-PECH-SC_{11}	146.0	643.3	4.41
A-PECH-SC_{12}	494.4	1,362.0	2.75
I-PECH-SC_{12}	398.6	1,669.5	4.19

passes through the solution. Polarimetry of all isotactic polyethers with thioether-containing pendant groups, A-PECH, and A-PECH-SC_6 in $CHCl_3$ was conducted at a typical concentration of 10 mg polymer/ 1 mL solution. As expected, the isotactic samples exhibited an optical activity, while the atactic samples had no optical activity. The specific rotation of *R*-(-)-ECH monomer is -35.4° in methanol which is essentially the same as the value reported by the manufacturer ($[\alpha]_D^{20}$ = -34° at *c* =1). In contrast, the optical activities of isotactic polyethers with thioether pendant groups were in the range of -12.5° to -17.8°, which are much lower than that of the monomer. This might result from different heteroatoms (Cl vs S) before and after the substitution reaction and different molar masses of the repeat unit. Assuming that the contributions of Cl and S-R to the optical activity are identical, we normalized the optical activities of isotactic samples on the basis of the molar mass of the repeat unit. All of the polarimetry results are summarized in Table 5.2, including the normalized optical activities which were found to be ranging from -27.3 to -38.6°, comparable to that of *R*-(-)-ECH. Thus, from the polarimetry and ^{13}C NMR spectroscopy data, we confirmed that isotactic polyethers with thioether pendant groups was successfully obtained through the synthetic procedure described above.

5.3.4. Synthesis of Isotactic and Atactic Polyethers with Monosulfone-Containing Pendant Groups

The synthesis of polyethers with monosulfone-containing pendant groups was accomplished by the oxidation of the thioether in the side chain to a sulfone group using oxidizing agent *meta*-chloroperoxybenzoic acid (*m*-CPBA) in chloroform at room

Table 5.2. Summary of Polarimetry Data Acquired Including the Measured Activity and Normalized Activity

	$[\alpha]_{589}^{20}$ (°)	Molar Mass[a]	Molar Mass Ratio[b]	Normalized $[\alpha]_{589}^{20}$ (°)
R -(-)-ECH	-35.4	92.52		
I-PECH-SC_5	-17.8	160.28	1.73	-30.8
A-PECH-SC_6	0.0			
I-PECH-SC_6	-17.8	174.30	1.88	-33.5
I-PECH-SC_7	-14.7	188.33	2.04	-29.9
I-PECH-SC_8	-12.5	202.36	2.19	-27.3
I-PECH-SC_9	-12.8	216.38	2.34	-29.9
I-PECH-SC_{10}	-13.6	230.41	2.49	-33.9
I-PECH-SC_{11}	-12.7	244.44	2.64	-33.6
I-PECH-SC_{12}	-13.8	258.46	2.79	-38.6

[a] Molar mass of the polymer repeat unit. [b] Molar mass ratio of repeat unit to monomer *R*-(-)-ECH.

temperature for 2 h. The reaction mixture was then diluted with additional chloroform and transferred to a separatory funnel. The polymer was washed with 1 M NaOH solution twice. The organic layer was collected and concentrated under an air stream. The solubility of the oxidized samples in common organic solvents ($CHCl_3$, CH_2Cl_2, THF, etc.) was found to be poor after the polymers were fully dried. Nevertheless, ^{1}H NMR spectroscopy was performed and shown in Figures 5.16 – 5.23. From the ^{1}H NMR spectra, we observed that the CH_2 groups adjacent to the sulfone shifted from 2.80 – 2.48 ppm to 3.40 – 2.92 ppm after the oxidation reaction. The complete shift indicated that the polyethers were fully oxidized. After precipitation in methanol from chloroform once, the polymers were collected and fully dried under high vacuum for thermal analysis. These samples were named in a similar fashion as mentioned earlier, with the addition of O_2 after S signifying the presence of a sulfone group in the pendant group.

5.3.5. Thermogravimetric Analysis of Polyethers with Monosulfone-Containing Pendant Groups

The oxidized products, polyethers with sulfone-containing pendant groups, were characterized by TGA for thermal stability. The TGA profiles for all polymers are presented in Figures 5.24 – 5.27. The temperatures at the 95% weight retention for all polymers are summarized in Table 5.3. We found that the isotactic polymers were observed to generally have higher thermal degradation temperatures than the atactic polyethers with the same pendant group, although there were some exceptions: PECH-SO_2C_7, PECH-SO_2C_9, and PECH-SO_2C_{10}. The underlying reasons for these exceptions are unclear. The generally higher thermal stability of isotactic polyethers with sulfone-containing pendant

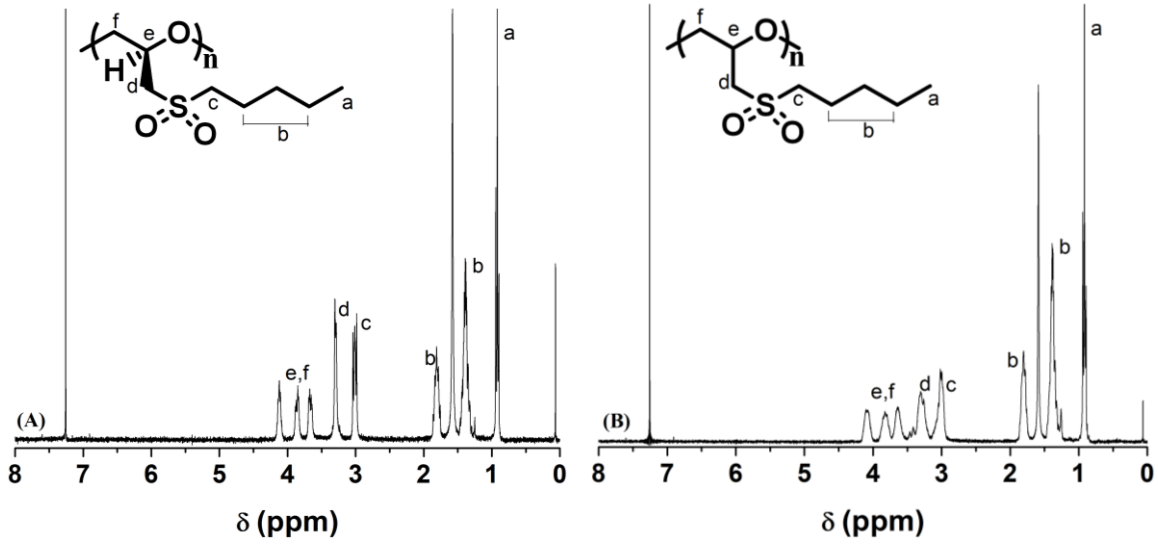

Figure 5.16. ^{1}H NMR spectra of (A) I-PECH-SO_2C_5 and (B) A-PECH-SO_2C_5 in $CDCl_3$.

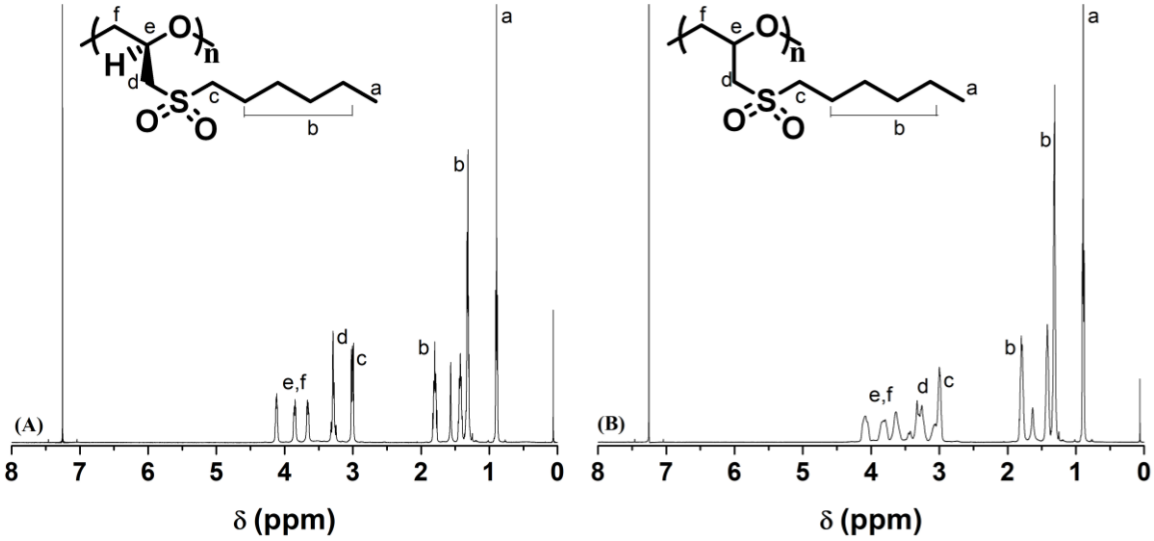

Figure 5.17. ^{1}H NMR spectra of (A) I-PECH-SO_2C_6 and (B) A-PECH-SO_2C_6 in $CDCl_3$.

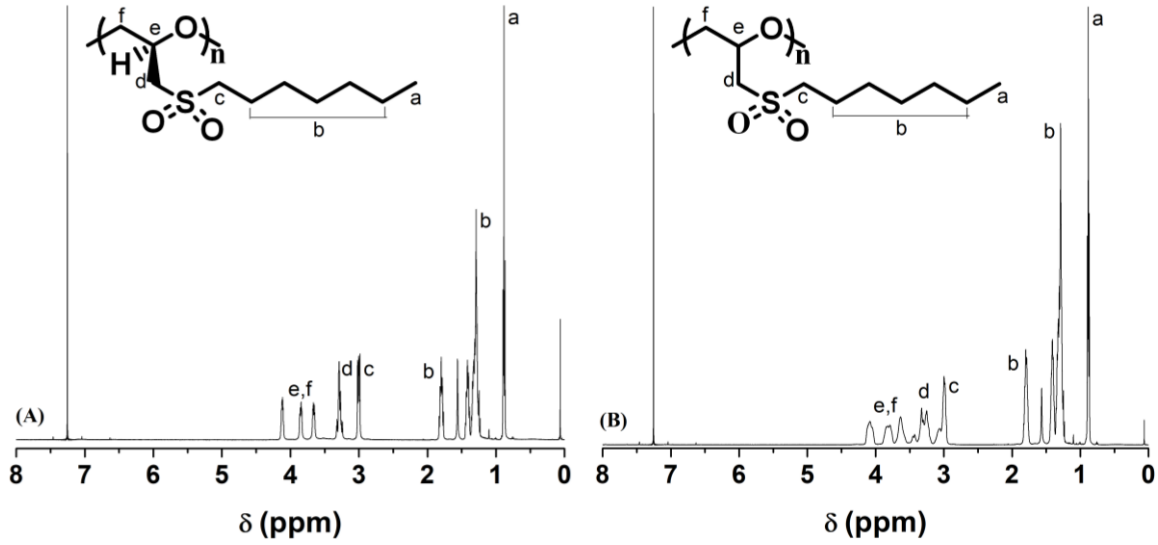

Figure 5.18. ^{1}H NMR spectra of (A) I-PECH-SO_2C_7 and (B) A-PECH-SO_2C_7 in $CDCl_3$.

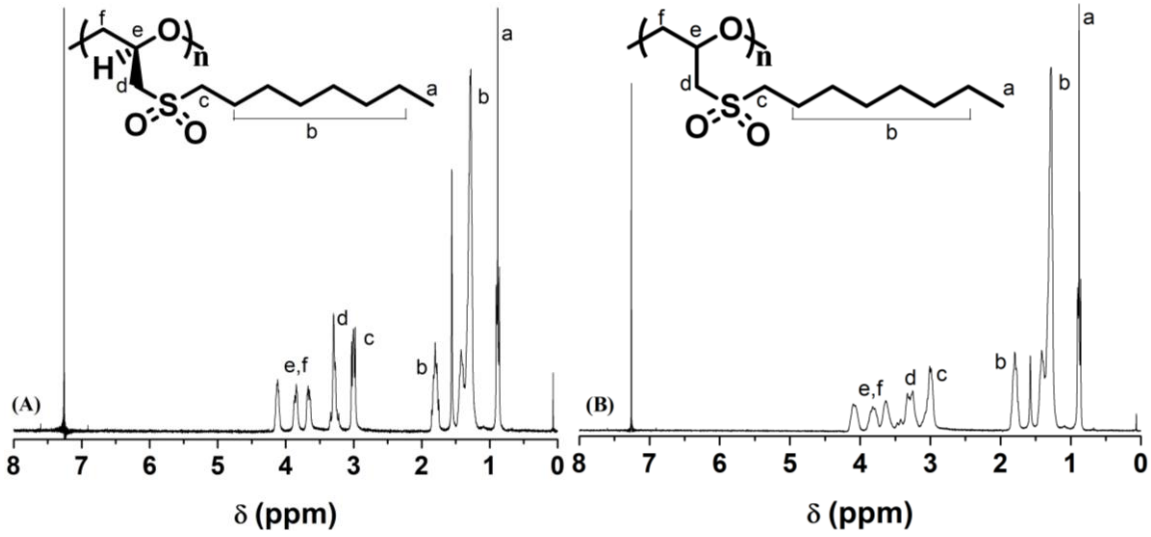

Figure 5.19. ^{1}H NMR spectra of (A) I-PECH-SO_2C_8 and (B) A-PECH-SO_2C_8 in $CDCl_3$.

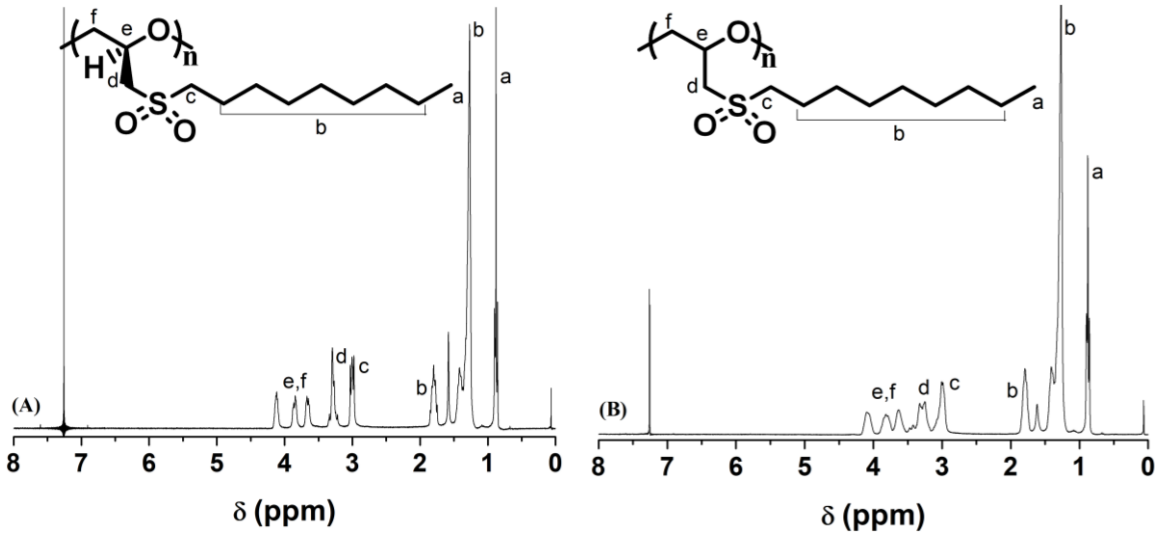

Figure 5.20. ^{1}H NMR spectra of (A) I-PECH-SO_2C_9 and (B) A-PECH-SO_2C_9 in $CDCl_3$.

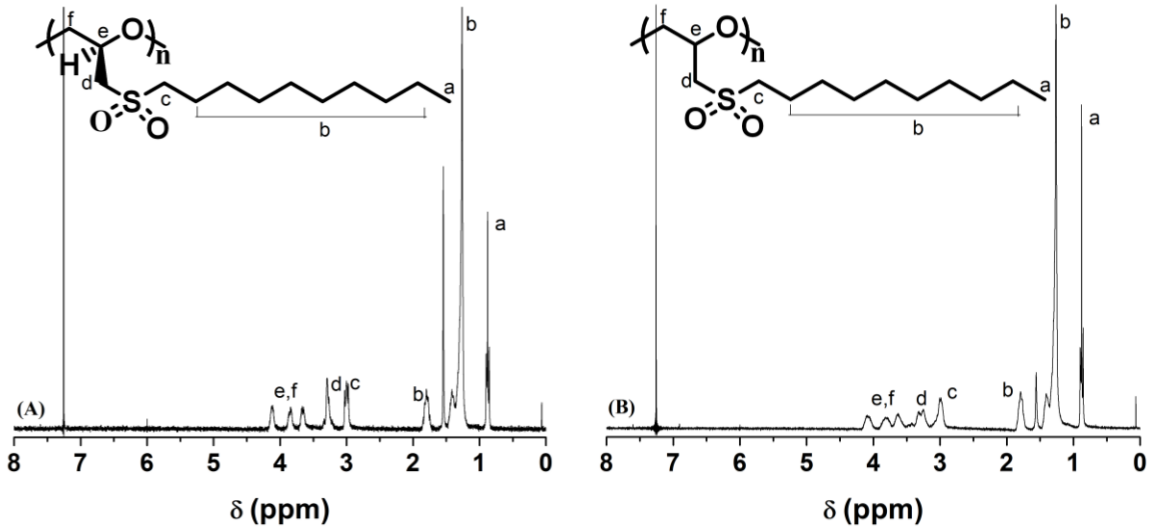

Figure 5.21. ^{1}H NMR spectra of (A) I-PECH-SO_2C_{10} and (B) A-PECH-SO_2C_{10} in $CDCl_3$.

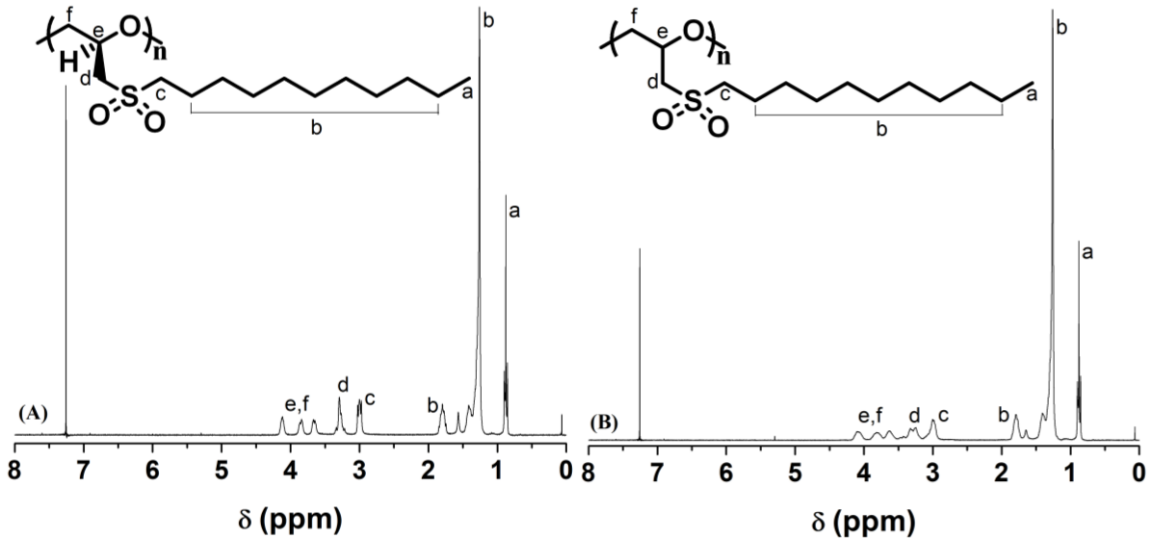

Figure 5.22. ^{1}H NMR spectra of (A) I-PECH-SO_2C_{11} and (B) A-PECH-SO_2C_{11} in $CDCl_3$.

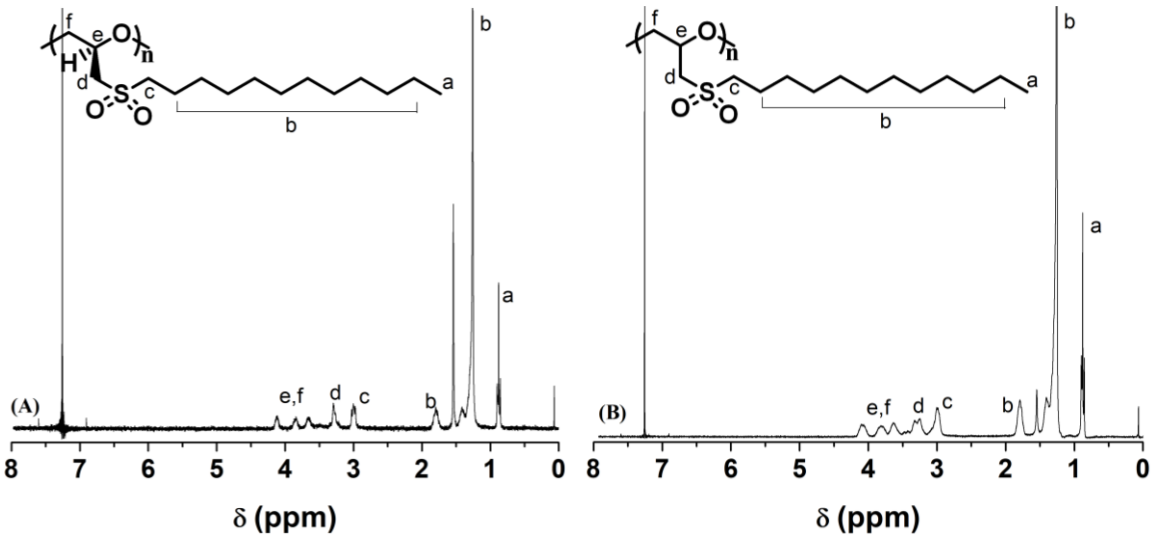

Figure 5.23. ^{1}H NMR spectra of (A) I-PECH-SO_2C_{12} and (B) A-PECH-SO_2C_{12} in $CDCl_3$.

Table 5.3. Summary of TGA Data of Polyethers with Monosulfone-containing Pendant Groups

	Temperature (°C)[a]		Temperature (°C)[a]
A-PECH-SO_2C_5	254	I-PECH-SO_2C_5	275
A-PECH-SO_2C_6	257	I-PECH-SO_2C_6	311
A-PECH-SO_2C_7	255	I-PECH-SO_2C_7	238
A-PECH-SO_2C_8	250	I-PECH-SO_2C_8	310
A-PECH-SO_2C_9	287	I-PECH-SO_2C_9	285
A-PECH-SO_2C_{10}	288	I-PECH-SO_2C_{10}	280
A-PECH-SO_2C_{11}	290	I-PECH-SO_2C_{11}	319
A-PECH-SO_2C_{12}	263	I-PECH-SO_2C_{12}	281

[a] Temperature of each sample was determined at 95% Weight Retention from TGA.

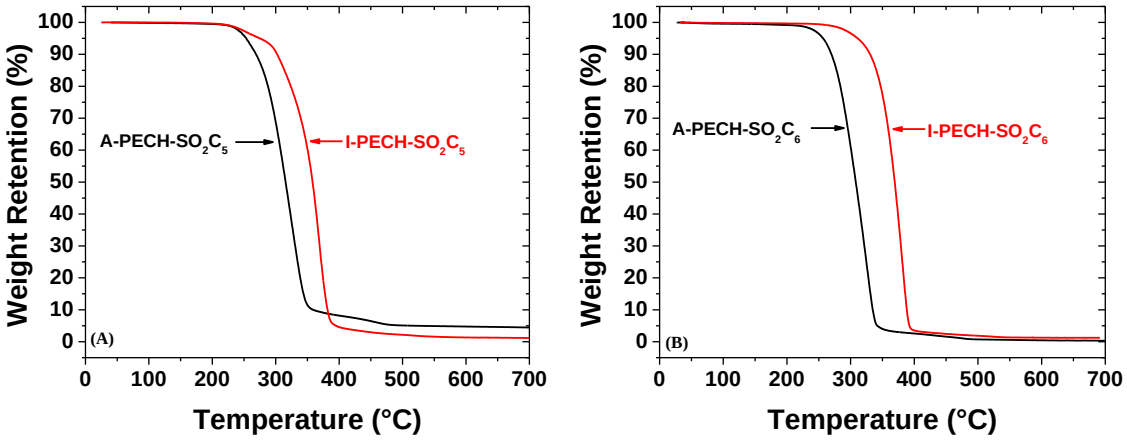

Figure 5.24. Thermogravimetric analysis (TGA) profiles of (A) A-PECH-SO_2C_5 and I-PECH-SO_2C_5 and (B) A-PECH-SO_2C_6 and I-PECH-SO_2C_6.

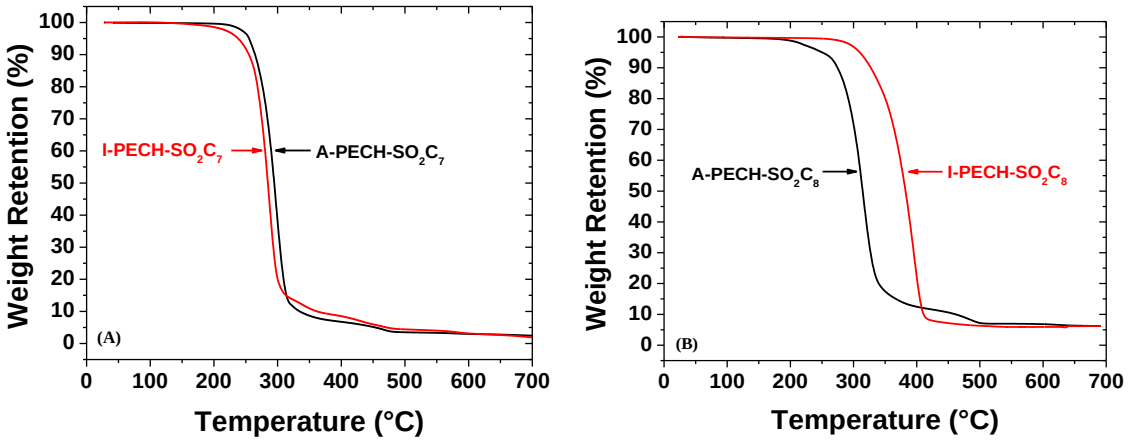

Figure 5.25. Thermogravimetric analysis (TGA) profiles of (A) A-PECH-SO_2C_7 and I-PECH-SO_2C_7 and (B) A-PECH-SO_2C_8 and I-PECH-SO_2C_8.

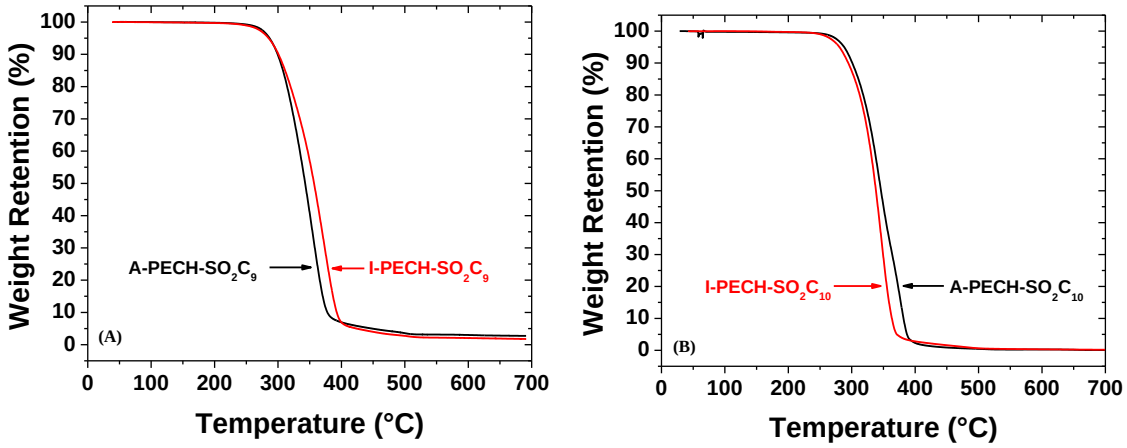

Figure 5.26. Thermogravimetric analysis (TGA) profiles of (A) A-PECH-SO_2C_9 and I-PECH-SO_2C_9 and (B) A-PECH-SO_2C_{10} and I-PECH-SO_2C_{10}.

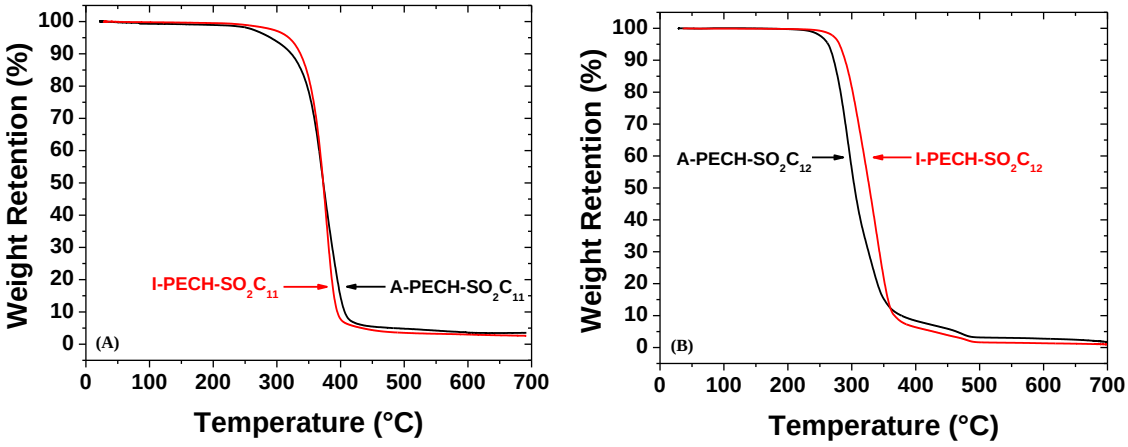

Figure 5.27. Thermogravimetric analysis (TGA) profiles of (A) A-PECH-SO_2C_{11} and I-PECH-SO_2C_{11} and (B) A-PECH-SO_2C_{12} and I-PECH-SO_2C_{12}.

groups is likely a result of higher crystallinity relative to atactic polymers. Note that this a collaborative study between our group and Professor Lei Zhu's group at Case Western Reserve University. Their group is currently conducting differential scanning calorimetry (DSC), small angle X-ray scattering (SAXS), and wide angle X-ray scattering (WAXS) studies on the described samples.

5.4. Conclusions

A series of chiral, isotactic polyethers with monosulfone-containing pendant groups with varying alkyl lengths were synthesized by ring-opening polymerization from *R*-(-)-epichlorohydrin and subsequent post-polymerization modifications. For comparison, atactic polyepichlorohydrin of a similar molecular weight, purchased from Sigma-Aldrich, was used for the synthesis of atactic, analogous polyethers. The two-step post-polymerization modifications were carried out to prepare the target polyethers, and various characterization techniques were performed throughout the synthesis. The first modification reaction was the substitution of the Cl from polyepichlorohydrin by an *n*-alkanethiol. These polymers, denoted as PECH-SC_X, where X represents the number of carbon atoms in the pendant group, were characterized by NMR spectroscopy, size exclusion chromatography, and polarimetry (for isotactic polyethers). ^{1}H NMR spectroscopy analysis indicated that the substitution reactions were complete for both isotactic and atactic PECHs. The thioether pendant groups in these polymers were then oxidized to sulfone groups, resulting in the desired polyethers, denoted as PECH-SO_2C_X. The thermal stabilities of all PECH-SO_2C_X samples were characterized by thermogravimetric analysis and found to be stable up to ~300 °C. Our collaborators are

currently studying these polyethers by differential scanning calorimetry and wide and small angle x-ray scattering.

References

1. Neese, B.; Chu, B.; Lu, S.-G.; Wang, Y.; Furman, E.; Zhang, Q. M. Large Electrocaloric Effect in Ferroelectric Polymers Near Room Temperature. *Science* **2008,** *321* (5890), 821-823.
2. Valant, M. Electrocaloric materials for future solid-state refrigeration technologies. *Prog. Mater. Sci.* **2012,** *57* (6), 980-1009.
3. Havelský, V.; Mečárik, K. Heat pump design with thermal storage. *Heat Recovery Syst. CHP* **1989,** *9* (5), 447-450.
4. Ma, R.; Zhang, Z.; Tong, K.; Huber, D.; Kornbluh, R.; Ju, Y. S.; Pei, Q. Highly efficient electrocaloric cooling with electrostatic actuation. *Science* **2017,** *357* (6356), 1130-1134.
5. Defay, E.; Crossley, S.; Kar-Narayan, S.; Moya, X.; Mathur, N. D. The Electrocaloric Efficiency of Ceramic and Polymer Films. *Adv. Mater.* **2013,** *25* (24), 3337-3342.
6. Defay, E.; Faye, R.; Despesse, G.; Strozyk, H.; Sette, D.; Crossley, S.; Moya, X.; Mathur, N. D. Enhanced electrocaloric efficiency via energy recovery. *Nat. Commun.* **2018,** *9* (1), 1827.
7. Jugsujinda, S.; Vora-ud, A.; Seetawan, T. Analyzing of Thermoelectric Refrigerator Performance. *Procedia Eng.* **2011,** *8*, 154-159.
8. Bai, Y.; Qin, S.; Nie, W.; Li, J.; Li, J.; Wang, H.; Qiao, L.; Guo, D. Influence of microstructure features on electrocaloric effect in ferroelectric ceramics. *Ceram. Int.* **2018,** *44* (7), 8263-8269.

9. Molin, C.; Neumeister, P.; Neubert, H.; Gebhardt, S. E. Multilayer Ceramics for Electrocaloric Cooling Applications. *Energy Technol.* **2018,** *6* (8), 1543-1552.
10. Li, M.-D.; Tang, X.-G.; Zeng, S.-M.; Liu, Q.-X.; Jiang, Y.-P.; Zhang, T.-F.; Li, W.-H. Large Electrocaloric Effect in Lead-free Ba(HfxTi1–x)O3 Ferroelectric Ceramics for Clean Energy Applications. *ACS Sustainable Chem. Eng.* **2018,** *6* (7), 8920-8925.
11. Zhuo, F.; Li, Q.; Gao, J.; Ji, Y.; Yan, Q.; Zhang, Y.; Wu, H.-H.; Xi, X.-Q.; Chu, X.; Cao, W. Giant Negative Electrocaloric Effect in (Pb,La)(Zr,Sn,Ti)O3 Antiferroelectrics Near Room Temperature. *ACS Appl. Mater. Interfaces* **2018,** *10* (14), 11747-11755.
12. Chen, X.; Han, X.; Shen, Q.-D. PVDF-Based Ferroelectric Polymers in Modern Flexible Electronics. *Adv. Electron. Mater.* **2017,** *3* (5), 1600460.
13. Basso, V.; Russo, F.; Gerard, J.-F.; Pruvost, S. Direct measurement of the electrocaloric effect in poly(vinylidene fluoride-trifluoroethylene-chlorotrifluoroethylene) terpolymer films. *Appl. Phys. Lett.* **2013,** *103* (20), 202904.
14. Lagerwell, S. T. Ferroelectric and Antiferroelectric Liquid Crystals. *Ferroelectrics* **2004,** *301* (1), 15-45.
15. Busson, P.; Ihre, H.; Hult, A. Synthesis of a Novel Dendritic Liquid Crystalline Polymer Showing a Ferroelectric SmC* Phase. *J. Am. Chem. Soc.* **1998,** *120* (35), 9070-9071.
16. Yoshino, K.; Ozaki, M.; Sakurai, T.; Sakamoto, K.; Honma, M. Ferroelectric Liquid Crystal with Extremely Large Spontaneous Polarization. *Jpn. J. Appl. Phys.* **1984,** *23* (Part 2, No. 3), L175-L177.

17. Lee, J.-C.; Han, S.-H.; Cha, S.-H.; Park, S.-Y.; Farmer, B. L. Synthesis and dipole-dipole interaction-induced mesomorphic behavior of poly(oxyethylene)s containing (n-octylsulfonyl)alkylthiomethyl or (n-octylsulfonyl)alkylsulfonylmethyl side groups. *Polymer* **2003,** *44* (24), 7413-7425.

18. Park, S. Y.; Farmer, B. L.; Lee, J. C. The structures of poly(oxyethylene)s having sulfone groups in the side chains. *Polymer* **2002,** *43* (1), 177-183.

19. Ferrier, R. C.; Pakhira, S.; Palmon, S. E.; Rodriguez, C. G.; Goldfeld, D. J.; Iyiola, O. O.; Chwatko, M.; Mendoza-Cortes, J. L.; Lynd, N. A. Demystifying the Mechanism of Regio- and Isoselective Epoxide Polymerization Using the Vandenberg Catalyst. *Macromolecules* **2018,** *51* (5), 1777-1786.

20. Brochu, S.; Ampleman, G. Synthesis and Characterization of Glycidyl Azide Polymers Using Isotactic and Chiral Poly(epichlorohydrin)s. *Macromolecules* **1996,** *29* (17), 5539-5545.

21. Vandenberg, E. J. Organometallic catalysts for polymerizing monosubstituted epoxides. *J. Polym. Sci.* **1960,** *47* (149), 486-489.

22. Iida, M.; Araki, T.; Teranishi, K.; Tani, H. Effect of Substituents on Stereospecific Polymerization of β-Alkyl- and β-Chloroalkyl-β-propiolactones. *Macromolecules* **1977,** *10* (2), 275-284.

Chapter 6. Conclusions and Future Work

Nanoparticles (NPs), including metals, metal oxides, and metal sulfides, have been shown to function as friction reducers and anti-wear reagents when added into base oils such as polyalphaolefin (PAO) as additives. However, NPs have a high tendency to undergo aggregation and precipitation because of the small size and high surface energy. Once NPs phase separate from the base oil, their tribological benefits are lost. Built on our group's previous work and expertise,[1-8] this dissertation research is aimed to design, develop, and explore polymer brush-grafted NPs (hairy NPs) for potential use as lubricant additives for friction and wear reductions. A series of hairy NPs were successfully synthesized by surface-initiated reversible addition-fragmentation chain transfer polymerization (SI-RAFT) from RAFT chain transfer agent-functionalized, 23 nm silica NPs with the addition of a free CTA. The lubricating properties of these hairy silica NPs were investigated either alone in PAO or in combination with an oil-miscible phosphonium-phosphate ionic liquid (IL), another type of promising additives, by tribological testing and profilometry measurements, and the tribofilms were analyzed by scanning electron microscopy-energy dispersive X-ray spectroscopy (SEM-EDS). The insights gained from this research will provide guidelines for developing hairy NPs for practical use in the lubricant industry.

In Chapter 2, a set of hairy NPs composed of poly(alkyl methacrylate) brushes with varying pendant group lengths were synthesized by SI-RAFT with a goal of elucidating the effects of alkyl pendant group on oil dispersibility, stability, and tribological property of hairy NPs.[9] Six hairy NP samples were prepared: poly(*n*-hexyl methacrylate) (PC6)-, poly(ethylhexyl methacrylate) (PC8)-, poly(lauryl methacrylate) (PC12)-, two batches of

poly(tridecyl methacrylate) (PC13)-, and poly(hexadecyl methacrylate) (PC16)-grafted silica NPs. We found that hairy NPs with sufficiently long alkyl pendant groups (12, 13, and 16 carbon atoms in the side group) readily formed homogeneous dispersions at room temperature, and exhibited high stability at -15 °C, 18 °C, and 100 °C for 60 days as revealed by visual inspection and dynamic light scattering (DLS) studies. In contrast, PC6 and PC8 hairy NPs formed cloudy mixtures in PAO at room temperature, but interestingly PC8 hairy NPs could be dispersed in PAO at 80 °C. Significant friction and wear reductions were achieved for the homogenous dispersions relative to PAO base oil. We found that the primary function of the grafted polymer chains in hairy NPs is the stabilization of silica NPs in hydrophobic PAO.

Chapter 3 aims to increase the function of polymer brushes in hairy NPs with the incorporation of a triboactive element, phosphorus, into the brushes grafted on 23 nm silica NPs. The functional polymer brush-grafted NPs were prepared by SI-RAFT copolymerizations of a long alkyl methacrylate monomer with a phosphonate-containing monomer from CTA-functionalized silica NPs at feed molar ratios of 95 : 5, 90 : 10, 85 : 15, and 80 : 20. Three phosphonate-functionalized monomers were designed and synthesized: diethyl (4-vinylbenzyl)phosphonate (StP), 11-(diethoxyphosphoryl)undecyl methacrylate (MAC11P), and 2-(diethoxyphosphoryl)ethyl methacrylate (MAC2P). The dispersibilities of the functional hairy NPs in PAO were investigated, and it was found that the hairy NPs made from hexadecyl methacrylate and MAC2P are the most promising.

Chapter 4 presents a study of the combination of oil-soluble hairy NPs and an oil-miscible phosphonium-phosphate IL as additives for friction reduction.[10] The hypothesis

was that both silica from hairy NPs and phosphate from the IL could react with each other and with the iron substrate to strength the tribofilm, which may result in a synergistic effect. We found that the lubricating performance was indeed improved significantly, relative to hairy NPs alone or ionic liquid alone, when the additives were mixed at certain ratios while the total concentration of additives was kept constant at 2 wt%. SEM-EDS revealed the tribofilm was enriched with both Si and P, suggesting that hairy NPs and IL participated in the tribo-chemical reaction.

Chapter 5 presents a side research project. A series of isotactic and atactic polyethers with monosulfone-containing pendant groups of varying lengths were synthesized by reacting corresponding poly(epichlorohydrin) polymers with various *n*-alkanethiols and subsequent oxidation of thioether groups. The atactic poly(epichlorohydrin) was purchased, and the isotactic poly((*R*)-epichlorohydrin) was synthesized by ring-opening polymerization of *R*-(-)-epichlorohydrin with a commercially available MAO catalyst. The isotacticity of the synthesized polymer was confirmed by ^{13}C NMR spectroscopy, and ^{1}H NMR spectroscopy analysis showed that substitution reactions went to completion. Our collaborators are characterizing the structures of these polymers.

Hairy NPs are a unique class of hybrid materials with great potential in friction and wear reduction applications. Possible future work in the exploration of hairy NPs as oil additives for friction reduction would include further studies on functional polymer brushes. The work presented Chapter 3 shows that homogenous phosphonate-functionalized NP dispersions in PAO are possible. Tribological testing of these samples is needed to analyze the lubricating properties. The hairy NPs synthesized by the

copolymerization of hexadecyl methacrylate and MAC2P exhibited increased dispersibility in PAO at higher levels of phosphonate incorporation relative to other hairy NPs. The study indicated that it is possible to further increase the phosphonate content beyond 20 mol%, which may lead to an even better lubrication property.

References

1. Wright, R. A. E.; Wang, K.; Qu, J.; Zhao, B. Oil-Soluble Polymer Brush Grafted Nanoparticles as Effective Lubricant Additives for Friction and Wear Reduction. *Angew. Chem., Int. Ed.* **2016,** *55* (30), 8656-8660.
2. Bao, C. H.; Tang, S. D.; Wright, R. A. E.; Tang, P.; Qiu, F.; Zhu, L.; Zhao, B. Effect of Molecular Weight on Lateral Microphase Separation of Mixed Homopolymer Brushes Grafted on Silica Particles. *Macromolecules* 2014, 47, 6824–6835.
3. Bao, C. H.; Tang, S. D.; Horton, J. M.; Jiang, X. M.; Tang, P.; Qiu, F.; Zhu, L.; Zhao, B. Effect of Overall Grafting Density on Microphase Separation of Mixed Homopolymer Brushes Synthesized from Y-Initiator-Functionalized Silica Particles. *Macromolecules* **2012**, *45*, 8027-8036.
4. Bao, C. H.; Horton, J. M.; Bai, Z. F.; Li, D. J.; Lodge, T. P.; Zhao, B. Stimuli-Triggered Phase Transfer of Polymer-Inorganic Hybrid Hairy Particles between Two Immiscible Liquid Phases. *J. Polym. Sci. Part B: Polym. Phys.* **2014**, *52*, 1600-1619.
5. Horton, J. M.; Bao, C. H.; Bai, Z. F.; Lodge, T. P.; Zhao, B. Temperature- and pH-triggered reversible transfer of doubly responsive hairy particles between water and a hydrophobic ionic liquid. *Langmuir* **2011**, *27*, 13324-13334.
6. Horton, J. M.; Bai, Z.; Jiang, X.; Li, D.; Lodge, T. P.; Zhao, B. Spontaneous Phase Transfer of Thermosensitive Hairy Particles between Water and an Ionic Liquid. *Langmuir* **2011**, *27*, 2019-2027.

7. Wright, R. A. E.; Henn, D. M.; Zhao, B. Thermally Reversible Physically Crosslinked Hybrid Network Hydrogels Formed by Thermosensitive Hairy NPs. *J. Phys. Chem. B* **2016**, *120*, 8036-8045.
8. Wright, R. A. E.; Hu, B.; Henn, D. M.; Zhao, B. Reversible Sol-Gel Transitions of Aqueous Dispersions of Silica Nanoparticles Grafted with Diblock Copolymer Brushes Composed of a Thermosensitive Inner Block and a Charged Outer Block. *Soft Matter* **2015**, *11*, 6808-6820.
9. Seymour, B. T.; Wright, R. A. E.; Parrott, A. C.; Gao, H.; Martini, A.; Qu, J.; Dai, S.; Zhao, B. Poly(alkyl methacrylate) Brush-Grafted Silica Nanoparticles as Oil Lubricant Additives: Effects of Alkyl Pendant Groups on Oil Dispersibility, Stability, and Lubrication Property. *ACS Appl. Mater. Interfaces* **2017,** *9* (29), 25038-25048.
10. Seymour, B. T.; Fu, W.; Wright, R. A. E.; Luo, H.; Qu, J.; Dai, S.; Zhao, B. Improved Lubricating Performance by Combining Oil-Soluble Hairy Silica Nanoparticles and an Ionic Liquid as an Additive for a Synthetic Base Oil. *ACS Appl. Mater. Interfaces* **2018,** *10* (17), 15129-15139.

Vita

Bryan Thomas Seymour was born in Atlanta, GA. In 2014, he received his B. S. degree in Chemistry from Georgia Southern University in Statesboro, GA. After completing his undergraduate studies, he enrolled as a graduate student at the University of Tennessee, Knoxville and joined Professor Bin Zhao's research group. His research focused on the synthesis and application of oil-soluble polymer brush-grafted nanoparticles as additives for friction and wear reduction. He went on to receive a Doctor of Philosophy Degree in Chemistry from the University of Tennessee, Knoxville in May 2019.